ÇUKUROVA UNIVERSITY
INSTITUTE OF NATURAL AND APPLIED SCIENCES

PhD THESIS

Enhanced Control Structure for Grid Connected Photovoltaic Systems Under Different Operating Conditions

Ibrahem Mahmoud Abed Alhameed HUSSEIN

Department Of Electrical and Electronics Engineering

August, 2024

ÇUKUROVA UNIVERSITY
INSTITUTE OF NATURAL AND APPLIED SCIENCES

PhD THESIS APPROVAL

Enhanced Control Structure for Grid Connected Photovoltaic Systems Under Different Operating Conditions

Ibrahem Mahmoud Abed Alhameed HUSSEIN

Department Of Electrical and Electronics Engineering

This Doctorate Thesis was evaluated by the following Jury Members on 18/07/2024 and was approved by unanimity / majority of votes.

Jury : Prof. Dr. Ahmet TEKE (Advisor) …………

: Assoc. Prof. Dr. Özgür ÇELIK …………

: Asst. Prof. Dr. Oğuzhan TİMUR …………

: Asst. Prof. Dr. Murat FURAT …………

: Asst. Prof. Dr. Kasım ZOR …………

This Thesis was written in the Department of Electrical and Electronics Engineering, Institute of Natural and Applied Sciences.
Thesis Number:

Prof. Dr. Sadık DİNÇER
Director
Institute of Natural and Applied Sciences

This work was supported by the Scientific Project Unit of Çukurova University.
Project ID: FDK-2021-14048

CONTENTS

CUKUROVA UNIVERSITY

INSTITUTE OF NATURAL AND APPLIED SCIENCES

PhD THESIS

Enhanced Control Structure for Grid Connected Photovoltaic Systems Under Different Operating Conditions

Ibrahem Mahmoud Abed Alhameed HUSSEIN

Advisor: Prof. Dr. Ahmet TEKE

Department of Electrical and Electronics Engineering

ABSTRACT

Increasing the penetration level of grid-connected photovoltaic systems poses challenges to the utility grid power quality (PQ) and raises significant concerns regarding the interharmonics in the injected grid current. Delivering efficient power that meets grid PQ standards depends on the enhancements to be made in the control structure of the inverters. This thesis is devoted to investigating the characteristics of interharmonics generation, mechanisms of emission, and their effects on the inverter performance, as well as proposing mitigation techniques under various operating conditions. For these purposes, a strong relationship has been identified between the interharmonics generating characteristics and the parameters of the maximum power point tracking (MPPT) algorithms, such as the perturbation step size and sampling rate. Utilizing a large step size and fast sampling rate enhances the tracking performance but also increases the injected interharmonics in the frequency spectrum of the grid current. The relation between interharmonics generating characteristics and the developed control systems is analyzed under active and reactive power support, utility grid abnormalities, e.g., low-voltage ride-through (LVRT), voltage sag/swell conditions, deviation of grid frequency, and the variation in the dc-link capacitance. Accordingly, new mathematical expressions are proposed to predict the interharmonics frequencies based on these parameters. Additionally, a mathematical development is proposed that relates the parameters of the MPPT algorithms to the dc-link voltage of the inverter. These equations can be used in the detection process of interharmonics. The proposed technique is applied to modify the various MPPT algorithms to mitigate the emission of interharmonics in single-phase grid-connected PV systems. The proposed methods are based on modifying various MPPT algorithms to maximize their performance characteristics and tracking efficiencies while effectively minimizing the generated interharmonics and total harmonic distortion (THD). Therefore, the distribution of interharmonics in the frequency spectrum is modified, and the power quality of the injected grid current is improved.

Keywords: Grid-Connected Inverter, MPPT, Photovoltaic, Power Quality, Interharmonics.

ÇUKUROVA ÜNİVERSİTESİ
FEN BİLİMLERİ ENSTİTÜSÜ

DOKTORA TEZİ

Farklı Çalışma Koşullarında Şebeke Bağlantılı Fotovoltaik Sistemler İçin Gelişmiş Kontrol Yapısı

Ibrahem Mahmoud Abed Alhameed HUSSEIN

Danışman: Prof. Dr. Ahmet TEKE

Department of Electrical and Electronics Engineering

ÖZ

Şebekeye bağlı fotovoltaik sistemlerin şebekeye artan entegrasyonu, elektrik şebekesinde güç kalitesi (PQ) için zorluklar oluşmakta ve şebekedeki interharmonikler konusunda önemli problemler doğurmaktadır. Şebeke için gerekli PQ standartlarına uygun bir güç sağlamak, invertörlerin kontrol yapısının doğru gerçekleştirilmesine bağlıdır. Bu tez çalışması, interharmonik üreticilerin özelliklerini, emisyon sıcaklıklarını, performans üzerindeki çeşitli değişkenleri ve farklı sistem koşulları altında azaltma tekniklerini önermektedir. Bu amaç için, interharmonik üreten karakteristik özelliğiyle ile maksimum güç noktası izleme (MPPT) programlarının bozulmayan adım boyutu ve hareket hızı gibi parametreleri arasında güçlü bir ilişki tanımlanmıştır. Büyük adım boyutu ve hızlı vuruş hızı takip performansını arttırabilir fakat şebeke akımının frekans spektrumunda ölçülen ara harmonikleri artırıbilir. İnterharmonik üretme karakteristiği ile geliştirilen kontrol sistemleri arasındaki ilişkiler aktif ve reaktif güç desteği, şebeke anormallikleri, düşük voltajlı sürüş desteği (LVRT), voltajın düşmesi/yükselmesi koşulları, şebeke dağılımının sapması ve dc-link kapasitanındaki değişimler için analiz edilmiştir. Buna göre, bu parametrelere bağlı olan interharmonik frekanslarını tahmin etmek için yeni matematiksel denklemler önerilmiştir.. Ek olarak, MPPT algoritmalarının parametrelerini eviricinin DC hat voltajıyla ilişkilendiren bir matematiksel iyileştirme önerilmiştir. Böylece bu denklemler ara harmoniklerin tespit edilmesinde kullanılabilmektedir. Önerilen teknik, tek fazlı şebekeye bağlı PV sistemlerinde ara harmoniklerin emisyonunu azaltmak amacıyla çeşitli MPPT algoritmalarını değiştirmek için uygulanabilir. Önerilen yöntemler, çeşitli MPPT algoritmalarının, performans özelliklerini ve izleme verimliliklerini en üst düzeye çıkarırken, üretilen interharmonikleri ve toplam harmonik bozulmayı (THD) etkili bir şekilde en aza indirecek şekilde değiştirilmesine dayanmaktadır. Bu nedenle, frekans spektrumundaki ara harmoniklerin dağılımı değiştirmekte ve enjekte edilen şebeke akımının güç kalitesi iyileştirmektedir.

Anahtar Kelimeler: Şebekeye Bağlı İnvertör, MPPT, Fotovoltaik, Güç Kalitesi, Ara Harmonikler.

EXTENDED ABSTRACT

Research into energy-generating systems has become increasingly crucial for different countries due to the extensive use of energy resources. Even though conventional electric power infrastructure plays a vital role in supplying energy, the use of distributed generating systems, such as grid-connected renewable generating units, has become common in these networks. Supplying the power from these generating systems should be in an optimal way to reduce the effects of different power quality issues resulting from the connection to the utility grid. The number of grid-connected customers utilizing different types of renewable generating systems is rapidly increasing, particularly for solar energy and PV technology, which are gaining popularity due to the decreasing cost of these systems with time. From the technological point of view, the continuous development of PV systems, including innovations in shapes and materials, has led to more effective PV cells being produced with higher efficiency and lower cost. These advancements have impacted the PV system's penetration and integration levels to the utility grid. Consequently, operational residential and megawatt-scale grid-connected PV systems are being increasingly installed around the world.

Recently, the affordability of constructing a PV-generating system, either at local or large-scale levels, has enabled more customers to contribute to the total generation reserve. However, a typical PV system lifespan of around 25 years, along with other factors, suggests an optimal usage of PV equipment. The complex relationship between solar irradiance, temperature, and internal resistance affects the total extracted power from the PV cell. The nonlinear behavior of the power-voltage (P-V) curve, which results in a nonlinear efficiency value, created a unique point reflecting the PV cell's maximum power point. Thus, extracting the maximum power and the operation at this point is crucial. The utilization of an MPPT method is required to identify different operating power points and to choose the global maximum power point, ensuring the highest power harvesting out of the PV cell.

The rapid growth and the popularity of installing more PV systems, especially grid-connected systems, have increased the overall capacity and the applications of PV systems. Nevertheless, more enhancement and development of the control structure are demanded to cope with the development of grid-connected PV systems. This will ensure proper operation for the PV systems integrated into the grid regarding power quality, reliability, and stability. Therefore, inspecting the power delivery and the current being injected into the grid is essential; hence, the research on this topic is still premature.

In practice, challenging the utility grid integration standards by increasing the distributed PV renewable generating system's penetration level becomes a vital issue threatening the power quality at the distribution level. One of the main issues characterizing this situation is the interharmonics being injected into the power system network at the point of common coupling. Supplying pure sinusoidal current waveforms with rated values is one of the main interests and concerns in this field

of PQ. From the electrical grid point of view, increasing the number of connected PV systems can distribute the electrical distribution system, leading to many undesirable consequences. Hence, the signal distortion level, power losses, and disturbance of power electronic devices are essential issues for grid-connected PV systems. Integrating the PV systems into the electric grid should comply with different standards and rules set by electrical companies. Various existing grid-integration standards deal with different issues, e.g., interconnection criterion and power quality requirements. Nevertheless, regarding interharmonics, and due to the fact that this issue is currently under research, no obvious standard is imposed under this condition, and this suggests more investigations about their consequences.

The extensive use of grid-connected inverters, along with the conventional control structure of the PV inverter, requires investigations to enhance the system performance from the PQ perspective. The control algorithm used to control the inverter should be examined for each stage to reveal the main origin behind interharmonics emission to the electrical grid. The insufficient monitoring process at the point of common coupling from the utility grid side ensures power quality and reliability issues. Besides, the interharmonics propagated through the utility electric grid can cause smart metering issues, tripping of protection devices, interruption of power, and mis-operation of circuit breakers and relays. Therefore, exposing the existence of interharmonics emission from the grid-connected PV inverter and enhancing the control structure is demanded.

The utilization of different techniques to extract the maximum amount of PV power that is being injected into the electrical grid from the PV system comes with its consequences. The fluctuating nature of the solar irradiance and the partial shading issues change the amount of the injected power to the electrical grid. While focusing on efficiency and maximum power harvesting is extremely important, minimizing interharmonics in the injected current is indispensable. Some of the maximum power point tracking techniques impose perturbation on the DC-link voltage of the inverter. In the conventional maximum power point tracking techniques, the perturbations are highly dependent on the controller parameters and the grid synchronization process. The changing nature of the DC-link voltage during the allocation of the maximum power point creates additional terms in the frequency spectra resulting from DC-link voltage. This will interact with the synchronization process based on the grid frequency to create modulated interharmonics that vary with the control parameters of the inverter controller and fluctuate in their magnitudes.

The synchronization process characterizes the interaction with the electrical grid; the spatial distance between interharmonics changes with the controller parameters, and the modulation process results from the synchronized injected current to the grid. Under this situation, the process of interharmonics detection and mitigation becomes a challenging task due to the frequency and magnitude variation of interharmonics. The investigations about interharmonics issues, the mechanism of their generation, and the possible ways to mitigate their effects are essential under high penetrating levels of grid-connected PV systems. In practice, harmonics and interharmonics are considered to be the measure of how much a signal is distorted. Under high integration levels, grid-connected photovoltaic systems (PVS) are considered a source of interharmonics that are injected into the utility grid network, which in turn leads to many financial and technical problems. The investigations behind the origins of interharmonics are still premature, and further studies should be carried out to bridge the gap in the literature and to justify the attributes and mitigation techniques for this issue.

Accordingly, to cope with these challenges, the control structure of the inverter can be effectively enhanced and improved by utilizing advanced power electronics controllers and enhancing the maximum power point tracking technique with an effective control structure. A strong relationship has been observed and identified between the control parameters of the MPPT algorithms, e.g., P&O, and the generation nature of interharmonics. Controlling the perturbation step size and sampling rate will affect tracking performance and efficiency. However, the values of these control parameters can lead to high magnitudes of interharmonics with variations in their frequencies. The MPPT control structure can be modified to achieve both a reduction in the generated interharmonics and an improvement in mitigating the effect of interharmonics emissions on the grid current. The investigations and the mitigation techniques of interharmonics should consider the system's operation under different operating conditions, especially with low irradiance scenarios. The injected current grid current under low power operating conditions, e.g., low irradiance or partial shading, is distorted, and the magnitudes of interharmonics rise with a varying frequency nature of their spatial frequency distribution. Therefore, investigations should be carried out under full and low-power operating conditions. Furthermore, the new technology in intelligent inverters enables the grid-connected PV inverter to support reactive power to the grid, and under this scenario, the investigation of interharmonics generating characteristics can improve the system stability under grid dynamic support. In addition, the investigation toward enhancing the control algorithm can be extended under active and reactive power support.

The first step toward successful interharmonics detection is to allocate the frequency spatial distribution of interharmonics mathematically. This can be done while considering the modulation effect from the synchronization process and the impact of the MPPT control parameters. In addition, the mathematical expressions can relate the control parameters of the MPPT algorithms to the DC-link voltage variation. Under this criteria, the main challenge can be depicted due to the randomly changing nature of interharmonics throughout the frequency spectrum. Another important aspect is to investigate the various types of MPT techniques and their effects on the generating characteristic of interharmonics. Different algorithms are available and employed in the control structure of single-phase and three-phase grid-connected PV systems. The dominant part, which includes the extensive use of single-phase inverters, drives the force toward investigating them in a comprehensive way. A comparison between the nature of interharmonics and how they behave under different normal and abnormal operating conditions will support the development of an enhanced control structure and improved technology used to control the single-phase grid-connected PV inverters.

Considering the daily increase in the number of connected PV inverters to the utility electric grid, the interharmonics emission increases throughout the network and adds up to create more significant distortion, which affects mainly the quality of power being delivered and the circulation of interharmonics through in the utility grid. The application of the proposed interharmonics mitigation technique and the enhancements to the MPPT algorithms will ensure the long lifespans of the inverter, the minimization of losses, and the maximization of efficiency with minimal possible THD values that comply with the grid integration standards. The proposed enhanced control structure of the inverter will ensure the operation of the grid-connected PV systems while minimizing the interharmonics emission to the utility grid. This will ensure the support of high-quality active and reactive power to the electric network. This will eliminate various types of power quality issues and improve the overall performance of the PV system at the point of common coupling.

This thesis focuses on the control structure of the inverter and the maximum power point tracking architecture, considering the interconnection standards regarding the PV inverters while maximizing the PV system's power quality, efficiency, and reliability. The following approach ensures high-quality power transfer between the PV grid-connected customer and the electric utility grid. This thesis presents investigations about grid-connected PV systems' power quality issues, focusing on single-phase systems and providing advanced and enhanced topological control solutions to significantly improve the system's performance.

This thesis aims to investigate the generating characteristics and the mechanism of interharmonics emission through the control system of the inverter. In addition, the factors that influence the generation of interharmonics are determined and analyzed. Mathematical expressions are proposed to specify the generated frequency of each individual interharmonic in the frequency spectra of the injected grid current. A mathematical development will also be proposed to relate the MPPT controller parameters to the generation and injection of interharmonics in the DC-link voltage controller and the modulation process in the grid current. Accordingly, this thesis will propose an interharmonics mitigation technique that applies to different MPPT algorithms to minimize their interharmonics-generating characteristics while maximizing their efficiency and tracking performance. A comparison between the various proposed mitigation techniques is presented in terms of efficiency, THD, and interharmonic emission values to validate the proposed method.

In this context, a multimission enhanced control structure of a single-phase grid-connected PV inverter is proposed to investigate the interharmonics generating characteristics under normal and abnormal operating conditions, which include utility grid voltage sag/swell, deviation of grid frequency, LVRT, active and reactive power support, and variation of DC-link capacitance due to the aging effect of the component. An extensive simulation-based analysis is performed on the proposed interharmonics mitigation technique and the modified MPPT algorithms to validate their effectiveness under these operating conditions with low, full, and dynamic solar irradiances.

The developed mathematical modeling, along with proposed interharmonics mitigation techniques for different MPPT algorithms, are considered good candidates to enhance the control structure of the inverter, mitigate the interharmonics in the frequency spectra of the grid current, and improve the quality of power being injected into the grid.

GENİŞLETİLMİŞ ÖZET

Enerji üretim sistemleri üzerindeki araştırmalar, enerji kaynaklarının geniş çapta kullanımından dolayı farklı ülkeler için giderek daha önemli hale gelmektedir. Geleneksel elektrik güç altyapısı enerji sağlama konusunda kritik bir rol oynasa da, şebeke bağlantılı yenilenebilir enerji üretim üniteleri gibi dağılmış üretim sistemlerinin kullanımı bu ağlarda yaygın hale gelmiştir. Bu üretim sistemlerinden enerji sağlanması, şebeke bağlantısının neden olduğu çeşitli güç kalitesi sorunlarının etkilerini azaltmak için optimal bir şekilde yapılmalıdır. Yenilenebilir enerji sistemlerinin çeşitli türlerini kullanan şebeke bağlantılı müşteri sayısı hızla artmakta, özellikle güneş enerjisi ve PV teknolojileri, zamanla bu sistemlerin maliyetlerinin azalması nedeniyle popülerlik kazanmaktadır. Teknolojik açıdan, PV sistemlerinin sürekli gelişimi, şekil ve malzeme yenilikleri dahil, daha yüksek verimlilik ve daha düşük maliyetle daha etkili PV hücrelerinin üretilmesini sağlamıştır. Bu ilerlemeler, PV sistemlerinin şebekeye penetrasyon ve entegrasyon seviyelerini etkilemiştir. Sonuç olarak, dünya genelinde operasyonel konut ve megavat ölçeğinde şebeke bağlantılı PV sistemleri giderek daha fazla kurulmaktadır.

Son zamanlarda, yerel veya büyük ölçekli seviyelerde bir PV üretim sistemi kurmanın maliyetinin düşmesi, daha fazla müşterinin toplam enerji üretim rezervine katkıda bulunmasını sağlamıştır. Ancak, tipik bir PV sistem ömrü olan yaklaşık 25 yıl ve diğer faktörler, PV ekipmanının optimal kullanımını önermektedir. Güneş ışınımı, sıcaklık ve iç direnç arasındaki karmaşık ilişki, PV hücresinden elde edilen toplam gücü etkilemektedir. Güç-gerilim (P-V) eğrisinin doğrusal olmayan davranışı, doğrusal olmayan bir verimlilik değeri ile sonuçlanarak, PV hücresinin maksimum güç noktasını yansıtan benzersiz bir nokta oluşturur. Bu nedenle, maksimum gücün elde edilmesi ve bu noktada işletilmesi kritik öneme sahiptir. Farklı işletim güç noktalarını belirlemek ve global maksimum güç noktasını seçmek için MPPT (Maksimum Güç Noktası Takibi) yönteminin kullanılması gereklidir. Bu, PV hücresinden en yüksek gücün elde edilmesini sağlamaktadır.

PV sistemlerinin, özellikle şebeke bağlantılı sistemlerin, hızlı bir şekilde büyümesi ve popülerliği, toplam kapasiteyi ve PV sistemlerinin uygulama alanlarını artırmıştır. Bununla birlikte, şebeke bağlantılı PV sistemlerinin gelişimiyle başa çıkmak için kontrol yapısının daha fazla geliştirilmesi ve iyileştirilmesi gerekmektedir. Bu, şebekeye entegre edilen PV sistemlerinin güç kalitesi, güvenilirlik ve kararlılık açısından düzgün bir şekilde çalışmasını sağlayacaktır. Bu nedenle, güç iletiminin ve şebekeye enjeksiyon yapılan akımın incelenmesi önemlidir; dolayısıyla, bu konudaki araştırmalar henüz başlangıç aşamasındadır.

Pratikte, dağıtılmış PV yenilenebilir üretim sistemlerinin penetrasyon seviyesini artırmak, dağıtım seviyesinde güç kalitesini tehdit eden bir sorun haline gelmektedir. Bu durumun karakterize ettiği başlıca sorunlardan biri, ortak bağlantı noktasında güç sistemi ağına enjekte edilen interharmoniklerdir. Bu alandaki güç kalitesi (PQ) sorunlarından biri, belirlenen değerlerde saf sinüzoidal akım dalgalarının sağlanmasıdır. Elektrik şebekesi açısından, bağlı PV sistemlerinin sayısının artması, elektrik dağıtım sistemini yayarak birçok istenmeyen sonuca yol açabilir. Bu nedenle, sinyal bozulma seviyesi, güç kayıpları ve güç elektroniği cihazlarının rahatsızlığı, şebeke bağlantılı PV sistemleri için önemli sorunlardır. PV sistemlerinin elektrik şebekesine entegrasyonu, elektrik şirketleri tarafından belirlenen farklı standart ve kurallara uymalıdır. Mevcut çeşitli şebeke entegrasyon standartları, bağlantı kriterleri ve güç kalitesi gereksinimleri gibi farklı sorunlarla ilgilenmektedir. Bununla birlikte, interharmonikler konusunda, bu sorunun halen araştırma aşamasında olması nedeniyle, bu koşul altında belirgin bir standart uygulanmamaktadır ve bu durum, etkilerinin daha fazla araştırılmasını gerektirmektedir.

Şebeke bağlantılı inverterlerin geniş çapta kullanımı ve PV inverterlerin geleneksel kontrol yapısı, sistem performansını güç kalitesi (PQ) perspektifinden geliştirmek için araştırmalar yapılmasını gerektirmektedir. İnverteri kontrol etmek için kullanılan kontrol algoritması, interharmonik emisyonlarının elektrik şebekesine olan ana kökenini ortaya çıkarmak amacıyla her aşamada incelenmelidir. Şebeke tarafında ortak bağlantı noktasında yetersiz izleme süreci, güç kalitesi ve güvenilirlik sorunlarına yol açmaktadır. Ayrıca, şebeke elektriği aracılığıyla yayılan interharmonikler, akıllı ölçüm sorunlarına, koruma cihazlarının devreye girmesine, güç kesintilerine ve devre kesiciler ile rölelerin yanlış çalışmasına neden olabilir. Bu nedenle, şebeke bağlantılı PV inverterlerden interharmonik emisyonlarının varlığının ortaya konması ve kontrol yapısının geliştirilmesi gerekmektedir.

Farklı tekniklerin, PV sisteminden elektrik şebekesine en yüksek miktarda güç aktarımını sağlamak amacıyla kullanılması bazı sonuçlarla birlikte gelmektedir. Güneş ışınımının değişken doğası ve kısmi gölgeleme sorunları, şebekeye enjekte edilen güç miktarını değiştirmektedir. Verimlilik ve maksimum güç hasadına odaklanmak son derece önemli olmakla birlikte, enjekte edilen akımda interharmoniklerin minimuma indirilmesi de zorunludur. Bazı maksimum güç noktası izleme (MPPT) teknikleri, inverterin DC-link voltajında perturbasyonlar uygulamaktadır. Geleneksel MPPT tekniklerinde, perturbasyonlar büyük ölçüde kontrolör parametrelerine ve şebeke senkronizasyon sürecine bağlıdır. Maksimum güç noktasının tahsisi sırasında DC-link voltajının değişken doğası, DC-link voltajından kaynaklanan frekans spektrumunda ek terimler oluşturur. Bu durum, şebeke frekansına dayanan senkronizasyon süreci ile etkileşime girerek, inverter kontrolörünün kontrol parametrelerine bağlı olarak değişen ve büyüklükleri dalgalanan modüle edilmiş interharmonikler yaratmaktadır.

Senkronizasyon süreci, elektrik şebekesi ile etkileşimi tanımlar; interharmonikler arasındaki mekânsal mesafe kontrolör parametrelerine bağlı olarak değişir ve modülasyon süreci, şebekeye senkronize edilmiş akımın sonucudur. Bu durumda, interharmoniklerin tespiti ve azaltılması süreci, interharmoniklerin frekans ve büyüklük değişimleri nedeniyle zorlu bir görev haline gelmektedir. Şebeke bağlantılı PV sistemlerinin yüksek penetrasyon seviyelerinde, interharmonik sorunları, bunların üretim mekanizması ve etkilerini azaltma yöntemleri üzerine yapılan araştırmalar hayati öneme sahiptir. Pratikte, harmonikler ve interharmonikler, bir sinyalin ne kadar bozulduğunu ölçen bir gösterge olarak kabul edilmektedir. Yüksek entegrasyon seviyelerinde, şebeke bağlantılı fotovoltaik sistemler (PVS), şebeke ağına enjekte edilen interharmoniklerin bir kaynağı olarak görülmektedir ve bu durum, birçok finansal ve teknik probleme yol açmaktadır. Interharmoniklerin kökenleri üzerine yapılan araştırmalar hala başlangıç aşamasındadır; literatürdeki boşlukları kapatmak ve bu sorunun özelliklerini ve azaltma tekniklerini haklı çıkarmak için daha fazla çalışma yapılmalıdır.

Bu zorluklarla başa çıkabilmek için, inverterin kontrol yapısı, ileri düzey güç elektroniği kontrolörlerinin kullanılması ve etkili bir kontrol yapısıyla maksimum güç noktası izleme tekniğinin iyileştirilmesi yoluyla etkin bir şekilde geliştirilebilir ve iyileştirilebilir. MPPT algoritmalarının, örneğin P&O, kontrol parametreleri ile interharmoniklerin üretim doğası arasında güçlü bir ilişki gözlemlenmiş ve tanımlanmıştır. Perturbasyon adım boyutunu ve örnekleme hızını kontrol etmek, izleme performansını ve verimliliği etkileyecektir. Ancak, bu kontrol parametrelerinin değerleri, frekanslarındaki değişimlerle birlikte yüksek büyüklükte interharmonikler üretebilmektedir. MPPT kontrol yapısı, üretilen interharmoniklerin azaltılmasını ve interharmonik emisyonlarının şebeke akımı üzerindeki etkilerinin azaltılmasını sağlamak için modifiye edilebilir. Interharmoniklerin araştırılması ve azaltma teknikleri, sistemin farklı çalışma koşullarındaki operasyonunu, özellikle düşük ışınım senaryolarında göz önünde bulundurmalıdır. Düşük güç çalışma koşullarında, örneğin düşük ışınım veya kısmi gölgeleme, enjekte edilen şebeke akımı bozulur ve interharmoniklerin büyüklükleri, mekânsal frekans dağılımının değişen frekans doğası ile artmaktadır. Bu nedenle, tam ve düşük güç çalışma koşulları altında araştırmalar yapılmalıdır. Ayrıca, akıllı inverterlerdeki yeni teknoloji, şebeke bağlantılı PV inverterinin şebekeye reaktif güç desteklemesini sağlar ve bu senaryoda, interharmoniklerin üretim özelliklerinin incelenmesi, sistemin şebeke dinamik desteği altındaki stabilitesini iyileştirebilir. Ayrıca, kontrol algoritmasının iyileştirilmesine yönelik araştırmalar, aktif ve reaktif güç desteği altında genişletilebilir.

Başarılı interharmonik tespiti için ilk adım, interharmoniklerin frekans mekânsal dağılımını matematiksel olarak belirlemektir. Bu, senkronizasyon sürecinden kaynaklanan modülasyon etkisini ve MPPT kontrol parametrelerinin etkisini dikkate alarak yapılabilir. Ayrıca, matematiksel ifadeler, MPPT algoritmalarının kontrol parametrelerini DC-link voltajı değişimi ile ilişkilendirebilir. Bu kriter altında, interharmoniklerin frekans spektrumu boyunca rastgele değişen doğası nedeniyle ana zorluk ortaya çıkabilir. Bir diğer önemli husus, çeşitli MPPT tekniklerinin ve bunların interharmoniklerin üretim özellikleri üzerindeki etkilerinin araştırılmasıdır. Tek fazlı ve üç fazlı şebeke bağlantılı PV sistemlerinin kontrol yapısında kullanılan farklı algoritmalar mevcuttur ve uygulanmaktadır. Özellikle tek fazlı inverterlerin geniş kapsamlı kullanımı, bunların kapsamlı bir şekilde incelenmesi yönündeki çabayı artırmaktadır. Interharmoniklerin doğası ve farklı normal ve anormal çalışma koşulları altındaki davranışları arasındaki karşılaştırma, tek fazlı şebeke bağlantılı PV inverterlerin kontrolünü geliştirmek ve kullanılan teknolojiyi iyileştirmek için destek sağlayacaktır.

Günlük olarak şebekeye bağlı PV inverter sayısındaki artışı dikkate aldığımızda, interharmonik emisyonu ağ boyunca artar ve daha büyük bozulmalara yol açarak, temel olarak sağlanan gücün kalitesini ve interharmoniklerin şebeke içinde dolaşımını etkiler. Önerilen interharmonik azaltma tekniği ve MPPT algoritmalarındaki iyileştirmelerin uygulanması, inverterlerin uzun ömürlerini garanti edecek, kayıpları minimize edecek ve verimliliği artıracaktır; aynı zamanda, şebeke entegrasyon standartlarına uygun olarak mümkün olan en düşük THD (Toplam Harmonik Distorsiyon) değerlerini sağlayacaktır. Önerilen geliştirilmiş inverter kontrol yapısı, şebeke bağlantılı PV sistemlerinin operasyonunu sağlarken, interharmonik emisyonunu şebekeye en aza indirecektir. Bu, elektrik şebekesine yüksek kaliteli aktif ve reaktif güç desteği sağlayacak ve çeşitli güç kalitesi sorunlarını ortadan kaldırarak, ortak bağlantı noktasında PV sisteminin genel performansını artıracaktır.

Bu tez, inverterlerin kontrol yapısı ve maksimum güç noktası izleme mimarisine odaklanarak, PV inverterler ile ilgili bağlantı standartlarını dikkate alırken, PV sisteminin güç kalitesini, verimliliğini ve güvenilirliğini maksimize etmeyi hedeflemektedir. Bu yaklaşım, şebekeye bağlı PV müşterisi ile elektrik şebekesi arasında yüksek kaliteli güç transferini sağlamak için geliştirilmiştir. Tez, şebeke bağlantılı PV sistemlerinin güç kalitesi sorunlarına dair araştırmalar sunmakta olup, özellikle tek fazlı sistemler üzerine yoğunlaşarak sistem performansını önemli ölçüde artıracak ileri düzey ve geliştirilmiş topolojik kontrol çözümleri önermektedir.

Bu tez, inverter kontrol sistemi aracılığıyla interharmonik emisyonlarının üretim özelliklerini ve mekanizmasını araştırmayı amaçlamaktadır. Ayrıca, interharmoniklerin üretimini etkileyen faktörler belirlenip analiz edilecektir. Enjekte edilen şebeke akımının frekans spektrumunda her bir bireysel interharmoniğin üretilen frekansını belirlemek için matematiksel ifadeler önerilecektir. MPPT kontrolör parametrelerini DC-link voltajı kontrolörü ve şebeke akımındaki modülasyon süreci üzerindeki interharmoniklerin üretimi ve enjeksiyonu ile ilişkilendirmek için matematiksel bir gelişim önerilecektir. Buna bağlı olarak, bu tez, çeşitli MPPT algoritmalarına uygulanabilen ve interharmonik üreten özelliklerini minimize ederken verimlilik ve izleme performansını maksimize eden bir interharmonik azaltma tekniği önerecektir. Önerilen yöntemleri doğrulamak için çeşitli önerilen azaltma tekniklerinin verimlilik, THD ve interharmonik emisyon değerleri açısından karşılaştırması sunulacaktır.

Bu bağlamda, tek fazlı şebeke bağlantılı PV inverter için çok işlevli geliştirilmiş bir kontrol yapısı önerilmektedir. Bu yapı, normal ve anormal çalışma koşullarındaki interharmonik üretim özelliklerini araştırmayı amaçlamaktadır; bu koşullar arasında şebeke voltajı düşüşü/şişmesi, şebeke frekansındaki sapmalar, düşük voltajlı sağlamlık (LVRT), aktif ve reaktif güç desteği, ve komponent yaşlanması nedeniyle DC-link kapasitansındaki değişiklikler yer almaktadır. Önerilen interharmonik azaltma tekniği ve modifiye edilmiş MPPT algoritmalarının etkinliğini doğrulamak amacıyla, düşük, tam ve dinamik güneş ışınımı koşullarında kapsamlı bir simülasyon tabanlı analiz gerçekleştirilmiştir.

Geliştirilen matematiksel modelleme ve farklı MPPT algoritmaları için önerilen interharmonik azaltma teknikleri, inverterin kontrol yapısını geliştirmek, şebeke akımının frekans spektrumundaki interharmonikleri azaltmak ve şebekeye enjekte edilen gücün kalitesini artırmak için iyi çözümler olarak değerlendirilmiştir.

ACKNOWLEDGEMENTS

First and foremost, I would like to express my great appreciation to my supervisor, Prof. Dr. Ahmet TEKE, for his patience, guidance, expertise, and assistance in completing this thesis. His scientific approach has allowed me to accomplish this research.

I owe my most profound appreciation to Assoc. Prof. Dr. Özgür Çelik for his constant support, ideas, inspiration, and guidance to beat all the challenges. His vast knowledge and vital recommendations have assisted me in completing this thesis.

In addition, I would like to extend my sincere appreciation to the members of the jury Assoc. Prof. Dr. Özgür Çelik, Asst. Prof. Dr. Oğuzhan TİMUR, Assoc. Prof. Dr. Murat Furat, and Asst. Prof. Dr. Kasım ZOR, for many generous and helpful suggestions.

I also would like to acknowledge the financial support of the Scientific Research Project Unit of Çukurova University(Project Number: FDK-2021-14048), which is gratefully appreciated.

I would like to thank my parents, Mahmoud and Nada, for being patient with me during all these years and for their constant support and caring.

I would like to express my appreciation and gratitude to my wife, Yasmeen, and my daughter, Emily, for their unwavering support and love.

To my friends in Adana, thank you for your continuous support and loving care during my stay in this beautiful city.

.

LIST OF TABLES

LIST OF FIGURES

LIST OF ABBREVIATIONS

AC	:	Alternating Current
CSI	:	Current Source Inverter
CT	:	Clarke Transformation
CV	:	Constant Voltage
DC	:	Direct Current
DER	:	Distributed Energy Recourses
DG	:	Distributed Generation
DSP	:	Digital Signal Processor
FP	:	Full-Power
GW	:	Giga Watt
HF	:	High Frequency
ICC	:	Indirect Current Control
IEA	:	International Energy Agency
IEC	:	International Electrotechnical Commission
IEE	:	Institution of Electrical Engineers
IEEE	:	The Institute of Electrical and Electronic Engineers
IET	:	The Institution of Engineering and Technology
InCon	:	Incremental Conductance
LP	:	Low-Power
LPF	:	Low Pass Filter
LVRT	:	Low-Voltage Ride-Through
MInCon	:	Hybrid Random Modified Incremental Conductance
MInCon-f	:	Modified Incremental Conductance -Frequency
MInCon-v	:	Modified Incremental Conductance -Voltage
MP&O	:	Hybrid Random Modified Perturb and Observe
MP&O-f	:	Modified Perturb and Observe-Frequency
MP&O-v	:	Modified Perturb and Observe-Voltage
MPPT	:	Maximum Power Point Tracking
MSE	:	Mean Square Error
MW	:	Miga Watt
NN	:	Neural Network
P&O	:	Perturb and Observe
PCC	:	Point of Common Coupling
PD	:	Proportional-Derivative

PI	:	Proportional-Integral
PID	:	Proportional-Integral-Derivative
PLL	:	Phase Lock Loop
PQ	:	Power Quality
PR	:	Proportional Resonant
PSO	:	Particle Swarm Optimization
PV	:	Photovoltaic
PVS	:	Photovoltaic Systems
PWM	:	Pulse Width Modulation
REF	:	Reference
RMS	:	Root Mean Square
RP	:	Rated-Power
SPWM	:	Sinusoidal Pulse Width Modulation
SRF	:	Synchronous Reference Frame
THD	:	Total Harmonic Distortion
VSI	:	Voltage Source Inverter
d	:	Direct
q	:	Quadrature

1. INTRODUCTION

This chapter introduces the thesis research methodology. Firstly, an overview of PV systems and the importance of renewable energy resources are presented. The importance of PQ in renewable energy generating systems is discussed with more emphasis on grid-connected PV systems. Secondly, detailed information about the categories of different PQ issues, including the waveform events, is introduced. The technical and economic challenges that face the high level of grid-connected PV integration are depicted in detail. Further, the PQ requirements for each level through the electrical network are provided. At the end of this chapter, the scope of this research, the thesis objectives, the thesis contributions, and the organization of this thesis are given.

1.1. Background and Motivation

Electrical energy is considered the backbone of industry and manufacturing. The continuous rise in electricity demands increases the importance of investigating more reliable and cost-effective generating systems, which drive the force toward renewable and sustainable sources of energy (Sinsel, Riemke, and Hoffmann 2020). According to several studies (Alaaeddin et al. 2019; Choudhary and Srivastava 2019; Dogga and Pathak 2019; Hernández-Callejo, Gallardo-Saavedra, and Alonso-Gómez 2019; Shubbak 2019; Sinsel et al. 2020; Srivastava, Tiwari, and Giri 2020), solar energy is considered as one of the most promising energy sources toward fulfill the raising electricity demand, which will be increased by 48% in the coming 25 years (Srivastava et al. 2020). For instance, photovoltaic systems (PVS) are the technology responsible for converting solar energy to usable electrical energy by utilizing photovoltaic panels that convert the incident sunlight into electricity.

Following the decreasing cost of PV systems, several studies have shown that in the oncoming years and around 2022 -2025, the price of electricity generation by solar PV systems will be competitively compared with the conventional generating systems (Srivastava et al. 2020). With not only mentioning the current PV systems lower production, operational, and maintenance costs along with the high reliability and availability but also promoting this technology for further advancements and investigations, and therefore, to become one of the most promising renewable generating systems (Alaaeddin et al. 2019). It can be predicted that the penetration level of PVS, which includes the grid-connected PVS, is expected to increase. The advances in power electronics and storage systems drive the forces toward extensive integration of this technology in the near future.

For instance, Figure 1.1 depicts the global capacity additions of PVS installed worldwide, implementing more than 507 GW of installed solar power in 2023, which is almost 50% higher than in 2022 (IEA 2023). Among this vast power share, Turkey occupied 12th place with more than 3.2% share of PVS with respect to the total worldwide installed power capacity, with expectations to increase soon. Countries like Japan and China lead the market share with more than 50% of PVS share with an installed capacity of 131 GW, followed by European countries with more than 28% of the total global shares. Many countries have set ambitious target goals. Denmark, where the sunshine is even limited, is targeting 100% of installed renewable energy systems by 2035.

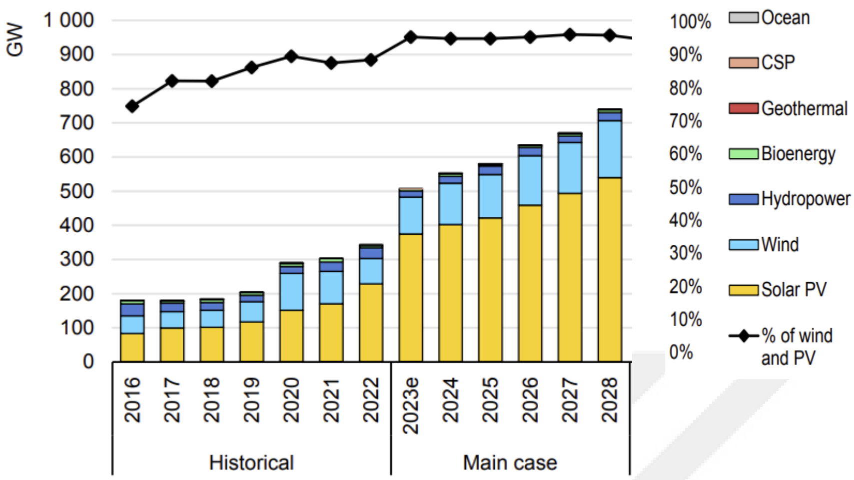

Figure 1.1. Global growth of cumulative PV capacity in GW (IEA 2023)

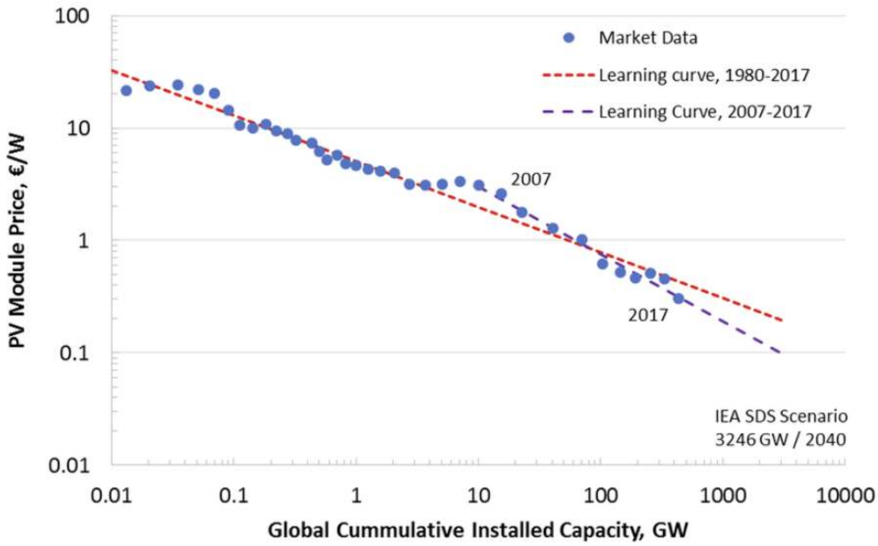

Figure 1.2. Cost reduction trend in PV modules versus the global cumulative installed PV systems capacity in GW (Taylor and Jäger-Waldau 2019)

In this context, another essential point is the cost; the continuous reduction of PVS capital cost per kWh is noticeable in the last seven years (Yang et al. 2019). Figure 1.2 indicates the cost of a PV module in euros per watt, which indicates that more than 90% reduction in the total cost will be achieved by 2040. Therefore, it is evident that the total installed capacity is increasing worldwide, especially for PV energy systems. However, the enormous additions of these Gigawatts should be followed by the technical implementation barriers, which should be addressed in the various PVS applications.

The last discussion leads to the importance of the appropriate adoption and integration of PV systems, with more attention on grid-connected PVS. However, increasing the integration level comes with its cost. The adverse side effects of high penetration levels of PVS could be characterized by reliability issues, availability, and power quality, which may affect both the end-users or consumers and the operators of distribution systems. These problems could be propagated further to the higher levels, such as the transmission network. There are many active codes, standards, and requirements for successful grid integration, and they are continuously updated to adopt the continuous change in the total capacity to enhance the overall performance. This will require not only improvement in the field of power electronics, which is the key, but also the control strategies applied for every specific application. These standards are usually applied to three-phase grid-connected systems with medium and higher voltage levels to address utility grid stability issues. However, most of the efforts and concerns have been driven toward islanding protection and maximum power generation in low-voltage networks.

Therefore, more investigations should be carried out to assess the impacts of the grid-connected PV converters, and not only for three-phase systems, which will enhance the penetration levels and PQ in the residential sectors. The low-voltage network-level corporate converter-based issues and abnormalities, which are strongly related to power quality and the associated faults, either from the grid or converter side. Table 1.1 depicts some of these integration concerns with respect to the system's level (Yang et al. 2019). Power quality is one of the main concerns at the first level; the direct connection with PV converters at the local distribution level may negatively impact the local distribution grid and challenge the grid's power quality standards. One of the main issues in the power quality field is the harmonics and interharmonics generation and emission due to power electronics switching and perturbations at the converter level (Ravindran, Busatto, et al. 2019; Sangwongwanich et al. 2017a, 2018a). These additive frequency components will not only affect the distribution grid by interrupting the power protection devices but also will result in power quality issues through the injected grid current, which contains the interharmonics current. Moreover, power interruptions may lead to isolating the PV inverter from the grid (Nduka and Pal 2017; Ravindran, Busatto, et al. 2019; Sangwongwanich et al. 2017a, 2018a; Sangwongwanich and Blaabjerg 2019; Žnidarec et al. 2019).

Table 1.1. PV requirements throughout different levels of the network.

Systems level (vVoltage).	Grid-connected PVS specifications and requirements
PV modules and Converter levels	Cost, power optimization, efficiency, power quality, voltage sag/swell, anti-islanding, reliability, power controllability, etc.
Distribution network level	Power flow, network local stability (V&F), etc.
Transmission network level	Utility grid stability, faults analysis, reactive power, power quality, etc.

The massive use, and sometimes the irresponsible one, of power electronics devices, inverters in PVS, and time-varying loads has led to so-called power quality (PQ) issues, the distortion of the current and voltage waveforms, or the deviations of their frequencies and amplitudes. Back then, PQ problems were not considered serious issues for grid-connected PVS. However, the recent advancement in power electronics, e.g., inverters and switch mode power supplies, added more sophisticated loads that cannot bear the effects of a significant disturbance caused by power quality issues. Even the new protection systems could be interrupted by a distorted waveform.

There are three main types of major events regarding PQ, which are (Jain 2014):

1. Waveform events.
2. Voltage events.
3. Frequency events.

Figure 1.3 depicts the classifications of each type according to each major event. Frequency events are infrequent; hence, the main frequency of the grid is directly associated with the rotational speed of the electrical generator. However, voltage events are considered as the voltage deviation from its nominal value, which is more likely to happen. The deviation of the voltage and current waveforms from their regular sinusoidal shapes is considered a waveform event. It could happen in a steady state or at transient periods related to the system dynamics, as indicated in Figure 1.3.

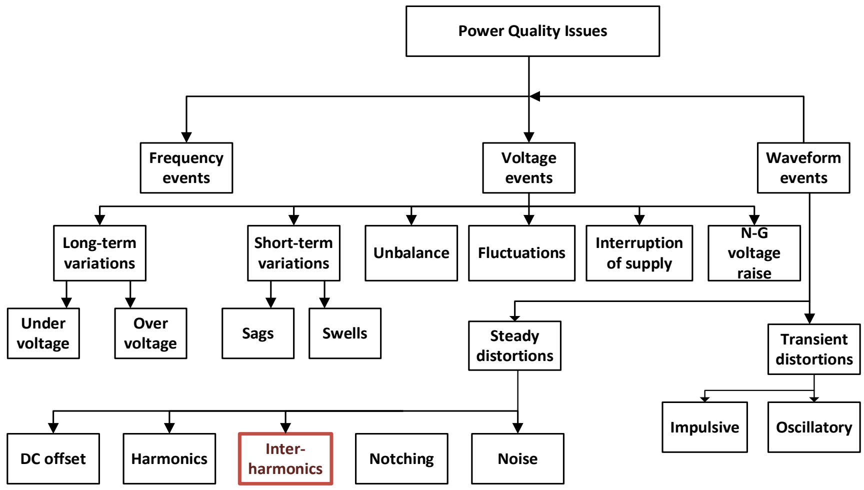

Figure 1.3. Classifications of PQ issues based on the type of waveform event

Waveform events are classified into two main categories: steady state and transient distortions. The latter has two forms: impulsive and oscillatory disturbances. In the steady-state distortion case, five main events can happen, which are: DC offset, harmonics, interharmonics, notching, and noise. This work is devoted to dealing with one of the waveform events that causes steady-state distortion, namely interharmonics.

Interharmonics and harmonics are considered one of the main challenges in the field of power quality and a source of significant disturbances. They are similar in their conceptional description but different in their frequency characteristic. Interharmonics distortion happens due to the existence of additional frequency components within the voltage or the current waveform, which are non-integer multiples of the main or fundamental frequency component. On the other hand, harmonics are the additional frequency components, which are integer multiples of the main frequency component (Testa et al. 2007). Usually, harmonic distortion is periodic, e.g., each cycle is repetitive with the same shape. In the case of interharmonics, the waveform distortion changes from one cycle to another. Therefore, their detection in practice is a challenging process (Karimi-Ghartemani and Iravani 2005). In PV systems, harmonics are generated by the non-ideal switching of the power converters and the interaction of different controllers, i.e., voltage and current control loops, and methods to mitigate them are found in the literature (Du et al. 2013, 2015). The literature discussed the effects of harmonics in power systems and its measurement techniques (Fekete, Klaic, and Majdandzic 2012; Menti, Zacharias, and Milias-Argitis 2011; Montoya et al. 2019; de Oliveira et al. 2021; Oliveira, Filho, and Cormane 2019; Yu et al. 2020). Nevertheless, the research work on interharmonics is still premature, and more investigations should be carried out to bridge the gaps in the literature on mitigation techniques.

Interharmonics emerge as a result of several influencing factors. For instance, the presence of time-varying or non-linear loads plays a substantial role in the generation of harmonics and interharmonics. Moreover, recent research (Roberto Langella et al. 2016; Sangwongwanich et al. 2018b) highlights that grid-connected photovoltaic systems (PVS), particularly PV inverters, are also significant contributors to interharmonics generation. Few research works have demonstrated the generational nature of interharmonics while trying to reveal its origin. Different studies have shown various sources of interharmonics. The authors (Roberto Langella et al. 2016; Sangwongwanich et al. 2018b) proposed that interharmonics are presented due to perturbations of the maximum power point tracking algorithm during the maximum power point searching process. Furthermore, it has been shown that its origin may belong to the perturbation of the DC-link voltage. Hence, the main absolute reason behind interharmonics is still under research. Therefore, this work will focus on this issue while trying to model the actual disturbance phenomena and discuss the possible mitigation solutions extensively.

1.2. Scope of the Thesis

This thesis will focus on analyzing the previous research findings related to interharmonics generation from grid-connected PV systems. The specific gaps in the literature will be addressed, and practical solutions will be proposed to address those issues. Following the thesis objectives, the current control algorithms of the single-phase grid-connected inverter will be investigated and developed. The interharmonics generating characteristic from a single-phase grid-connected PV system will be simulated on string single-stage single-phase grid-connected PVS. A simulation model for the system will be developed and simulated using MATLAB-SIMULINK software. The designed model will follow the thesis objectives and be used to simulate and validate the proposed control algorithms, which aim to mitigate interharmonics under different operating power conditions and with the developed multimission case studies integrated into the control system.

1.3. Thesis Objectives

The main objective of this thesis is to investigate the operation of grid-connected photovoltaic systems for interharmonics distortion effects under different operating and multimission conditions. In addition, this thesis proposes diagnostic tools and mathematical expressions for the injected interharmonics in single-phase grid-connected photovoltaic systems. The particular objectives in this thesis are summarized as the following:

- Conduct a complete literature survey on interharmonics issues related to single-phase grid-connected photovoltaic systems.

- Investigate the interharmonics generation process, the emission mechanism through the system control loops, and the effects on the injected current to the grid; the results will be compared to the findings of the literature.
- Investigate the various control structures of the single-phase grid-connected PV inverter. This step includes the development of the control structure and the overall model that will be used to analyze the proposed interharmonics mitigation techniques.
- Investigate the effects of different MPPT algorithms and and the control parameters on the generation characteristics of interharmonics, as well as their frequency distribution and magnitudes.
- Develop mathematical expressions that relate the variations of the interharmonics frequency distribution to the control parameters of various MPPT algorithms. These analytical expressions can be used to mimic the DC-link voltage error and the propagated interharmonics through the outer control loop.
- Develop a mathematical equation that specifies the frequency separation between each interharmonic and relates their spatial variation to the control parameters of the MPPT algorithms for the DC-link voltage error and the injected current into the grid.
- Propose a mathematical-based interharmonics mitigation technique based on modifying the control parameters of the MPPT algorithms and, thus, proposing modifications to the MPPT algorithms to minimize the magnitudes of the frequency-varying interharmonics in the inject grid current at the point of common coupling. The proposed MPPT algorithms will ensure that the system delivers the maximum power to the grid with the maximum tracking efficiency and minimum THD.
- Conduct a simulation analysis for the developed single-phase grid-connected photovoltaic system under different power operating conditions, including the system's dynamical response under various irradiance values for the proposed interharmonics mitigation technique. In addition, a multimission analysis is considered to investigate the

developed system under grid abnormalities, including dynamic grid support, LVRT, grid frequency variation, and DC-link capacitance aging effect.

- Investigate the dependency between the injected power and the characteristics of interharmonics in terms of their magnitudes and frequency allocation.
- It is planned to meet the international grid integration standards for the THD (IEC 61727, IEE1547, IEC 61727, and VDE 0126-1-1) while minimizing the interharmonics emission.

1.4. Contribution of the Thesis

The grid-connected PV systems have been reported as a source of interharmonics. The research contributions in this regard are still premature, and more extensive studies are still needed to address this problem comprehensively. This thesis investigates the possible enhancement techniques for the control structure of a single-phase grid-connected PV system to mitigate interharmonics emissions with the proposed modifications to the MPPT algorithms. The proposed mitigation techniques will be investigated, compared, and evaluated based on the inverter control structures, tracking efficiencies, power quality performance, and grid integration requirements. Therefore, it is an open subject of improvement for present and future grid integration with many research scopes.

The original contributions of the current research are summarized as the following:

- The main origin behind interharmonics is still under research; this thesis is devoted to discussing this issue, confirming the previous findings, and contributing to the literature in terms of confirming the power dependency from the input irradiance and the interharmonics emission.
- Propose a mathematical-based modified MPPT algorithm that enhances the inverter's control structure. The proposed MPPT algorithms will be based on modifications to the parameters that control the overall performance of the MPPT algorithm.
- Propose mathematical expressions to specify the frequency allocation under the frequency-varying characteristics of each interharmonic in the frequency spectrum of the injected grid current, which depends on the MPPT parameters.
- Propose mathematical expressions that relate the DC-link voltage to the control parameters of the MPPT algorithms. This will assist the process of mathematically modeling the

interharmonics generated from the DC-link control loop and propagated to the inner current control structure.

- A comparison between the proposed MPPT methods and the existing algorithms in the literature will be presented. This comparison will focus on confirming the proposed methods to fulfill the standard grid integration codes and minimize the THD while maximizing the MPPT efficiency.
- Investigate the interharmonics generating characteristics under dynamic grid support, LVRT, grid frequency deviation, and capacitance aging effects. Different proposed MPPT algorithms will be compared under different power operating conditions.
- This work will contribute to the current research by publishing articles in SCI journals.

With these contributions mentioned above, a significant enhancement to the control structure of the grid-connected PVS will be achieved. This is mainly characterized by improving the quality of power being injected into the grid.

1.5. Organization of the Thesis

The organization of the thesis is as follows:

Chapter 1: Introduction

This chapter introduces the importance of investigating the high-level penetration of grid-connected PV systems and the impact of increasing the total installed PVS capacity on the power quality. Also, the research objectives, the contributions of this thesis, and the organization of the thesis are given.

Chapter 2: Literature Review On Interharmonics Generation from Grid PV Systems

This chapter presents extensive and comparative investigations about the generating characteristics of interharmonics, their mechanism of emission, and their PQ impact on grid-connected PV systems.

Chapter 3: Fundamentals of Grid-Connected PV Systems

This chapter depicts the fundamentals of grid-connected PV systems, the topologies of PV systems, and their configurations. In addition, it emphasizes the control topologies of single-phase grid-connected inverters and their structures. The chapter also presents the various types of MPPT algorithms, some of their techniques, and their relations to interharmonic.

Chapter 4: Interharmonics from Single-Phase Grid-Connected PV Systems

This chapter investigates and analyses the generating characteristics of interharmonics and the propagation mechanism through the inverter control structure. This chapter also discusses the impact of the MPPT algorithms' control parameters on the magnitudes and the frequency separation of interharmonics. Mathematical expressions are proposed to specify the frequency allocation of each interharmonic in the frequency spectra for the DC-link voltage error and the injected grid current to the grid. The proposed mitigation methods of interharmonics are presented and compared under different power operating conditions. In addition, a mathematical development is proposed to relate the DC-link voltage characteristic to the control parameters of the MPPT algorithms. The performances of the proposed techniques are compared based on emission levels of interharmonics, the tracking efficiencies of the MPPT algorithms, and their THD for different case studies. The developed equations are used to construct the DC-link voltage control loop and the current control structure to investigate the generated interharmonics in the frequency spectra.

Chapter 5: Investigations of Interharmonics Emissions under Different Operating Conditions

This chapter extends the proposed mitigation technique of interharmonics for the enhanced control structure of various MPPT algorithms under different operating conditions. This analysis includes comparing six proposed modified MPPT algorithms, the developed neural network-based MPPT algorithm, and the conventional methods. The dynamical response performance under different irradiances is investigated for the proposed MPPT technique. A multimission analysis is presented for the developed model under dynamic grid support, LVRT, grid frequency deviation, and the variation of DC-link capacitance. A PLL-based voltage sag/swell detection algorithm is employed in the developed model for active and reactive power support.

Chapter 6: Conclusions and Future Work

This chapter summarizes the main contributions and highlights several concluding remarks. In addition, the future research perspectives and directions are discussed.

The organization of the thesis is depicted in Figure 1.4.

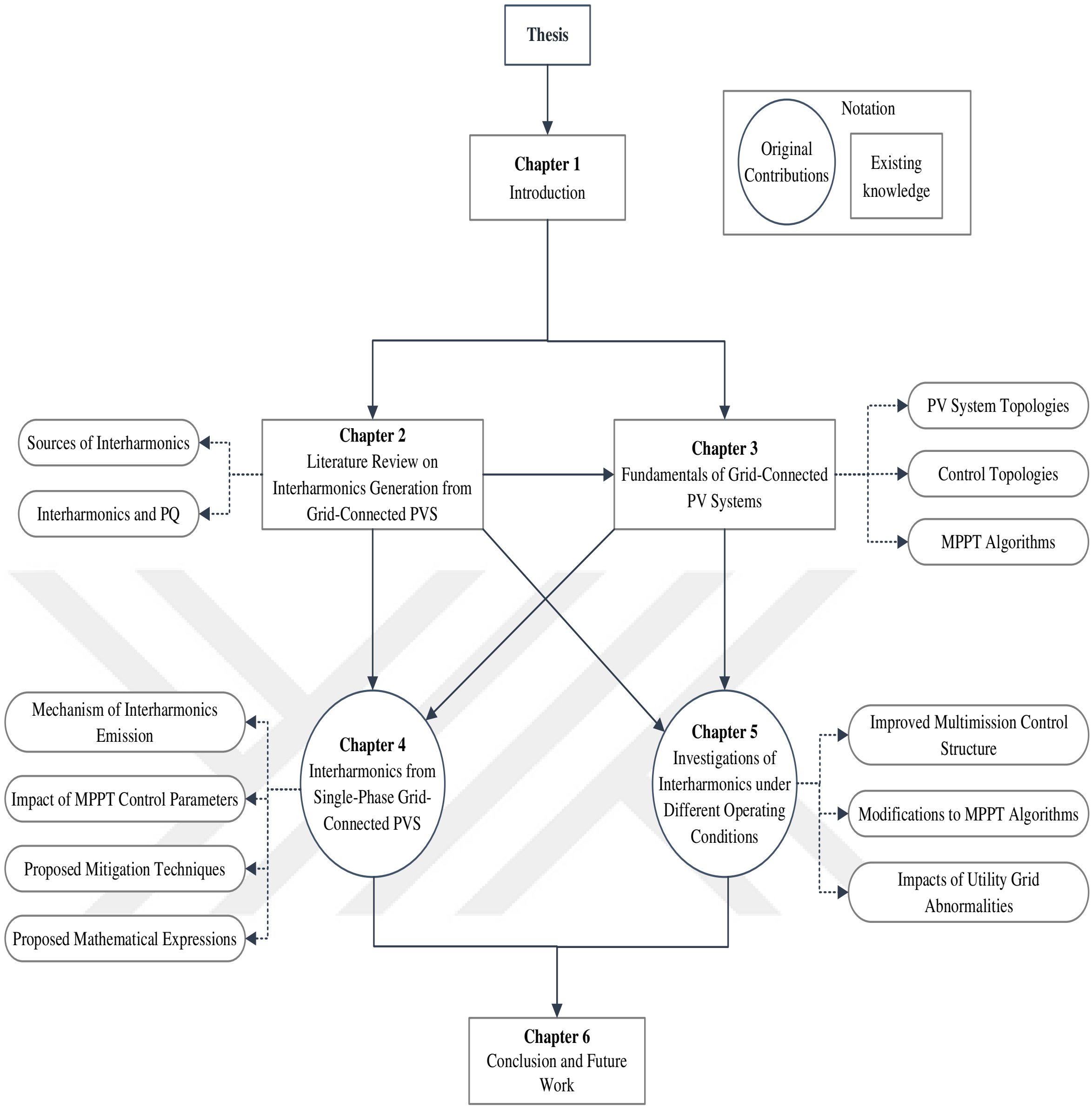

Figure 1.4. The organization of the thesis

2. LITERATURE REVIEW ON INTERHARMONICS GENERATION FROM GRID-CONNECTED PV SYSTEMS

2.1. Introduction

The rapid growth of renewable energy technologies, including photovoltaic systems, has a significant impact on the existing infrastructure of the conventional grid's power quality (Ravindran, Rönnberg, and Bollen 2019). Distributed generating systems, especially with variable output power, such as photovoltaic systems, have a wide application on grid-connected PV systems. Due to the continuous decrease in price and the development of this technology, high penetration has started to be encountered, especially for single-phase grid-connected PV systems. This interface requires power electronic components or, more specifically, PV inverters that will affect the existing conventional network at the point of common coupling and challenge its power quality (Blaabjerg et al. 2017; Katiraei and Agüero 2011; Katiraei, Mauch, and Dignard-Bailey 2007; Li 2018; Oliva and Balda 2003). The literature reported many studies indicating that some of the main arising issues are harmonics and interharmonics delivered to the grid (Enslin and Heskes 2004; Gallo et al. 2013; Infield et al. 2004; Messo et al. 2014; Ravindran, Rönnberg, et al. 2019; Varma et al. 2016; Yang, Zhou, and Blaabjerg 2016). The extraordinary growth in this sector raises the importance of investigating their impact on the PQ of the conventional grid.

Interharmonics are attributed to many reasons (Testa et al. 2007), e.g., time-varying or non-linear loads (Beites et al. 2001), motor drives in double asynchronous conversion systems (De Rosa et al. 2005), and mechanical vibrations, e.g., wind turbines (Vilar, Usaola, and Amarís 2003) have contributed significantly to the generation of interharmonics. However, grid-connected PV systems are usually not considered as a source of interharmonics. The first work has been done regarding interharmonics and the attributes behind them is conducted in (Djokic et al. 2015). In addition, some attempts have been conducted to mitigate (Sangwongwanich et al. 2017b, 2018b) and investigate (R. Langella et al. 2016; Roberto Langella et al. 2016) the interharmonics in PVS. The literature reported that the MPPT algorithms are responsible for generating interharmonics. However, obtaining the commercial inverter's control parameters is sometimes tricky. However, mapping the interharmonics frequencies to the control parameters of various MPPT algorithms is possible. The origins of interharmonics and their characteristics need to be explored more, and research on their mitigation methods is still premature.

This chapter will first introduce a review of the general power quality issues and emphasize the impacts of interharmonics on the power quality of the delivered current to the grid. The following section will review the interharmonics emission in PV systems under dynamic grid support. Finally, the last section will demonstrate a summary of the presented literature.

2.2. Power Quality Issues from Grid-Connected PVS with Impact of Interharmonics

The classifications of power quality issues are presented in the first chapter. Three main types of major events are directly related to power quality concerns. This section will review the recent advances and issues faced in this regard related to grid-connected PV systems.

The authors (Santhoshi, Sundaram, and Padmanaban 2019) presented an overview of the current challenges that grid-connected PV systems confront. In addition, the concepts of ancillary services and reactive power injection are also presented. The authors highlighted the inverters' topologies, synchronization methods, grid requirements, and standards for successfully integrating the PV systems into the electric network. Consequently, the authors (Singh, Goyal, and Siddiqui 2019) emphasized the current issues and the impact of PV systems integration on the grid. Hence, residential sectors widely adopt this technology, and the integration into the grid will be highly employed at this level. Accordingly, this rapid rise of adaptation will stress the electrical utility grid. In other words, if the utility grid is not monitored, then many grid-connected PV systems will negatively impact the grid's power quality. Furthermore, if this source of power is not dispatchable, then it will be hard to control the power as well as the effects under large penetration of grid-connected PV systems.

The impacts of PV systems on the utility grid can be summarized into the following points:

1. Impact on voltage stability: several studies have shown that the most important technical problem is the voltage stability at the distribution level. It could be the effect of transient cloud coverage; the transformer at the distribution level will not be able to change the voltage instantaneously, thus resulting in voltage variation. In addition, the distance between the feeder and the PV system at the distribution level should be minimized and optimally allocated. It is suggested that a large-scale PV system be investigated to determine how voltage profiles are affected under uncertain conditions such as cloud coverage, irradiance, and temperature variations (Singh et al. 2019).
2. Impact on frequency stability: In literature, there is an argument about the effect of high penetration of PV systems on grid frequency stability. The authors (Abdlrahem, Venayagamoorthy, and Corzine 2013) simulated a 200 MW grid-connected PV system formed by four 50MW subsystems. It has been stated that the frequency stability is not drastically affected by the grid integration level of the PV systems. However, the authors (Silva, Lopez-Botet-Zulueta, and Wang 2016) concluded a noteworthy effect.
3. Impact on active power generation: This effect is characterized by the various available algorithms to track the MPP of the PV systems. The system will be utilizing the MPPT algorithms under different operating conditions. However, the utility grid performance will negatively deviate under different uncertainty conditions, such as transient cloud coverage,

e.g., power mismatch and economic dispatch. In addition, the system will experience high levels of power ramp (Guerrero-Lemus et al. 2015).

4. Impact on dynamic grid support: The grid-connected PV inverter should support the control function of reactive power and LVRT (Ellis et al. 2012). However, it is not required by IEEE-1547 standards for grid-connected PVS. In some recent inverter technologies, the PQ control has not been integrated into the control system, even with the latest advancements. On the other hand, the authors (Liu et al. 2008) argued that an inverter under high penetration levels could replace a capacitor bank connected to a feeder for reactive power compensation.
5. Impact on equipment loading, voltage regulation devices, and power losses: The literature reported that grid-connected PV systems can reduce the various losses associated with the utility grid.
6. Impacts on Harmonics and Interharmonics: Hence, the main focus of this thesis is the study of interharmonics issues from single-phase grid-connected PV systems; the following discussion will emphasize this issue and will review the research conducted in this manner.

Recent studies (Roberto Langella et al. 2016; Ravindran, Busatto, et al. 2019; Sangwongwanich et al. 2017b, 2018b) indicated that the grid-connected PV inverters may contribute to the generation and emissions of interharmonics, which results in flickering and overloading. The presence of harmonics and interharmonics in the injected grid current spectrum could lead to undesirable outcomes. It can result in damage to the power electronic devices, impose thermal stress, shorten the lifespan of rotating electrical machines, increase electromagnetic interference, and in the most severe cases and under high penetrations, it may trip the protection devices and isolate the PV inverter (Jithin et al. 2023), which could affect the system stability and the overall performance of the systems (Chicco, Schlabbach, and Spertino 2009). The environmental factors, such as the varying temperature and irradiance, along with the use of power converters, such as inverters with their nonlinear characteristics, will lead to the distortion of utility grid current and imposing harmonics and interharmonics in the current and voltage signals (Elvira-Ortiz et al. 2019). Harmonics and interharmonics will lead to many undesirable outcomes, such as sub-synchronous harmonics oscillation during the paralleling operation of inverters, unstable operation of PLL and inaccurate measurements, and amplification of interharmonics emissions around the resonant frequency. Many codes and standards have been employed to cope with these issues, such as EN 50160 and IEEE 519-2014 (Elvira-Ortiz et al. 2019). However, these codes do not impose any limitation on the emissions of interharmonics.

Nevertheless, the EN 50160 code limits the interharmonics to flicker values. More investigations should be carried out on the analysis of interharmonics to assist the higher penetration of grid-connected PV systems. The literature briefly discusses this issue, as depicted in Table 2.1.

Table 2.1. Latest research work done to investigate interharmonics generation

Reference	Topology	Rated power	System Voltage	THD	Efficiency
(Sangwongwanich et al. 2017b)	Single-stage with LCL-filter, Transformerless	3KW	450V	-	-
(Sangwongwanich et al. 2018b)	Single-stage, H4 with LC-filter	3KW	440-460V	-	-
(Ravindran, Busatto, et al. 2019)	Single-stage, Transformerless, H4	4.6KW	647-663V	<3%	-
(Sangwongwanich and Blaabjerg 2019)	Single-stage, H4	3KW	395-420V	-	<97.5%
(Roberto Langella et al. 2016)	LF-transformer and transformerless	4.6KW	388-392V	<5%	-

The authors (Sangwongwanich and Blaabjerg 2019) illustrated that during the MPP searching process and due to the variation at the DC-link voltage, additional frequency components are generated and propagated to the current controller. A conclusion has been made that the interharmonics can be generated from grid-connected PV systems. The significance of investigating these challenges faced with interharmonics emissions is presented in (Ravindran, Rönnberg, et al. 2019), which can be summarized with the time-varying characteristic of low-frequency components of interharmonics around the fundamental and the second components. Also, the intermodulation process and interaction of interharmonics with the harmonics themselves and the fundamental frequency component create high and low nonstationary interharmonics. In addition, the dependency of interharmonics on the MPPT sampling rate and the voltage perturbations under different solar irradiance operating conditions. It is mentioned by (Ravindran, Rönnberg, et al. 2019) that interharmonics emission increases particularly at low power operating levels, making this process of detecting these nonstationary interharmonics more challenging. However, other studies show that interharmonics generation is independent of the operating power conditions (Roberto Langella et al. 2016; Ravindran, Busatto, et al. 2019; Sangwongwanich et al. 2017b, 2018b). Furthermore, the frequency distribution for interharmonics consists of varying frequency components that are noninteger multiples of the fundamental frequency, which challenge the detection process, especially with the grid frequency deviation.

The authors (Elvira-Ortiz et al. 2019) conducted a study on the calculation of harmonics and interharmonics distortion levels for a grid-connected PVS. They developed an MLR model that estimates the distortion of the voltage signal injected by the inverter to the grid. The authors showed a relation between harmonic distortion and variations in temperature and irradiances. The authors (Ravindran, Rönnberg, et al. 2019) presented a summary of the research work that focused on the interharmonics issue, and they provided significant guidelines and considerations for investigating interharmonics emission in grid-connected PVS. The authors indicated that the detected level of interharmonics emissions from grid-connected PVS depends on the applied analysis method. Therefore, special attention should be paid to choosing the most appropriate analysis technique that yields the best estimation of interharmonics. The authors highlighted the impacts of the MPPT algorithms control parameters on the generating mechanism of interharmonics. The authors suggest finding a correct estimation of the sampling rate of the MPPT under different operating irradiances and DC-link voltage perturbation conditions.

In (Anurangi, Rodrigo, and Jayatunga 2018), the authors investigated the effects of harmonics on the low voltage distribution networks incorporating multiple 2kW grid-connected PV systems. The authors in this study determined the total harmonic distortion and the impact of integrating more grid-connected PV systems at the distribution level. The study showed that the location at which the PV system is installed, the control strategy of the inverter, the inverter loading, and the transmission line impedance are the main influencing factors affecting the injected grid current and the voltage at the PCC. The authors (Du and Lu 2018) investigated the effects of the total harmonic distortion on the injected grid-connected PV inverter's current. This paper considered the voltage change and the ripples across the decoupling capacitor. Analytical expressions are developed to calculate the harmonics' amplitude by modeling the time-varying DC-link voltage variations.

In (Etier et al. 2016), the impact of integrating a 150 kW large-scale grid-connected PV system is investigated. This research work investigated two case studies, operating the system in a standalone scenario, while the second case involved integrating the PV system into the grid. The current harmonic distortion obtained in the first case was 4.7%. However, the second case included the effects of temperature and irradiance variation, and the THD obtained in this case was 13%. This research shows the impact of the high penetration level of grid-connected PV systems on PQ.

Consequently, the authors (Pinto et al. 2016) investigated the effect of a rural 3.6 kW grid-connected PV system on the power quality at the PCC. This research investigated the reasons behind the undesirable inverter operating characteristics and the disconnections during the inverter operation. This study focused on the utility grid's voltage, frequency, and harmonic variations. This study also considered the changes to the system after some modifications to the distribution grid at PCC made by the electrical utility company. It is worth mentioning that during sunny hours and whenever the inverter is connected to the grid, the voltage is raised at the connection point.

2.3. Interharmonics from Grid-Connected PV systems

A few recent studies have been found in the literature that investigated the interharmonics generation from grid-connected PV systems. The first work conducted to outline the expected attributes of interharmonics is presented in (Roberto Langella et al. 2016). The same authors investigated the harmonics and interharmonics generation of grid-connected PV systems from the control perspective and the reasons behind interharmonics, emphasizing the MPPT algorithm and the DC-link voltage variations. According to the literature, this is the first work stating that the MPPT is responsible for the generation and emissions of interharmonics. This research was an extension of the work that has been done by (Djokic et al. 2015).

The literature reported a recent study (Sangwongwanich et al. 2017b) that attempted to analyze interharmonics and investigate their mitigation methods. The authors indicated that the MPPT algorithm is operated with stable movements between several optimal points. However, the injected grid current is highly distorted under the case of 5% of the rated power and contains higher contents of interharmonics. This behavior was explained by the resulting DC-link voltage controller error, which contains some frequency components that propagate through the PI controller of the DC-link voltage and then modulated with the grid phase angle to be injected into the utility grid. This study shows a sort of power dependency regarding interharmonics generation; hence, at low-power operating conditions, the peaks of interharmonics are almost doubled in the frequency range between 0 and 150 Hz. However, the same authors (Sangwongwanich et al. 2018a) indicated that the interharmonics generation is almost identical for low and rated power operating conditions.

The literature reported a recent attempt to modify the grid-connected PVS's control structure, aiming to mitigate and reduce the effects of interharmonics. The authors (Sangwongwanich et al. 2017b) proposed solutions to improve the DC-link voltage control loop. Under this situation, the MPPT algorithm imposes a step change at the beginning of the search process. Besides, the DC-link voltage controller responds quickly to those changes and in a step manner. Therefore, the PI controller encounters a fast transient response in the conventional control structure.

Nevertheless, the proportional coefficient of the PI controller could be reduced, and the abrupt change in the grid current could be decreased. However, this will mainly affect the perturbation rate of the MPPT; hence, this rate depends on the settling time, which will be reduced to alleviate this problem. Therefore, other methods should be implemented while maintaining the tracking efficiency of the MPPT algorithms and operating principles. As proposed by the authors, some of these methods include the use of adaptive gain for the voltage controller; the second method is characterized by utilizing a rate limiter or notch filter for the DC-link voltage controller. A third method is the utilization of the constant voltage (CV) MPPT method. However, the MPPT tracking efficiency should be investigated with these methods. The authors reported mainly simulation and some experimental results, showing that the CV MPPT method is the best candidate for reducing the emissions of interharmonics to the grid.

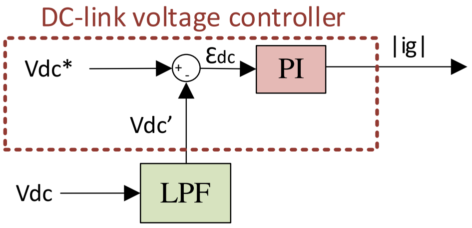

Figure 2.1. The DC-link outer control loop

For the adaptive gain mitigation technique, which is related to the DC-link voltage controller, and, as mentioned before, the DC-link voltage should reach a steady state value before the next perturbation of the MPP and therefore, the settling time will determine the MPPT perturbation rating. The slow response could be eliminated by changing the proportional gain in an adaptive way (PI controller). The proportional constant of the PI controller will be a function of the PV power, as shown in Figure 2.1. This adaptive function will allow a low value during low-power operation conditions and maintain the controller dynamics at high power. Nevertheless, in the rate limiter topology, the DC-link voltage perturbation is changed in a ramp manner from one set point to another, which the rate limiter can achieve. This method aims to reduce the overshoots and steep changes during the operation of MPPT perturbation. Notably, the rate limiter does not affect the MPPT tracking efficiency, as the power oscillation during steady state is the main contributor to losses. However, by utilizing this method, the DC-link voltage should reach its steady state value before the next perturbation step for the whole MPPT period. Another technique discussed is the constant voltage MPPT algorithm.

This solution relies on canceling the DC-link voltage perturbation. A constant DC voltage is fed to the controller, which is 71%-78% of the open circuit voltage of the PV array. The interaction between the DC-link voltage controller and the current controller is avoided by providing a constant voltage value, and the interharmonics due to the DC-link perturbations are eliminated. The drawback of this method is the deterioration of inverter efficiency, which reduces the total PV system energy yields. This implies that this method should be used at lower power operating conditions along with other practical algorithms, such as the perturb and observe (P&O) algorithm under normal power operating conditions (Hybrid). This work declares that the third method is the best among the other proposed solutions to reduce the effect of interharmonics. However, the constant voltage-based MPPT method provides an approximation of the reference voltage, which may affect the MPP tracking efficiency and performance.

More detailed analysis and modeling of interharmonics are presented in (Sangwongwanich et al. 2018a). The authors specified that the problem of interharmonics is limited to the DC-link voltage perturbation due to the MPPT searching process, irrespective of the PV power limit as an influencing factor on the interharmonics characteristics. However, this conclusion could be argued with the recent previous research findings mentioned in (Sangwongwanich et al. 2017b) and (R.

Langella et al. 2016). The authors (Sangwongwanich et al. 2017b, 2018b) investigated the effect of MPPT control parameters such as the step size and sampling rate. By changing the step size, the amplitudes of the interharmonics become more comparable with the amplitude of the fundamental component. Nevertheless, the interharmonics frequency characteristic is still the same. On the other hand, increasing the sampling rate will increase the amplitudes and change the frequency distribution and the allocation of interharmonics in the inject grid current. Therefore, increasing the sampling rate, which is limited by some extent to the DC-link voltage steady state settling time, will affect the utility grid's power quality.

Accordingly, a mitigation method based on modifying the MPPT algorithm sampling rate is proposed in (Sangwongwanich and Blaabjerg 2019) based on the analysis performed in (Sangwongwanich et al. 2018a). The authors outlined the effect of the MPPT sampling rate and the perturbation step size under the P&O MPPT algorithm. The effect is characterized as if the step size or the sampling rate increases, the interharmonics amplitudes will increase with peaks depending on these parameters' values. However, the interharmonics' frequency will vary for sampling rate variations only. This concludes the significat impacts of the MPPT control parameters on interharmonics characteristics. This method is mainly focusing on varying the sampling rate of the MPPT algorithm to minimize the dominant interharmonics in the frequency spectrum. This change will include fast and slow rates hence at higher sampling rate, the interharmonics amplitudes are somehow doubled per doubling the sampling rate (Sangwongwanich and Blaabjerg 2019). However, this study did not consider the effect of the MPPT step size, which is dominate on the magnitudes of interharmonics generation and emission.

This method affects the perturbations of the DC-link voltage controller and the spikes generated at low irradiance operating conditions. The authors validated the proposed method experimentally with an MPPT efficiency of 97.2%. This research was performed on enhancing one of the MPPT algorithms, which is P&O. Besides, the modification was conducted to the sampling rate while excluding a significant dominant parameter, the voltage step size. Furthermore, the developed mitigation algorithm was investigated using a trapezoidal solar irradiance waveform. However, a step-changing solar irradiance can be used to investigate the developed method's dynamic and steady-state response. Finally, there should be a comparison between the methods presented by the authors about the best mitigation method in terms of efficiency and performance.

2.4. Impact of Dynamic Grid Support on Interharmonics Emission

The intermittent behavior of the PV renewable energy-generating systems under high penetration levels brings adverse consequences on the power quality, reliability, and stability of the utility grid for the distribution level. The injection of active power, under high production of PV energy, through the distribution network's different points may affect the grid's stability and challenge the voltage regulation standards. The current grid standards for the conventional grid-connected PV inverters required working on a near unity power factor (more than 0.99) along with MPPT algorithms to maximize the power extraction from the PV panels. Meanwhile, grid-connected PV systems are interrupted in case of grid abnormalities, e.g., voltage sag/swell, grid faults, and protection device failures due to harmonics and interharmonics.

Increasing the adoption of grid-connected PV systems may lead to voltage rise at the distribution level (PCC), e.g., reactive current along with interharmonics being injected into the utility grid. Following the IEEE 1547-2003 standard, conventional grid-connected inverters continuously monitor the voltage and frequency of the grid without significant attention to the power quality. In case of voltage abnormalities, the PV system will be disconnected from the network. This may further complicate the problem; hence, if a group of inverters disconnected from the grid, a sharp rate reduction will occur, and voltage disturbance may further be exacerbated.

The same situation is encountered due to power ramping up while the inverters are returned back into service (NREL 2014). Possible solutions in this case are to reduce the maximum power limit generated by the PV system or by reducing the total number of installed grid-connected PV systems, which is, in either of these cases, against the global goals of reducing carbon dioxide and emissions (Yang, Wang, and Blaabjerg 2014). Another solution is compensating for voltage abnormalities by installing additional expensive distribution network components such as under-load tap changing transformers (ULTCT), step voltage regulators (SVR), etc. In this regard, reactive power compensation such as Static var compensator (SVC), STATCOM, and switched capacitors for reactive power support. However, this will require additional costs and increase the system's complexity. A viable solution is to consider advanced grid-connected PV inverters as a reactive power source, which absorbs or injects the reactive power as a part of the ancillary services in the distributed energy resources (DER) while minimizing any additional costs. This will maintain voltage stability, which is one of the major concerns at the point of common coupling.

While the current inverter technology and standards adopt disconnecting them from the network under voltage disturbances, advanced inverter technologies have the “ride through” capability. This will enhance the grid stability under the grid’s frequency and voltage variations by keeping the PV system online and connected under minor events. One way to achieve this purpose is by enhancing the control structure of the grid-connected PV inverter by controlling the active power (or limit) and reactive power (dynamic grid support) (NREL 2014). An amendment was published in 2014 (IEEE 1547a-2014), allowing DER to perform advanced inverter capabilities, such as voltage regulation, under specific agreements between the customers and the grid operators. The high-speed dynamic response of PV inverters promoted them to act as the fast-local reactive power compensator at the point of common coupling, with a significant amount of PV active-reactive power. The local loads absorb the supplied VAR to the PCC, enhancing the power factor, improving voltage regulation, reducing transmission loss, and maximizing power transmission. Therefore, the oncoming generation of grid-connected PV systems is recommended to adopt dynamic grid support and reactive power injection in terms of low-voltage ride-through (LVRT) capability (Yang et al. 2014).

The authors (V, M, and K 2018) investigated a novel control strategy of a single-phase transformerless grid-connected PV system for active power and reactive power compensation. A novel control method with a switching strategy is investigated to improve the power quality in terms of power factor and THD.

2.5. Summary

This section summarizes the most related research on the impact of interharmonics generation from grid-connected PV systems, as depicted in Table 2.2.

Table 2.2: Summary of literature on the related research work investigating the PQ issues for grid-connected PV systems

Reference\specifications	PVS size	Grid Voltage (V)	Influences factors	PCC-feeders	Power Quality Index
(Sangwongwanich and Blaabjerg 2019)	3 kW	230	Dc-link voltage controller	1	Interharmonics
(Elvira-Ortiz et al. 2019)	100 KW	L.V	Temperature, solar irradiance	1	Harmonics, THD
(Ravindran, Rönnberg, et al. 2019)	Miga-size	L.V	Active power-grid voltage	Many	PQ analysis
(Sangwongwanich et al. 2018a)	3 kW	230	Dc-link voltage controller	1	Interharmonics
(Sangwongwanich et al. 2017b)	3 kW	230	Dc-link voltage controller	1	Interharmonics
(Du and Lu 2018)	-	70	solar irradiance.	-	Harmonics, THD
(Etier et al. 2016)	50 kW	33 kV	Temperature, solar irradiance	1	Harmonics, THD
(Pinto et al. 2016)	3.45 kW	230V	Active power-grid voltage	1	PQ analysis
(R. Langella et al. 2016)	3 kW	230	Solar irradiance and MPPT algorithm	1	Interharmonics
(Djokic et al. 2015)	4.6 kW	230	Solar irradiance and MPPT algorithm	1	Interharmonics

3. OVERVIEW OF GRID-CONNECTED PV SYSTEMS

3.1. Introduction

Several topologies exist for the solar PV power conversion process, especially for grid-connected PV systems. A typical configuration is shown in Figure 3.1, where the source or the generating units represent a series of parallel PV panels or strings. The incompatibility between the source and the load (i.e., the grid) raises the importance of utilizing a power electronic-based converter to match the load amplitude and frequency. To achieve grid standards and requirements at the PCC, the conversion systems and their control structure should be advanced to enhance the PQ and power delivery; hence, integrating these systems into the grid is considered a source of waveform events, e.g., interharmonics. Furthermore, enhancing the performance of system components will improve the lifetime of the conversion system (Enslin and Heskes 2004; Gallo et al. 2013; Infield et al. 2004; Messo et al. 2014; Ravindran, Rönnberg, et al. 2019; Varma et al. 2016; Yang et al. 2016).

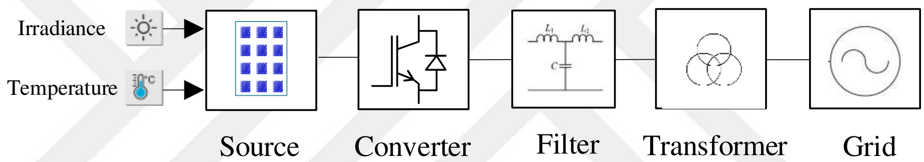

Figure 3.1. The general structure of a grid-connected PV system

The PV systems can be classified into single- or three-phase grid-connected or stand-alone topologies based on the inverter connections. These configurations could be found in single or double-staged systems with central, string, multi-string, or module inverters (Kabalcı 2020), as shown in Figure 3.2 and Figure 3.3. For instance, in Europe, more than 98% of the systems are grid-connected PV systems, which means that part of the generated power is transferred to the utility grid. A great deal of research has been done on improving the efficiency, cost, and integration structure of these inverters. However, the effects of high penetration and integration of grid-connected PV systems is still a premature topic, and more studies should be conducted in this field to justify the impact on the quality of the delivered power.

According to the state-of-the-art, three main topologies exist for interfacing grid-connected PV systems. The PV source is formed by a series of paralleled panels connected to the AC grid using DC-AC inverters with optional DC-DC converters. The utilization of power converters depends on the power rating as well as the voltage ratings. Central inverter topologies are used for a power range from tens up to hundreds of kW, as indicated in Figure 3.2-C. They are mainly targeting cost reduction and decreasing the system's conversion losses. This configuration depends on a single central inverter and a central MPPT algorithm for many strings, which usually increases the mismatch, energy losses, and challenges to the system's reliability; therefore, one or several central inverters are used. The literature reported that the DC-link voltage is around 1000 Vdc. However, the current technology requires increasing the voltage level to 1500 Vdc to reduce energy losses (Raveendhra et al. 2023).

The string inverter topology is a promising solution for the mentioned issues; hence, it utilizes the power converters and a dependent MPPT algorithm for each string. However, the mismatch between the series of connected modules is still encountered. Therefore, the module inverter topology or microinverters are presented. They are plug-and-play modules where the inverter is attached to the back of each PV module and uses a single MPPT algorithm. However, a high DC gain or conversion ratio is required, reducing the system's overall efficiency. The module's voltage is boosted by utilizing a DC-DC converter to a suitable level for the inverter's input; in this case, a double-stage configuration is obtained. Another technology derived from string inverters is multi-string topology, which is considered an in-between solution between module and string topologies. Each string is controlled separately by a dedicated converter or inverter, which will increase overall efficiency and reduce the mismatch problem. The system's reliability is also improved; hence, the failure of one inverter keeps the system partially functioning with no complete loss of energy. String and multi-string topologies are implemented and installed mainly in residential sectors. Two-stage topologies are obtained by utilizing DC-DC converters when the string voltage is not within the minimum input DC link voltage of the inverter; for instance, this will simplify the control structure of the inverter (Nyamathulla and Chittathuru 2023). On the other hand, three-phase central single-stage inverters are spread in a fast manner. However, with the advancement of single-phase inverter topologies and control, three single-phase inverters with central or string topology have started to overtake the industrial and commercial markets, mainly for reliability purposes.

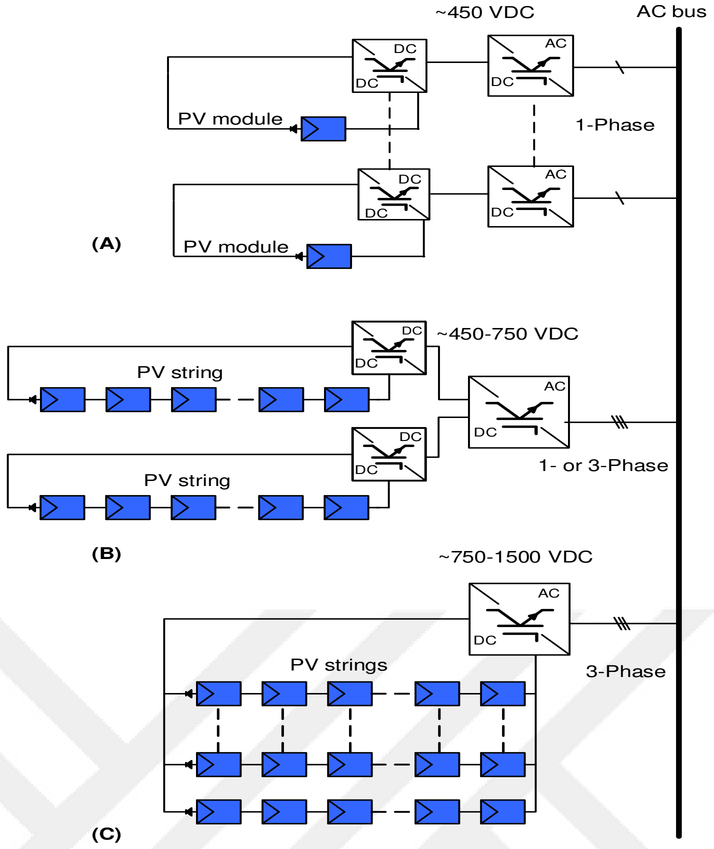

Figure 3.2. On-grid PV system interface to the low voltage grid side: (A) Module PV inverter for low power applications, (B) string/multi-string topology for medium power applications, (C) Central inverter topology for higher power applications

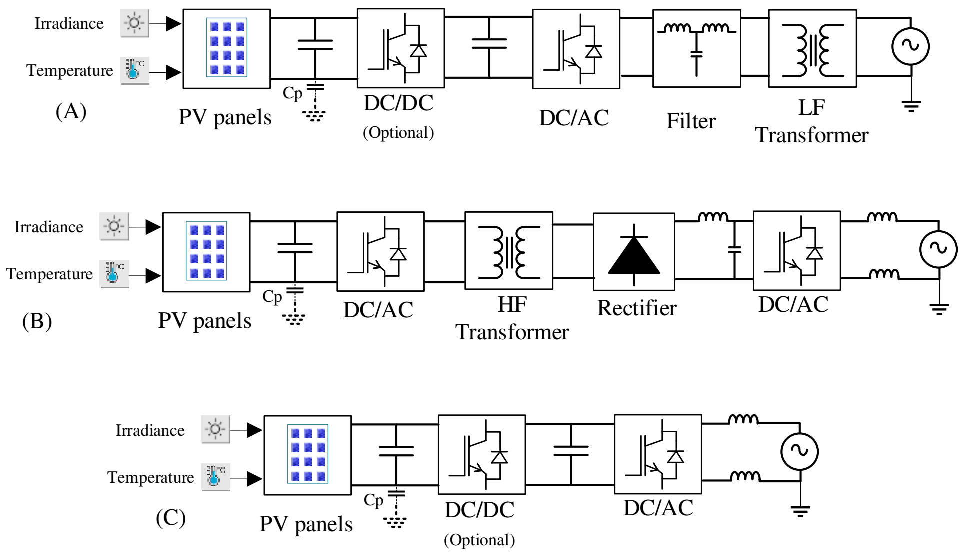

Figure 3.3. Single-phase grid-connected PV systems: (A) LFT with galvanic isolation, (B) HFT with galvanic isolation, and (C) transformerless topology, where Cp indicates the parasitic capacitance between the ground and the PV system

Recall from Figure 3.3 that the transformer's existence is mainly to offer galvanic isolation, and in case of its absence in the PV system, the configuration is called transformerless topology. The isolation transformer could be at the grid side with low-frequency operation or operated at high frequencies when installed as an intermediate stage. Figure 3.3 shows the existing grid-connected photovoltaic system topologies according to the existence and location of the transformer. Generally, the efficiency of these topologies (with isolation transformers) is less than that of transformerless inverters, and the efficiency of transformerless systems is more than 95% (Alam, Prasad, and Asim 2022). However, the latter suffers from current leakage issues and raises safety concerns, and thus, it is considered a trade-off by increasing efficiency after removing the transformer. These issues can be overcome by utilizing extra switches in the inverter design and modifying the modulation technique. Transformerless inverters are much lighter in weight, cost-effective, and provide more power density. The literature includes a good deal of work that has been conducted on transformerless inverters; they have been used practically in many countries, including Europe. The markets are expected to understand better these inverters, which will increase the share and penetration levels of PV systems integrated into the utility grid.

3.2. PV Inverter Topologies and Structures

The backbone of the PV systems is the inverters, and special attention should be paid to their design, control, and operation. This is mainly to achieve efficiency, reliability, and high power quality delivery. The power converters are reviewed here based on their power ratings and topologies, i.e., module, string, and central inverters (Boscaino et al. 2024).

3.2.1. Module Converters

There are two topologies of module converters, namely microinverters and power optimizers. The latter is simply a DC-DC converter aiming to maximize energy harvesting from PV modules. Power optimizers are connected to DC loads or as the input stage for standalone or grid-connected inverters. Under module inverter topology, the PV module voltage is typically low (30-60 V), and therefore, power optimizers are connected in series for grid-connected PVS applications. The utilization of power optimizers enhances efficiency and enables the MPPT to be achieved at the module level. This will reduce the effects of partial shading, nonuniform solar irradiation on panels and improve the reliability in case of failure, such as partial coverage of dust or other factors affecting the individual PV modules. Under these circumstances, the overall performance is not deteriorated. Power levels can be increased by paralleling the power optimizers or utilizing differential power processing. The classical DC-DC converters include buck, boost, buck-boost, and Cuk converters. The application of step-up converters is essential for grid-connected converters in module topology. High-gain and voltage conversion ratio converters are required to reduce the number of paralleled units. It is worth mentioning that some converter topologies are non-isolated. Therefore, other topologies are developed, such as flyback converters, which are considered as one of the most popular topologies. This converter enjoys higher efficiency, reliability, simple structure, and lower cost than the classical boost converter. However, the optimizer's voltage gain depends not only on the duty cycle but also on the transformer turn ratio. Other topologies of power optimizers, such as full or half-bridge converters with HF transformers, impedance-source converters, and switched-capacitors or inductor converters, can be used. More understanding of these converters is expected in the market due to their performance and the ability to track the power under nonuniform solar irradiance conditions. A double-stage configuration will form when the power optimizer is connected to the inverter's input. Under this configuration, the MPPT process is taken by the DC-DC converter, and the inverter performs the DC-LINK voltage control and current loop regulation. A capacitor is typically used at the DC-link voltage, where the voltage variation is presented at a frequency equal to two times the grid frequency to buffer and decouple the AC and DC power.

In terms of control, the double-stage configuration is more straightforward; hence, the control functions are separated. Nevertheless, the overall efficiency degrades and worsens when connecting a galvanic isolation transformer. Other topologies are introduced in the literature to improve performance and overall efficiency, and they are referred to as single-stage configurations. The first topology is the universal microinverter, which has a wide range of operating conditions such as buck, boost, or buck-boost mode. This configuration is suffering from zero-crossing current distortion. Therefore, two other promising topologies are presented: differential buck-boost and buck-boost integrated microinverters. Under these topologies, two out-of-phase voltages are produced to alleviate the zero-cross distortion, where a common mode source is adopted.

3.2.2. String Inverters

Connecting multiple PV modules in series will form a PV string, and the allowed input voltage of the inverter is easily achieved by increasing the number of series connected modules (for a single-phase, it is around 400 V). Also, the power rating can be increased by paralleling more than one string to form a multi-string inverter. String inverters can be classified as single or double-stage configurations and galvanic isolated or transformerless inverters. Out of these configurations, transformerless and single-stage topologies target the overall performance to enhance efficiency. Nevertheless, these structures are more complex in their design and control function, i.e., the inverter performs the MPPT, DC-link voltage, and grid current regulation. In addition, for transformerless inverters, the design should consider mitigating and suppressing the leakage current produced by the parasitic capacitance.

String inverters applications are mainly found in single-phase systems where the inverters are connected to single-phase feeders with power ratings typically less than 10 kW. Therefore, this section will review single-phase string inverter topologies focusing on transformer, transformerless, and double-stage inverters by considering the widely used single-phase string inverter, which is the full bridge inverter. It is still the most common topology; hence, it contains the lowest number of switching devices due to its simplicity in control and design. Figure 3.4 presents a transformerless single-phase string inverter connected to an LCL filter.

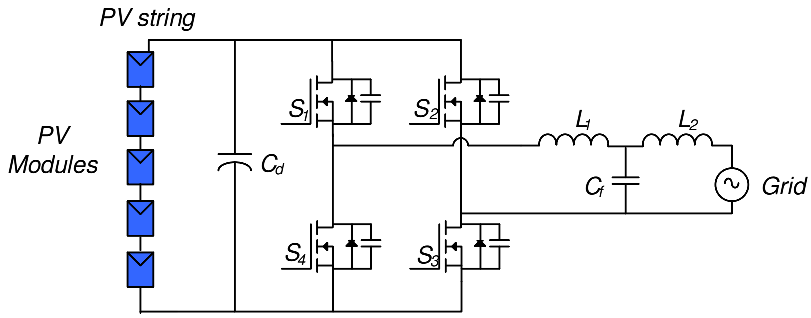

Figure 3.4. Single-phase full-bridge transformerless inverter topology

Even though single-stage PV systems are preferred in string topologies, double-stage configurations are also acknowledged in the literature. Under this case, another stage is presented, much similar to microinverters' DC-DC conversion stage, reducing the tasks performed by the inverter. Full or half-bridge inverter topologies or transformerless configurations can be used in the second stage. However, in the later topology, special attention should be taken to the DC-DC converter design to reduce the leakage current.

The power level below 10 kWp is referred to as a single-phase string inverter. However, to increase the PV system's power level, many strings can be connected in series or parallel, with each string connected to a DC-DC converter, as in the case of microinverters, and interfaced to two or multilevel inverters. Thus, the energy harvesting is optimized on the string level. The last configuration is called multi-string topology and typically referred to three-phase inverters connected to low voltage networks, with DC-link voltage up to 1500 V. It is worth mentioning that compared to microinverters, the switching frequency of string inverters is lower, which improves the efficiency and alleviate the EMI effect. Nevertheless, higher switching frequency in microinverters reduces the inverter size from one side, challenging efficiency and EMI effects.

3.2.3. Central Inverters

Increasing the power level through multi-string and central inverters drives the force toward multilevel inverters, and only in single stage configuration where the efficiency and cost are improved. The input power can be increased by paralleling the strings together to form a PV array. Under this situation, 3L NPC inverters are preferred. The high output voltage level of these inverters, and compared to 2L inverters, improves the efficiency by reducing the output filter requirements. The power switch's voltage stress is also reduced, and typical or conventional power devices (1.2 kV) can be used.

For higher power ratings in the scale of MW, multilevel inverters, more than 3L, or modular multilevel converters can be utilized. The overall system efficiency and voltage stress should be considered carefully in the design of these converters. Modular technology brings the benefits of fault-tolerant operation and control. It consists of submodules or cells connected in series and is typically implemented by a half-bridge converter, which is the most widely used. PV modules can be connected across the modular modules or attached to each cell. For maximum energy harvesting, MPPT can be utilized either as a common algorithm or on the module level, and thus, the power mismatch between PV strings and modules is reduced.

3.3. PV Panel Modeling

The PV panels are the exposed part of the PV system; they are just as important as the power electronic converters, which are used to condition the panel's output power. Panels are mounted on the rooftops, in open areas, or integrated into building materials. Solar-to-electrical energy conversion is based on the photovoltaic effect and depends highly on the efficiency and reliability of the module. Therefore, capturing the maximum amount of solar energy improves the system's performance and enhances overall efficiency. A great deal of research is conducted on PV cells to increase module efficiency and reduce manufacturing costs. Among the different types of PV cells, which include thin-film, perovskite, dye-sensitized, and organic cells, crystalline silicon PV cells are still the most widely used in grid-connected PV systems. Modeling and emulating the PV system will assist the design process and provide a deep understanding of the PV system's behavior and its performance characteristics under different operating conditions. In addition, mathematical modeling of the PV cells and the power electronics interface is considered the first step in coping with unexpected operating conditions. Therefore, the mathematical modeling of crystalline silicon PV cells in string topology is introduced (Mlazi et al. 2024). However, modeling of the PV system can be performed on a level of cell, panel, string, or multistring, depending on the application and power ratings.

The single-diode circuit model is the most commonly used implementation of a PV cell; this nonlinear model consists of four components, as shown in Figure 3.5. When the PV cell voltage is positive on the I-V curve, the operation is called forward bias, where the maximum power point of the cell is located.

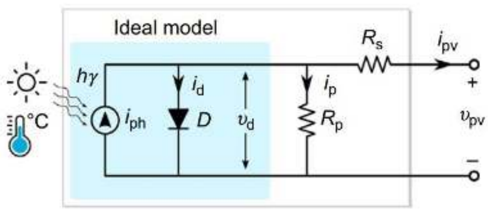

Figure 3.5. The electric model of a PV cell in the forward-bias mode condition.

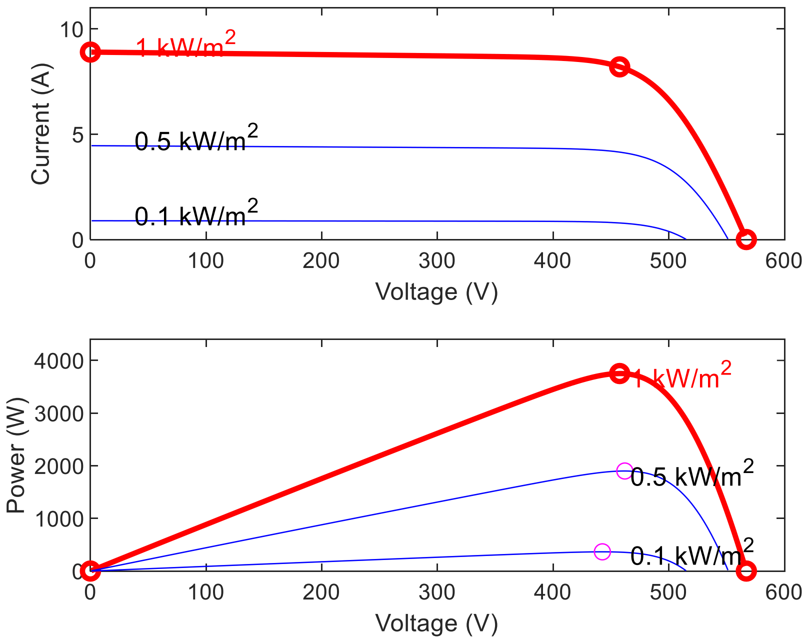

Figure 3.6. I-V and P-V characteristics of a PV string under different operating irradiancies

Where i_{ph} is the photocurrent resulting from the solar irradiance, D is the diode component represents the PV cell surface, R_p, R_s are the parallel and series parasitic resistances required for more accurate modeling of the PV cell, where the photocurrent source and the diode alone represent the idea PV cell model.

The main factors that affect the PV cell characteristic are the solar irradiance on the cell surface G, and the cell temperature T. Under standard conditions, G is equal to G_n 1000 W/m^2 and T is T_n 25^0 C.

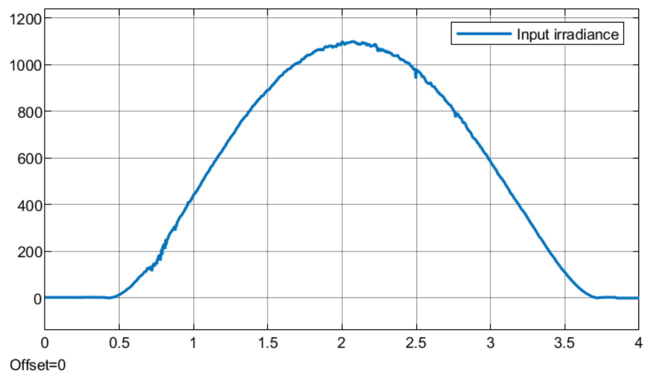

Figure 3.7. Input irradiance (a realistic curve)

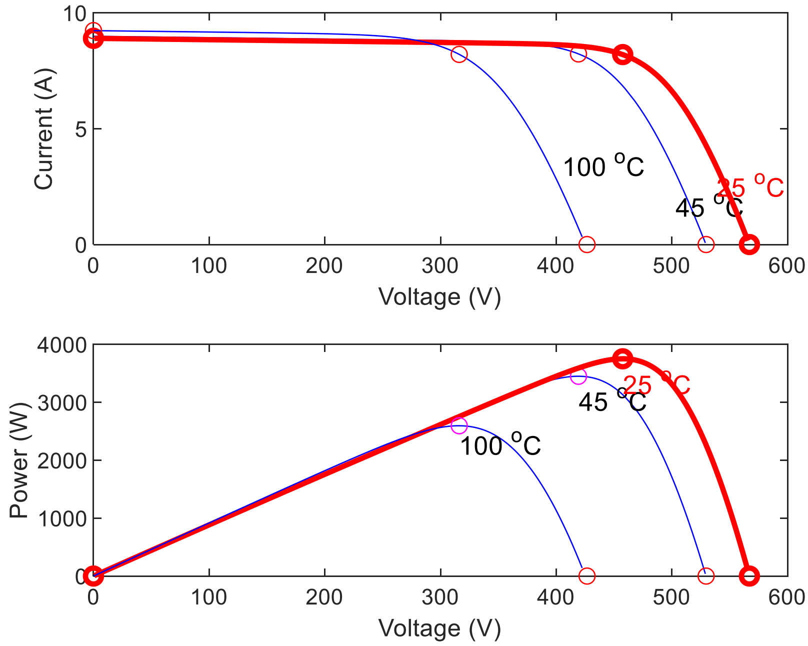

Figure 3.8. I-V and P-V characteristics under different operating temperatures (string topology)

The $I - V$ characteristic is affected by two temperature coefficients K_i and K_v. Besides, the open circuit voltage V_{oc} and short circuit current I_{sc} are two essential parameters that have a significant impact on the I-V characteristic of the PV cell. Mathematically, the PV cell's parameters related to the environmental factors are given by:

$$i_{ph} = \left[I_{sc} \frac{(R_p + R_s)}{R_p} + K_i(T - T_n) \right] \tag{3.1}$$

The diode's current i_d with the voltage across it v_d is given as:

$$i_d = I_s \left[\exp\left(\frac{v_d}{\alpha V_t} \right) - 1 \right] \tag{3.2}$$

$$V_t = \frac{k_\beta T}{q} \tag{3.3}$$

Where $I_s, \alpha, V_t, k_\beta, q$ are the diode saturation current, the ideality factor, the single-cell thermal voltage of the semiconductor junction, Boltzmann's constant, and the electronic charge, respectively. Finally, the PV cell voltage can be obtained as:

$$I_{pv} = i_{ph} - i_d - i_p \tag{3.4}$$

$$V_{pv} = v_d - i_{pv} R_s \tag{3.5}$$

Under some operating conditions, the PV cell junction became reversed-biased, and it can be modeled by modifying the single-diode circuit to include the reverse-biased situation. By passing a certain threshold, the PV cell junction breaks down, increasing the reverse current to the PV cell.

3.4. Control Of Single-Phase Grid-Connected PV Systems

Different varieties of power converters are used in single-phase grid-connected PV systems and, more commonly, with two-level inverters. Both single-stage and double-stage PV systems are adopted in practical applications for these systems. The design of these systems should meet the maximum power point requirements under uniform and nonuniform weather and solar irradiance conditions. Also, a high-quality injected current with minimum total harmonic distortion (THD) is required. Typically, the control of grid-connected PV systems is characterized by two cascaded loops; the first loop (outer loop) is responsible for regulating the voltage (or the active power) and generating the reference current, while the second loop (inner loop) performs the regulation of the injected grid current, which maintains its power quality (Morey et al. 2023).

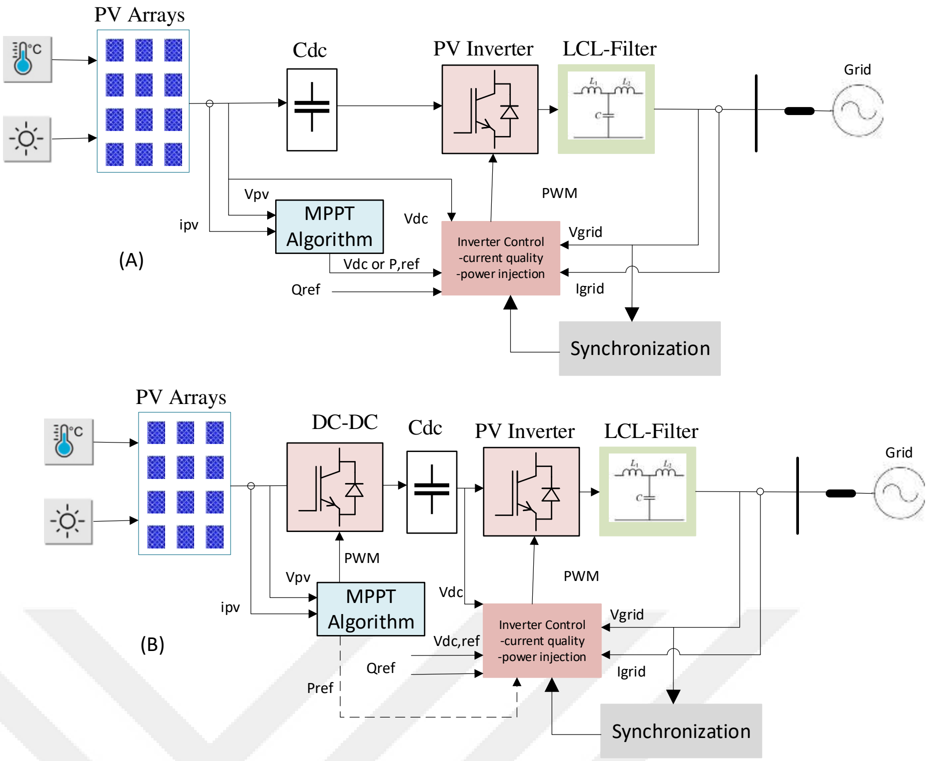

Figure 3.9. The general control diagram of a single-phase grid-connected PV system in (A) with single-stage configuration and (B) with double-stage configuration

For single-stage configuration, the inverter is required to perform two tasks: power optimization, utilizing a proper MPPT algorithm for maximum energy harvesting, and controlling the power injection to the grid. Nevertheless, a double-stage configuration separates these tasks and decouples the input PV power dynamical control from the inverter controller. Specifically, the DC-DC converter regulates the MPPT dynamics (Morey et al. 2023).

Decoupled power control should be employed to regulate the power exchange between the grid and inverter, i.e., the injected active and reactive power. Two orthogonal signals can be generated to control the active and reactive injected power. The active injected power is controlled by extracting the maximum power using a proper MPPT algorithm. A PLL is used to extract the grid phase and frequency. This yields synchronized reference signals with the grid voltage. Accordingly, a current controller is used to drive the error between the output and reference currents, which will control the PWM of the inverter to minimize the output error.

Many linear and nonlinear methods are classified under current control methods for the VSI. Table 3.1 depicts the current control classifications and algorithms used in VSI (Boscaino et al. 2024).

Table 3.1. Classification of the current loop control algorithms

Control type	Control algorithm	Reference frame
Linear	PI (proportional Integral)	Synchronous reference frame
	PR (proportional Resonant)	Stationery reference frame
	DBC (Dead beat current)	Natural reference frame
Non-linear	CHC (Current hysteresis)	
	MPCC (Model predictive)	

Under the case of utilizing a PI-current controller, the control signals are transformed to a reference frame that rotates with the fundamental frequency of the grid voltage. This will result in a DC quantity, which refers to D (direct) and Q (quadrature) in the dq reference frame. To achieve the decoupling process and to control the active and reactive power, two orthogonal signals should be generated for the grid current and voltage signals. One way to perform this is by delaying the voltage and current signals by a specific fraction of the original fundamental period; a fictitious orthogonal signal is generated.

Single- and three-phase grid-connected PV systems can be controlled in three reference frames: the natural abc-reference frame, rotating dq-reference frame, and stationary alpha-beta reference frame. The only control parameter in single-phase systems is the injected current, where the control is feasible using reference frames other than the natural frame by creating an imaginary AC system in quadrature with the original single-phase system. The grid's voltage phase is essential for this transformation and for controlling the inverter. This phase is obtained in the grid synchronization process through phase-lock-loops (PLL) (Gawhade and Ojha 2021). Therefore, as will be introduced in Chapter 4 of this thesis, three main tasks should be conducted: MPPT, inverter control, and grid synchronization.

3.4.1. Current Feed-in Control

The last sections discussed the main objectives for grid-connected PV inverters. However, controlling the injected feed-in current into the grid with minimum THD is essential. By utilizing dual loop control structure, with the outer loop as the DC-voltage control loop or the power control loop, the inner loop reference current can be generated. The synchronous or stationary reference frames can be utilized for designing the current controller, as shown in Figure 3.10 (Yang et al. 2019), which indicates the inverter general control structure in (A) with a synchronous reference frame and PI controllers and in (B), which is based on PI and PR controllers, where the latter is designed in the stationary reference frame based on single-phase PQ theory. The reference frame theory is introduced since the control system is based on Park and Clark transformation, especially for single-phase systems (Murillo-Yarce et al. 2020).

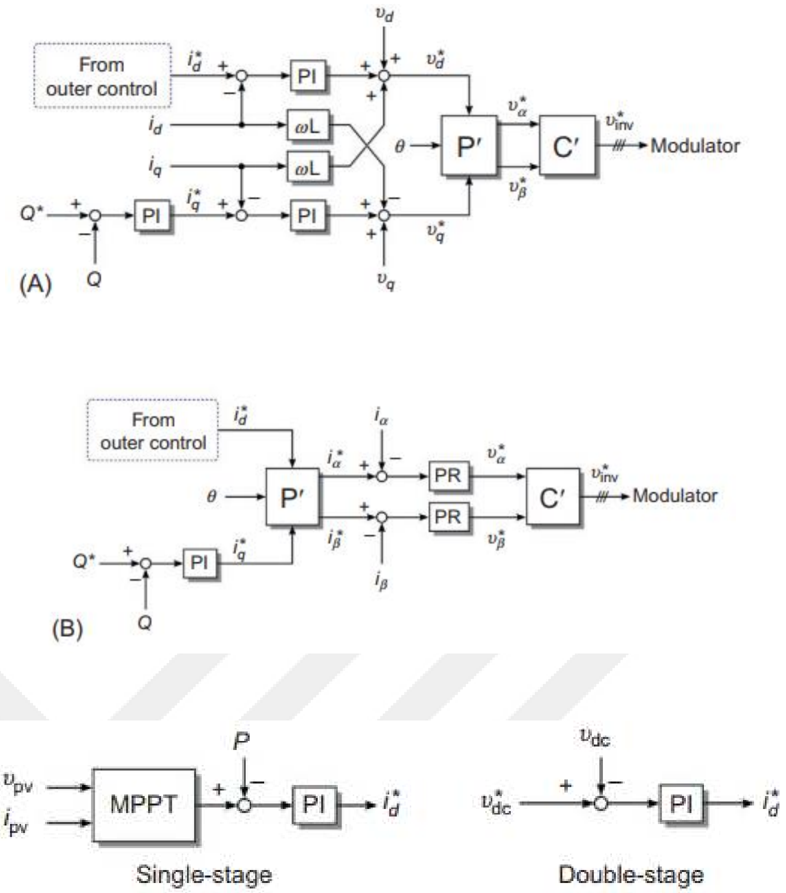

Figure 3.10. Grid-connected control structures (Yang et al. 2019)

For three-phase 2L inverters, there are two sets of three-phase quantities apart 120 degrees between each other, which are the voltages V_{abc} and the currents I_{abc}. Clark's transformation is given as:

$$[x_{\alpha}, x_{\beta}] = C\ [x_a\ x_b\ x_c] \tag{3.6}$$

Where C is

$$C = \frac{2}{3}\begin{bmatrix} 1 & -\frac{1}{2} & -\frac{1}{2} \\ 0 & \frac{sqr(3)}{2} & -\frac{sqr(3)}{2} \end{bmatrix} \tag{3.7}$$

The three AC variables are reduced to two AC qualities, which reduces the control complexity and the number of controllers. PI controllers cannot track AC variables and steady-state errors. Therefore, Park transformation is adopted to transform these variables into constant signals by transformation matrix P as:

$$P = \begin{bmatrix} cos\theta & sin\theta \\ -sin\theta & cos\theta \end{bmatrix} \tag{3.8}$$

A fictitious orthogonal system can be created for single-phase systems to utilize the PI controller in the synchronous reference frame. The principle is explained in Figure 3.11 below:

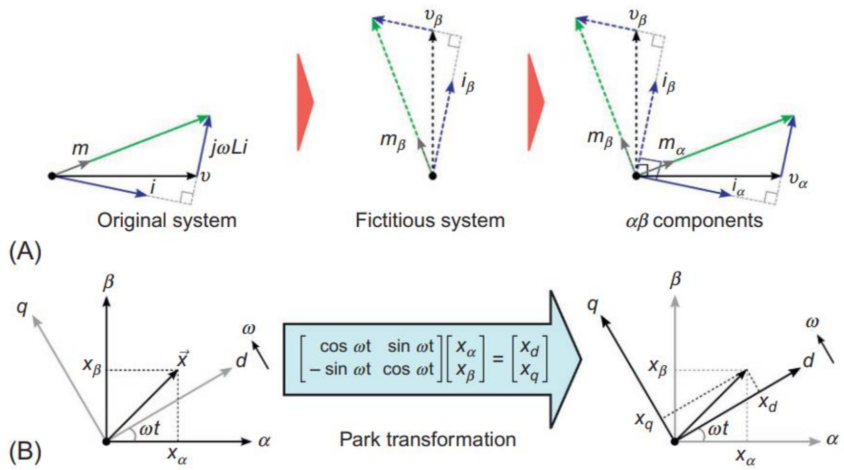

Figure 3.11. Park transformation for single-phase systems (Yang et al. 2019)

3.4.2. Outer Control Loop

An input capacitor is essential for grid-connected voltage source inverters to balance, buffer, and decouple the input power DC and output AC power. The input DC power is regulated and smoothed at the DC-link, and then routed to the grid side through a grid-connected inverter. It is worth mentioning that the minimum DC-link voltage should be higher than the grid peak voltage value and typically more than 400 V for single-phase systems. Therefore, the DC-link voltage is held constant for grid-connected applications (Yang et al. 2019).

$$\begin{aligned} P_{dc} &= v_{dc}i_{dc} - v_{dc}C_{dc}\frac{dv_{dc}}{dt} \\ P_{dc} &= \frac{2}{3}\left(v_d i_d + i_q v_q\right) \\ P_{dc} &\approx P_{ac} \\ v_{dc}i_{dc} - v_{dc}C_{dc}\frac{dv_{dc}}{dt} &= \frac{2}{3}\left(v_d i_d + i_q v_q\right) \end{aligned} \tag{3.9}$$

When the synchronous frame's d-axis component is aligned with the grid, the quadrature component is equal to zero, and therefore, $V_d = V_m$. The above equation became:

$$v_{dc}(s) = G_{p-dc}(s)i_d(s) = \frac{3V_m}{2\,(2I_{dc} - sC_{dc}V_{dc})}\,i_d(s) \tag{3.10}$$

$$i_d^* = -G_{p-dc}(s)i_d(s)(v_{dc} - v_{dc}^*) \tag{3.11}$$

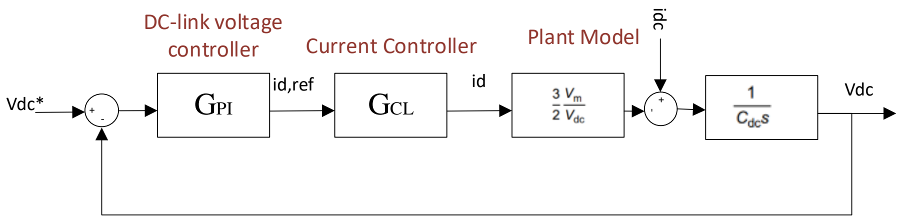

Figure 3.12. The close control loop of the DC-link for the d-axis current

When designing the DC-link voltage, a practical approximation for the current loop can be given as:

$$G_{CL-cc}(s) = \frac{1}{1 + 3T_s\,s} \tag{3.12}$$

According to PQ theory, the instantaneous active and reactive power can be written as:

$$\begin{aligned} P &= \frac{3}{2}(v_d i_d + i_q v_q) \\ Q &= \frac{3}{2}(v_q i_d - i_q v_d) \end{aligned} \tag{3.13}$$

Therefore, the d- and q-axis currents can be used to regulate the active and reactive power.

$$\begin{bmatrix} i_d^* \\ i_q^* \end{bmatrix} = \begin{bmatrix} G_{PI-P}(s)\,(P^* - P) \\ G_{PI-Q}(s)(Q^* - Q) \end{bmatrix} \tag{3.14}$$

3.4.3. Inner Control Loop

In this part, different control algorithms are implemented based on the reference frame used in the current controller design. For a three-phase inverter system (also for single-phase), the voltage equation can be written as:

$$L\frac{di_p}{dt} + Ri_p = v_{op} - v_p \tag{3.15}$$

To control the system in the synchronous reference frame, Park transformation is applied to the last equation, which yields:

$$L\frac{di_d}{dt} + Ri_d - \omega Li_q = m_d v_{dc} - v_d$$
$$L\frac{di_q}{dt} + Ri_q - \omega Li_d = m_q v_{dc} - v_q \quad (3.16)$$

It can be noticed that the d- and q- axises equations contain mutual terms, and decouple terms are added, which yields the following equations:

$$m_d^* = m_d + \frac{\omega L\, i_q}{v_{dc}} - \frac{1}{v_{dc}}\, v_d$$
$$m_q^* = m_q + \frac{\omega L\, i_d}{v_{dc}} - \frac{1}{v_{dc}}\, v_q \quad (3.17)$$

The transformed equations to stationary reference frames are used to implement the inverter control system by utilizing PR controllers. The transformation to a stationary reference frame is obtained by:

$$L\frac{di_\alpha}{dt} + Ri_\alpha = m_\alpha v_{dc} - v_\alpha$$
$$L\frac{di_\beta}{dt} + Ri_\beta = m_\beta v_{dc} - v_\beta \quad (3.18)$$

In S-domain, it can be written as:

$$(Ls + R)i_{\alpha\beta}(s) = v_{dc}m_{\alpha\beta}(s) - v_{\alpha\beta(s)} \quad (3.19)$$

In other words, by proper regulation of out voltage ($m_{\alpha\beta}$), the injected grid current can be controlled, and thus:

$$m_{\alpha\beta}^* = \frac{1}{v_{dc}} G_{cc-\alpha\beta}(s)\left(i_{\alpha\beta}^* - i_{\alpha\beta}\right)\ v_{dc}m_{\alpha\beta}^* \quad (3.20)$$

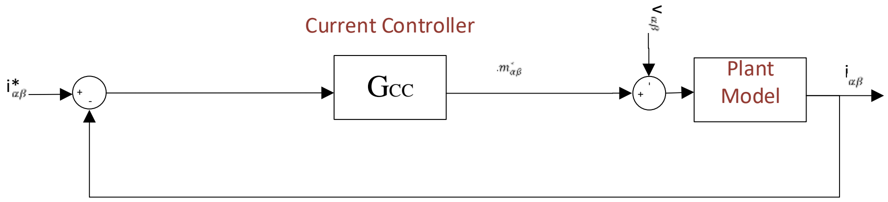

Figure 3.13. Closed-loop current control system under stationary reference frame

3.5. Maximum Power Point Tracking Technology

Besides the development of the controller, the overall performance should meet and comply with the design codes, such as the allowed THD (IEC 61727, IEE1547, IEC 61727, and VDE 0126-1-1), auxiliary services, and the use of MPPT algorithms. A unique PV cell operating point is characterized by a specific voltage and current, where the maximum power point (MPP) is obtained. This point changes with many factors, such as the cell's temperature and solar irradiance. Usually, the temperature change is slower (in the order of minutes) than the irradiance, which exhibits a rapid fluctuation (in the order of milliseconds), e.g., in instant cloud coverage. Following this continuous change of the MPP throughout the day is indispensable, and proper control is essential to maximize the system's output power and overall efficiency. Many algorithms have been developed for this purpose, and most of them divide the control action into two loops: the inner loop, which keeps a fixed value while the outer loop updates it using a specific MPPT algorithm (Motahhir, El Hammoumi, and El Ghzizal 2019). Although many different MPPT algorithms have been developed in the last decades, they can be generally divided into characteristic-based and extreme-seeking algorithms. In the first type, sensors measure the voltage (and current) or the operating point of the PV panel and modify it according to predefined data, e.g., the panel datasheet.

Nevertheless, the second method deals with MPPT as an optimization problem to allocate the maximum point in the power curve. These algorithms are designed to perform the same task and to realize the objective of finding the MPP. However, they have many varieties and differences, which include, but are not limited to, the level of complexity for implementation, oscillations around the MPP, convergence speed to the MPP, measured control variables, true MPPT, and array-based methods (Ahmad, Murtaza, and Sher 2019). Figure 3.14 and Figure 3.15 show the flow charts of the P&O and IncCon MPPT algorithms for implementing the control algorithm. Table 3.2 presents a summary of the most commonly used and well-documented MPPT algorithms in the literature. These algorithms are a strong candidate for enhancing overall efficiency and maximizing input source power.

Table 3.2. Different MPPT algorithms with performance parameters

MPPT Method	True MPPT	Complexity	Conv. speed	Array-Based	Control parameter	Type	Oscillations
Perturb & Observe	Yes	Low	Variable	No	V and I	Online	High
Incremental Conductance	Yes	Medium	Variable	No	V and I	Online	Medium
Sliding Mode	Yes	Medium	Fast	No	V and I	Online	-
Capacitor Control	No	Low	Medium	No	V	Online	-
Load I-V Control	No	Low	Fast	No	V and I	Online	-
Open-Circuit Voltage	No	Low	Medium	Yes	V	Offline	High
Constant Voltage	No	Low	Medium	Yes	V	Offline	-
Short-Circuit Pulse-Based	No	Medium	Medium	Yes	V	Offline	-
Short Circuit Current	NO	Low	Low	Yes	I	Offline	High
dP/dV and dP/dI feedback	Yes	Medium	Fast	No	V and I	Online	-
Fuzzy Logic Control	Yes	High	Fast	Yes	V	Offline	Low
Artificial Neural Network	Yes	High	Fast	Yes	V	Offline	Low
Genetic Algorithm	Yes	High	Fast	Yes	V	offline	Low
Particle Swarm Optimization	Yes	High	Fast	Yes	V	Hybrid	Low

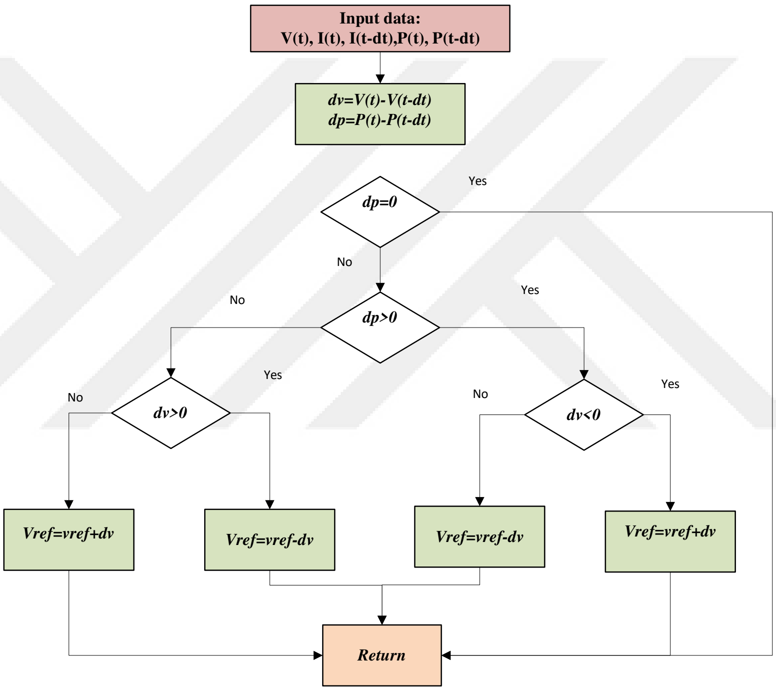

Figure 3.14. The P&O MPPT algorithm

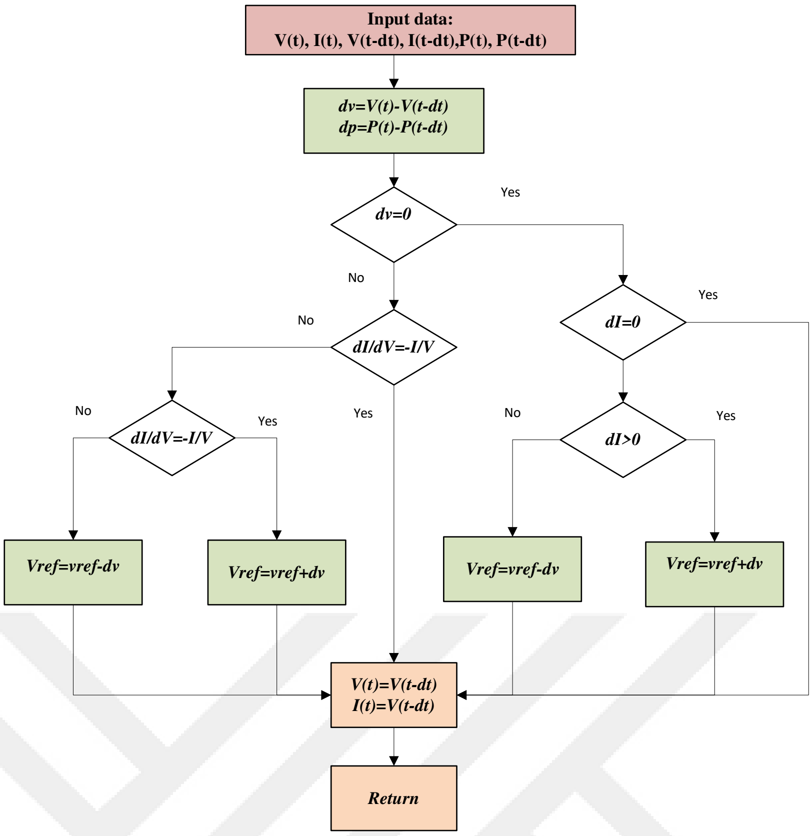

Figure 3.15. The InCon MPPT algorithm

Particular attention should be paid to the parameters of the MPPT algorithm, as recent studies show a relation between the interharmonics emissions and generation and the parameters of the control structure. Besides the conventional MPPT methods, such as the P&O and InCon algorithms, other algorithms depend on artificial neural networks, fuzzy logic, and genetic algorithms (Elsheikh et al. 2019). It is worth mentioning that other methods use extra sensors for temperature and solar irradiance measurements for more accurate modeling. However, this increases the total complexity and cost and raises the issue of occasional recalibration necessary due to cell aging and other environmental factors; and therefore, frequent outer loop measurements are needed to keep the system functional. Alternative MPPT techniques demand reduced intervals for measurement.

In open-circuit voltage and frictional short-circuit current MPPT algorithms, periodical measurements are conducted to update the value of the operating point; a pilot cell can be used as a representative of the other modules, and therefore, the system will keep its continuity. Nevertheless, the most widely used MPPT algorithms in practical applications are P&O and InCon due to their control simplicity and implementation.

3.6. Summary

This chapter presents an overview of the topologies, configurations, and structures for single-phase grid-connected PV systems. Accordingly, the control techniques used in single-phase systems, including the feed-in and dual-loop control, are discussed. In addition, a review of the PV panel modeling and design is provided. Finally, the widely used MPPT algorithms are compared, emphasizing the utilized control parameters, their convergence speed, tracking efficiencies, and steady-state oscillations.

4. INTERHARMONICS FROM SINGLE-PHASE GRID-CONNECTED PV SYSTEMS

This chapter presents the investigation of interharmonics under different operating conditions, the generating characteristic of interharmonics, the mechanism of emission, and the proposed mitigation technique, along with the proposed mathematical development and analysis of the injected interharmonics into the grid current.

4.1. The Inverter Configuration and its Control

To investigate the interharmonics generation characteristics and their mitigation techniques, extensive simulation analysis has been conducted on a single-stage, single-phase grid-connected PV system shown in Figure 4.1 (Blaabjerg et al. 2006), with parameters indicated in Table 4.1. The PV system contains four parts: The PV arrays, the PV inverter, the LCL-filter, and the grid. The PV inverter implements the critical part of controlling and interfacing the PV power to the ac grid. The maximum power extraction from the PV arrays is ensured by utilizing MPPT algorithms, e.g., Perturb and Observe (P&O), and the value of the reference dc-link voltage V_{dc}^{*} is determined. Accordingly, the Proportional Integral (PI)-based dc-link voltage controller controls the grid current i_g and regulates the dc-link voltage V_{dc}. Due to the interaction between the dc side (PV side) and the grid (ac side), double frequency component $2f_g$ is presented in the dc-link voltage. Therefore, a low pass filter (LPF) is used, resulting in V_{dc}' to improve the control performance (M. Ciobotaru 2009). A phase-locked loop (PLL) is considered for the synchronization process, and this yields the phase angle of the grid voltage $\sin(\theta_g)$, which is used for generating the reference grid current i_g^{*}. A Proportional Resonant (PR) controller with harmonics compensation for the inner control loop is used to regulate the grid current. Accordingly, the Pulse width modulation (PWM) generates the switching signals (G_p) to control the outputs of the inverter.

The operation of the PV system and its control structure is demonstrated during steady state with a constant dc-link voltage, e.g., constant voltage MPPT operation, to investigate interharmonics under this case. Figure 4.4 shows the rated power dc-link voltage, injected grid current, and dc-link voltage error. The frequency spectrum of the injected current is shown in Figure 4.5; it can be seen that the amplitudes of the interharmonics are negligible under this operating condition, and the frequency spectrum contains only the dominant fundamental component. It can be concluded that the interharmonics are strongly related to the perturbation of the dc-link voltage and its error value, e.g., the MPPT perturbation.

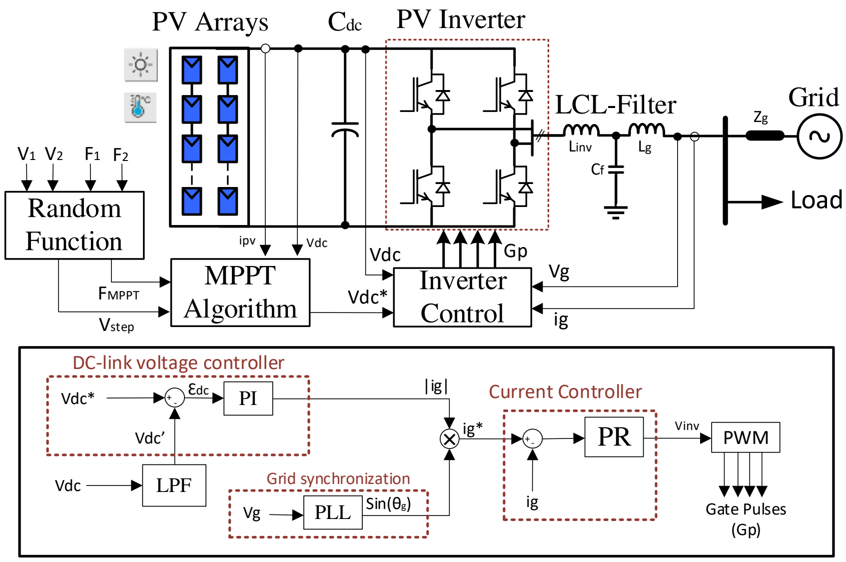

Figure 4.1. The power topology and control structure of the single-stag single-phase grid-connected PV system

Table 4.1. Parameters of the simulated single-phase grid-connected PV system

c	3.75 kW
Capacity of the DC-link	$C_{dc} = 1400\ \mu F$
LCL-filter	$L_{inv} = 5\ mH, C_f = 5.2\ \mu F, L_g = 2\ mH$
Transformer leakage inductance	$Z_g = 2\ mH$
Sampling frequency of the controller	$f_s = 20\ kHz$
Switching frequency	$f_{sw} = 8\ kHz$
Nominal grid voltage	$V_g = 230\ V$
Nominal grid frequency	$f_g = 50\ Hz$
DC-link voltage	$V_{dc} = 450\ V$
MPPT sampling rate	$F_{mppt} = 20\ Hz$
MPPT step size	$V_{step} = 5\ V$

The designed system is implemented and simulated using the MATLAB/SIMULINK program. The schematic diagram of the power circuit and the control structure circuit is depicted in Figure 4.3 below. It should be mentioned that filter design is a critical part of the system; hence, it will be extremely effective in suppressing the switching frequency harmonics generated by the inverter. The LCL-filter is designed with harmonics compensation for the 3rd, 5th, and 7th harmonics. The interface with the grid could be implemented with an L-filter. However, this will increase the size, cost and reduce the overall performance of the system. Therefore, LCL-filters with harmonic compensation will yield the best performance characteristic.

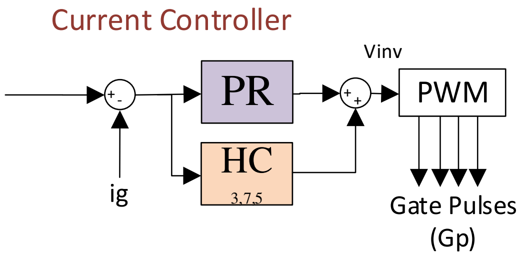

Figure 4.2. The current controller with HC

The complete power topology and the proposed modified control structure are shown below.

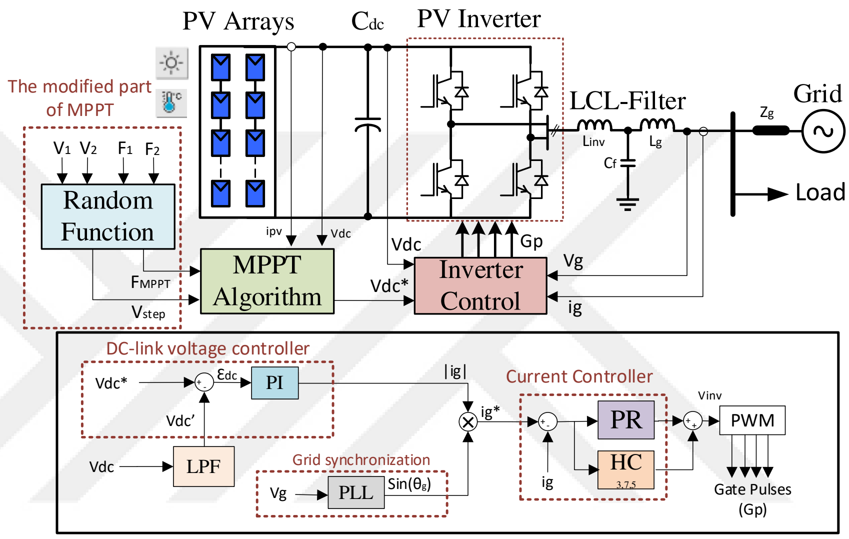

Figure 4.3. The power topology and the structure of the controller for the considered grid-connected PV system.

4.2. Operation under MPPT Algorithm

It has been reported by (Sangwongwanich et al. 2018a; Sangwongwanich and Blaabjerg 2019) that the MPPT operation is a source of interharmonics generation in single-phase grid-connected PV systems. In addition, the authors (Djokic et al. 2015; R. Langella et al. 2016; Roberto Langella et al. 2016; Sangwongwanich et al. 2017b), (Xiao et al. 2017) presented the so-called "power dependency" where the emission of interharmonics increase at low power operating conditions. Therefore, the single-phase PV system is investigated under MPPT operation and with two simulation cases under 100% and 5% of the rated power, as shown in Figure 4.6 and Figure 4.7. The literature reported the interharmonics emission from commercial single-phase inverters, which also utilized the widely used P&O MPPT algorithm. Therefore, it has been employed in this simulation as it is extensively used in industry (Sangwongwanich et al. 2018a).

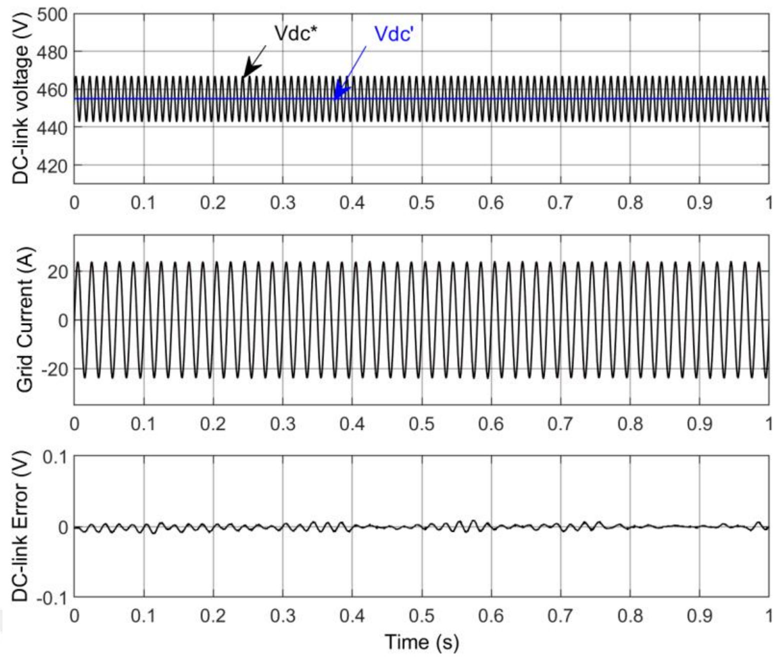

Figure 4.4. The dc-link voltage, grid current, and dc-link error of the single-phase grid-connected PV inverter under steady state and constant-voltage MPPT

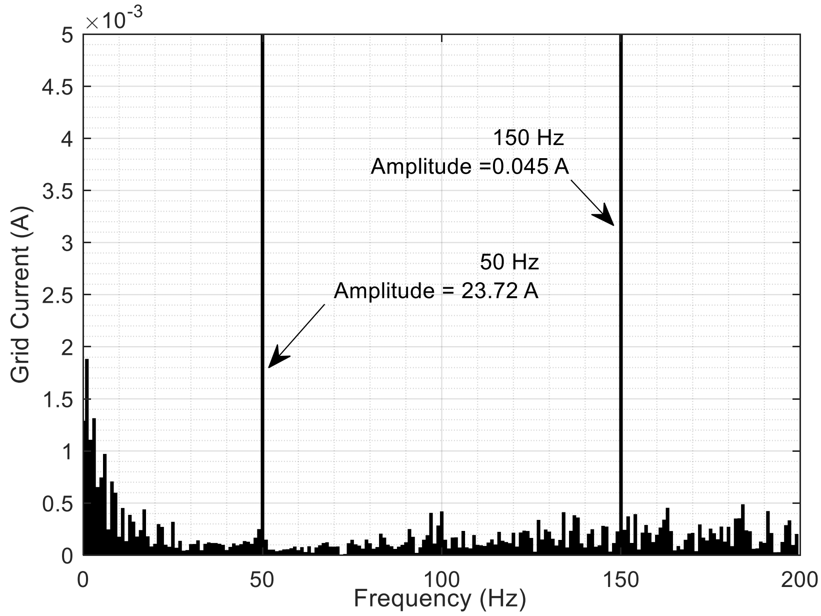

Figure 4.5. Frequency spectrum of grid current under constant-voltage MPPT operation

The hill-climbing type MPPT, e.g., P&O, maintains power oscillation during steady-state operation even under constant input irradiance and temperature. As can be observed from Figure 4.6 and Figure 4.7, the MPPT algorithm operation is stable and operates around three optimum points with similar input parameters (sampling rate, perturbation step size, and the PI dc-link controller) for both cases. This kind of operation with an MPPT sampling rate of 20 Hz is considered the optimal situation (Sangwongwanich and Blaabjerg 2019). The grid current distortion is encountered due to the perturbation, especially under low-power operating conditions, as indicated in Figure 4.7.

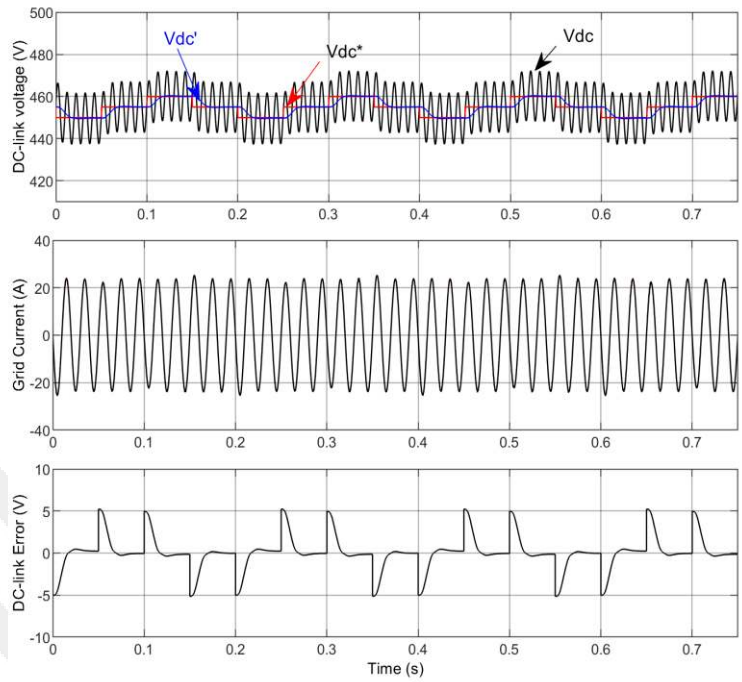

Figure 4.6. The obtained results of the PV inverter (dc-link voltage, grid current, and dc-link error) operated under 100% of the rated power

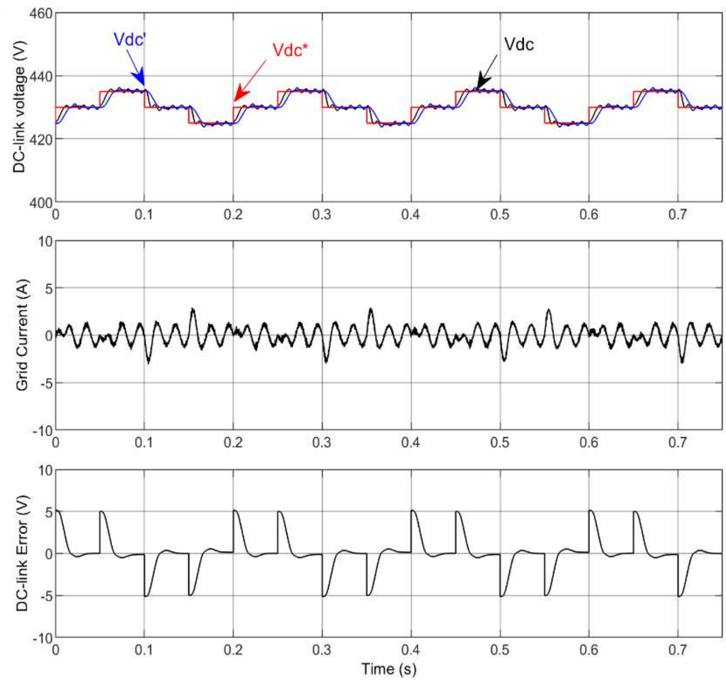

Figure 4.7. The obtained results of the PV inverter (dc-link voltage, grid current, and dc-link error) operated under 100% of the rated power

In grid-connected PV systems, the interharmonics generation process is strongly related to the operation of MPPT algorithms and the variation of the DC-link voltage. During the MPPT perturbation process, the error of the inverter's outer control loop will carry some frequency components that will be propagated through the PI controller and modulated with the grid phase angle, resulting in additional frequency components in the injected grid current. Therefore, enhancing the MPPT control structure will assist in the reduction of these frequency components. The grid current experiences periodic overshoots; these peaks are related to the parameters of the MPPT and the reason for the existence of interharmonics in the grid current, as will be discussed in the following section.

4.3. Interharmonics Characteristic and the Mechanism of Emission

To investigate the interharmonics generating characteristic in the grid current, the frequency spectrum is obtained under different operating power points, as shown in Figure 4.8, with a frequency resolution of 1 Hz. It is observed that the frequencies of interharmonics appear as a series of equally spaced components (frequency distribution). The proposed frequency separation d_h, in Hertz, between each consecutive dominant interharmonics is observed and given in (1), i.e., 10 Hz (e.g., 55 Hz, 65 Hz, 75 Hz, etc.).

$$d_h = \frac{f_{mppt}}{N} \tag{4.1}$$

Where N is the number of times the reference dc-link voltage changes its value, i.e., the MPPT step size, in one period.

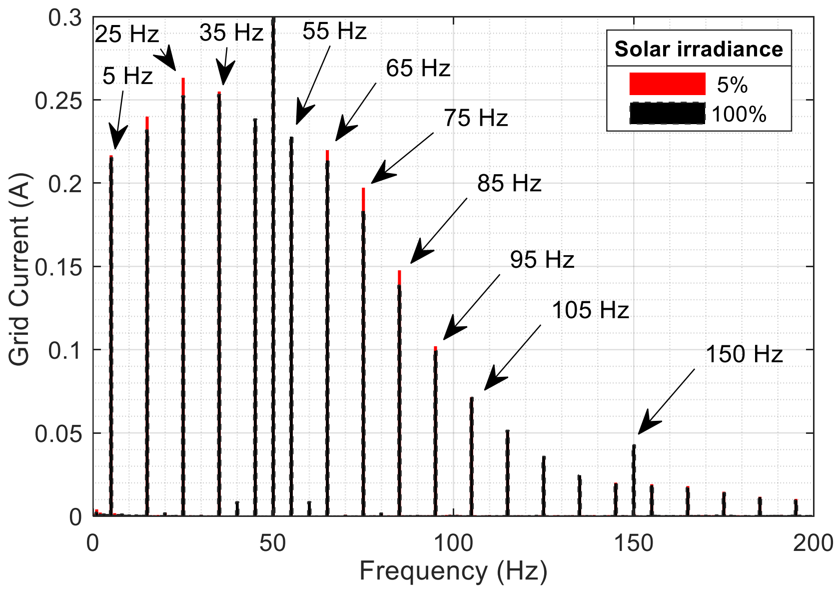

Figure 4.8. The injected grid current frequency spectrum under steady-state operating conditions for two different operating powers (100% and 5% of the rated power) and a frequency resolution of 1 Hz.

The dc-link voltage perturbation, due to the MPP searching process, will result in changing the value of the reference dc voltage V_{dc} by an amount equal to the step size of the MPPT perturbation, as shown in Figure 4.9. In addition, the frequency shift is controlled by the frequency of the reference dc-link voltage waveform, i.e., the sampling rate of the MPPT algorithm, hence $T_o = NT_{mppt}$ or $f_o = f_{mppt}/N$. This result spots the light on the frequency components in Figure 4.10 and the distance between them as indicated in (1). It can be concluded that the error in the dc-link occurs whenever the reference voltage changes its value with a specific rate corresponding to the MPPT sampling rate. The frequency components $f_{n,dc}$ of the dc-link voltage error are presented to the outer loop of the dc-link controller, which in turn will be propagated to the inner current control loop after a shifting process conducted by the amplitude modulation resulting from the multiplication with $\sin(\theta_g)$ of the grid's voltage.

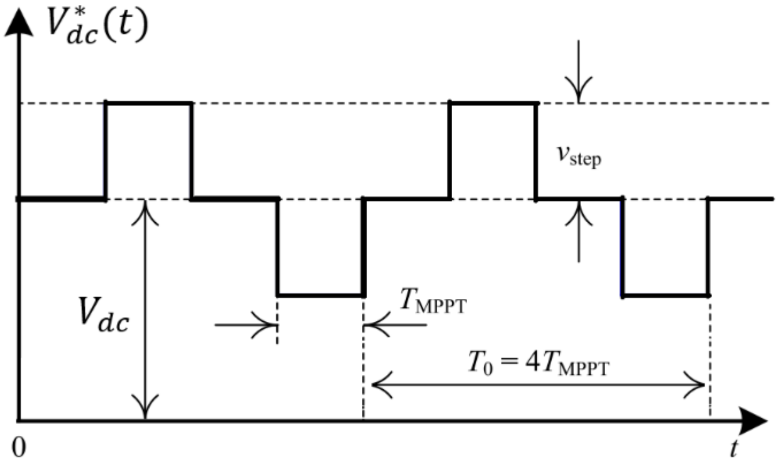

Figure 4.9. DC-link perturbations due to MPPT process

It is evident that the synchronization process is affecting the frequency distribution of interharmonics, where the nth order harmonic contributes to two frequency components. This means that $f_{n,dc}$ will be shifted by the value of f_g or $f_g \mp f_{n,dc}$, the amplitude of the original signal is equally split to these components with a 90-degree phase shift.

It is worth mentioning that the interharmonics spectrum is almost the same during the full-rated and low-power operating conditions. This conclusion can be drawn from the dc-link error values in Figure 4.6 and Figure 4.7, where the magnitude of step changes in the reference voltage are the same, which means that $f_{n,dc}$ and their amplitudes are the same for both cases.

Following the last discussion and for verification, the dc-link voltage frequency spectrum is obtained and depicted in Figure 4.10. As observed, the frequency components of interharmonics are the $n \times d_h$ where n is an odd number (e.g., 1, 3, 5, etc.). Therefore, the interharmonics frequency components of the grid current $f_{n,gh}$ are given in (14) as:

$$f_{n,gh} = f_g \mp \frac{nf_{mppt}}{N} \quad (4.2)$$

Thus, the dominant amplitudes in the grid current frequency spectrum will be the same as the ones in the spectrum of dc-link error voltage but shifted with f_g (e.g., the dominant frequency corresponding to 5 Hz, 15 Hz, and 25 Hz in the dc-link error voltage are 50±5 Hz, 50±15 Hz, and 50±25 Hz, respectively. This frequency mapping will be verified with more simulated cases in the following sections.

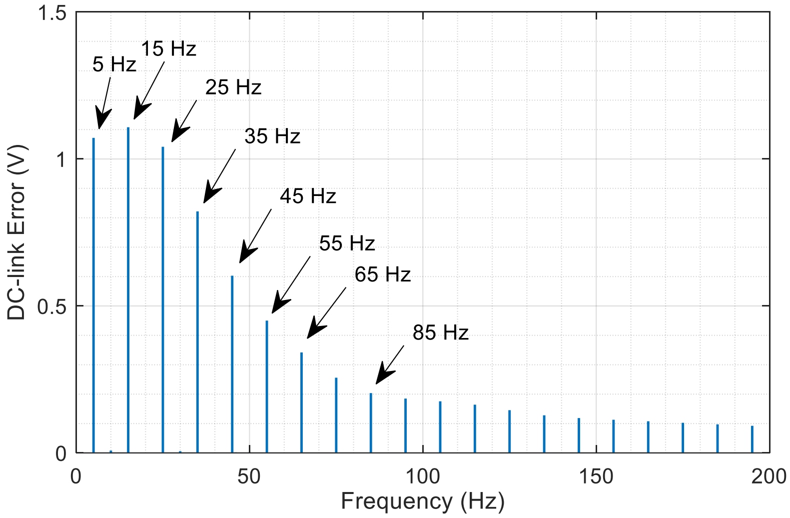

Figure 4.10. DC-link error voltage during steady-state operation of the MPPT under 5% of the rated power

4.4. Impact Of MPPT Control Parameters On Interharmonics

The last discussion and simulation results clarified that the MPPT algorithm is responsible for generating the interharmonics injected into the grid current. The analysis also indicated that the characteristics of interharmonics are almost the same under different operating power levels. Nevertheless, the frequency spectrum of the DC-link voltage and the grid current, as indicated in (2), suggests investigating the impact of MPPT controller parameters and its relation to the emission of interharmonics in single-phase grid-connected PV systems.

4.4.1. Influences of MPPT Perturbation Step Size

The perturbation step size of the MPPT algorithm is strongly related to the tracking efficiency. A larger step size will improve the tracking speed and improve the convergence process. On the other hand, it will cause steady-state power oscillation and will lead to power losses and efficiency reduction. This issue is demonstrated in Figure 4.11 for three perturbation step sizes of 2, 6, and 10 V. As can be observed, the interharmonics emission increases as the step size increases, which clearly affects the harmonics generation. It can be noticed that the amplitudes are increasing while the frequency characteristic is still the same; this is clearly shown in Figure 4.12.

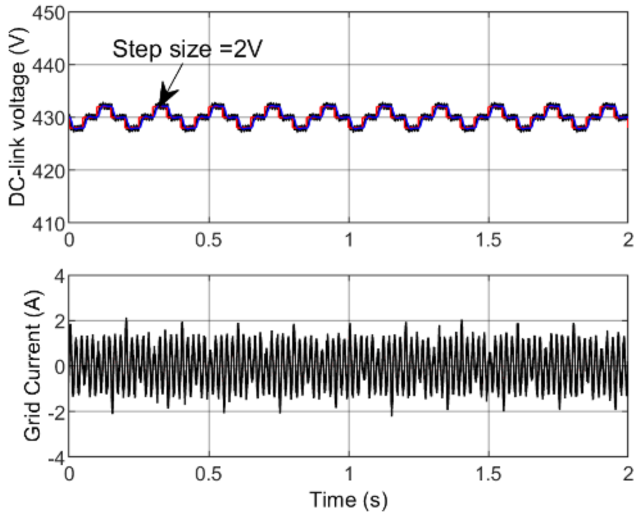

Figure 4.11. The simulation results for the on-grid PV system operated under 5% of the rated power with MPPT perturbation step size of 2 Volts

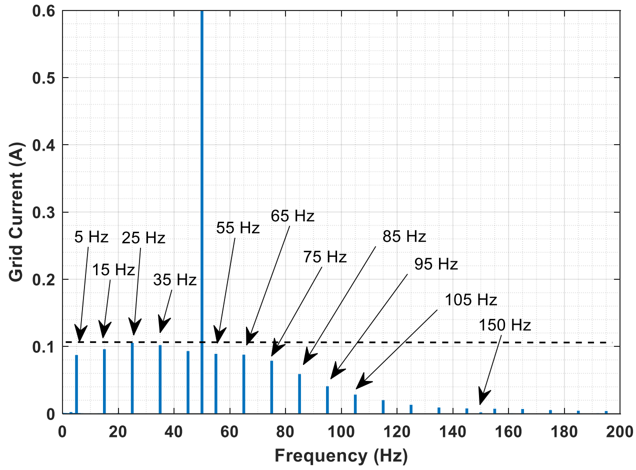

Figure 4.12. The simulation results for the on-grid PV system operated under 5% of the rated power with MPPT perturbation step size of 2 Volts

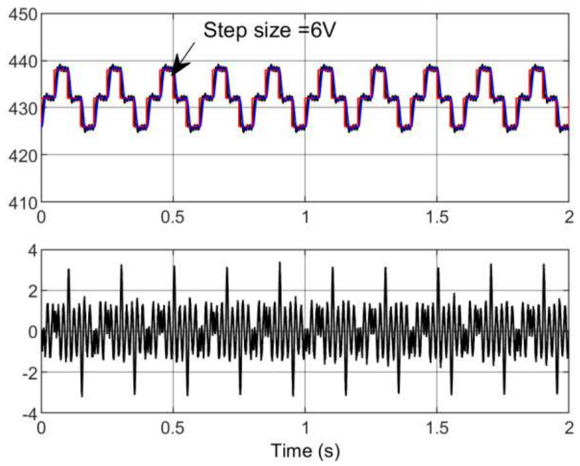

Figure 4.13. The simulation results for the on-grid PV system operated under 5% of the rated power with MPPT perturbation step size of 6 Volts

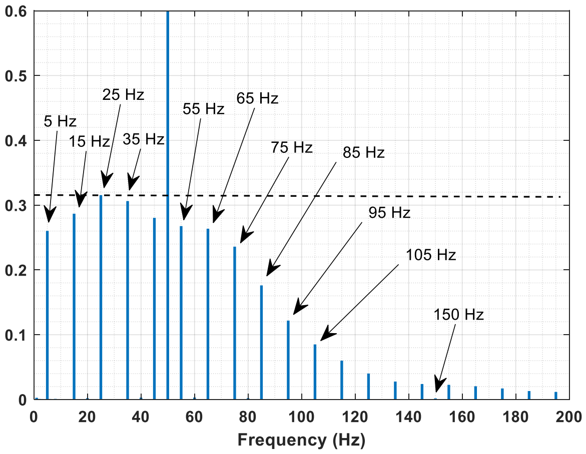

Figure 4.14. The simulation results for the on-grid PV system operated under 5% of the rated power with MPPT perturbation step size of 6 Volts

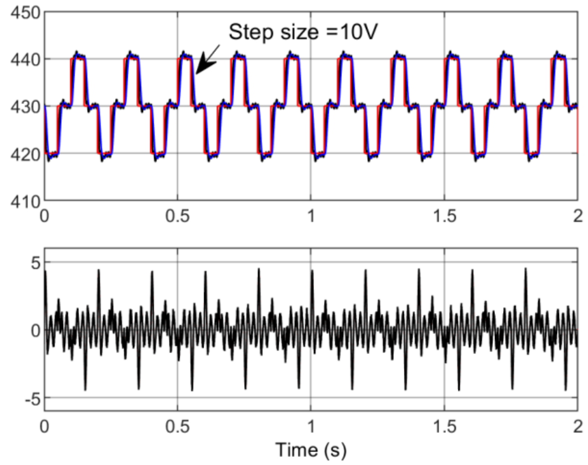

Figure 4.15. The simulation results for the on-grid PV system operated under 5% of the rated power with MPPT perturbation step size of 10Volts

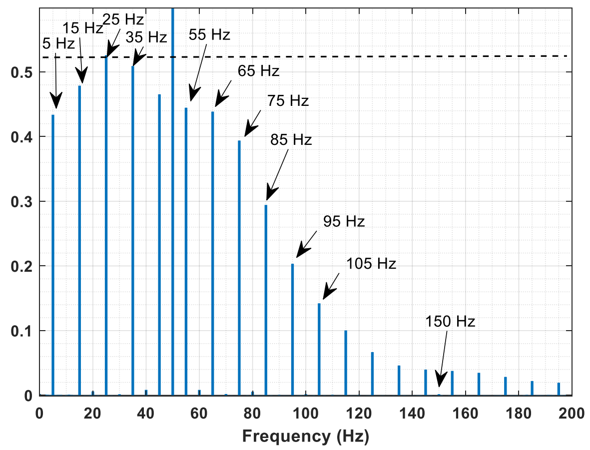

Figure 4.16. The simulation results for the on-grid PV system operated under 5% of the rated power with MPPT perturbation step size of 10Volts

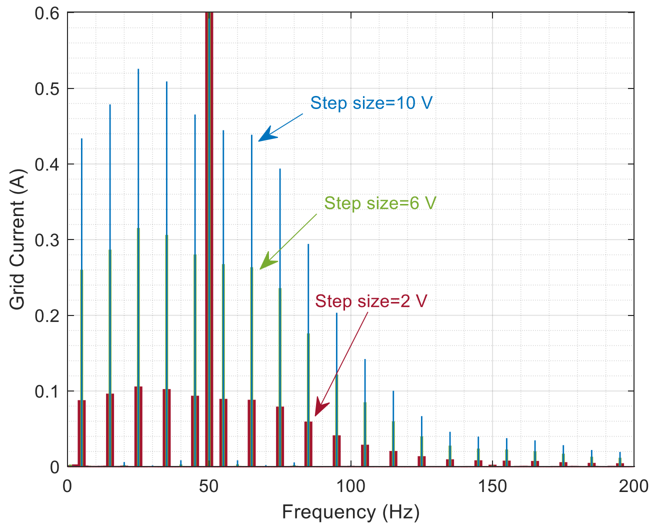

Figure 4.17. The effect of MPPT step size on the emission of interharmonics

4.4.2. Influences of MPPT Sampling Rate

The second important parameter to consider is the MPPT sampling rate. Increasing this rate will improve the tracking efficiency, especially under fast-changing irradiance conditions. Nevertheless, this rate should be limited to the steady state operation of the DC-link, where the voltage should be stabilized before the next perturbation. As reported in (Femia et al. 2005; Kivimaki et al. 2017), the optimal sampling rate is between 1 and 20 Hz.

This thesis uses the sampling rates of 8, 16, 32, and 20 Hz (used in the previous section) to show the effects above and between the optimal range. Figure 4.18 presents the simulation results; it is clearly shown that the characteristics of interharmonics increase as the sampling rate becomes faster. Moreover, the frequency spectrum of the grid current includes changing interharmonics components and amplitudes. Also, the frequency distance d_h is also increases. With the discussion mentioned above, the MPPT algorithm should be designed and modified in a way that pays attention to the step size and sampling rate of the MPPT algorithm.

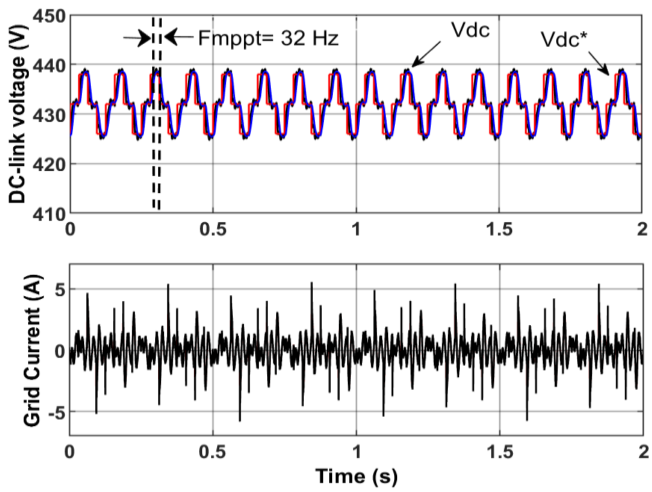

Figure 4.18. The simulation results for the on-grid PV system operated under 5% of the rated power with an MPPT sampling rate of 32 Hz

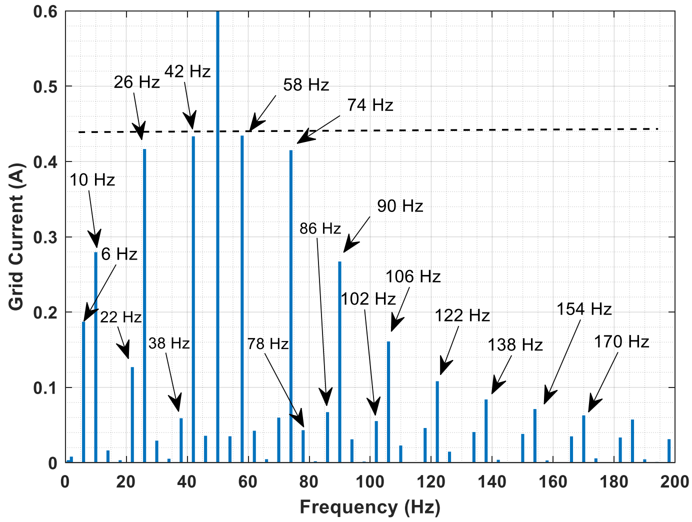

Figure 4.19. The simulation results for the on-grid PV system operated under 5% of the rated power with an MPPT sampling rate of 32 Hz

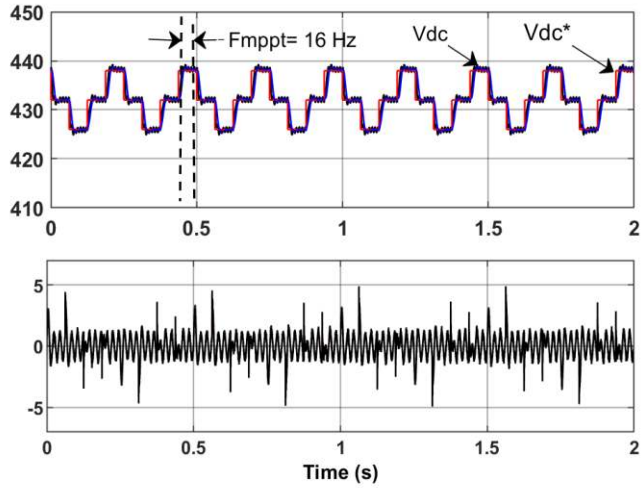

Figure 4.20. The simulation results for the on-grid PV system operated under 5% of the rated power with an MPPT sampling rate of 16 Hz

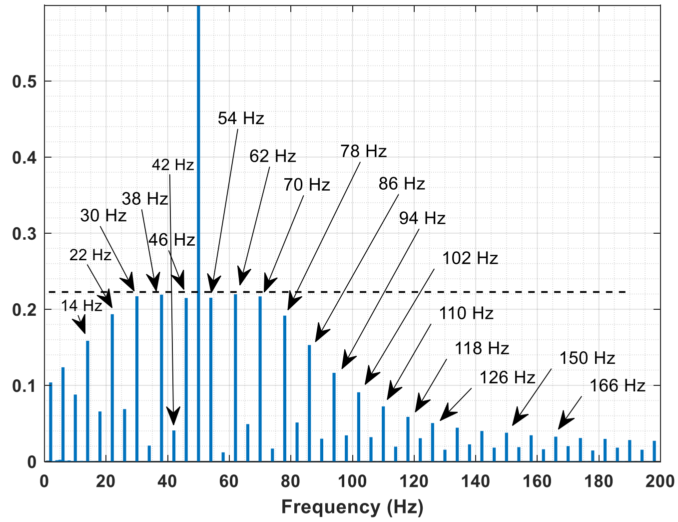

Figure 4.21. The simulation results for the on-grid PV system operated under 5% of the rated power with an MPPT sampling rate of 16 Hz

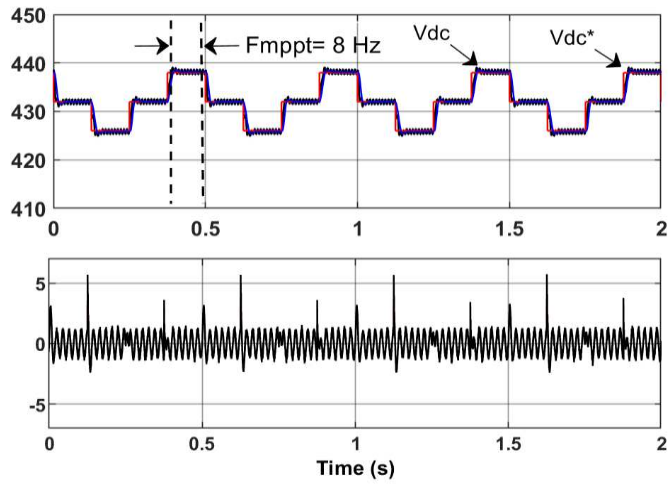

Figure 4.22. The simulation results for the on-grid PV system operated under 5% of the rated power with an MPPT sampling rate of 8 Hz

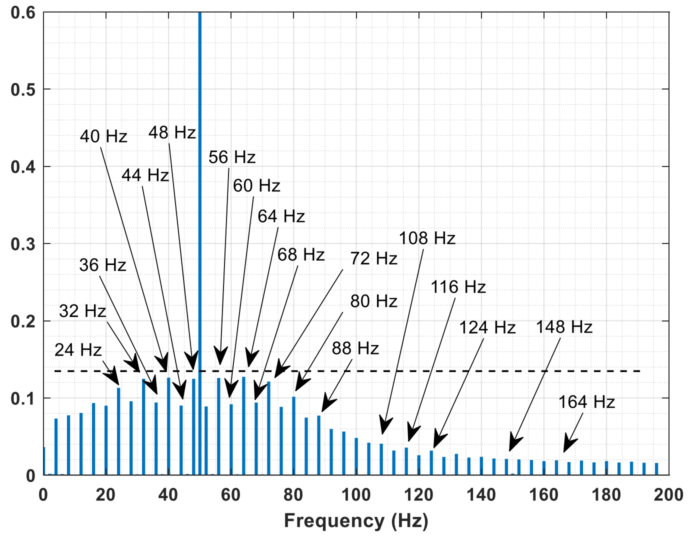

Figure 4.23. The simulation results for the on-grid PV system operated under 5% of the rated power with an MPPT sampling rate of 8 Hz

4.5. The Proposed Interharmonics Mitigation Method

This section will present the proposed interharmonics mitigation method based on a hybrid modifying technique for the step size and sampling rate of the MPPT algorithm.

4.5.1. Proposed MPPT Algorithm

Traditionally, the parameters of the MPPT algorithm are kept fixed, e.g., the step size and sampling rate, mainly to seek better tracking efficiency. The use of low perturbation step size and high MPPT sampling rate will enhance the tracking process and improve the overall efficiency, especially under variable environmental conditions, e.g., the input irradiance. However, as indicated in the previous section, this will present interharmonics, with dominant peaks injected into the grid current. This thesis proposes a method to keep the tracking efficiency within acceptable limits and reduce the interharmonics. One way to achieve this target is by randomly changing the MPPT parameters between their optimal values, e.g., the sampling rate and step size. The same concept is used for harmonic reduction by utilizing a random PWM (Blaabjerg, Pedersen, and Thoegersen 1997), and also used in (Sangwongwanich and Blaabjerg 2019) by employing a random sampling rate for the MPPT algorithm. Nevertheless, this thesis uses hybrid random MPPT parameters as the effect of step size perturbation on the interharmonics emissions is also dominant. Figure 4.24 presents a simple way to generate the randomly selected parameters V_1,V_2, f_1, and f_2. These variables can be generated using a function, such as:

$$\left[\, V_{step}(V_1, V_2), f_{mppt}(f_1, f_2) \,\right] = \begin{cases} V_1, f_1 & X \leq \dfrac{1}{2} \\ V_2, f_2 & X > \dfrac{1}{2} \end{cases} \tag{4.3}$$

Where X is a random number between 0 and 1, V_1,V_2 are the small and big step sizes, and f_1, f_2 are the slow and fast rates of the proposed MPPT algorithm, respectively. Figure 4.24 and Figure 4.25 shows the resulting random characteristics of the MPPT parameters (i.e., step size and sampling rate).

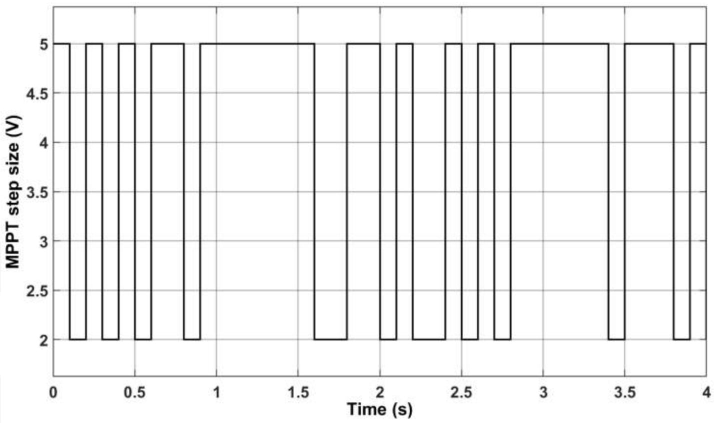

Figure 4.24. The randomly generated step size of perturbation of the MPPT algorithm (between 2 and 5 Volts)

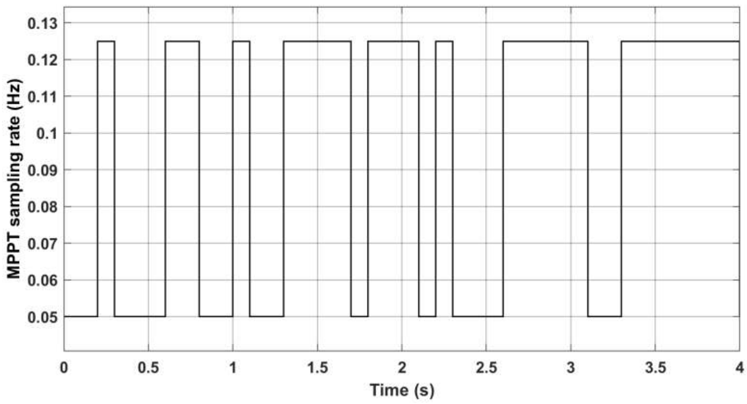

Figure 4.25. The randomly generated sampling rate of the MPPT algorithm (between 8 and 20 Hz)

Figure 4.24 and Figure 4.25 demonstrate the generated random step sizes and MPPT sampling rates. As proposed, the selected values are located within the optimal range for the MPPT parameters. It is worth mentioning that the other parameters are maintained, as in the cases discussed in the last section. Figure 4.24 and Figure 4.25 show the effect of the proposed method; it is reflected directly in the dc-link perturbation process. Also, the changeable state of the DC-link voltage is clearly shown due to the random step size and sampling rate selection of the MPPT method.

4.5.2. Reduction of Interharmonics

The generated random MPPT parameters, i.e., step sizes and sampling rates, are applied to the system, and the simulation results are shown in Figure 4.26 to Figure 4.31. The resulting DC-link perturbation and grid current are presented under random step sizes, as shown in Figure 4.26, random sampling rates, as shown in Figure 4.27, and with combined hybrid random variables, as shown in Figure 4.28. It is clearly shown in Figure 4.26 to Figure 4.28 that the dc-link voltage perturbation and the grid current variation are less than that in Fig. 4-(b), and the best case is obtained for Figure 4.28. The frequency spectrums of the grid currents comparing the interharmonics characteristics between these cases are shown in Figure 4.29. The minimum peak value between the dominant individual interharmonics components is 0.08 A, which belongs to the hybrid random variable method. If this value is compared with 0.26 A, 0.16 A, and 0.11 A obtained from the fixed step size and sampling rate, random step sizes, and random sampling rate, it is almost three times less than the peak value with fixed MPPT parameters. Moreover, this random process resulted in a distributed frequency distribution, which assists the stability by avoiding the trigger of specific undamped resonances created by interharmonics.

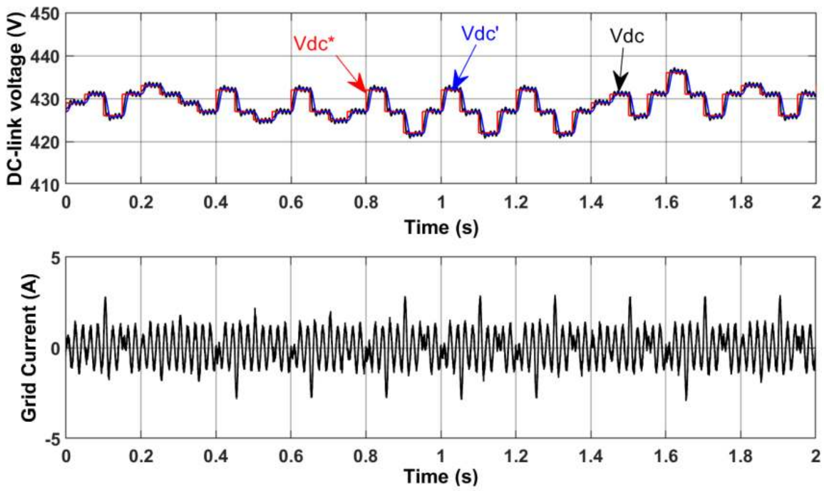

Figure 4.26. The simulation results for the on-grid PV system operated under 5% of the rated power with the modified MPPT algorithm under random step size condition

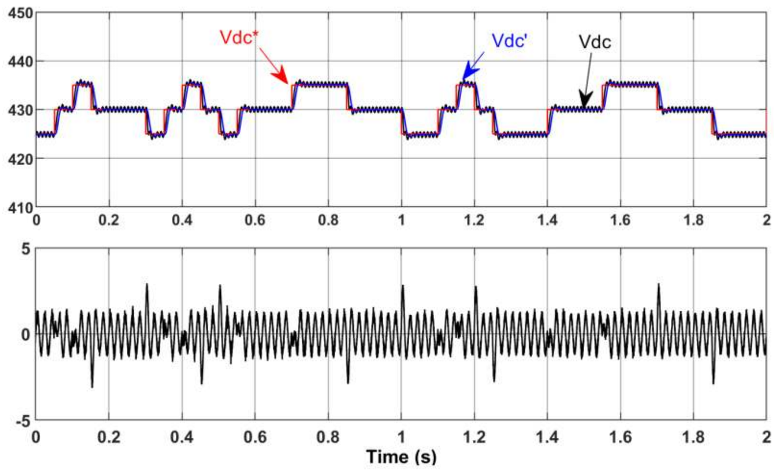

Figure 4.27. The simulation results for the on-grid PV system operated under 5% of the rated power with the modified MPPT algorithm under random sampling rate condition

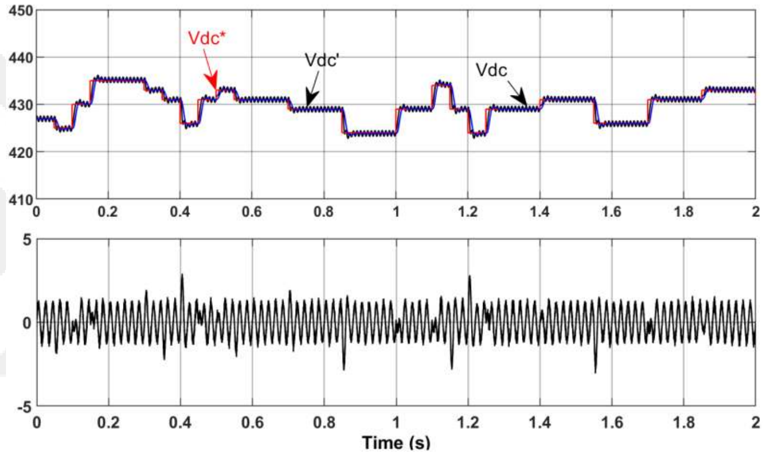

Figure 4.28. The simulation results for the on-grid PV system operated under 5% of the rated power with the modified MPPT algorithm under the hybrid method (random step size and sampling rate)

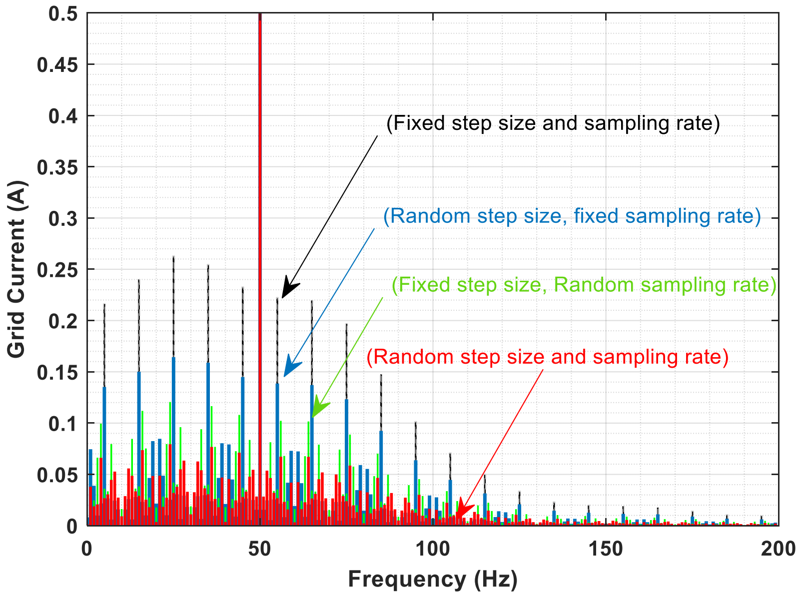

Figure 4.29. Frequency spectrum of grid current, comparison between the mitigation methods

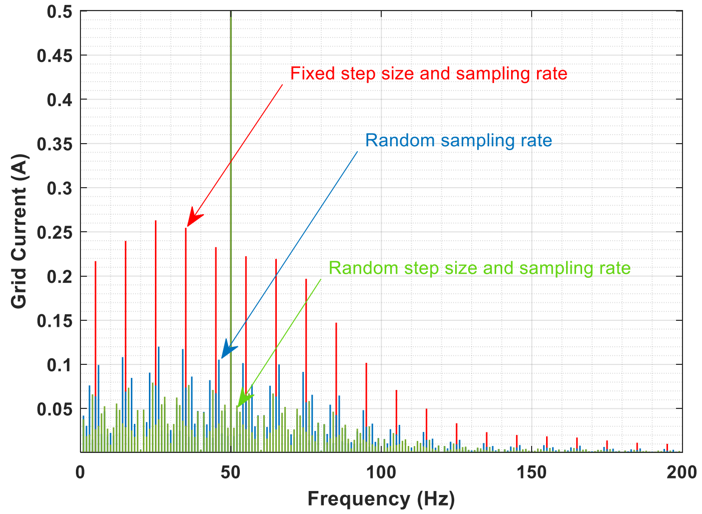

Figure 4.30. Frequency spectrum of grid current, comparison between the mitigation methods

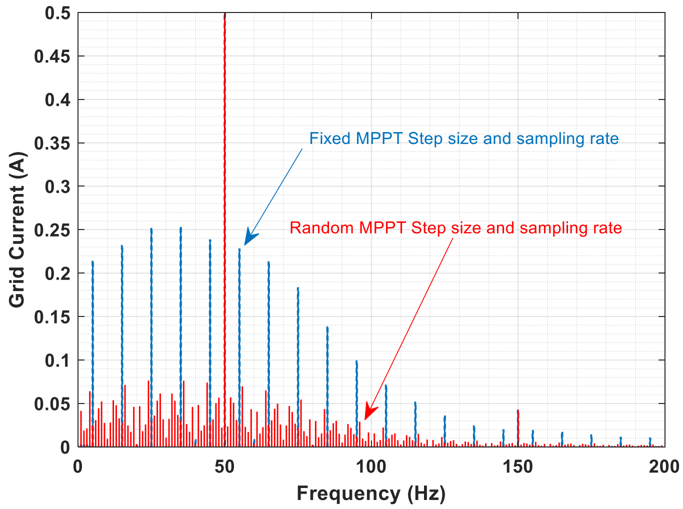

Figure 4.31. Frequency spectrum of grid current, comparison between the conventional and proposed method

4.6. Efficiency of the Proposed MPPT Algorithm

To investigate the tracking efficiency of the proposed MPPT algorithm, a trapezoidal solar irradiance profile is utilized to observe the MPPT operation under ramping and steady-state conditions. The efficiency η_{mppt} calculation of MPPT is based on $\eta_{mppt} = E_{pv}/E_{av}$, where E_{pv} is the extracted PV energy from the PV power P_{pv}, and E_{av} is the available power. Table 4.2 compares the efficiency between the proposed method (case 4), the traditional MPPT (case 1, 2, 7, and 8), and the ones found in the literature (cases 3 and 9). It is evident that the highest obtained efficiency is for the minimum step size (i.e., 2 V) and the maximum sampling rate (i.e., 20 Hz). The MPPT tracking efficiencies with a fixed lower (V1=2 V, F1= 8 Hz) and upper (V2 = 5 V, F2= 20 Hz) MPPT input parameters are 97.63 % and 97.22 %, respectively. On the other hand, the tracking efficiency of the proposed method is obtained at 97.34 %, which is within the value of these cases. However, the emission of interharmonics is three times lower than the conventional method, as indicated in Table 4.2. Therefore, an efficient interharmonics mitigating solution is achieved with the proposed technique.

Table 4.2. The obtained efficiency of different MPPT parameters and their impact on the emission of interharmonics

Simulated cases	V_{step} **(V)**	f_{mppt} **(Hz)**	η **(%)**	**Interharmonics emission**
Case 1	2	20	97.63	+++++
Case 2	5	20	97.59	++++++
Case 3	5	Random	97.37	+++
Case **4**	**Random**	**Random**	**97.34**	**+**
Case 5	Random	8	97.31	+++
Case 6	Random	20	97.27	+++
Case 7	5	8	97.25	+++++
Case 8	2	8	97.22	++++
Case 9	2	Random	97.20	++

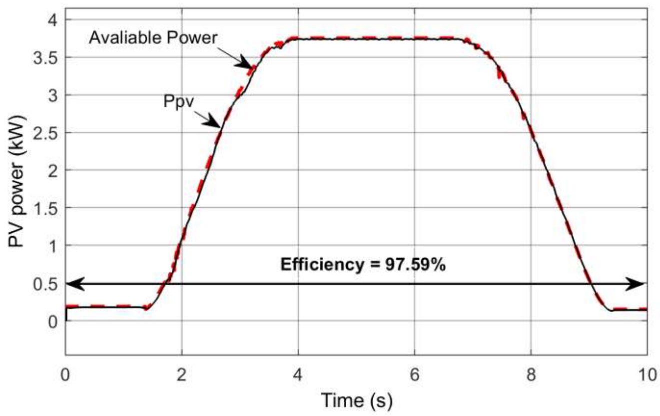

Figure 4.32. The efficiency resulted from the extracted PV power under trapezoidal irradiance conditions for case 2

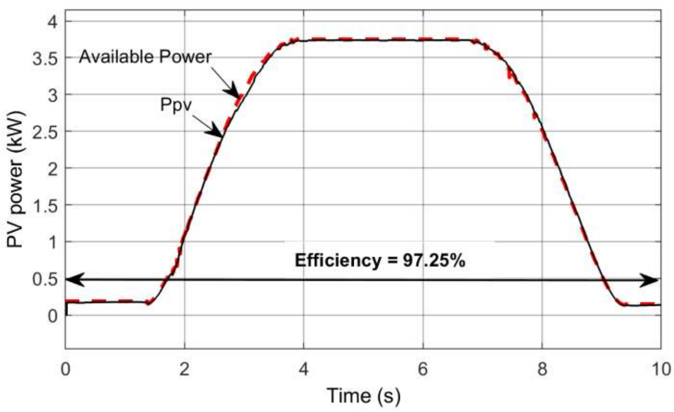

Figure 4.33. The efficiency resulted from the extracted PV power under trapezoidal irradiance conditions for case 7

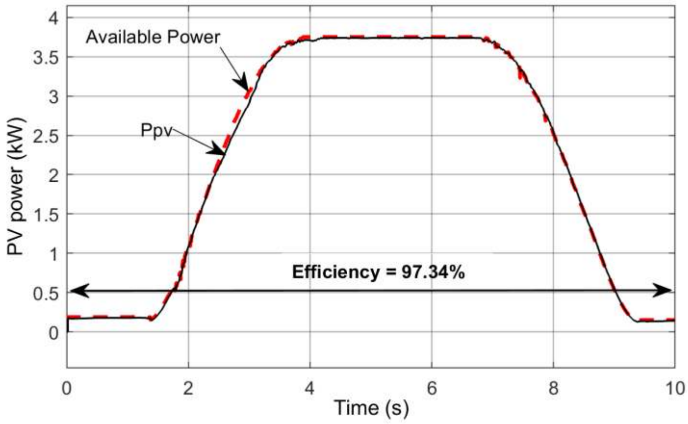

Figure 4.34. The efficiency resulted from the extracted PV power under trapezoidal irradiance conditions for case 4

4.7. Modeling of Interharmonics

The mathematical modeling of interharmonics is considered the first step toward an accurate mitigation technique for this problem. It was mentioned before that the DC-link voltage perturbation is the main reason behind interharmonics, and this perturbation is caused by the oscillations of the MPPT method. Also, mathematical modeling is required to map the effect of the MPPT parameters, i.e., the sampling rate and the step size, on the interharmonics generating characteristic. This process may be divided into four main steps: firstly, DC-link voltage variations should be represented accurately; secondly, the response to these components of the DC-link voltage should be obtained; thirdly, the effect of the grid synchronization process should be implemented, i.e., amplitude modulation. Finally, model validation should be carried out to compare the results of the proposed mathematical model with those of the simulation.

4.7.1. Representation of the DC-link Voltage

Mathematical development is proposed to investigate the impacts of the MPPT parameters on the emission of interharmonics, i.e., the sampling rate and the step size, and explain the generating characteristic of interharmonics. Due to the MPPT algorithm oscillation, the dc-link voltage is perturbated between three optimum points, which represent the steady-state operation with a fundamental period of $T = 4T_{mppt}$, where $T_{mppt} = 1/f_{mppt}$ (for $P\&O$ method). The interharmonics generation is highly dependent on this oscillation, and the representation of the input signal is required. Fourier series is one way to represent the DC-link voltage, and it has the advantage of decomposing the input signal into multiple components. The perturbation of dc-link voltage can be written as:

$$V_{dc}^{*}(t) = \begin{cases} V'_{dc} & 0 \leq t < T_{mppt} \\ V'_{dc} + V_{step} & T_{mppt} \leq t < 2T_{mppt} \\ V'_{dc} & 2T_{mppt} \leq t < 3T_{mppt} \\ V'_{dc} - V_{step} & 3T_{mppt} \leq t < 4T_{mppt} \end{cases} \tag{4.4}$$

Where V'_{dc} is the average dc-link voltage, $V_{step}, f_{mppt} = 1/T_{mppt}$ are the perturbation step size and sampling rate of the MPPT algorithm, respectively. It can be noticed that this representation contains the parameters of the MPPT algorithm, which will be used to map the effects of these parameters on the generation of the interharmonics. By utilizing Fourier analysis, the Fourier series and its coefficients can be written as:

$$V_{dc}^{*} = a_0 + \sum_{1}^{\infty} a_n \cos\left(\frac{2\pi nt}{T}\right) + b_n \sin\left(\frac{2\pi nt}{T}\right) \tag{4.5}$$

Where:

$$a_0 = \frac{2}{T}\int_0^T V_{dc}^{*}(t)\, dt \tag{4.6}$$

$$a_n = \frac{2}{T}\int_0^T V_{dc}^{*}(t) \cos\left(\frac{2\pi nt}{T}\right) dt \tag{4.7}$$

$$b_n = \frac{2}{T}\int_0^T V_{dc}^{*}(t) \sin\left(\frac{2\pi nt}{T}\right) dt \tag{4.8}$$

Where n denotes the harmonic order, a_0, a_n, b_n are the Fourier coefficients for the dc-component and the nth order harmonics. The Fourier series coefficients in (4.6) to (4.8) are calculated for V_{dc}^{*} in (4.4) as the following:

$$a_0 = \frac{2}{T}\left[\int_0^{T_{mppt}} V'_{dc}\, dt + \int_{T_{mppt}}^{2T_{mppt}} V'_{dc} + V_{step}\, dt + \int_{2T_{mppt}}^{3T_{mppt}} V'_{dc}\, dt + \int_{3T_{mppt}}^{4T_{mppt}} V'_{dc} - V_{step} dt\right] \tag{4.9}$$

Substituting $T = 4T_{mppt}$ and compute the integrations, yields:

$$a_0 = V'_{dc} \tag{4.10}$$

$$a_n = \frac{2}{4T_{mppt}} \left[\int_0^{T_{mppt}} V'_{dc} \, cos\left(\frac{2\pi nt}{4T_{mppt}}\right) dt \right.$$
$$+ \int_{T_{mppt}}^{2T_{mppt}} \left(V'_{dc} + V_{step}\right) \; cos\left(\frac{2\pi nt}{4T_{mppt}}\right) dt$$
$$+ \int_{2T_{mppt}}^{3T_{mppt}} V'_{dc} \, cos\left(\frac{2\pi nt}{4T_{mppt}}\right) dt \tag{4.11}$$
$$\left. + \int_{3T_{mppt}}^{4T_{mppt}} \left(V'_{dc} - V_{step}\right) \; cos\left(\frac{2\pi nt}{4T_{mppt}}\right) dt \right]$$

With computing each integration, yields:

$$a_n = \frac{2}{4n\pi T_{mppt}} \left[2T_{mppt} V'_{dc} \sin\left(\frac{\pi n}{2}\right) + 2T_{mppt}\left(V'_{dc} + V_{step}\right) \sin\left(\frac{\pi n}{2}\right) - \sin\left(\frac{\pi n}{2}\right) \right.$$
$$- \left(2T_{mppt} V'_{dc} \sin\left(\frac{\pi n}{2}\right) - \sin\left(\frac{3\pi n}{2}\right)\right) \tag{4.12}$$
$$\left. + 2T_{mppt}\left(V'_{dc} - V_{step}\right) \sin(2\pi n) - \sin\left(\frac{3\pi n}{2}\right) \right]$$

Yields:

$$a_n = \frac{-V_{step}}{n\pi} \left[\sin\left(\frac{\pi n}{2}\right) - \sin\left(\frac{3\pi n}{2}\right) \right] \tag{4.13}$$

The second term is zero for even n. In the same way, to find bn:

$$b_n = \frac{2}{4T_{mppt}} \left[\int_0^{T_{mppt}} V'_{dc} \, sin\left(\frac{2\pi mt}{4T_{mppt}}\right) dt \right.$$
$$+ \int_{T_{mppt}}^{2T_{mppt}} \left(V'_{dc} + V_{step}\right) \; sin\left(\frac{2\pi mt}{4T_{mppt}}\right) dt$$
$$+ \int_{2T_{mppt}}^{3T_{mppt}} V'_{dc} \, sin\left(\frac{2\pi mt}{4T_{mppt}}\right) dt \tag{4.14}$$
$$\left. + \int_{3T_{mppt}}^{4T_{mppt}} \left(V'_{dc} - V_{step}\right) \; sin\left(\frac{2\pi mt}{4T_{mppt}}\right) dt \right]$$

With computing each integration, yields:

$$b_n = \frac{2}{4n\pi T_{mppt}} \Big[4T_{mppt}V'_{dc}\sin\left(\frac{\pi n}{4}\right)^2 - \left(2T_{mppt}\left(V'_{dc} + V_{step}\right)\cos(\pi n) - \cos\left(\frac{\pi n}{2}\right)\right) + (2T_{mppt}V'_{dc}\cos(\pi n) - \cos\left(\frac{3\pi n}{2}\right) - \left(2T_{mppt}\left(V'_{dc} - V_{step}\right)\cos(2\pi n) - \cos\left(\frac{3\pi n}{2}\right)\right)\Big] \tag{4.15}$$

Or,

$$b_n = \frac{-2\left(\cos\left(\frac{\pi n}{4}\right)^2 - 1\right)}{n\pi} \left[\mathrm{v_{step}} + 2\mathrm{v_{step}}\cos\left(\frac{\pi n}{2}\right)\mathrm{v_{step}} + 4\mathrm{v_{dc}}\cos\left(\frac{\pi n}{2}\right)^2 - 4\mathrm{v_{step}}\cos\left(\frac{\pi n}{2}\right)^2 \right] \tag{4.16}$$

Or,

$$b_n = \frac{-2(\alpha - 1)}{n\pi} \left[\mathrm{v_{step}} + 2\,\beta\,\mathrm{v^2_{s\,tep}} + 4V'_{dc}\beta^2 - 4\mathrm{v_{step}}\,\beta^2 \right] \tag{4.17}$$

Where:

$$\alpha = \cos\left(\frac{\pi n}{4}\right)^2, \qquad \beta = \cos\left(\frac{\pi n}{2}\right) \tag{4.18}$$

The DC-link voltage can be written in a single sinusoid form as:

$$V^*_{dc,n} = a_0 + \sum_{1}^{\infty} A_n\, sin(\omega_n t + \phi_n) \tag{4.19}$$

Where

$$A_n = \sqrt{a_n^2 + b_n^2} \tag{4.20}$$

$$\phi = \tan^{-1}\left(\frac{a_n}{b_n}\right) \tag{4.21}$$

The output of the dc-link voltage controller can be calculated for each frequency component represented by the decomposed V^*_{dc} utilizing the individual transfer functions implementing the outer-loop of the DC-link voltage controller, as shown in Figure 4.35 (Teodorescu, Liserre, and Rodriguez 2011), (Yang et al. 2019). This model is based on the practical assumption that the inner-loop dynamics are faster than the outer-loop, and thus, the current (inner) and the voltage (outer) control-loops are decoupled. The rearrangement in the control structure is performed to obtain the grid current (amplitude) response to the perturbation in the dc-link voltage. The system can be simplified further to have the closed-form transfer function, as shown in Figure 4.35-(b).

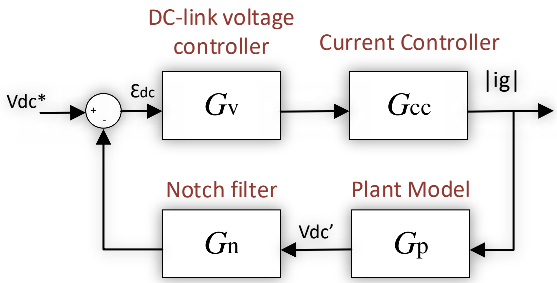

(a)

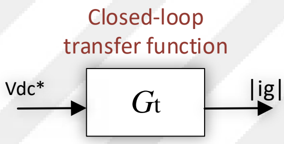

(b)

Figure 4.35. The outer control-loop of the dc-link voltage controller: (a) the block diagram of the transfer functions from the reference dc-link voltage to the grid current, and (b) the equivalent closed-loop transfer function

The transfer functions $G_v(s)$, $G_{cc}(s)$, $G_p(s)$, and $G_n(s)$ are the dc-link voltage controller, the current controller, the plant, and the notch filter, respectively; the total closed-loop transfer function is given by $G_t(s)$. These transfer functions are defined as the following:

$$G_v(s) = K_p + \frac{K_i}{S} \tag{4.22}$$

$$G_P(s) = \frac{V_g}{\sqrt{2}\, C_{dc} V'_{dc} S} \tag{4.23}$$

$$G_{cc}(s) = \frac{1}{1 + 3T_s S} \tag{4.24}$$

$$G_{cc}(s) = \frac{S^2 + \omega_h^2}{S^2 + k_h S + w_h^2} \tag{4.25}$$

$$G_t(s) = \frac{G_v(s)G_{cc}(s)}{1 + G_v(s)G_{cc}(s)G_n(s)G_p(s)} \tag{4.26}$$

Where K_p, K_i are the proportional and integral constants of the dc-link PI controller, V_g is the root-mean-square of the grid voltage, T_s is the sampling period of the digital controller, and k_h, w_h are the quality factor and frequency of the notch filter. The frequency response of the total transfer function at the nth order harmonic can be calculated at steady state by substituting $s = j\omega_n$, or $|G_t(j\omega_n)|\angle G_t(j\omega_n)$. Therefore, the amplitude and phase of the grid current at the nth order harmonic can be obtained as:

$$\left|i_g\right|_n(t) = A_n|G_t(j\omega_n)| \sin(\omega_n t + \angle G_t(j\omega_n) + \phi_n) \tag{4.27}$$

By summing the individual harmonic components, the amplitude grid current can be obtained (using the superposition principle):

$$|i_g|(t) = A_n|G_t(j\omega_n)| \sum_{n=1}^{\infty} \sin(2\pi f_n t + \angle G_t(j\omega_n) + \phi_n) \tag{4.28}$$

This analysis concludes that the closed-loop system's frequency response has modified the output signal's amplitude and phase angle. This affects changing the peaks of interharmonics without any change in their frequencies. The variation in interharmonics frequencies is standing behind the process of grid synchronization, which resulted from the amplitude modulation between the wideband spectrum of $i_g(t)$ and $\sin(\theta_g)$ of the grid system. The grid current can be mathematically calculated as:

$$|i_g|(t) \times \sin(2\pi f_g t) = A_n|G_t(j\omega_n)| \sum_{n=1}^{\infty} \sin(2\pi f_g t) \sin(2\pi f_n t + \angle G_t(j\omega_n) + \phi_n) \tag{4.29}$$

$$= \frac{A_n}{2}|G_t(j\omega_n)| \sum_{n=1}^{\infty} \left[cos\left(2\pi t(f_g - f_n) + \angle G_t(j\omega_n) + \phi_n\right) - cos\left(2\pi t(f_g + f_n) + \angle G_t(j\omega_n) + \phi_n\right)\right] \tag{4.30}$$

4.7.2. DC Link Voltage Based on the Mathematical Modeling

The main objective of the previous work is to decompose the DC-link voltage into multiple components; in this way, the output response of the controller can be determined for each frequency component. Figure 4.36 shows the close loop system with each transfer function to every block, which contains the PI controller, current controller, plant, and the notch filter transfer functions, respectively. For this close loop system, the assumption is that the dynamics of the inner loop are faster than the outer loop is held, and thus, the loops are decoupled.

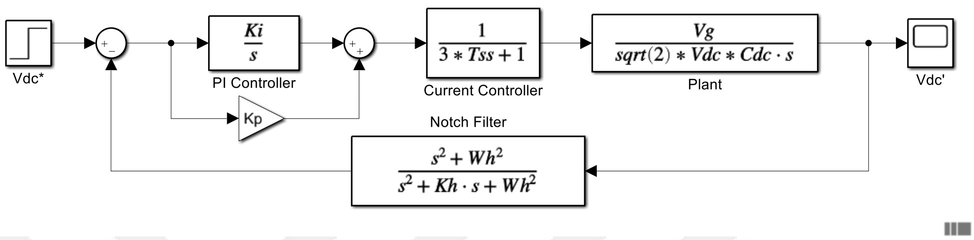

Figure 4.36. The control loop of the DC-link voltage, the transfer function of measured VDC to the reference value

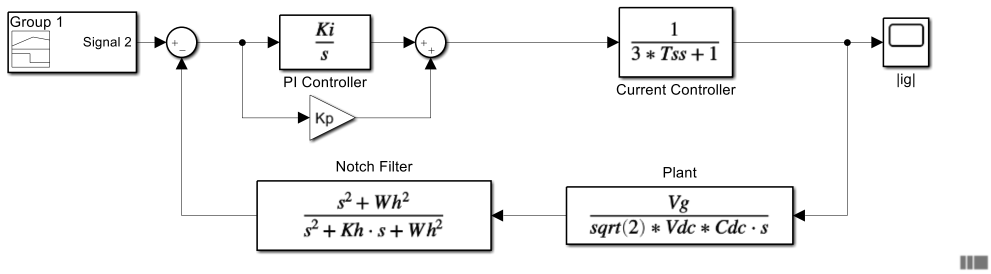

Figure 4.37. The control loop of the DC-link voltage: (a) the transfer function of measured VDC to the reference value, and (b) is the transfer function to the amplitude of the grid current

The resulting frequency response output of the simulated system is shown below for the case of 2 Hz and 20 Hz MPPT sampling rates, respectively. Figure 4.38 shows the frequency response to the DC-link, whereas Figure 4.39 depicts the analysis for the gid current.

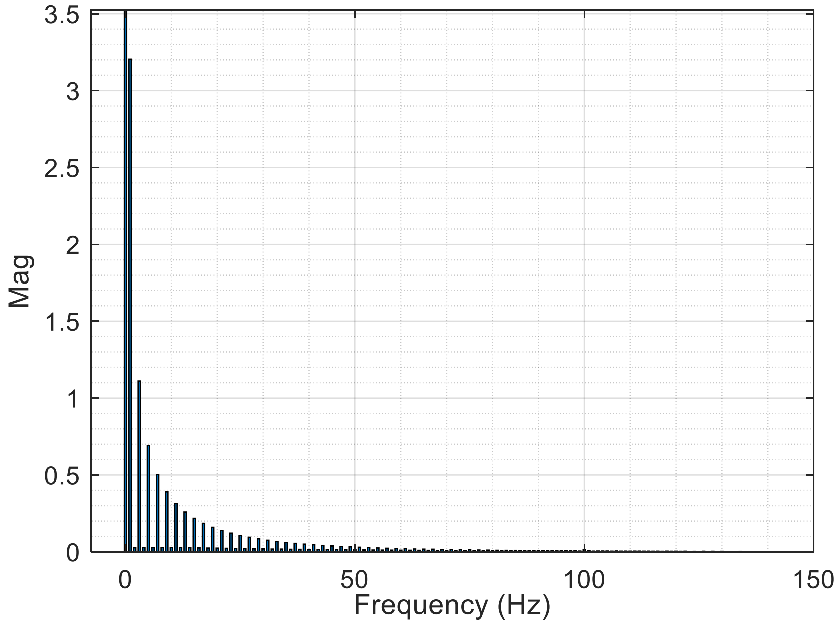

Figure 4.38. The frequency response of the measured VDC

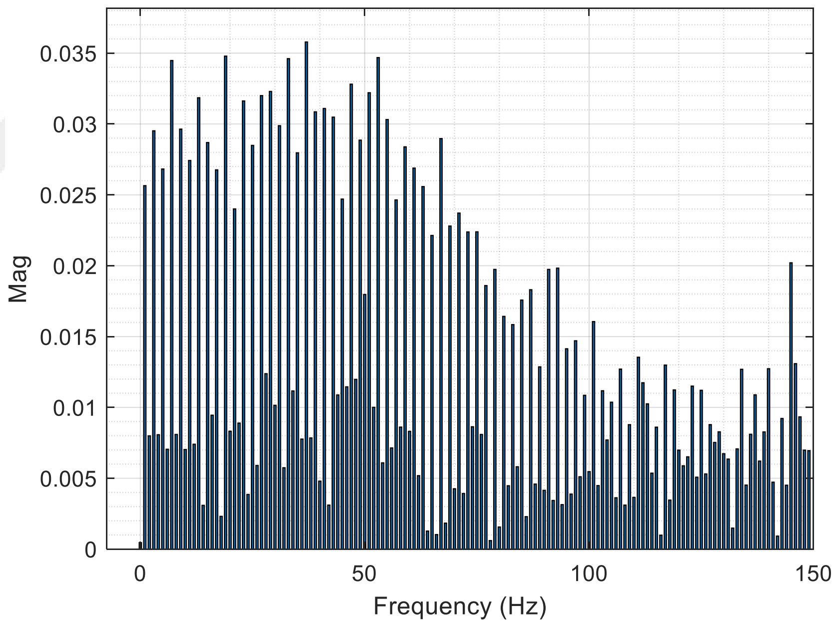

Figure 4.39. The frequency response of the grid current

In the case of 20 Hz MPPT sampling frequency, the results are shown below:

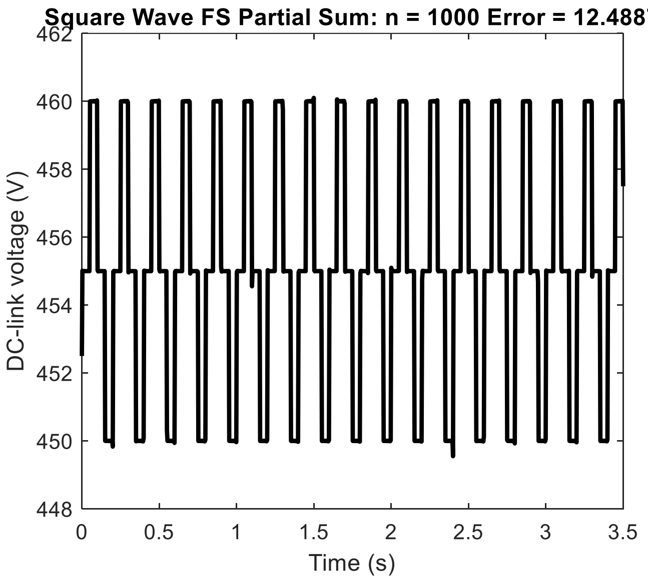

Figure 4.40. The DC-link voltage of the reference signal

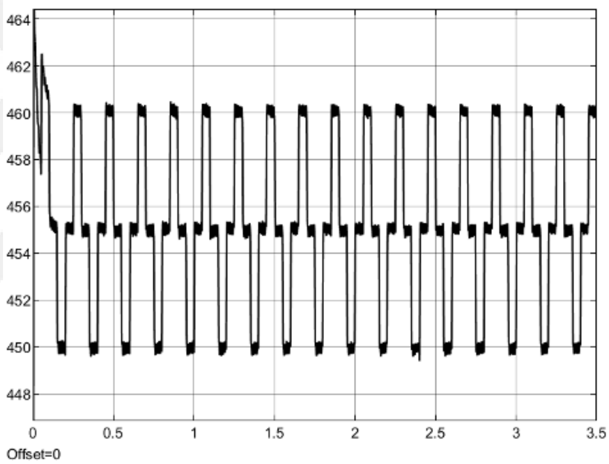

Figure 4.41. The DC-link voltage of the measured output

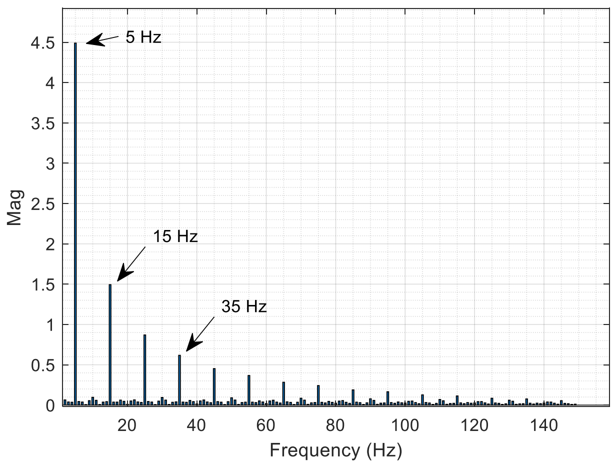

Figure 4.42. Frequency response of the DC link based on mathematical modeling

4.8. Summary

This chapter provides an extensive simulation analysis to investigate the generating characteristics and mechanism emissions for interharmonics with the developed single-phase grid-connected PV system. The primary origin behind interharmonics and the impact of the MPPT control parameters are considered in detail. The proposed mathematical expressions are developed to predict the frequency allocation of each interharmonics under the variation of the MPPT algorithm control parameters.

Accordingly, a mathematical development is proposed for the mitigation technique applied to the MPPT algorithm to reduce the peaks of interharmonics while maximizing its performance characteristics. Additionally, the control parameters are linked to the variation in the DC-link voltage mathematically, and the developed model simulates the effect of the generated and injected interharmonics in the DC-link voltage error. The proposed mitigation is applied to modify the MPPT operation and compared with other methods found in the literature, showing superior performance.

5. INVESTIGATIONS OF INTERHARMONICS EMISSIONS UNDER DIFFERENT OPERATING CONDITIONS

5.1. introduction

For a better understanding of interharmonics generating characteristics and emissions, more investigations with extensive analysis and case studies for the enhanced control structure of the developed single-phase grid-connected PV system are presented in this chapter. The analysis includes the application of the developed mitigation technique to different proposed MPPT algorithms, which include modified step voltage P&O (MP&O-v), modified sampling frequency P&O (MP&O-f), hybrid random step voltage-sampling frequency P&O (MP&O), modified step voltage InCon (MInCon -v), modified sampling frequency InCon (MInCon -f), hybrid random step voltage-sampling frequency InCon (MInCon), and neural network MPPT algorithms, respectively. Also, the proposed methods are compared to CV, P&O, and InCon MPPT algorithms. The enhanced control structure is developed to mitigate interharmonics using the proposed methods and includes multimission, such as dynamic grid support, LVRT, analysis of grid frequency deviation, and investigations of DC-link capacitance variations.

In practical situations, the grid-connected PV inverter is integrated into the grid side, and due to uncertainty in its operating conditions, it may raise significant issues at PCC and be considered a source of abnormalities. Different kinds of PQ disturbances affect the PV inverter from the grid side and the integrated PV inverter and their interaction, e.g., harmonics and interharmonics, voltage sag /swell, and frequency variations due to power mismatch between the load (grid) and the source (PV system). These disturbances can affect the grid-connected PV inverter's performance and even challenge the system's overall stability. For instance, the frequency variation primarily influences the current controller, which is frequency-dependent, such as the PR controllers, and leads to distortion of the injected current into the grid. Besides, recent studies revealed that single-phase grid-connected PV systems are considered a source of interharmonics, which are generated and injected with the delivered power to the grid. Therefore, special attention should be paid to the inverter and the grid sides. In addition, faults may occur from the grid side, which results in isolating the grid-connected PV inverter and may accelerate the collapse of the entire distribution system under high penetration levels. Therefore, low-voltage ride-through (LVRT) capabilities and dynamic grid support, i.e., reactive power injection, can be included in the inverter design to temporarily ride through faults and accelerate the restoration of normal operation. Thus, the PV inverters should have the functionality to stay connected and not cease power generation (Sufyan et al. 2019).

During the occurrence of grid faults, e.g., voltage sags, it is recommended for the PV inverter to stay active and connected, up to a specific time, as shown in Figure 5.1, to the grid while injecting reactive power to the PCC, which will help the grid resist this fault and prevent a complete outage. This operation is called LVRT, a sort of dynamic grid support in intelligent inverters. The purpose of LVRT is to limit the source from inducing a short circuit current at high voltage levels, especially under high penetration of PV systems, which leads to loss of power generation (Sufyan et al. 2019). Therefore, under LVRT operation in grid-connected PV systems, excess active power should be dissipated by:

1. Reduce the peak generated power – MPPT modification.
2. Integrating storage elements- Double stage configuration.
3. Utilization of DC chopper, as the case of wind systems.

Dynamic grid support requires online monitoring of the grid voltage states (using a PLL system), accurate generation of the reference current, according to grid codes, during the fault while avoiding the overcurrent and overvoltage tripping, and continuous monitoring after fault clearance.

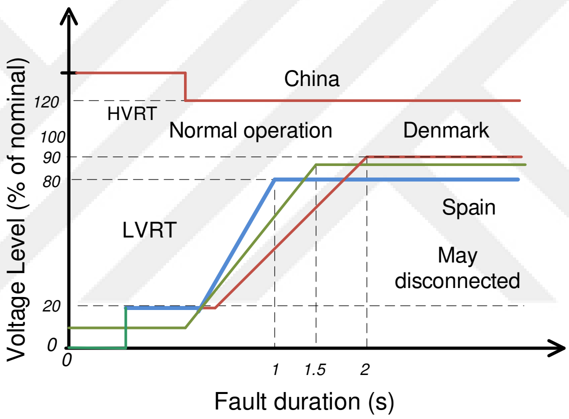

Figure 5.1. LVRT operation modes for different countries

5.2. The Improved Control Structure under Active and Reactive Power Support

It is possible to foresee expanded penetration to single-phase grid-connected PV systems, especially in low-voltage networks. Therefore, ancillary services such as LVRT and dynamic grid support are essential for grid-connected PV systems. A stationary reference frame-based single-phase PQ theory is utilized to control the inverter PQ injection, as shown in Figure 5.2.

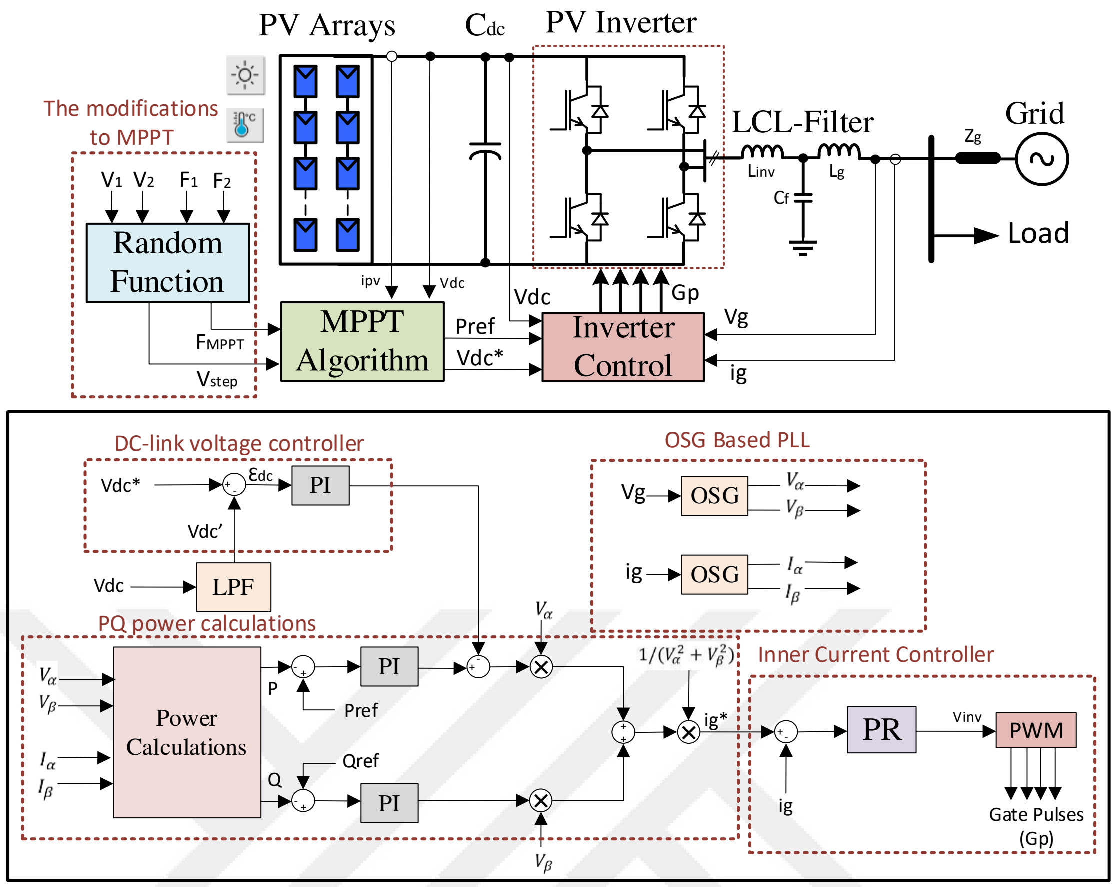

Figure 5.2. The power topology and the control structure of the grid-connected PV system

The realization of the control structure is based on instantaneous power theory for single-phase grid-connected PV systems. The active and reactive power values are given as:

$$P = \frac{1}{2}\left(v_\alpha i_\alpha + v_\beta i_\beta\right) \tag{5.1}$$

$$Q = \frac{1}{2}\left(v_\beta i_\alpha - v_\alpha i_\beta\right) \tag{5.2}$$

Where α, β are the components of the grid voltage and current generated by the orthogonal signal generator-based PLL. The realization of the loops with the reference values for the power with PI controllers can be given as:

$$\begin{bmatrix} i_\alpha^* \\ i_\beta^* \end{bmatrix} = \frac{2}{v_\alpha^2 + v_\beta^2}\begin{bmatrix} v_\alpha & v_\beta \\ v_\beta & -v_\alpha \end{bmatrix}\begin{bmatrix} P^* \\ Q^* \end{bmatrix} \tag{5.3}$$

5.3. Results of the Simulated Single-phase Grid-Connected PV system

Extensive simulation cases are presented in this section to assist and evaluate the performance of the enhanced grid-connected PV systems under different operating conditions. This section will depict the results under steady state operation for different irradiation levels, the dynamical response of the system under atmospheric changing conditions, and the case of deep changes in irradiance values. Furthermore, the proposed MPPT algorithms are compared to other techniques mentioned in the literature to evaluate the proposed method's performance. This thesis proposes the modified step voltage P&O (MP&O-v), modified sampling frequency P&O (MP&O-f), hybrid random step voltage-sampling frequency P&O (MP&O), modified step voltage InCon (MInCon -v), modified sampling frequency InCon (MInCon -f), hybrid random step voltage-sampling frequency InCon (MInCon), and neural network MPPT algorithms, respectively. Also, the developed methods are compared to CV, P&O, and InCon MPPT algorithms. The analysis also compares the THD, the tracking efficiencies, and the emission level of interharmonics between these proposed MPPT algorithms.

The results show the DC-link voltage, grid current, and DC-link voltage error with different MPPT methods. These results also compare injected grid current interharmonics frequency spectra for different MPPT techniques under different power operating conditions. The simulation parameters are depicted in Table 4.1 below.

Table 5.1. Parameters of the simulated single-phase grid-connected PV system

Rated PV Power	3.75 kW
Capacity of the DC-link	$C_{dc} = 1400\ \mu F$
LCL-filter	$L_{inv} = 5\ mH, C_f = 5.2\ \mu F, L_g = 2\ mH$
Transformer leakage inductance	$Z_g = 2\ mH$
Sampling frequency of the controller	$f_s = 20\ kHz$
Switching frequency	$f_{sw} = 8\ kHz$
Nominal grid voltage	$V_g = 230\ V$
Nominal grid frequency	$f_g = 50 \mp 0.5\ Hz$
DC-link voltage	$V_{dc} = 450\ V$
MPPT sampling rate	Proposed
MPPT step size	Proposed

5.3.1. Steady State Response under P&O MPPT Method

The steady-state performance characteristic for the developed system is simulated under low and full-power operating conditions with solar irradiances equal to 1000 W/m^2 and 185 W/m^2. The simulation results, shown in Figure 5.3 to Figure 5.7, under full-power operating conditions reveal that the tracking efficiency obtained under the P&O MPPT algorithm is 96.48%. The observed grid current interharmonics are high, and the total harmonics distortion level is 2.46%. The operation of the system under full power yields a power factor near unity (around 0.99). The system reaches the steady state operation in about 200 ms.

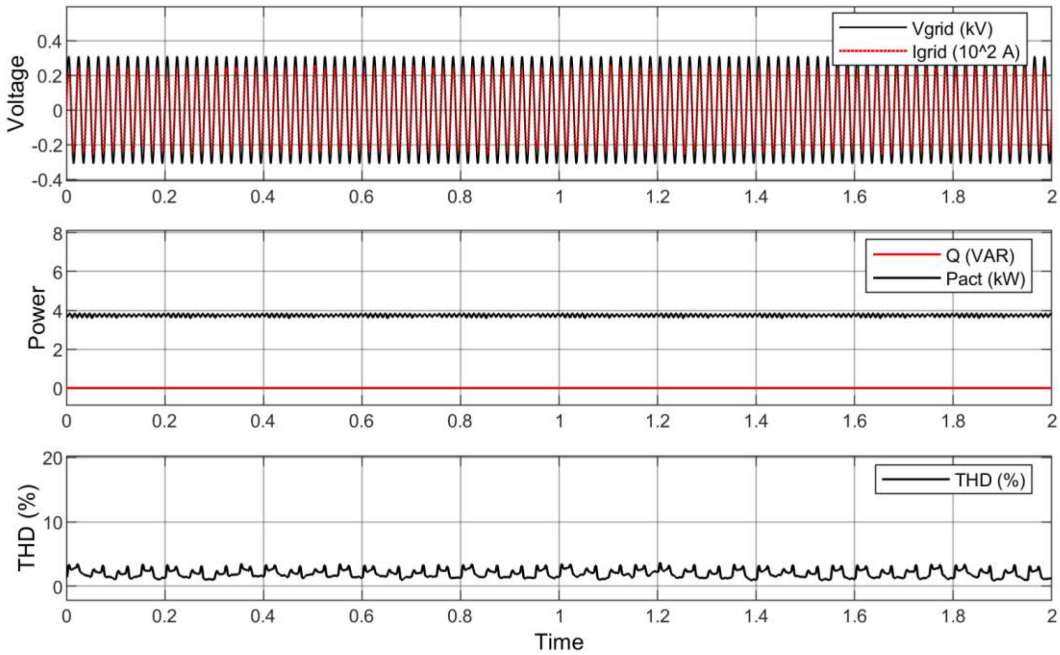

Figure 5.3. The obtained results of the developed grid-connected PV system (grid current and voltage, injected active and reactive power, and THD) under full-power operating condition

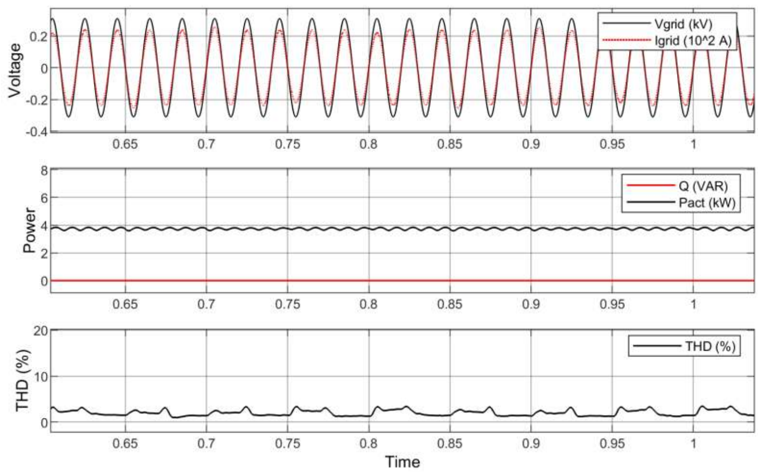

Figure 5.4. The detailed perturbation (grid current and voltage, injected active and reactive power, and THD) under full-power operating condition

The perturbation of DC-link voltage is shown in Figure 5.5 below. It can be noticed that a DC-link voltage error is presented with a magnitude of 5 volts corresponding to the perturbation step size.

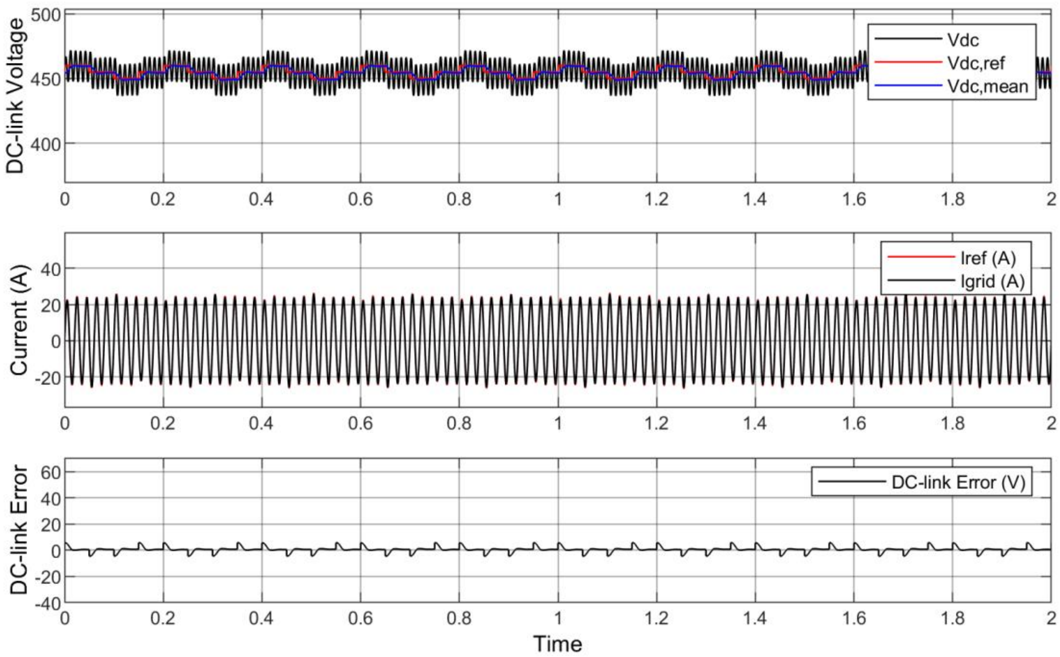

Figure 5.5. The obtained results of the grid-connected PV inverter (DC-link voltage, grid current, and DC-link error) under full-power operating condition

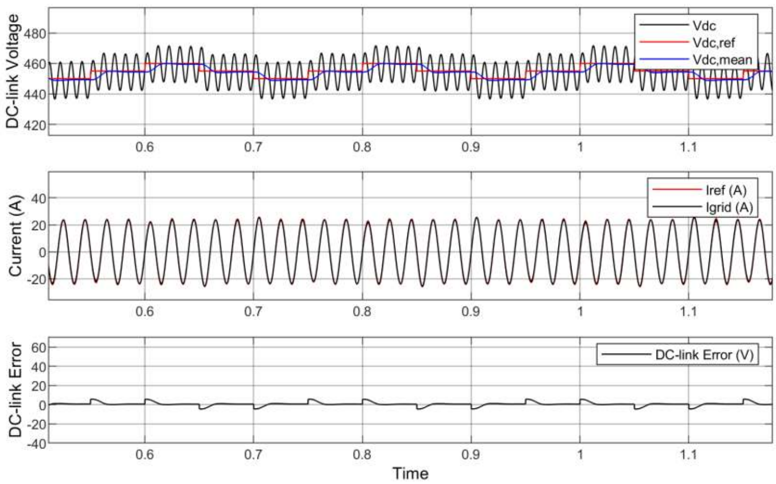

Figure 5.6. The detailed perturbation (DC-link voltage, grid current, and DC-link error) under full-power operating condition

The observed tracking efficiency of the MPPT algorithm under the full-power operating condition is 96.48%, as shown in Figure 5.7.

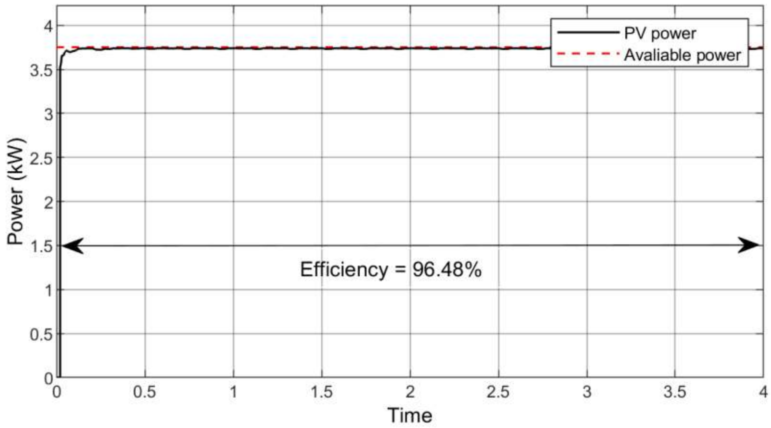

Figure 5.7. The efficiency resulted from the extracted PV power under 1000 W/m^2 solar irradiance for the full-power operating condition

However, under low-power operating conditions, the performance characteristic for the developed single-phase grid-connected PV system is also investigated in Figure 5.8 to Figure 5.11. The injected grid current is distorted, and the THD values are higher in this situation. In addition, the interharmonics peaks are high, and the frequency distribution is almost the same as that of the full-power operating condition.

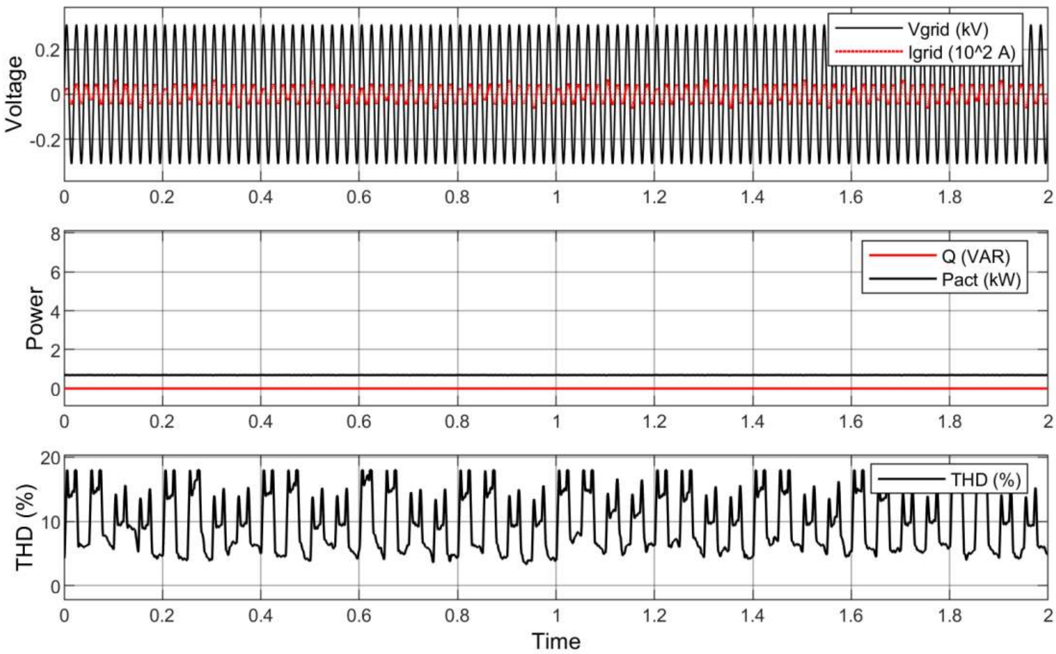

Figure 5.8. The obtained results of the developed grid-connected PV system (grid current and voltage, injected active and reactive power, and THD) under low-power operating condition

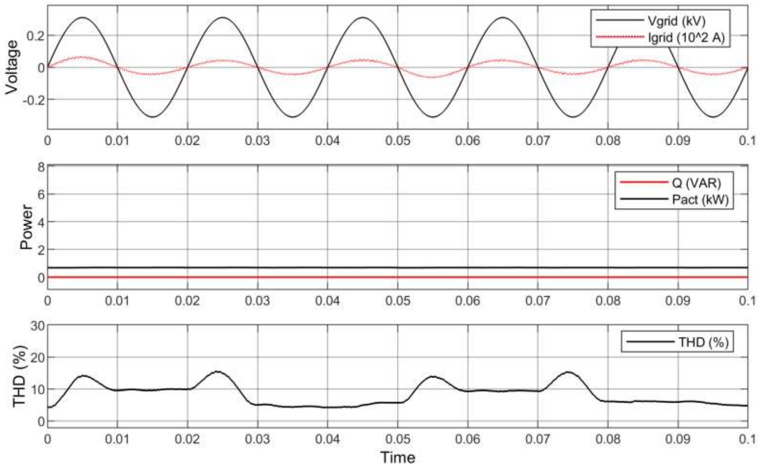

Figure 5.9. The detailed perturbation (grid current and voltage, injected active and reactive power, and THD) under low power operating condition

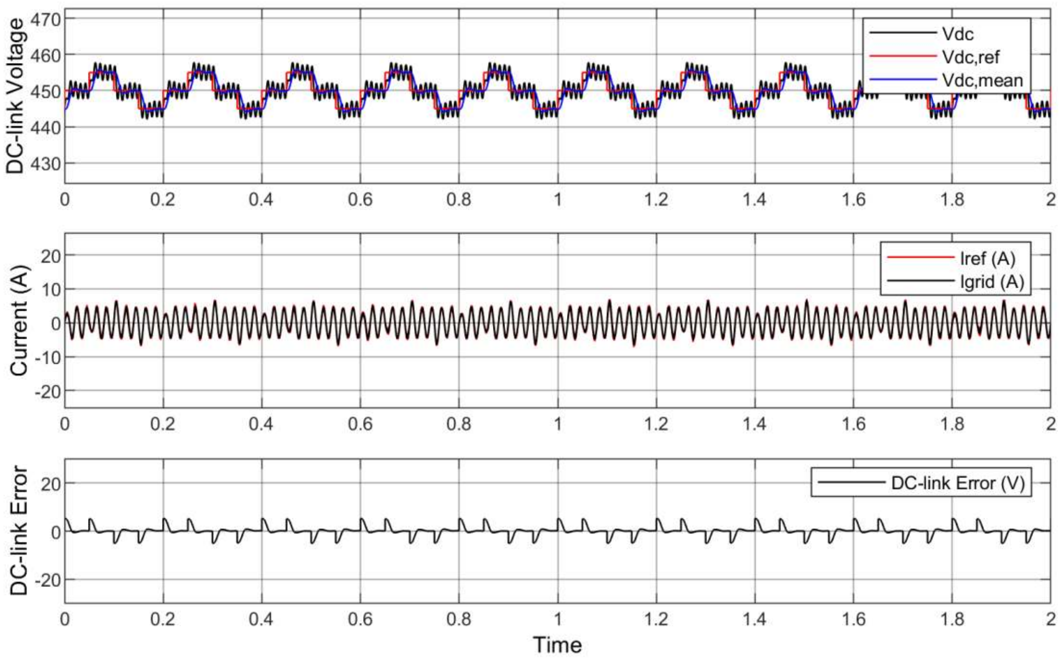

Figure 5.10. The obtained results of the grid-connected PV inverter (DC-link voltage, grid current, and DC-link error) operated under full-power operating condition

The perturbation of DC-link voltage is shown in Figure 5.10. It can be noticed that a DC-link voltage error is presented with a magnitude of 5 volts corresponding to the perturbation step size, and it is similar to the errors in Figure 5.5. Therefore, it can be concluded that interharmonics frequency distribution is almost the same for both cases, which makes it essential to apply the mitigation technique under different power operating conditions. The observed tracking efficiency of the MPPT algorithm under this condition is shown in Figure 5.11.

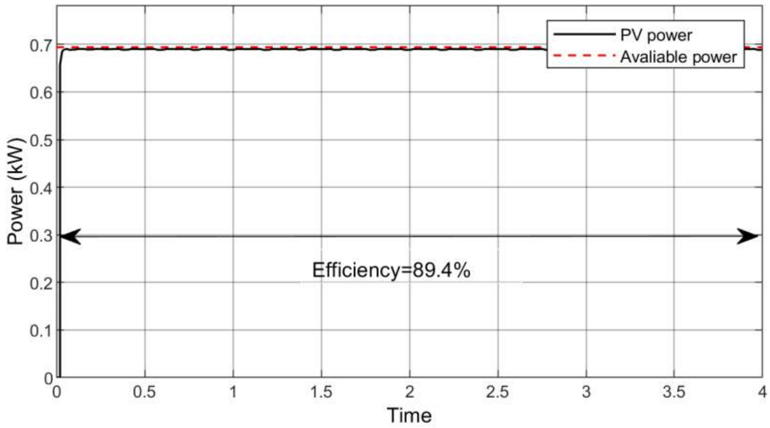

Figure 5.11. The efficiency resulted from the extracted PV power under 185 W/m^2 solar irradiance for the low-power operating condition

The performance under low-power operating conditions reveals that the efficiency is 89.4% and the THD is 12.43%. The performance characteristic of the system should be improved in terms of tracking efficiency, THD, and interharmonics emissions level. Therefore, the proposed methods in this thesis are investigated in the next subsections to enhance the overall performance of the developed system.

5.3.2. The Proposed Modified Step-Size P&O Method

The performance characteristics of the proposed MP&O-v MPPT algorithm are shown in Figure 5.12 to Figure 5.18. The analysis is performed for full- and low-power operating conditions.

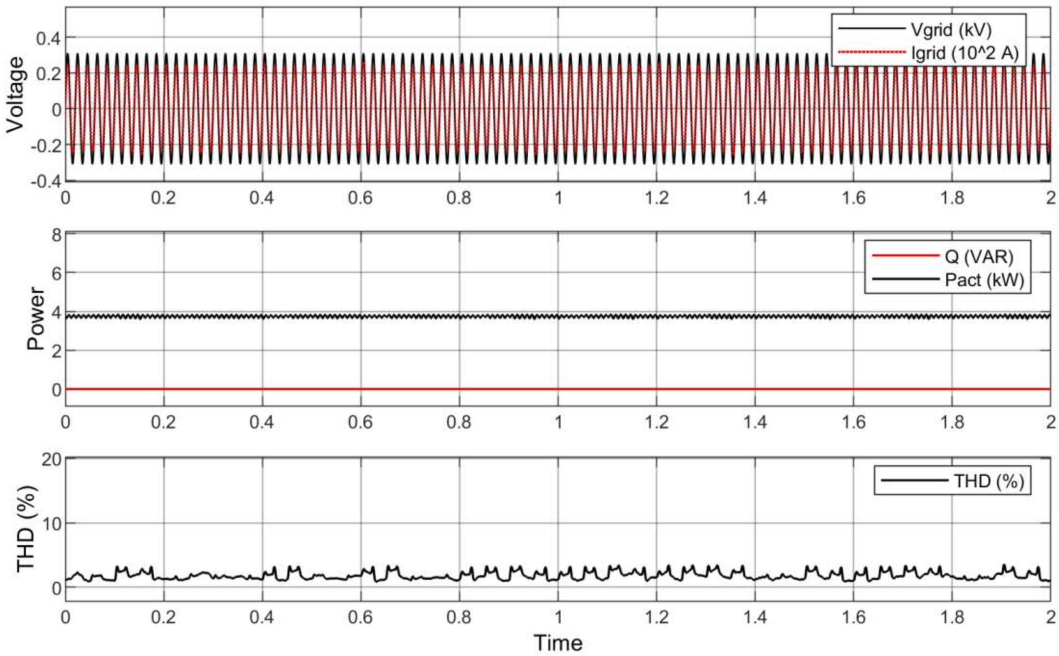

Figure 5.12. The obtained results of the developed grid-connected PV system utilizing MP&O-v MPPT algorithm (grid current and voltage, injected active and reactive power, and THD) under full-power operating conditions

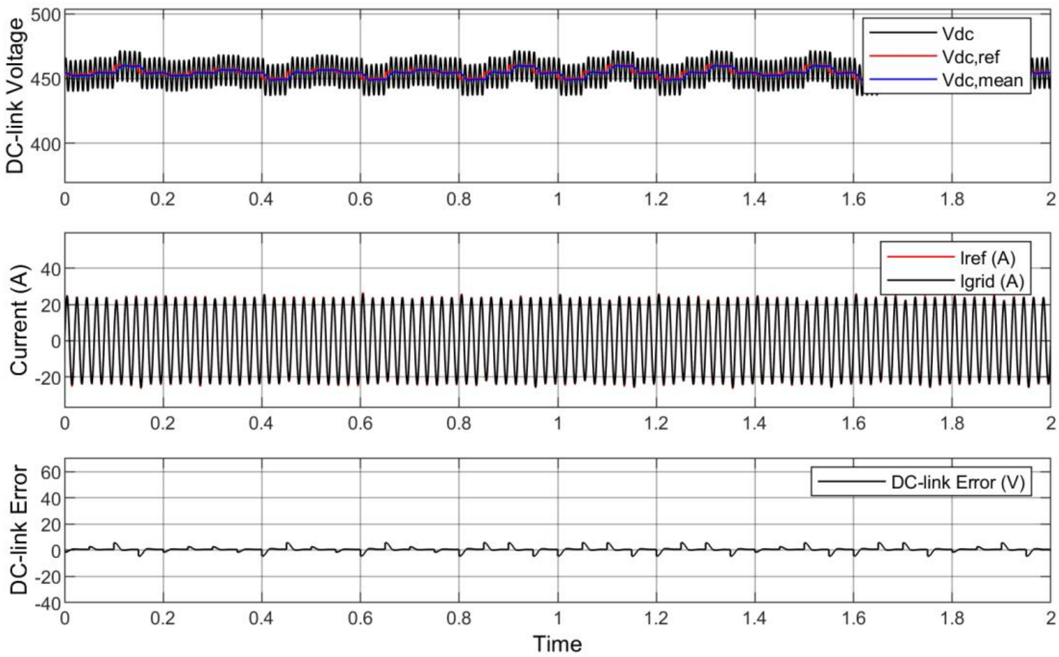

Figure 5.13. The obtained results of the developed grid-connected PV inverter utilizing MP&O-v MPPT algorithm (DC-link voltage, grid current, and DC-link error) at full-power operating conditions

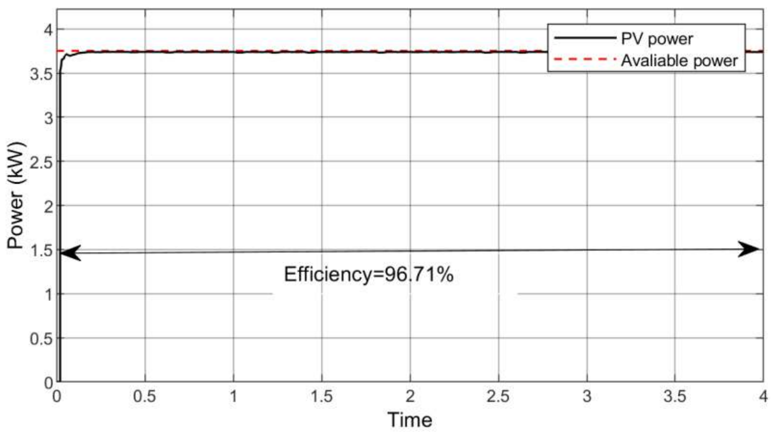

Figure 5.14. The efficiency resulted from the extracted PV power for the developed MP&O-v MPPT algorithm under 1000 W/m^2 solar irradiance at full-power operating condition

The simulation results under full-power operating conditions reveal that the tracking efficiency obtained under the MP&O-v MPPT algorithm is 96.71%. The observed grid current interharmonics are lower than the P&O MPPT method, and the total harmonics distortion level is 2.06% or 16.2% reduction of interharmonics and THD. The operation of the system under full power yields a power factor near unity (around 0.99). The system reaches the steady state operation in about 200 ms.

Under low-power operating conditions, the performance characteristic for the developed single-phase grid-connected PV system is also investigated in Figure 5.15 to Figure 5.17. The injected grid current distortion is decreased, and the THD values are relatively lower in this situation. In addition, the interharmonics peaks are also decreased.

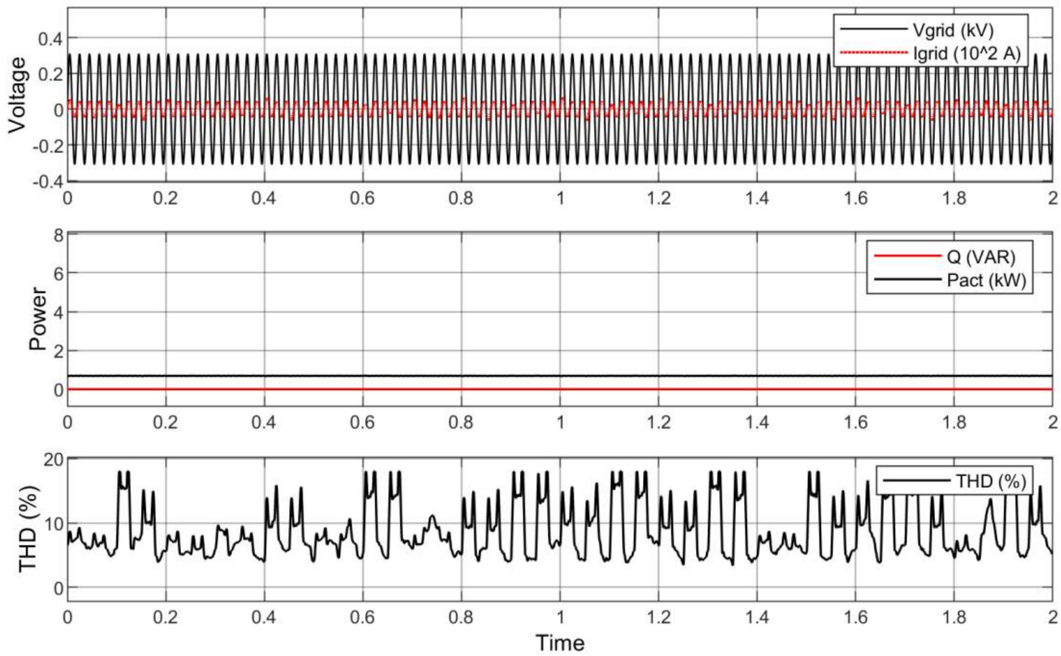

Figure 5.15. The obtained results of the developed MP&O-v MPPT algorithm (grid current and voltage, injected active and reactive power, and THD) operated under low-power operating conditions

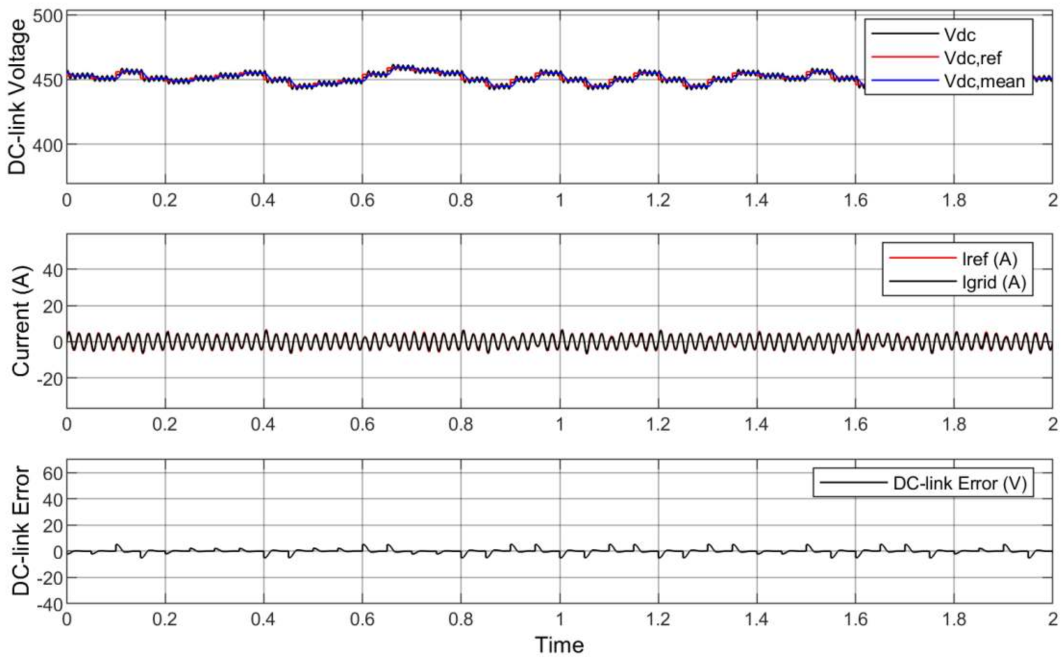

Figure 5.16. The obtained results of the developed MP&O-v MPPT algorithm (DC-link voltage, grid current, and DC-link error) at low-power operating conditions

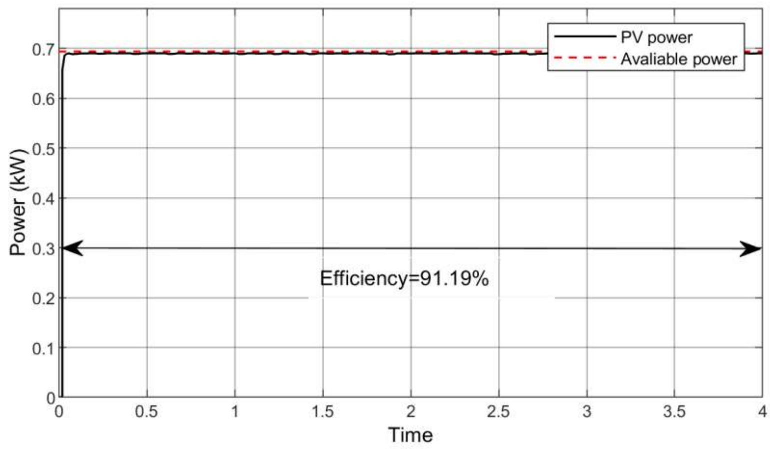

Figure 5.17. The efficiency resulted from the extracted PV power for the developed MP&O-v MPPT algorithm under 185 W/m^2 solar irradiance at low-power operating condition

The performance under low-power operating conditions with the proposed MP&O-v MPPT algorithm reveals that the efficiency is increased from 89.4% to 91.19%, and the THD is reduced from 12.43% to 10.33%. The frequency spectrum of the injected grid currents is presented in Figure 5.18, which compares the conventional P&O method with the proposed MP&O-v technique. It is evident that the developed MPPT method minimizes the interharmonics in the frequency spectrum and reduces the THD from 2.46% to 2.06% and from 12.43% to 10.33% under full and low-power operating conditions, respectively, by an improvement of 16.2%. The performance characteristics of the developed MP&O-v will be compared to other proposed methods in the following subsections.

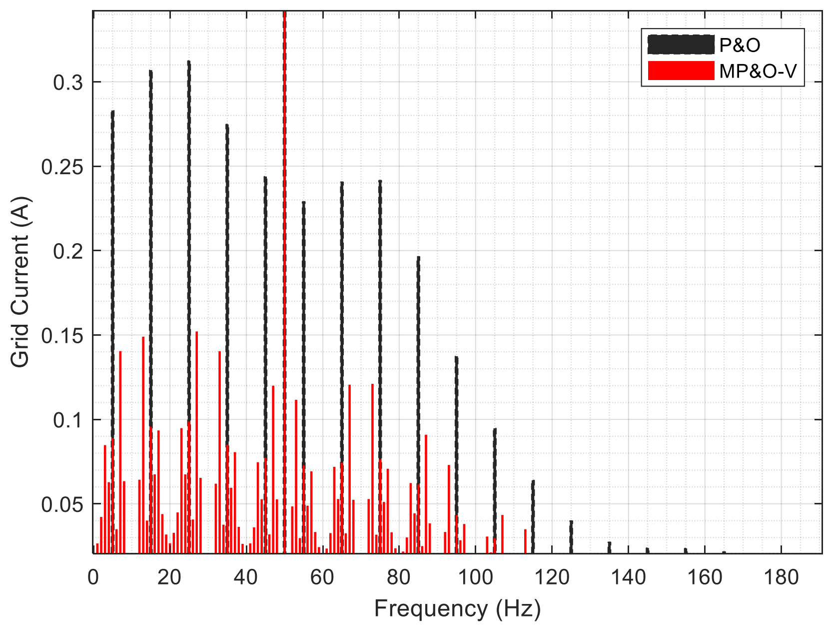

Figure 5.18. The injected grid currents frequency spectrum under steady-state and low-power operating conditions with a frequency resolution of 1 Hz

5.3.3. The Proposed Modified Sampling Frequency P&O Method

The investigation of the second proposed MPPT algorithm is presented in this section. The performance characteristics of the developed MP&O-f MPPT algorithm are shown in Figure 5.19 to Figure 5.25. The analysis is performed for full- and low-power operating conditions.

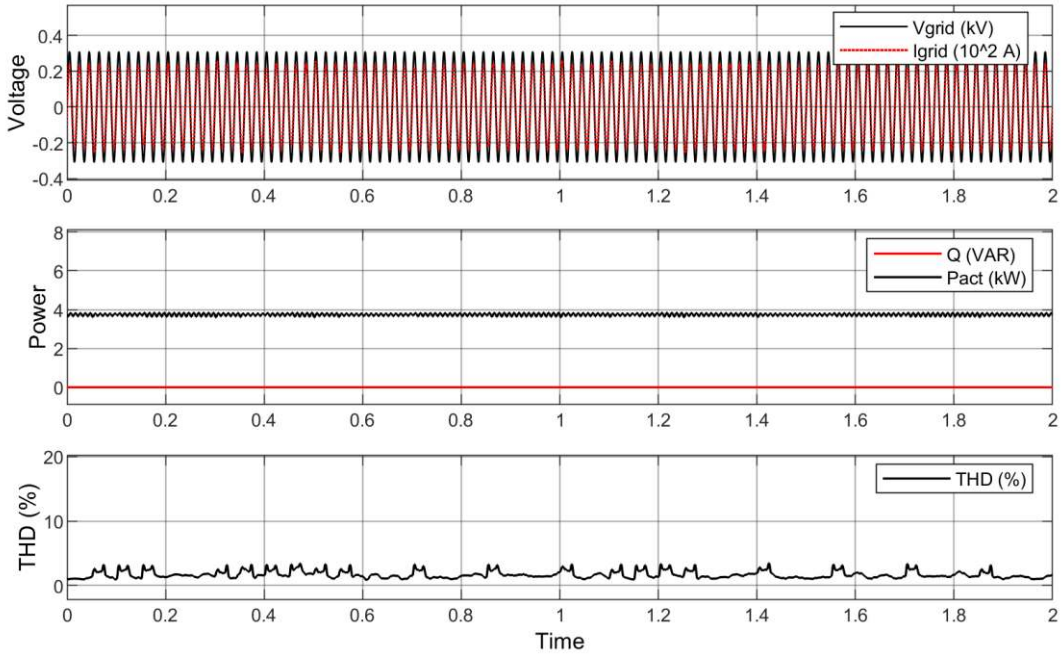

Figure 5.19. The obtained results of the developed MP&O-f MPPT algorithm (grid current and voltage, injected active and reactive power, and THD) under full-power operating conditions

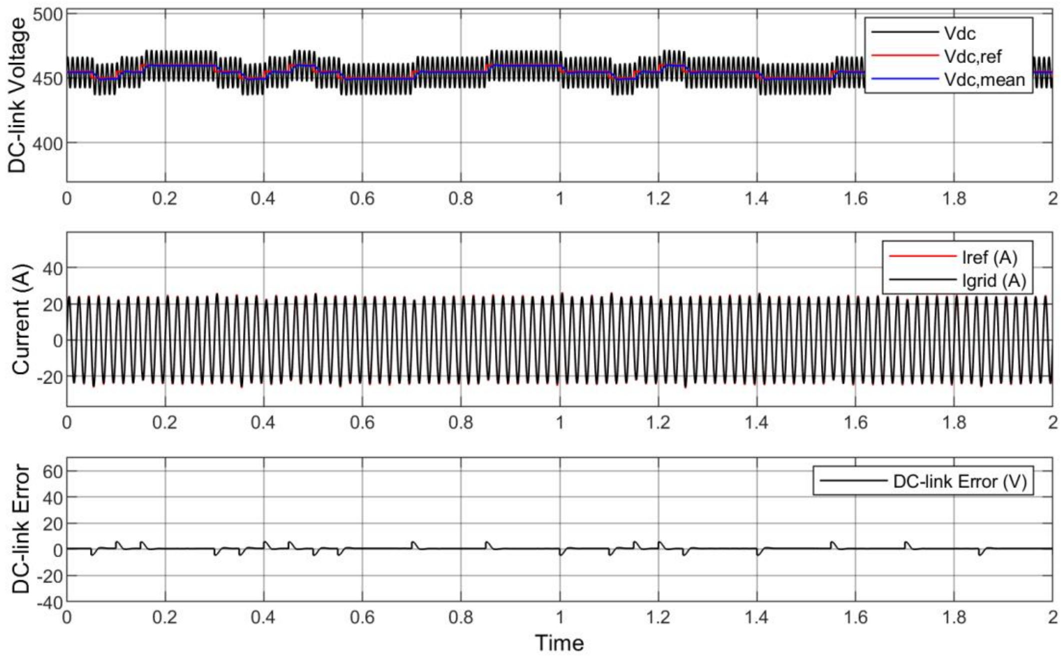

Figure 5.20. The obtained results of the developed MP&O-f MPPT algorithm (DC-link voltage, grid current, and DC-link error) at full-power operating conditions

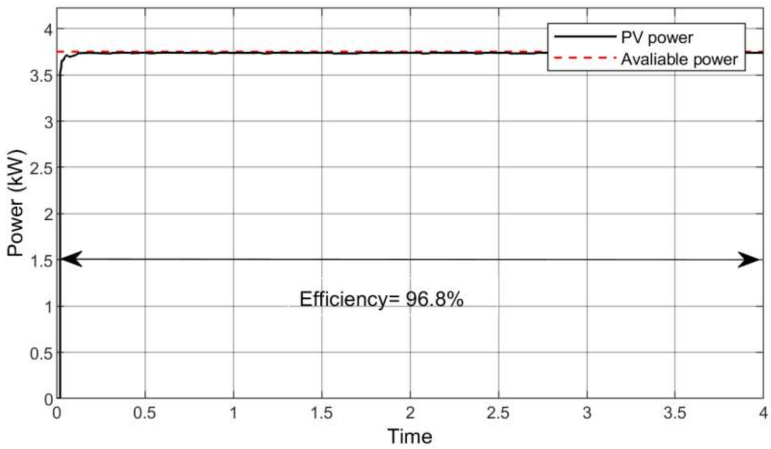

Figure 5.21. The efficiency resulted from the extracted PV power for the developed MP&O-f MPPT algorithm under 1000 W/m^2 solar irradiance at full-power operating condition

The simulation results under full-power operating conditions reveal that the tracking efficiency obtained under the MP&O-f MPPT algorithm is 96.8%. The observed interharmonics emissions are lower than the P&O MPPT method, and the total harmonics distortion level is 2.05% or 16.7% reduction of interharmonics and THD. The performance of the developed MPPT algorithm under low-power operating conditions is investigated in Figure 5.22 to Figure 5.24.

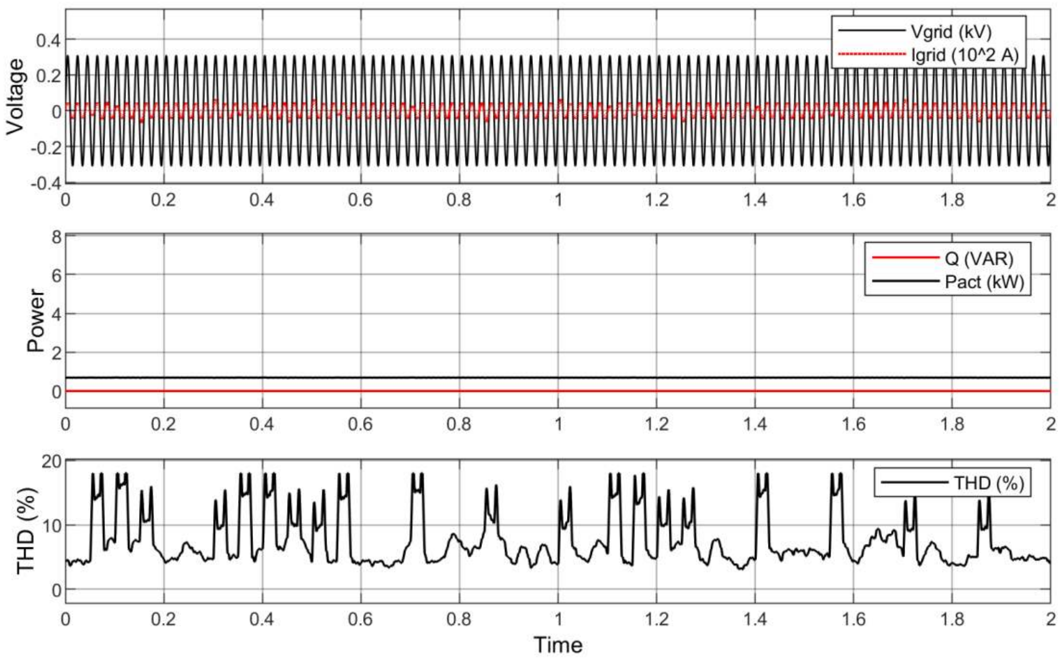

Figure 5.22. The obtained results of the developed MP&O-f MPPT algorithm (DC-link voltage, injected active and reactive power, and THD) operated under low-power operating conditions

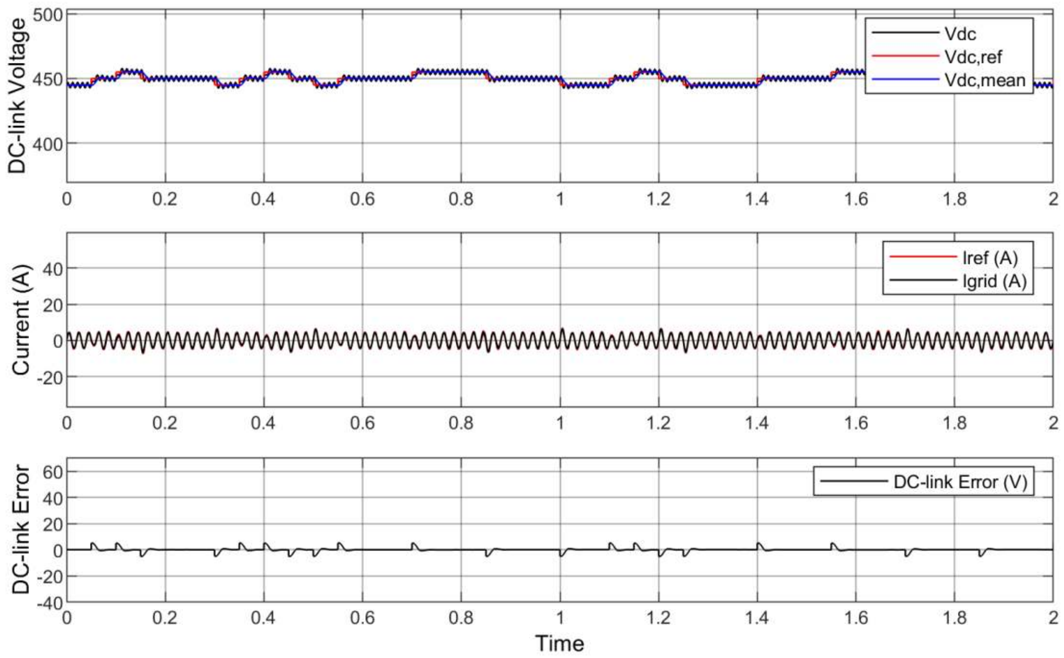

Figure 5.23. The obtained results of the developed MP&O-f MPPT algorithm (DC-link voltage, grid current, and DC-link error) under low-power operating conditions

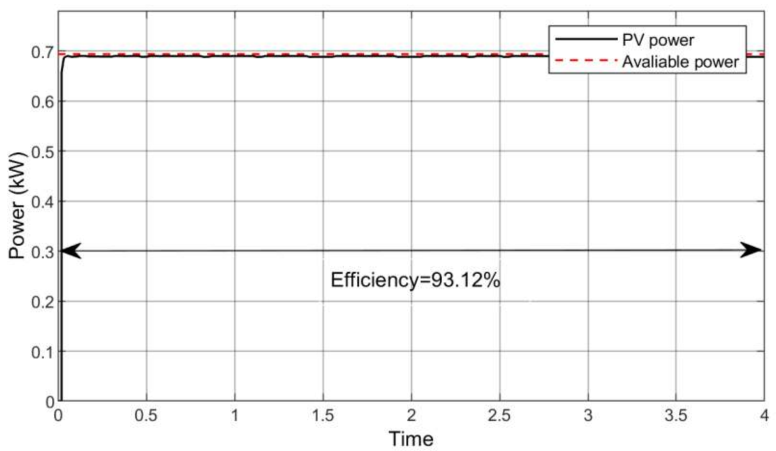

Figure 5.24. The efficiency resulted from the extracted PV power for the developed MPPT algorithm under 185 W/m^2 solar irradiance at low-power operating conditions

The mitigation technique performance characteristic under low-power operating conditions with the proposed MP&O-f MPPT algorithm shows that the efficiency is increased from 89.4% to 93.12%, and the THD is reduced from 12.43% to 10.14%. The frequency spectrum of the injected grid currents is presented in Figure 5.25. A comparison between the conventional P&O method and the proposed MP&O-f method is presented. It is obvious that the developed MPPT method reduces the interharmonics in the frequency spectrum and decreases the THD from 2.46% to 2.05% and from 12.43% to 10.14% under full and low-power operating conditions, respectively, by an improvement of 18.42%.

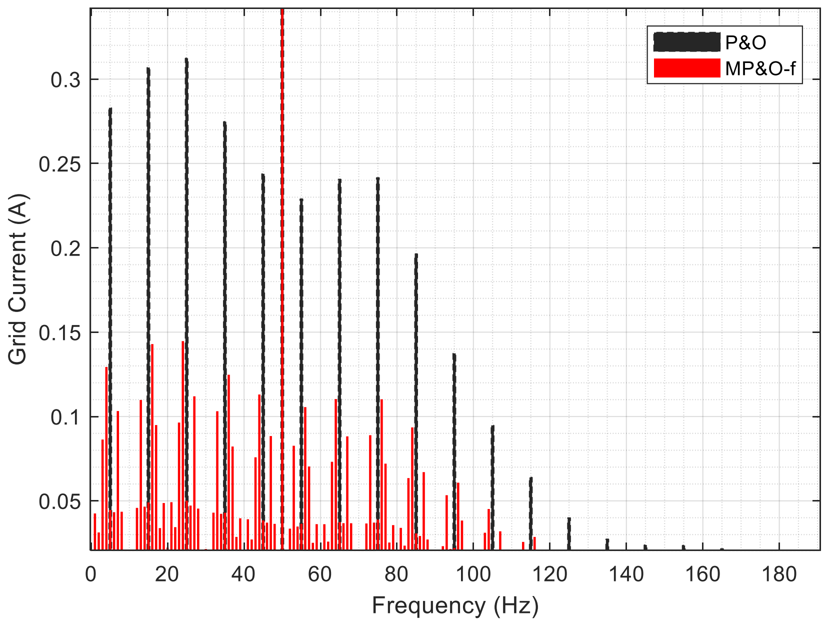

Figure 5.25. The injected grid currents frequency spectrum under steady-state and low-power operating conditions with a frequency resolution of 1 Hz

A comparison between different simulated cases is presented in Figure 5.26 to Figure 5.28 to show the effectiveness of the proposed MP&O-v and MP&O-f MPPT algorithms in mitigating interharmonics and improving overall tracking efficiency under full- and low-power operating conditions.

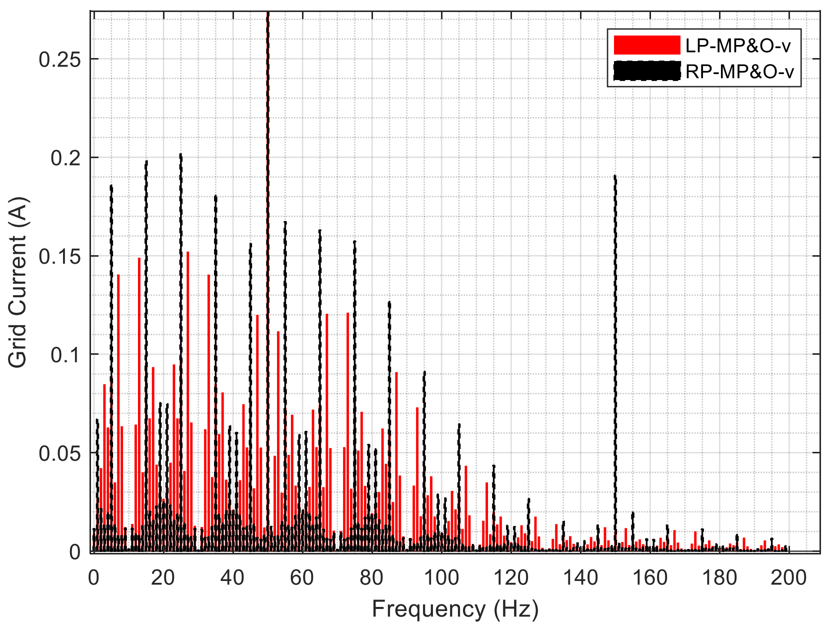

Figure 5.26. The injected grid currents frequency spectrum under steady-state operating conditions, a comparison between low- and full-power (LP and RP) operating conditions of proposed MPPT methods, with a frequency resolution of 1 Hz

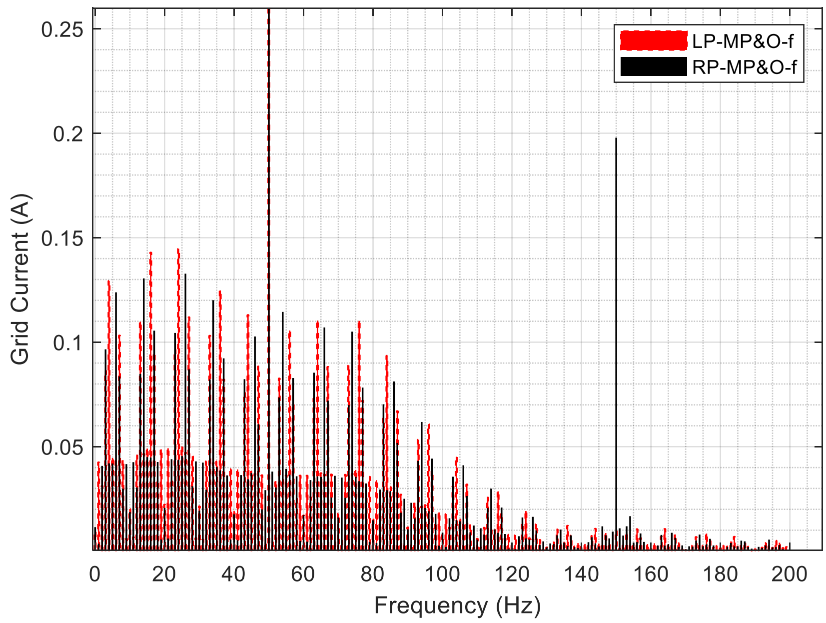

Figure 5.27. The injected grid currents frequency spectrum under steady-state operating conditions, a comparison between low- and full-power operating conditions of proposed MPPT methods, with a frequency resolution of 1 Hz

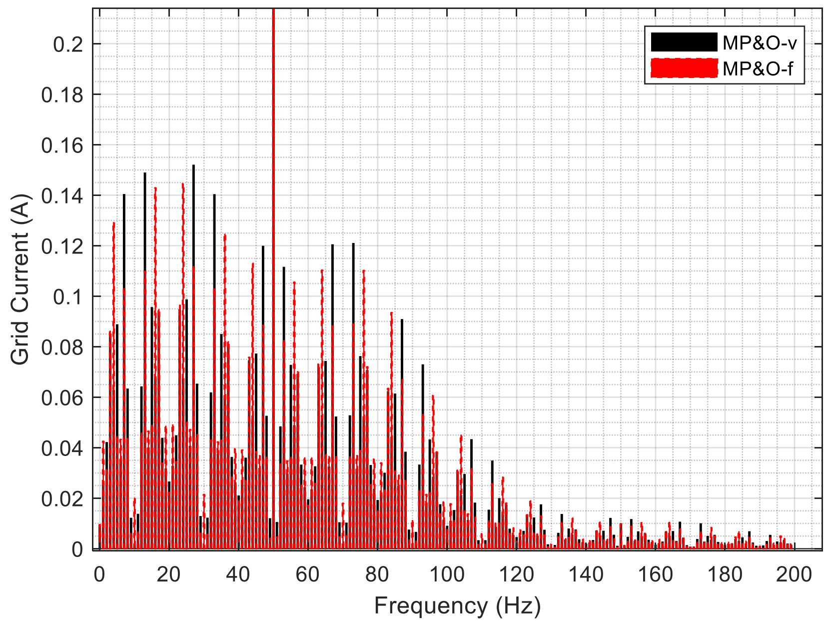

Figure 5.28. The injected grid currents frequency spectrum under steady-state low-power operating conditions, a comparison between proposed MPPT methods, with frequency resolution of 1 Hz

It can be noticed that interharmonics emissions are reduced by utilizing the proposed MP&O-v and P&O-f MPPT algorithms compared to the conventional P&O method. The reduction of interharmonics under MP&O-v for low-power operating conditions is evident, as shown in Figure 5.26. In addition, both developed methods show similar behavior, as shown in Figure 5.28.

5.3.4. The Proposed Hybrid Random P&O MPPT Algorithm

By combining the last two proposed mitigation techniques, the performance characteristics of the proposed hybrid random MP&O MPPT algorithm are presented in Figure 5.29 to Figure 5.35. The analysis is performed at full- and low-power operating conditions, respectively.

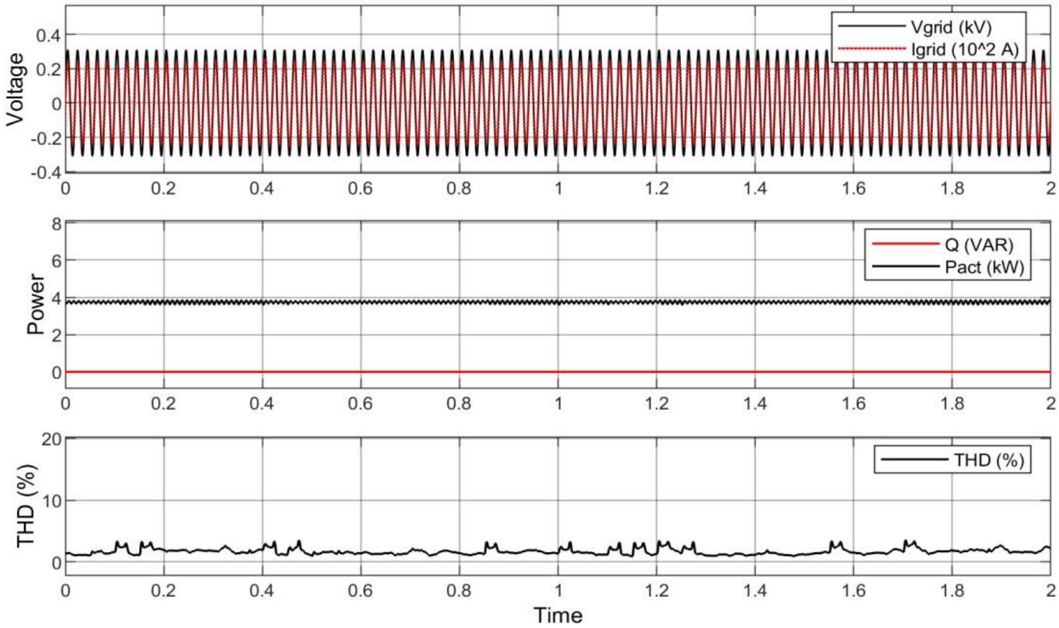

Figure 5.29. The obtained results of the developed MP&O MPPT algorithm with the proposed hybrid random technique (DC-link voltage, injected active and reactive power, and THD) under full-power operating conditions

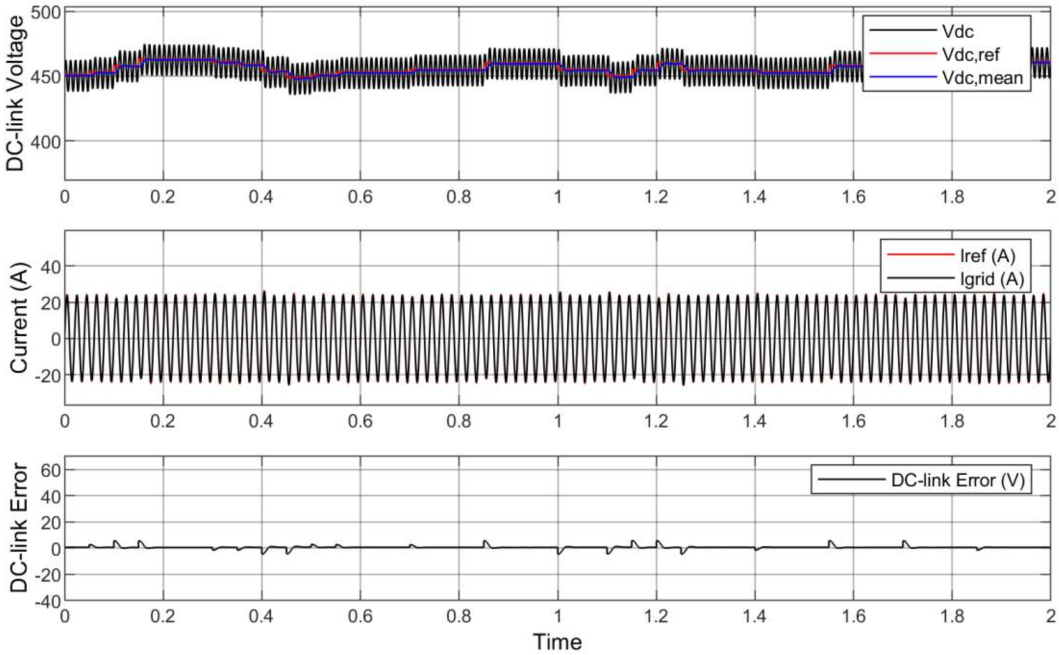

Figure 5.30. The obtained results of the developed MP&O MPPT algorithm with the proposed hybrid random MPPT technique (DC-link voltage, grid current, and DC-link error) under full-power operating conditions

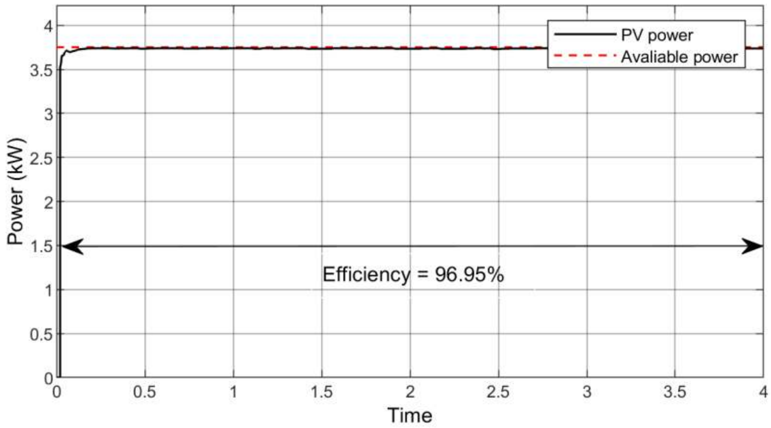

Figure 5.31. The efficiency resulted from the extracted PV power for the developed MP&O MPPT algorithm with the proposed hybrid random technique under 1000 W/m^2 solar irradiance at full-power operating conditions

The variation in the DC-lin voltage is modified by the proposed technique. The tracking efficiency of the developed method is 96.95%. Under low-power operating conditions, the performance characteristic is investigated for the proposed MP&O in Figure 5.32 to Figure 5.34. It can be observed from Figure 5.35 that the injected grid current distortion is superiorly decreased, and the THD values are highly lowered in this situation. In addition, the interharmonics peaks also decreased significantly.

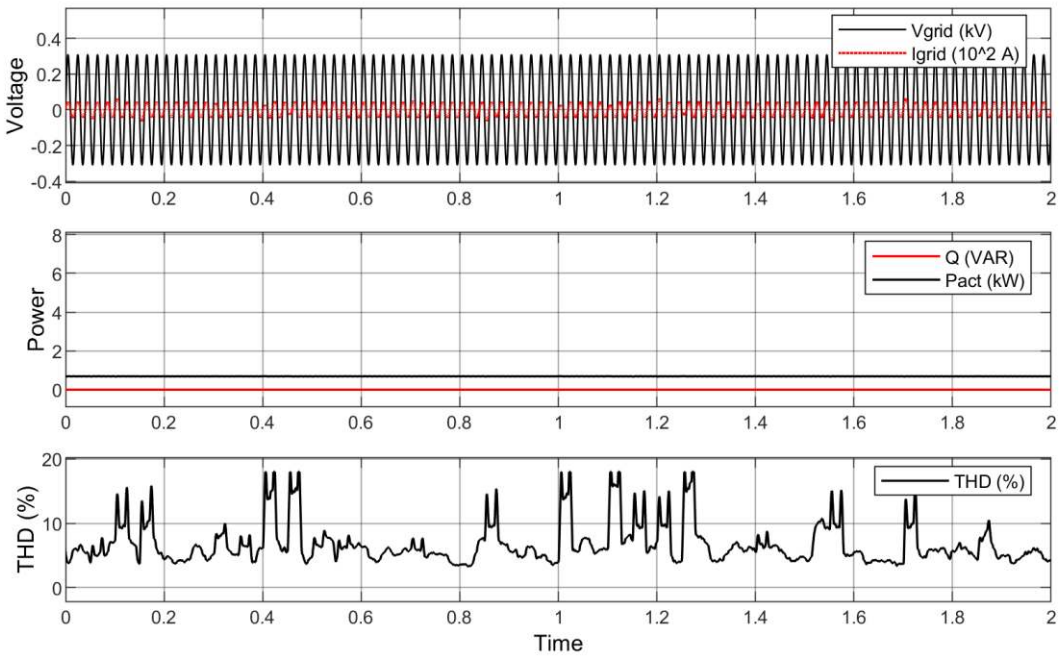

Figure 5.32. The obtained results of the developed MP&O MPPT algorithm with the proposed hybrid random MPPT algorithm (DC-link voltage, injected active and reactive power, and THD) under low-power operating conditions

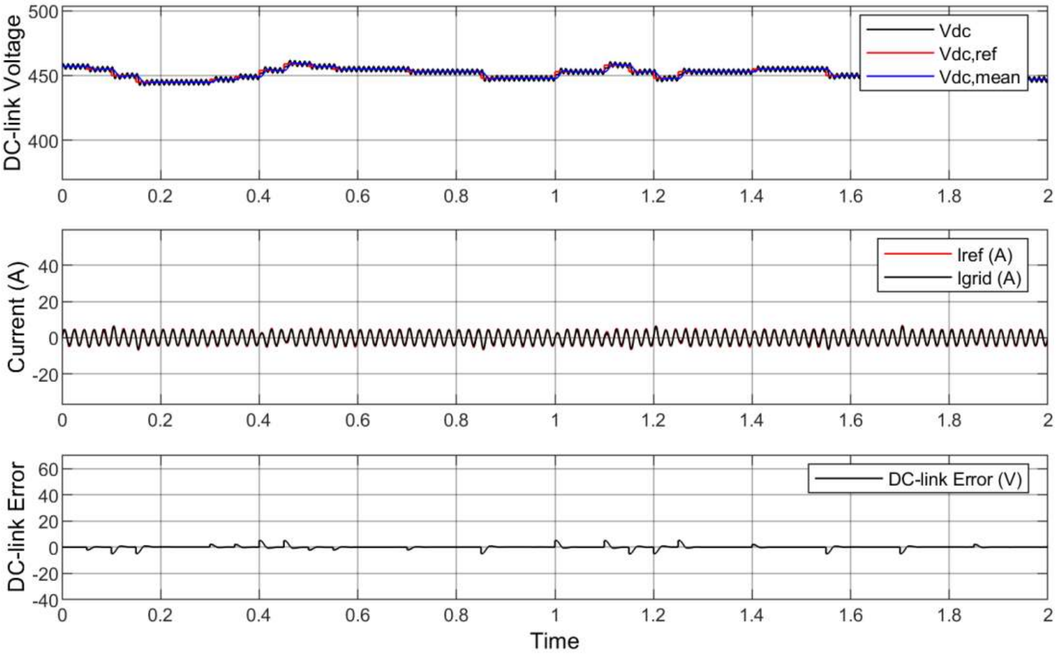

Figure 5.33. The obtained results of the developed MP&O MPPT algorithm with the proposed hybrid random MPPT technique (DC-link voltage, grid current, and DC-link error) operated under low-power operating conditions

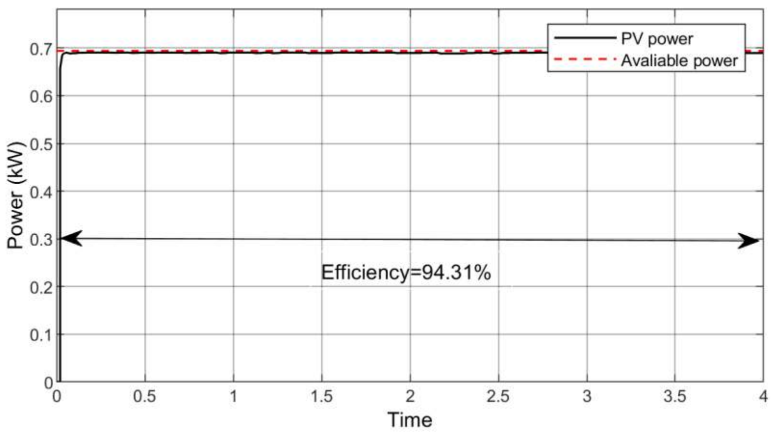

Figure 5.34. The efficiency resulted from the extracted PV power for the proposed MPPT algorithm with the hybrid random technique under 185 W/m^2 solar irradiance at full-power operating conditions

For low-power operating conditions, the performance characteristics of the proposed hybrid random MP&O MPPT algorithm show that the efficiency is increased from 89.4% under the conventional P&O method to 94.31%, and the THD is reduced from 12.43% to 8.07%. The frequency spectrum of the injected grid currents is presented in Figure 5.35, which compares the proposed interharmonics mitigation algorithms. It is evident that the proposed hybrid random MPPT is superior in minimizing the interharmonics in the frequency spectrum, which also reduces the THD from 2.46% to 1.86% under full-power operating conditions, by an improvement of 24.4%.

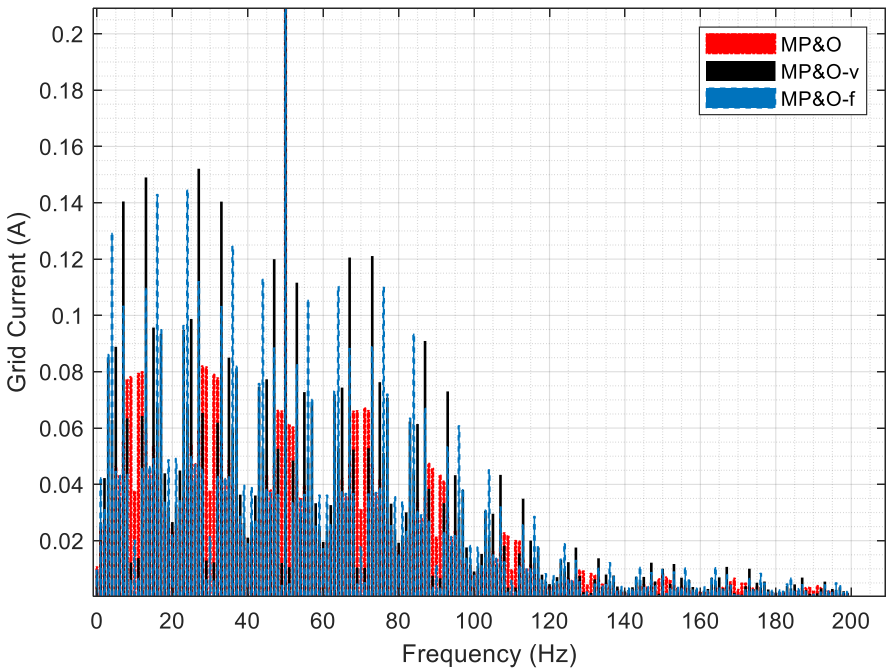

Figure 5.35. The injected grid current frequency spectrum under steady-state operating conditions, a comparison between proposed interharmonics mitigation techniques, MP&O-v, MP&O-f, and MP&O MPPT algorithms, with a frequency resolution of 1 Hz

The previous discussion shows that the proposed mitigation technique is a good candidate for reducing interharmonics emissions and THD and improving the MPPT algorithm's tracking efficiency. In addition, the performance of the proposed technique is evident under full- and low-power operating conditions.

5.3.5. Steady State Response under InCon MPPT Method

This section investigates the effect of other MPPT algorithms, such as the InCon MPPT algorithm, on the generating characteristic of interharmonics. The extension of the proposed interharmonics mitigation technique is introduced in the following subsections. The performance of the conventional InCon MPPT algorithm is shown in Figure 5.36 to Figure 5.42. The analysis is performed at full- and low-power operating conditions.

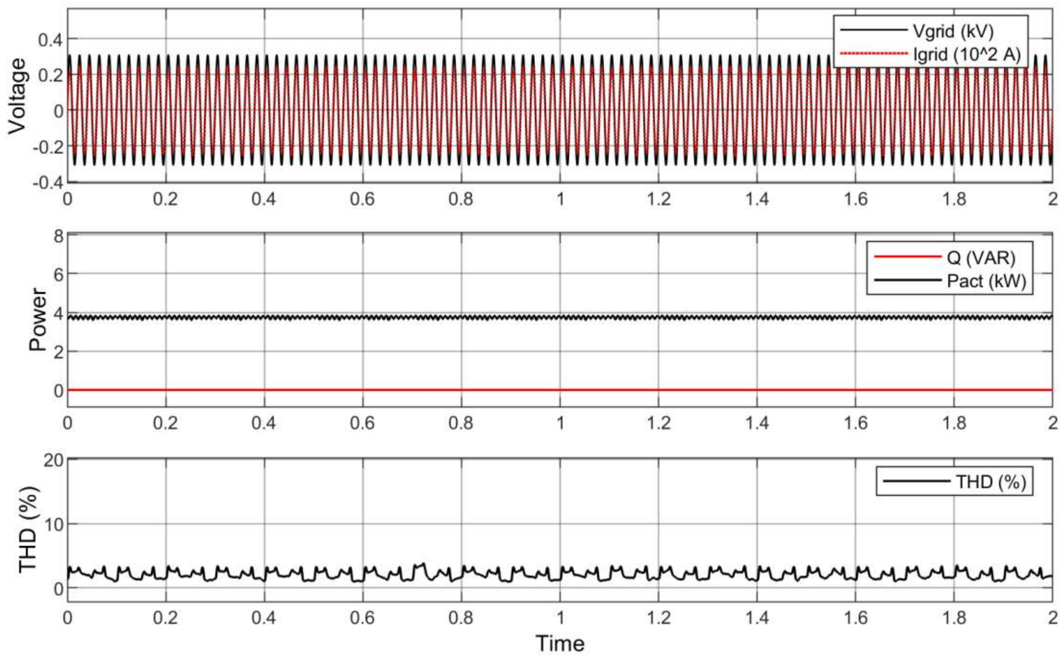

Figure 5.36. The obtained results of the InCon MPPT method (dc-link voltage, injected active and reactive power, and THD) under the full-power operating conditions

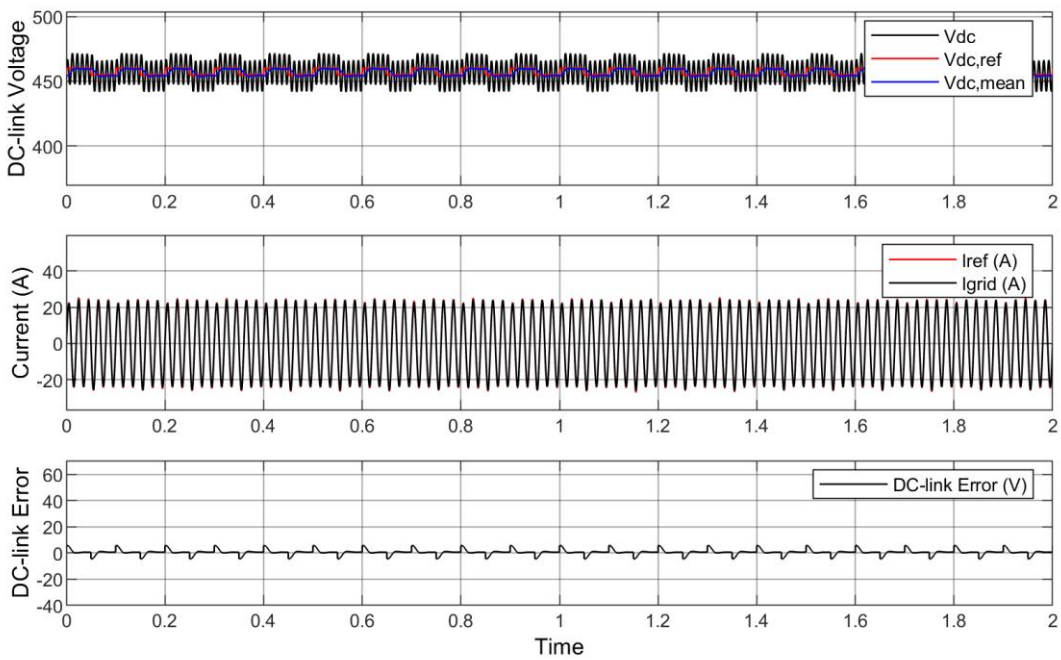

Figure 5.37. The obtained results of the InCon MPPT (DC-link voltage, grid current, and DC-link error) under full-power operating conditions

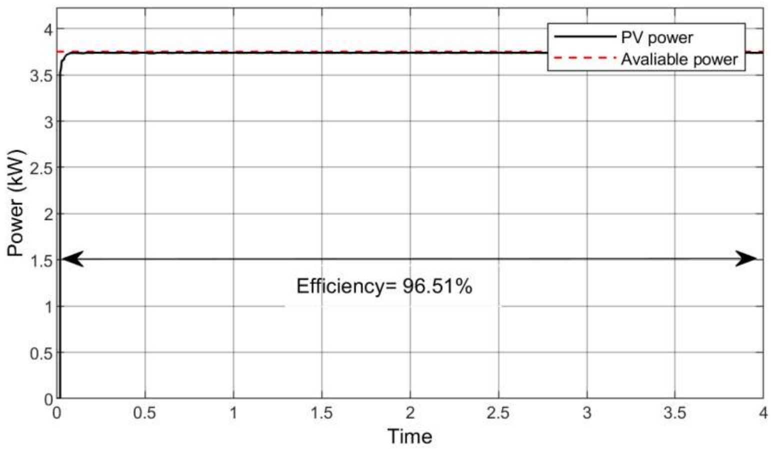

Figure 5.38. The efficiency resulted from the extracted PV power for the InCon MPPT algorithm under 1000 W/m^2 solar irradiance at full-power operating conditions

The previous results under full-power operating conditions reveal that the tracking efficiency obtained under the InCon MPPT algorithm is 96.51%. The observed grid current interharmonics are high, and the total harmonics distortion level is 2.49%. Under low-power operating conditions, the performance characteristic for the developed single-phase grid-connected PV system is also investigated in Figure 5.39 to Figure 5.41.

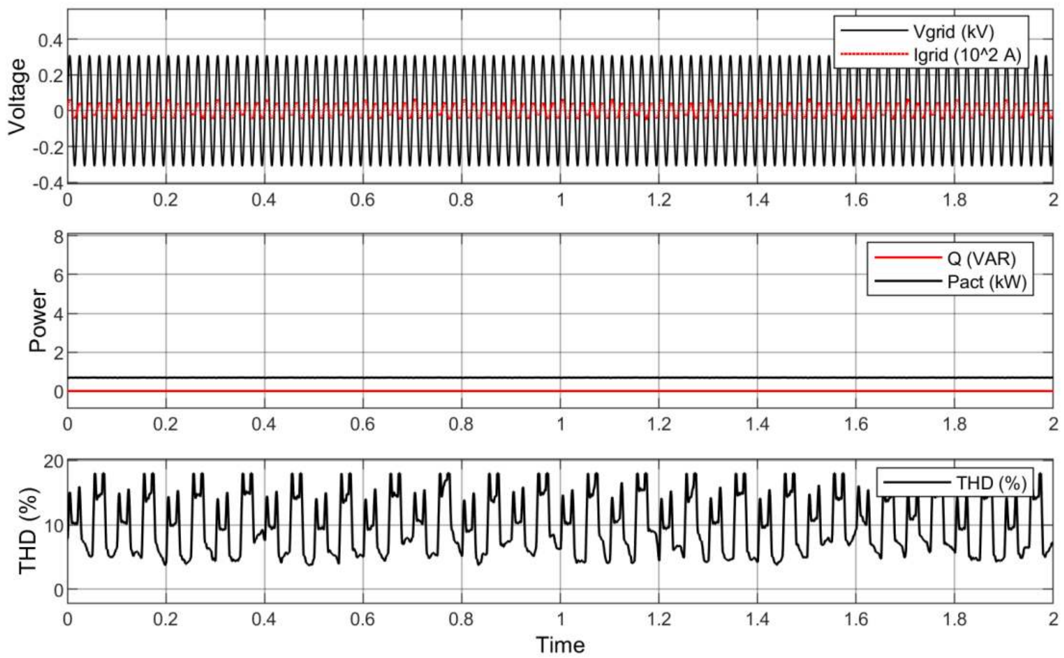

Figure 5.39. The obtained results of the InCon MPPT method (dc-link voltage, injected active and reactive power, and THD) under low-power operating conditions

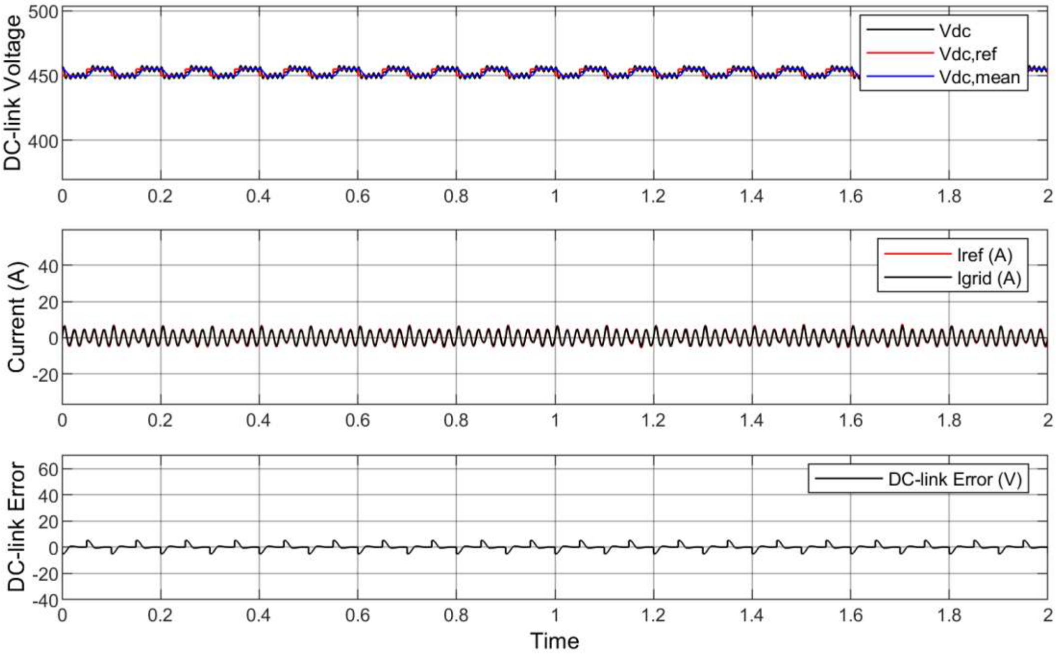

Figure 5.40. The obtained results of the InCon MPPT method (DC-link voltage, grid current, and DC-link error) under low-power operating conditions

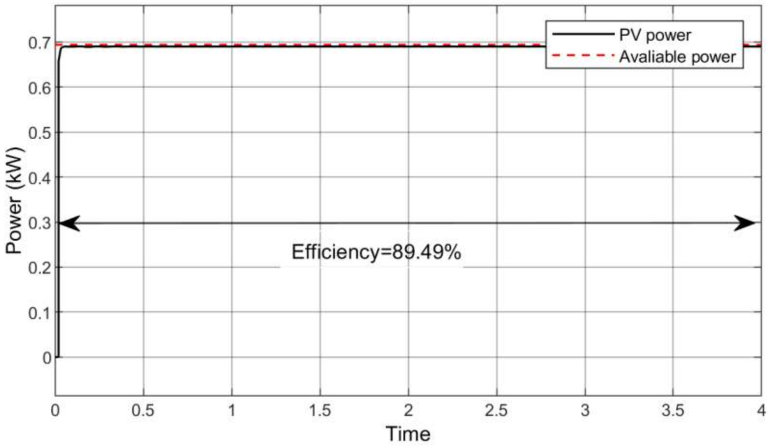

Figure 5.41. The efficiency resulted from the extracted PV power for the InCon MPPT algorithm under 185 W/m^2 solar irradiance at low-power operating conditions

The performance under low-power operating conditions with InCon MPPT algorithm reveals that the efficiency is 89.49% and the THD is 12.61%. The frequency spectrum of the injected grid currents is presented in Figure 5.42, which compares the conventional InCon method operating powers. As can be observed, the interharmonics peaks are high, and more enhancement should be employed to mitigate the emissions of interharmonics.

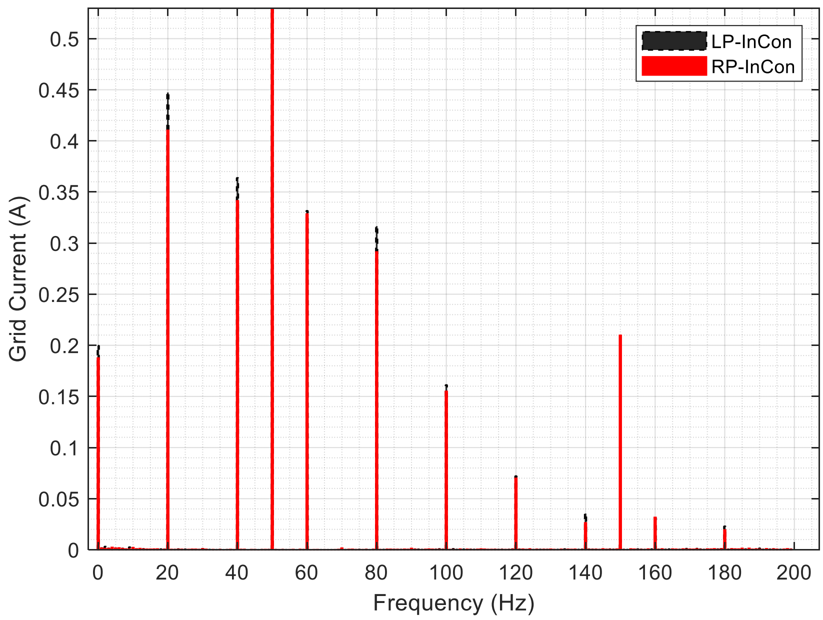

Figure 5.42. The injected grid current frequency spectrum under steady-state operating conditions, comparison between full- and low-power operation conditions with a frequency resolution of 1 Hz

5.3.6. The Proposed Modified Step-Size InCon Method

The performance of the proposed MinCon-v MPPPT algorithm is shown in Figure 5.43 to Figure 5.49. The analysis is performed for full- and low-power operating conditions.

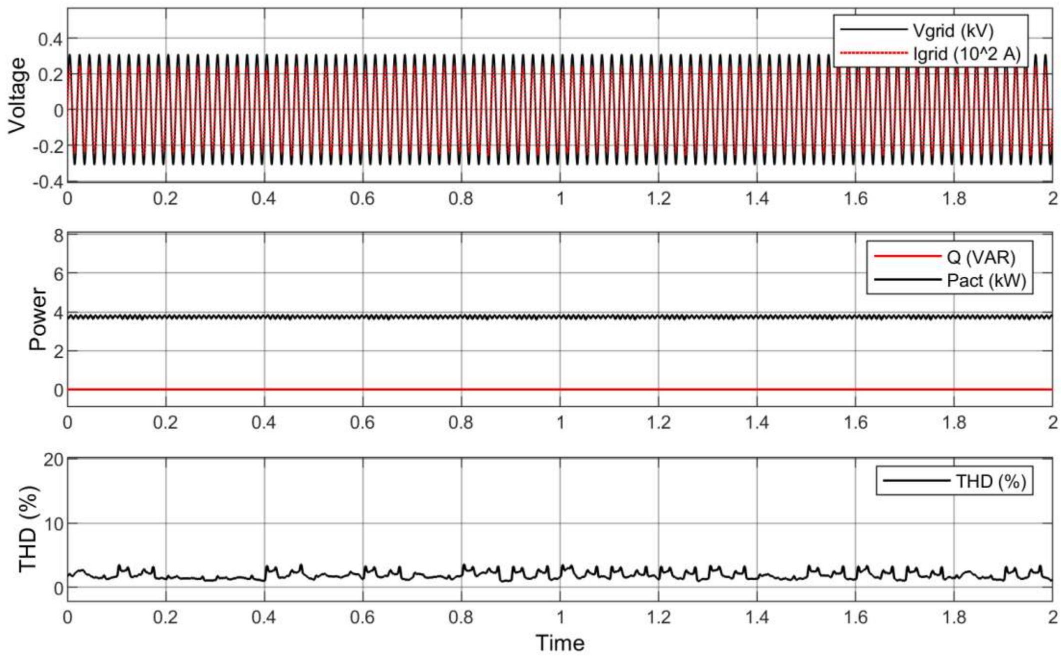

Figure 5.43. The obtained results of the proposed MInCon-v MPPT algorithm (dc-link voltage, injected active and reactive power, and THD) under full-power operating conditions

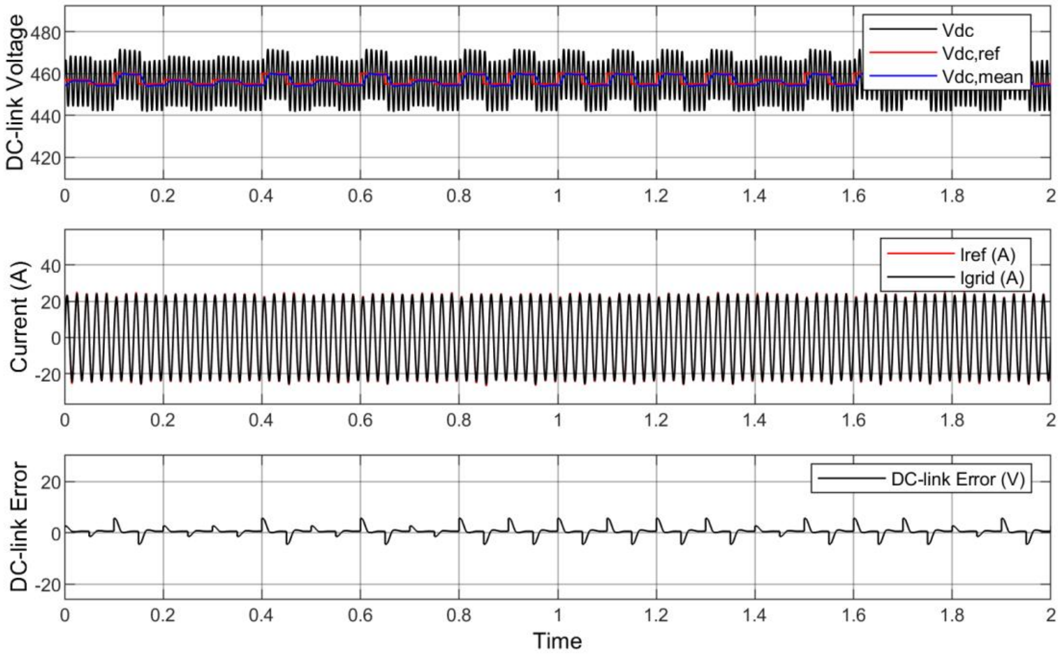

Figure 5.44. The obtained results of the developed MInCon-v MPPT algorithm with random step size (DC-link voltage, grid current, and DC-link error) operated under full-power operating conditions

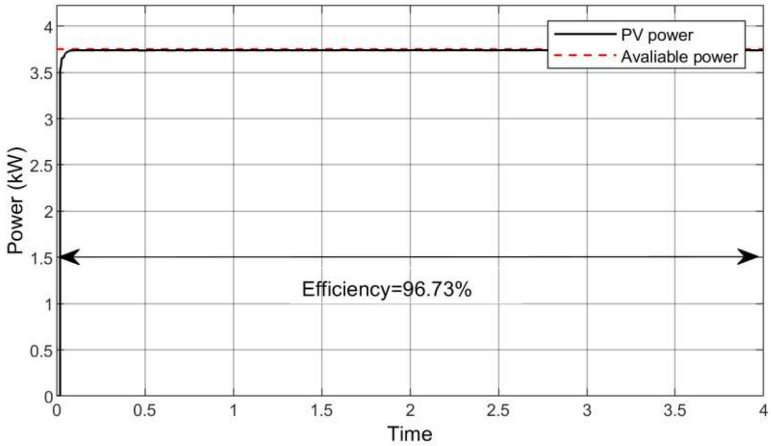

Figure 5.45. The efficiency resulted from the extracted PV power for the developed MInCon-v MPPT algorithm under 1000 W/m^2 solar irradiance at full-power operating conditions

The results under full-power operating conditions show that the tracking efficiency obtained under the MInCon-v MPPT algorithm is 96.73%, whereas it was 96.51%. The obtained grid current interharmonics are lower than the InCon MPPT method, and the total harmonics distortion level is 2.15%, whereas it was 2.49%. Figure 5.46 to Figure 5.48 below shows the operation under low-power operating conditions.

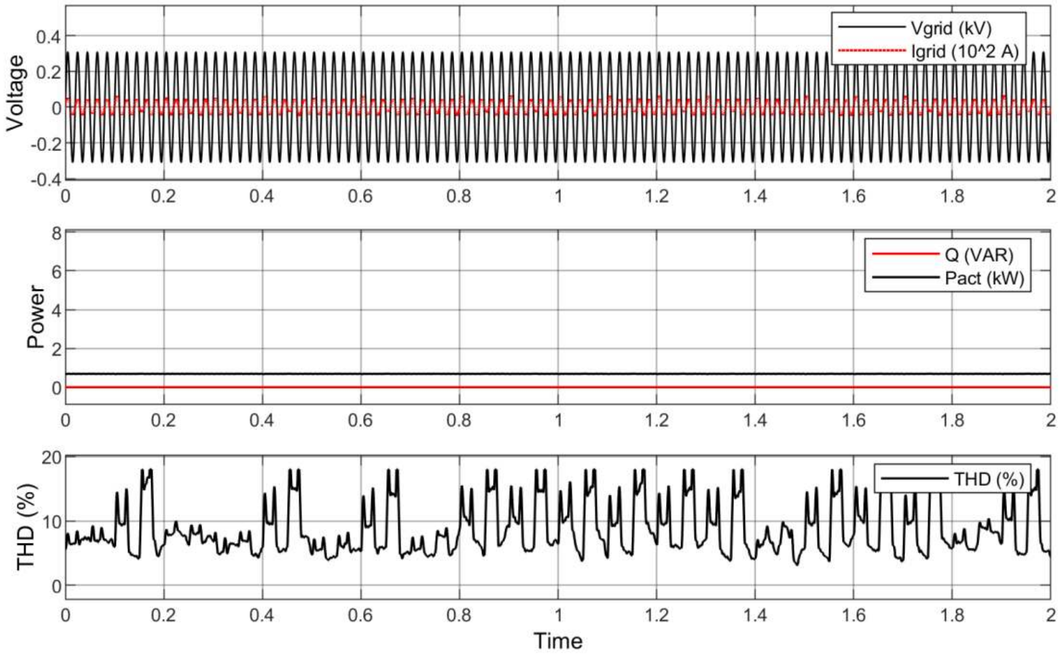

Figure 5.46. The obtained results of the developed MInCon-v MPPT algorithm (dc-link voltage, injected active and reactive power, and THD) under low-power operating conditions

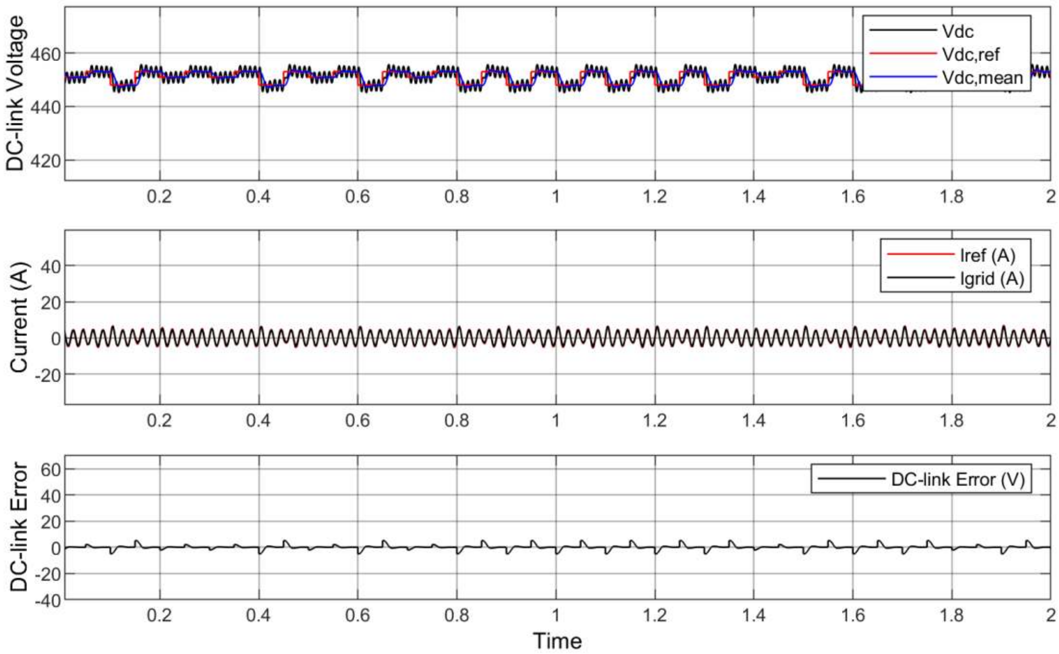

Figure 5.47. The obtained results of the developed MInCon-v MPPT algorithm (DC-link voltage, grid current, and DC-link error) under low-power operating conditions

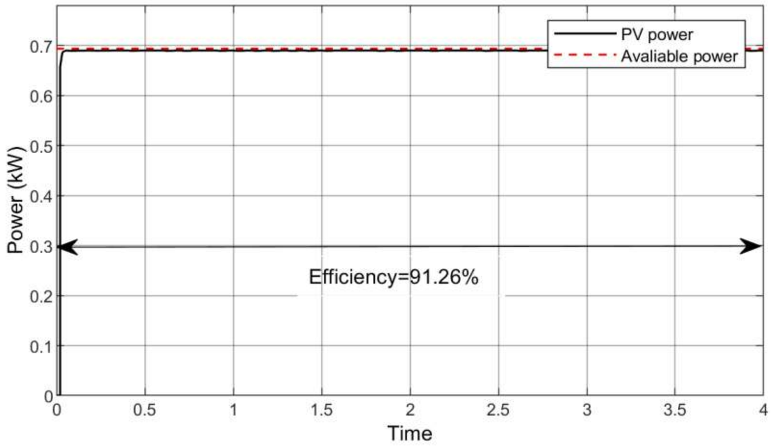

Figure 5.48. The efficiency resulted from the extracted PV power for the developed MInCon-v MPPT algorithm under 185 W/m^2 solar irradiance at low-power operating conditions

The results under low-power operating conditions show that the tracking efficiency obtained under the MInCon-v MPPT algorithm is 91.26%, which is improved from the conventional InCon of 89.49%. The obtained grid current interharmonics are lower than the InCon MPPT method, and the total harmonics distortion level is 10.3%, whereas it was 12.61%. The frequency spectrum of the injected grid current is shown in Figure 5.49, which compares the performance of the proposed MInCon-v with the InCon method under low-power operating conditions. It is evident that the proposed method is capable of mitigating the interharmonics resulting from the conventional InCon method.

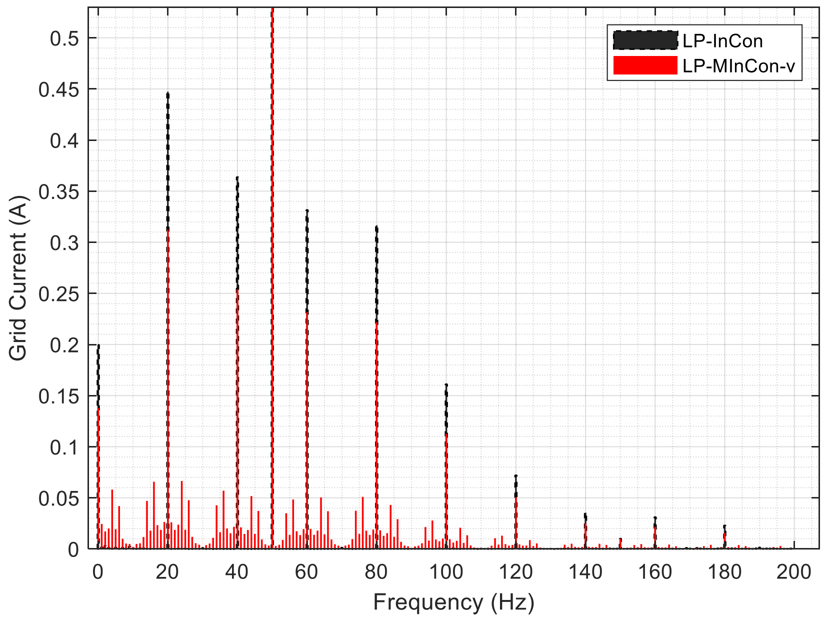

Figure 5.49. The injected grid current frequency spectrum under steady-state low-power operating conditions, comparison between the proposed MInCon-v with InCon MPPT algorithms with a frequency resolution of 1 Hz

5.3.7. The Proposed Modified Sampling Frequency InCon Method

The evaluation of the performance characteristics for the proposed MInCon-f MPPT algorithm is shown in Figure 5.50 to Figure 5.57. The analysis is performed at full- and low-power operating conditions.

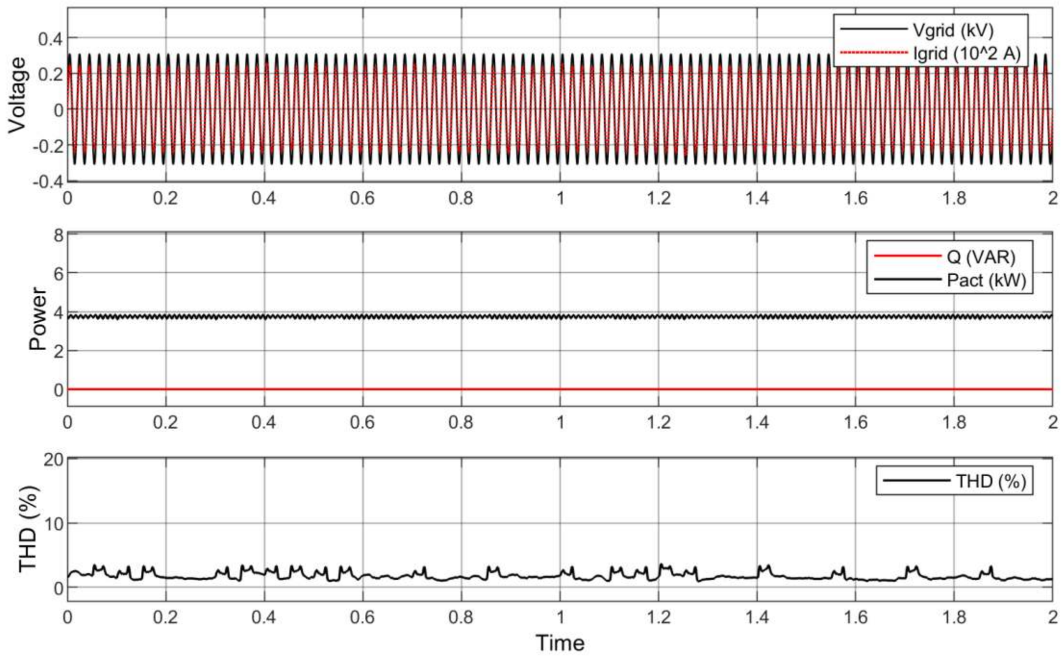

Figure 5.50. The obtained results of the developed MInCon-f MPPT algorithm (DC-link voltage, injected active and reactive power, and THD) operated under full-power operating conditions

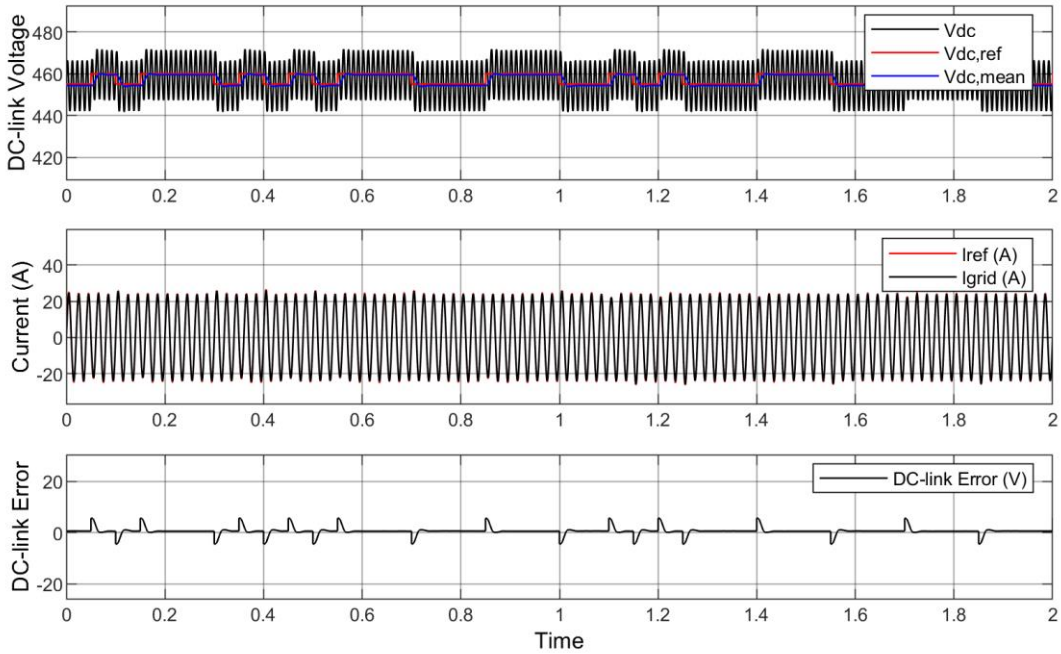

Figure 5.51. The obtained results of the developed MInCon-f MPPT (DC-link voltage, grid current, and DC-link error) operated under full-power operating conditions

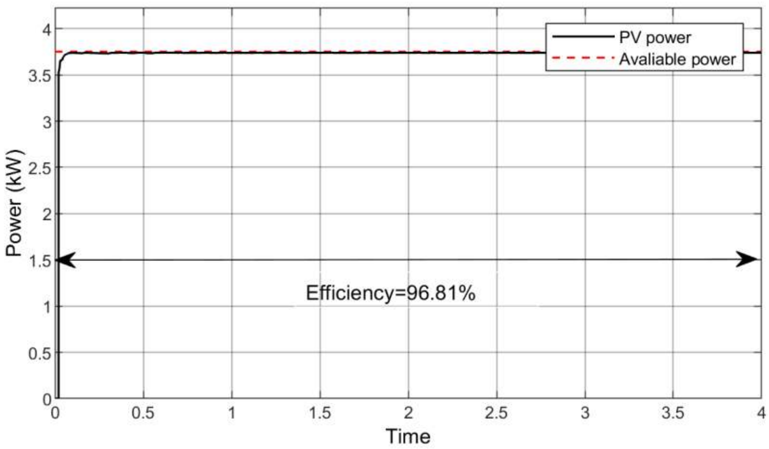

Figure 5.52. The efficiency resulted from the extracted PV power for the developed MInCon-f MPPT algorithm under 1000 W/m^2 solar irradiance at full-power operating conditions

The simulation results under full-power operating conditions depict the tracking efficiency in Figure 5.52 of 96.81% under the MInCon-f MPPT algorithm. The observed grid current interharmonics are lower than the InCon MPPT method, and the total harmonics distortion level is 2.13% or 16.9% reduction of interharmonics and THD. The system reaches the steady state operation in about 200 ms. The performance of the developed MInCon-f MPPT algorithm under low-power operating conditions is also investigated in Figure 5.53 to Figure 5.55 below.

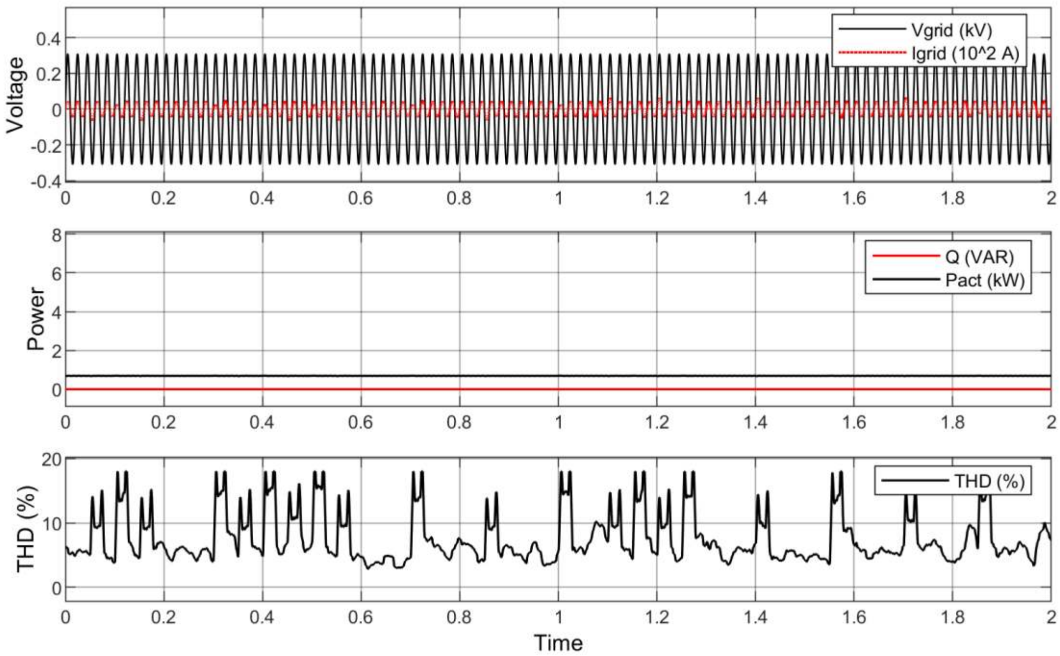

Figure 5.53. The obtained results of the developed MInCon-f MPPT algorithm (dc-link voltage, injected active and reactive power, and THD) operated under low-power operating conditions

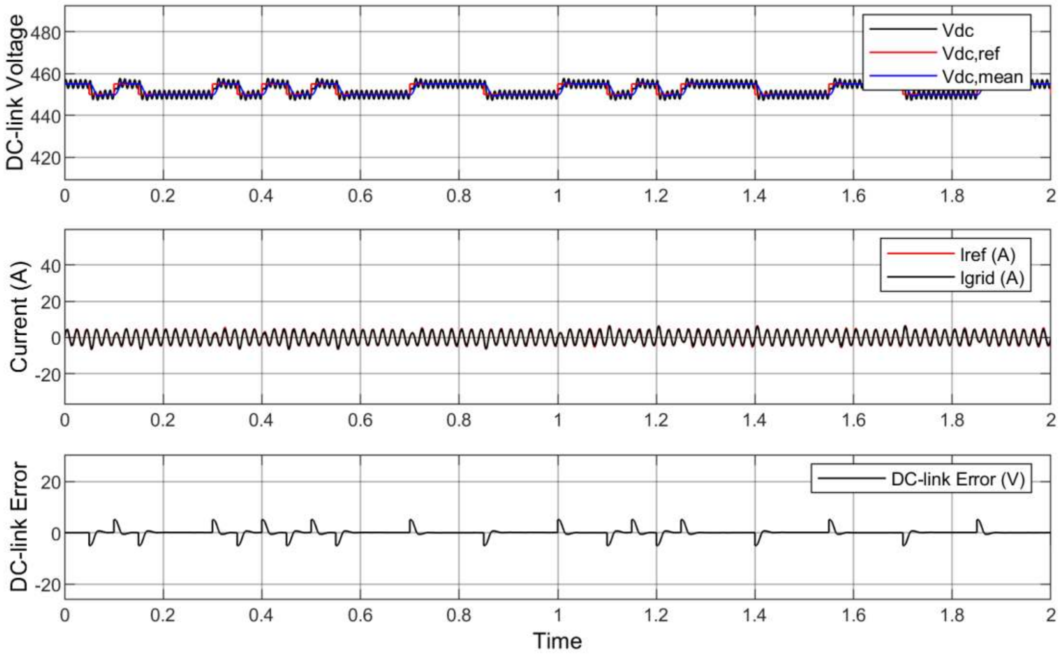

Figure 5.54. The obtained results of the developed MInCon-f MPPT (DC-link voltage, grid current, and DC-link error) operated under low-power operating conditions

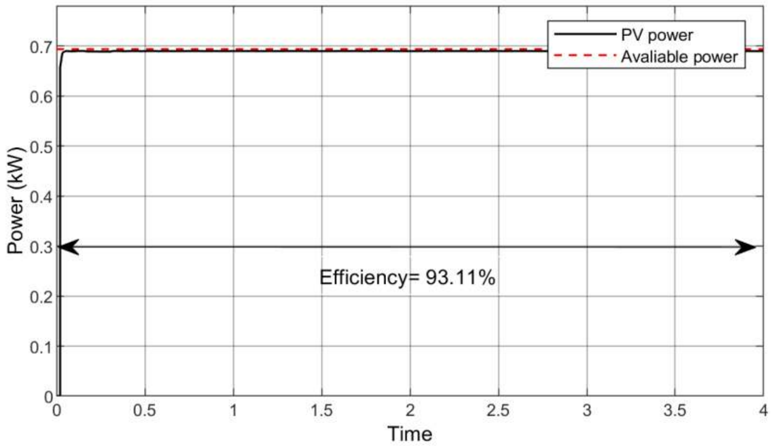

Figure 5.55. The efficiency resulted from the extracted PV power for the developed MInCon-f MPPT algorithm with random sampling frequency under 185 W/m^2 solar irradiance at full-power operating conditions

The frequency spectrum of the injected grid current is presented in Figure 5.56, and it compares the performance characteristics of the proposed MInCon-f and the conventional InCon MPPT algorithms under low-power operating conditions. Furthermore, a comparison between the proposed methods is conducted in Figure 5.56. It can be observed that MInCon-f is better than the MInCon-v in reducing the interharmonics peaks.

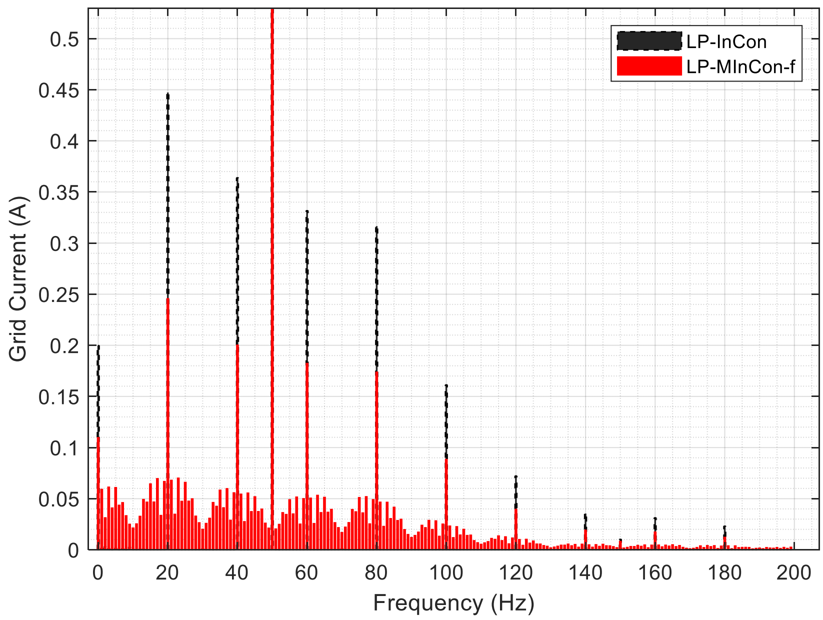

Figure 5.56. The injected grid current frequency spectrum under steady-state low-power operating conditions, comparison between MInCon-f and InCon MPPT algorithms with a frequency resolution of 1 Hz

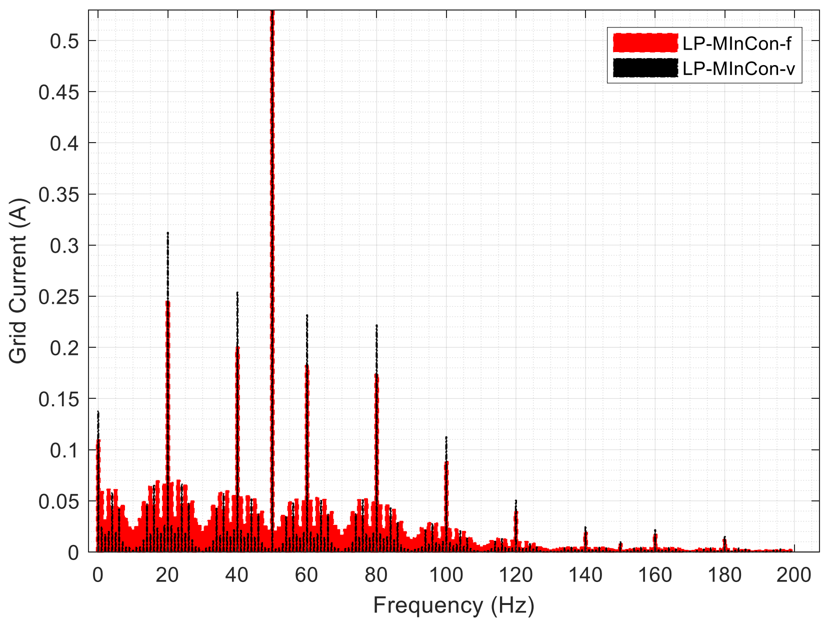

Figure 5.57. The injected grid current frequency spectrum under steady-state low-power operating conditions, comparison between MInCon-f and MInCon-v MPPT algorithms with a frequency resolution of 1 Hz

5.3.8. The Proposed Hybrid Random InCon MPPT Algorithm

In this section, the performance characteristics of the proposed hybrid random MPPT MInCon algorithm are presented in Figure 5.58 to Figure 5.67. The analysis is conducted under full- and low-power operating conditions.

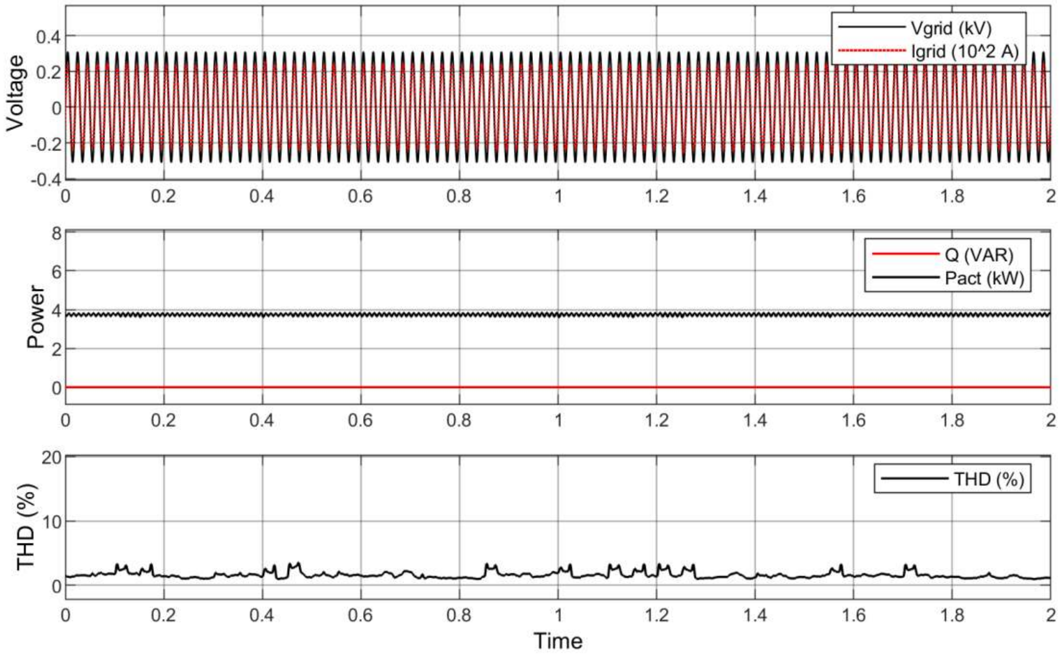

Figure 5.58. The obtained results of the proposed MInCon MPPT algorithm with the proposed hybrid random technique (dc-link voltage, injected active and reactive power, and THD) operated under full-power-operating conditions

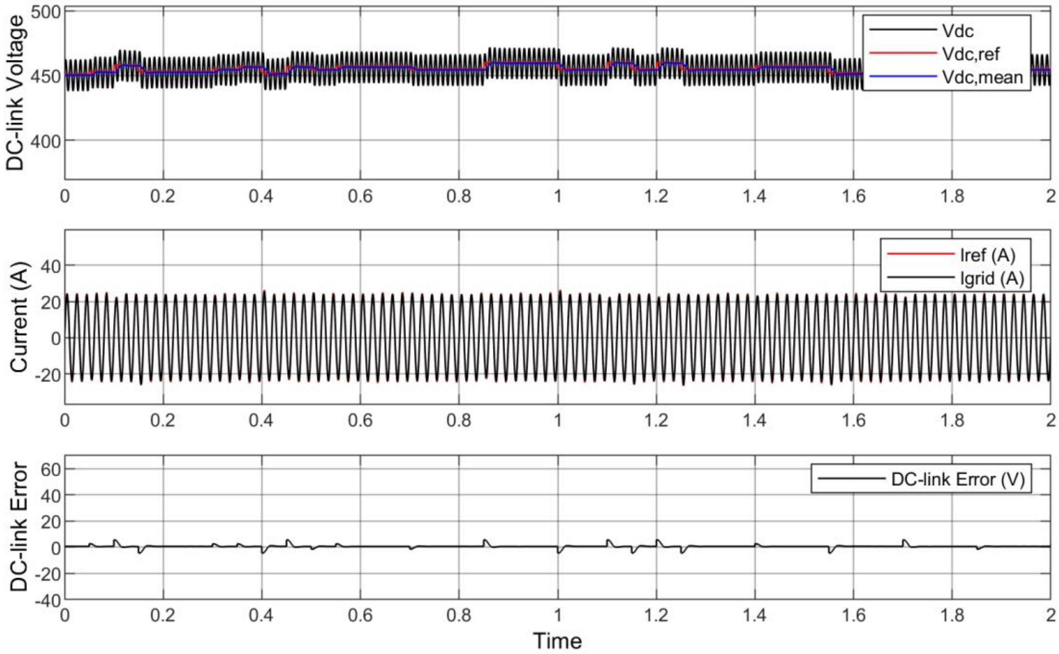

Figure 5.59. The obtained results of the proposed MInCon MPPT algorithm with proposed hybrid random technique (DC-link voltage, grid current, and DC-link error) operated under full-power-operating conditions

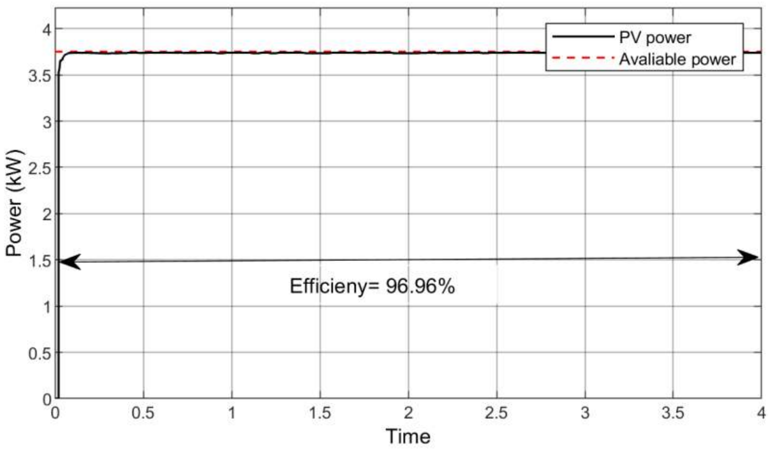

Figure 5.60. The efficiency resulted from the extracted PV power for the developed MInCon MPPT algorithm under 1000 W/m^2 solar irradiance at full-power-operating conditions

The results under full-power operating conditions reveal that the tracking efficiency obtained under the MInCon MPPT algorithm is 96.96%. The observed grid current interharmonics are lower than the InCon MPPT method, and the total harmonics distortion level is 1.82%. Figure 5.61 to Figure 5.63 depict the obtained results under low-power operating conditions for the developed MInCon MPPT algorithm.

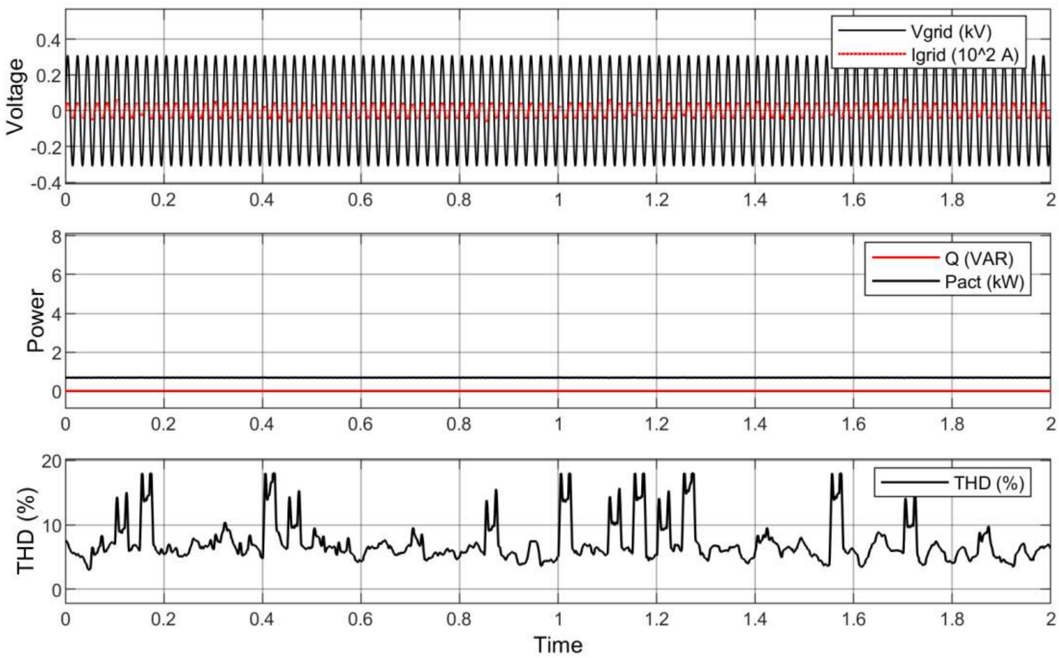

Figure 5.61. The obtained results of the proposed MInCon MPPT algorithm with proposed hybrid random technique (dc-link voltage, injected active and reactive power, and THD) under low-power-operating conditions

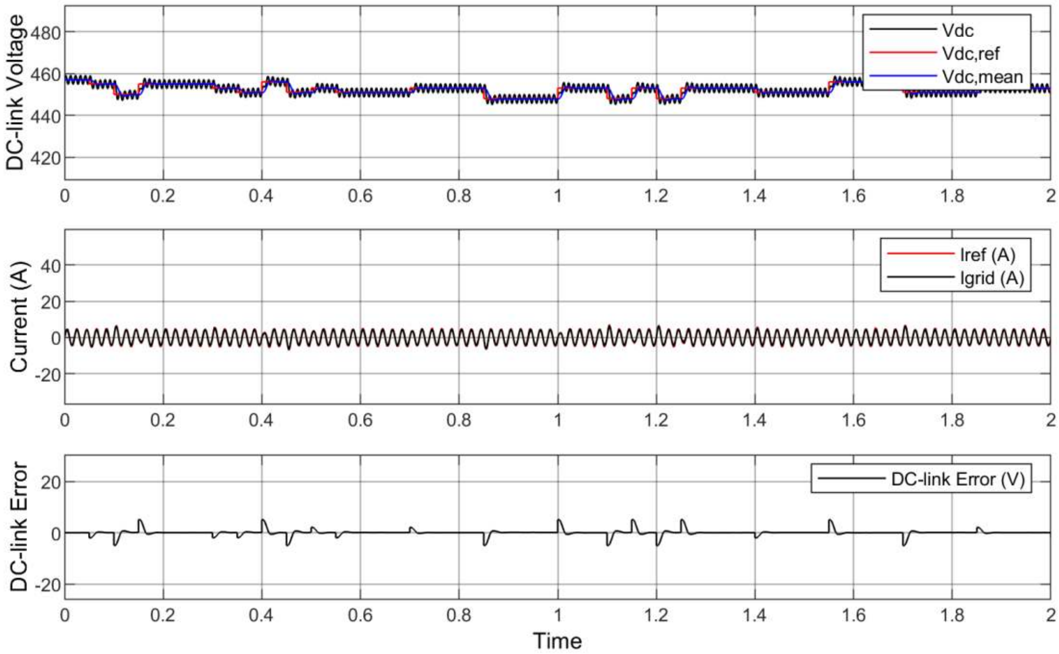

Figure 5.62. The obtained results of the proposed MInCon MPPT algorithm with proposed hybrid random technique (DC-link voltage, grid current, and DC-link error) under low-power-operating conditions

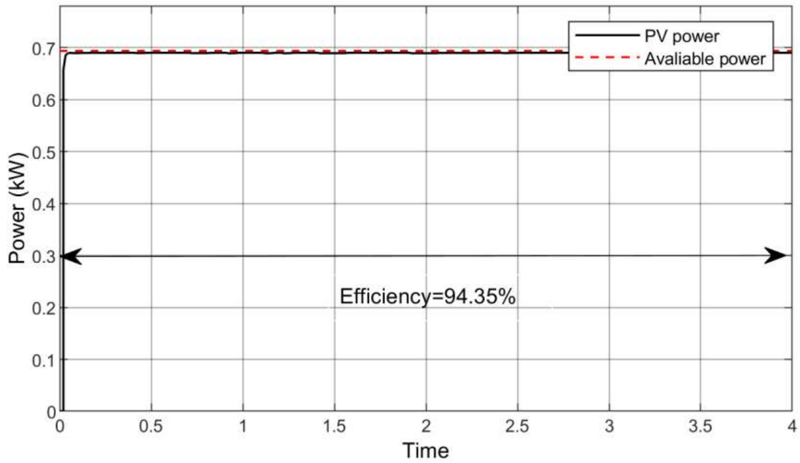

Figure 5.63. The efficiency resulted from the extracted PV power for the developed MPPT algorithm under 185 W/m^2 solar irradiance at low-power-operating conditions

Under the proposed MInCon MPPT algorithm, the performance at low-power operating conditions reveals that the efficiency is increased from 89.49% to 94.34%, and the THD is reduced from 12.43% to 8.41%. The frequency spectra of different proposed algorithms are shown in Figure 5.64 to Figure 5.67 to evaluate the interharmonics mitigation methods. It is evident that the developed MInCon and MP&O MPPT algorithms minimize the interharmonics in the frequency spectrum and reduce the THD from 2.49% to 1.82% and from 12.61% to 8.41% under full and low-power operating conditions, respectively, by an improvement of over than 26.91%.

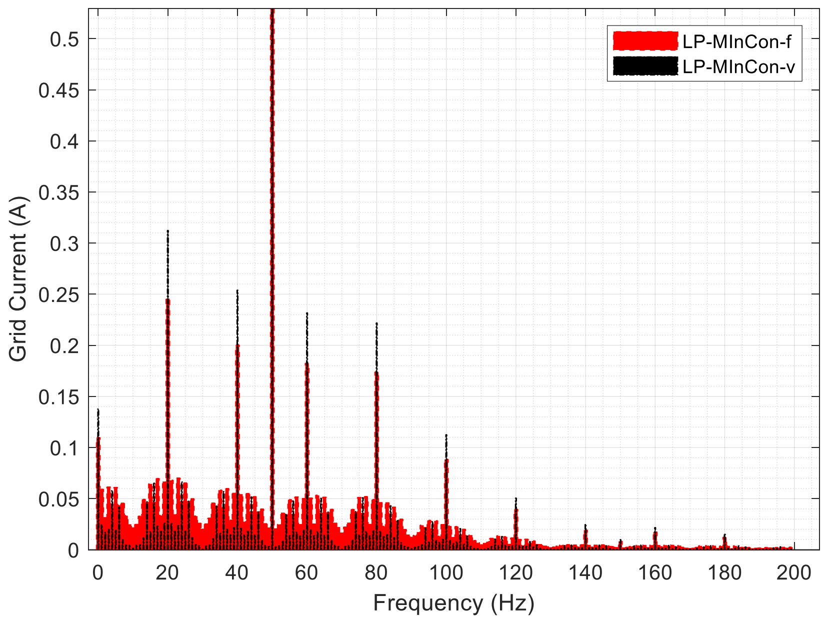

Figure 5.64. The injected grid current frequency spectrum under steady-state low-power operating conditions, comparison between MInCon-v and MInCon-f MPPT algorithms with a frequency resolution of 1 Hz

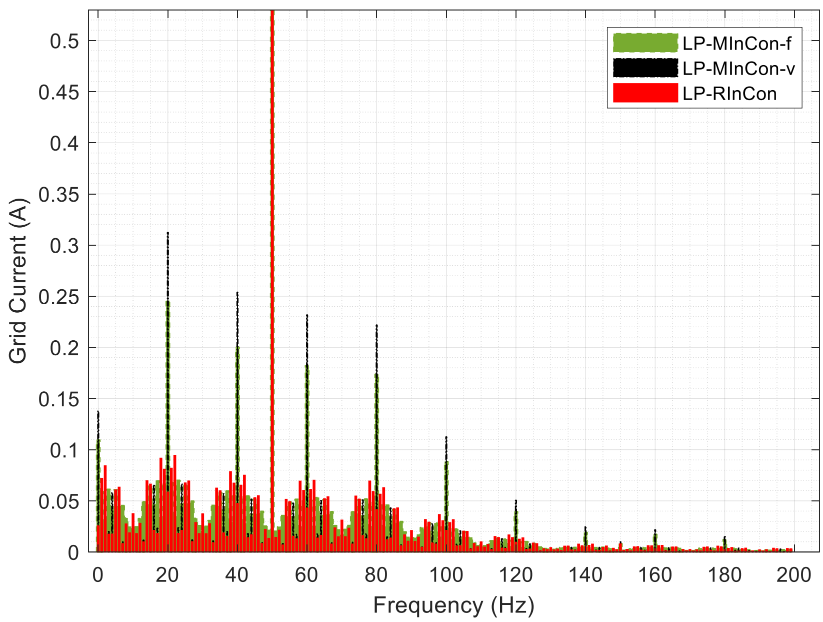

Figure 5.65. The injected grid current frequency spectrum under steady-state low-power operating conditions, comparison between MInCon-v, MInCon-f, and MInCon MPPT algorithms with a frequency resolution of 1 Hz

From Figure 5.65, it is evident that the performance of the proposed hybrid random MInCon in mitigation of the injected grid current interharmonics is superior to the proposed MInCon-v and MInCon-f. However, compared to the conventional InCon, all of the proposed methods significantly contribute to the reduction of interharmonics emissions in the frequency spectrum.

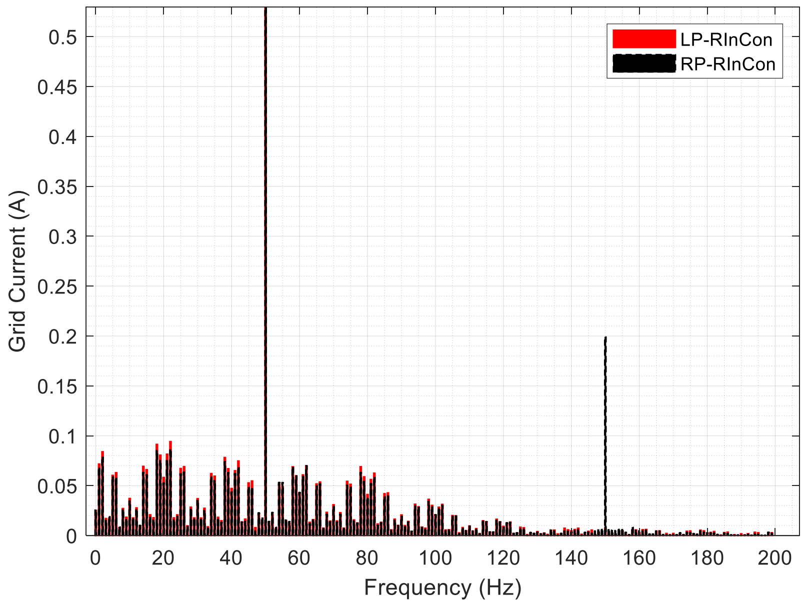

Figure 5.66. The injected grid current frequency spectrum under steady-state operating conditions, comparison of proposed MInCon MPPT algorithm between full- and low-power conditions with a frequency resolution of 1 Hz

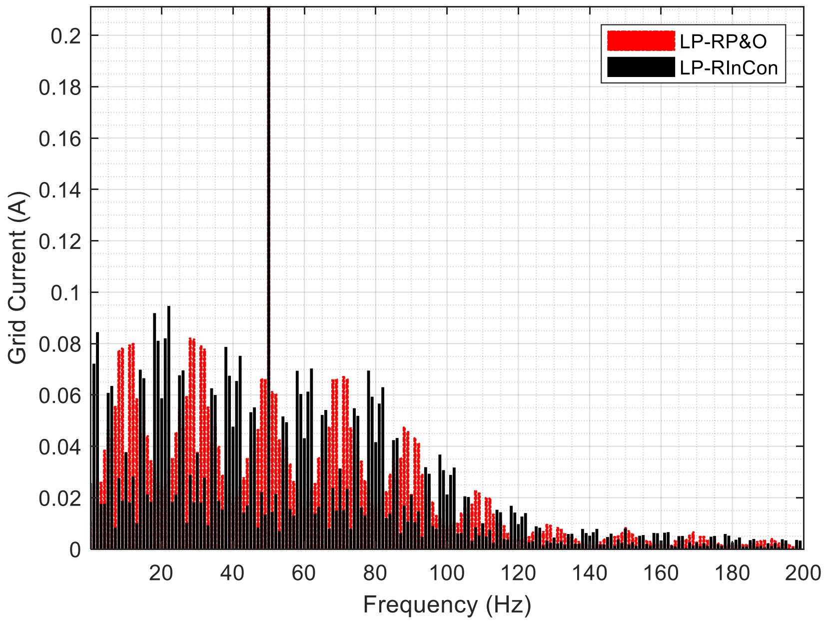

Figure 5.67. The injected grid current frequency spectrum under steady-state operating conditions, comparison of proposed MInCon (RInCon) and MP&O (RP&O) MPPT algorithms under low-power operating conditions with a frequency resolution of 1 Hz

The frequency spectrum of the injected grid current is shown in Figure 5.67 for the proposed hybrid random MInCon and MP&O MPPT algorithms under low-power operating conditions. It can be observed that both techniques significantly reduce the interharmonics emissions in the injected current and behave similarly with a slight shift of interharmonics in the frequency distribution.

5.3.9. The Proposed Neural Network Algorithm

As mentioned in previous chapters, the generating characteristics of interharmonics depend on the perturbations of the DC-link voltage. Therefore, the performance of neural network-based MPPT (NN-MPPT) algorithms is investigated in this section. The analysis is performed at full- and low-power operating conditions, as shown in Figure 5.68 to Figure 5.72.

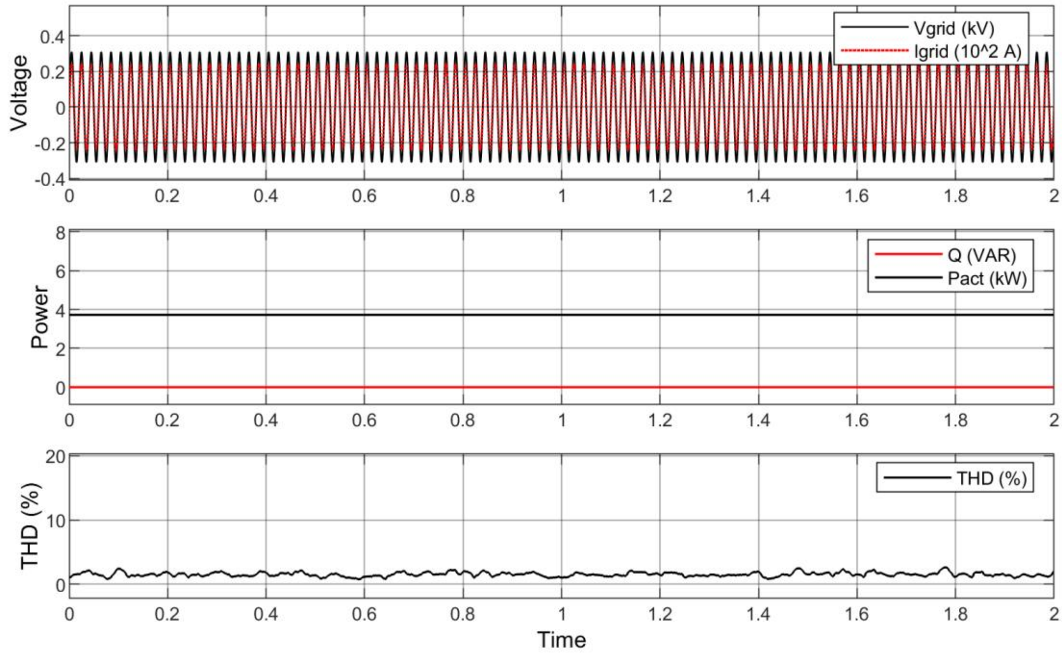

Figure 5.68. The obtained results of the proposed NN-MPPT algorithm (DC-link voltage, injected active and reactive power, and THD) under full-power operating conditions

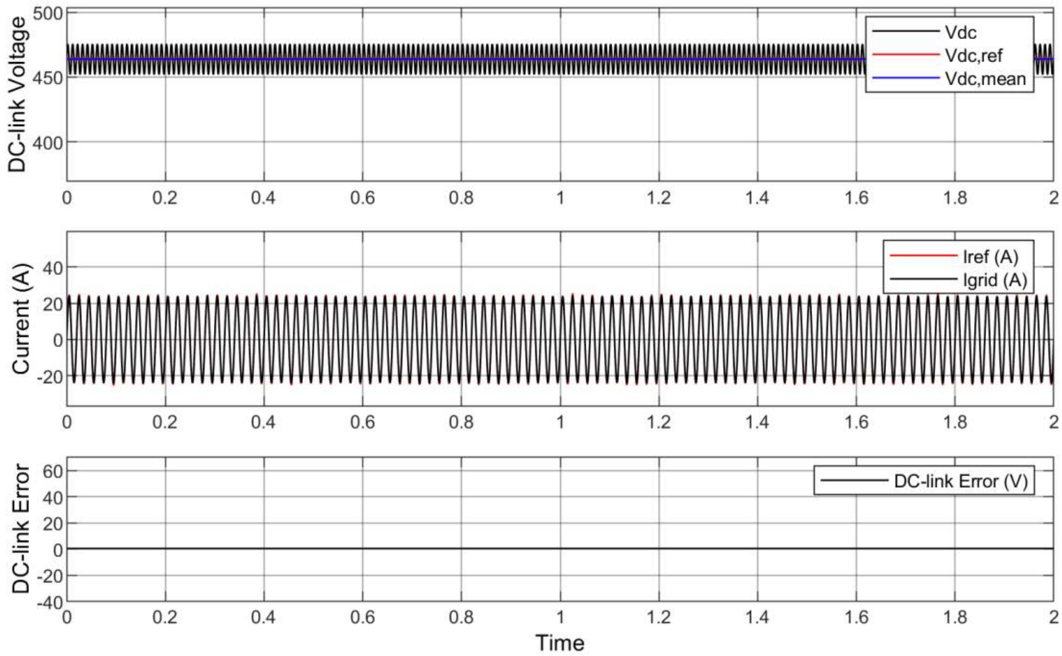

Figure 5.69. The obtained results of the proposed NN-MPPT algorithm (DC-link voltage, grid current, and DC-link error) under full-power operating conditions

The obtained efficiency under the proposed NN-MPPT algorithm is 97.12% with a THD of 1.54%. The performance of the developed MPPT algorithm under low-power operating conditions is also investigated, as shown below.

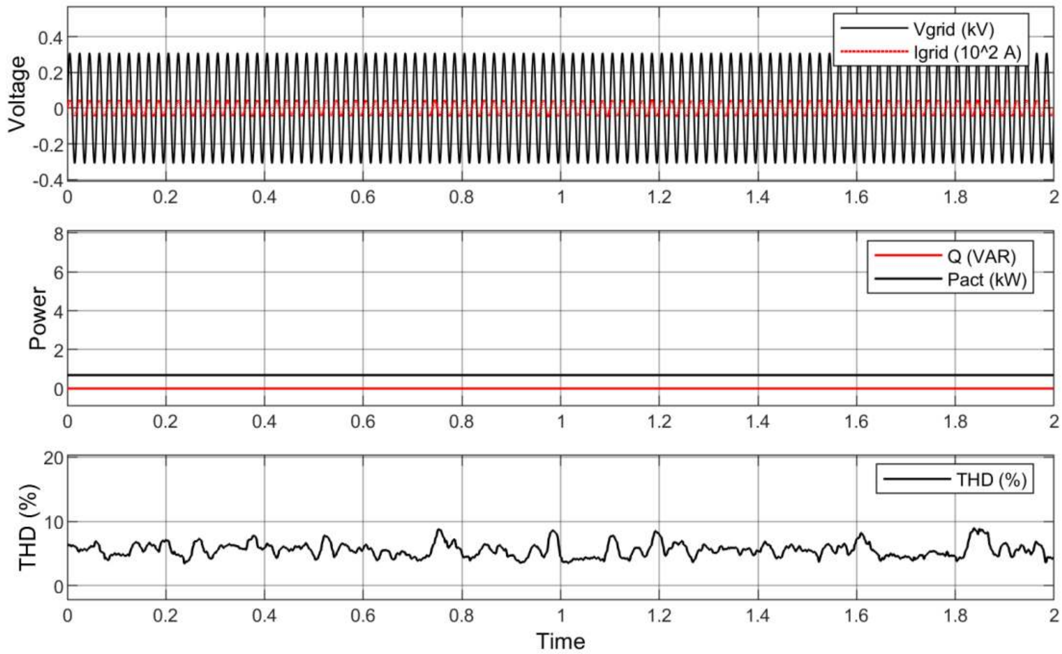

Figure 5.70. The obtained results of the proposed NN-MPPT algorithm (DC-link voltage, injected active and reactive power, and THD) under low-power operating conditions

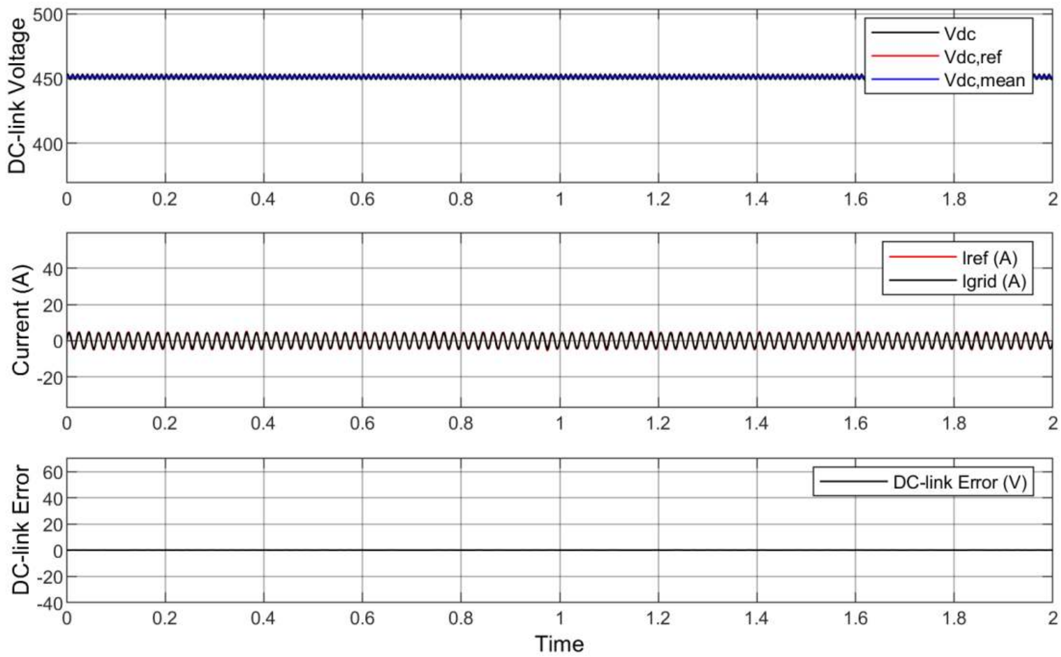

Figure 5.71. The obtained results of the proposed NN-MPPT algorithm (DC-link voltage, grid current, and DC-link error) under low-power operating conditions

Under this case, the obtained NN-MPPT tracking efficiency is 95.14%, whereas the resulting THD is 5.7%. The frequency spectrum of the injected grid current are presented in Figure 5.72, which compares the developed neural network method under low and full power conditions.

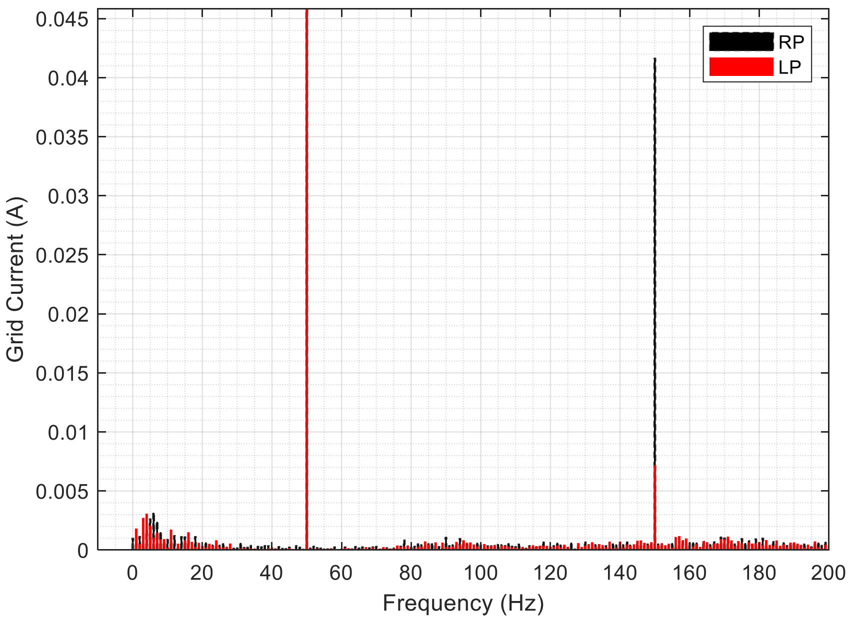

Figure 5.72. The injected grid current frequency spectrum under steady-state operating conditions, a comparison between NN-MPPT algorithm under full- and low-power operating conditions, with a frequency resolution of 1 Hz

5.3.10. The Performance Analysis under Constant-Voltage MPPT Algorithm

This section introduces the constant voltage MPPT (CV-MPPT) algorithm, which behaves similarly to the proposed NN-MPPT method. The performance of the conventional CV-MPPT algorithm is presented in Figure 5.73 to Figure 5.77. The analysis is performed at full- and -low-power operating conditions.

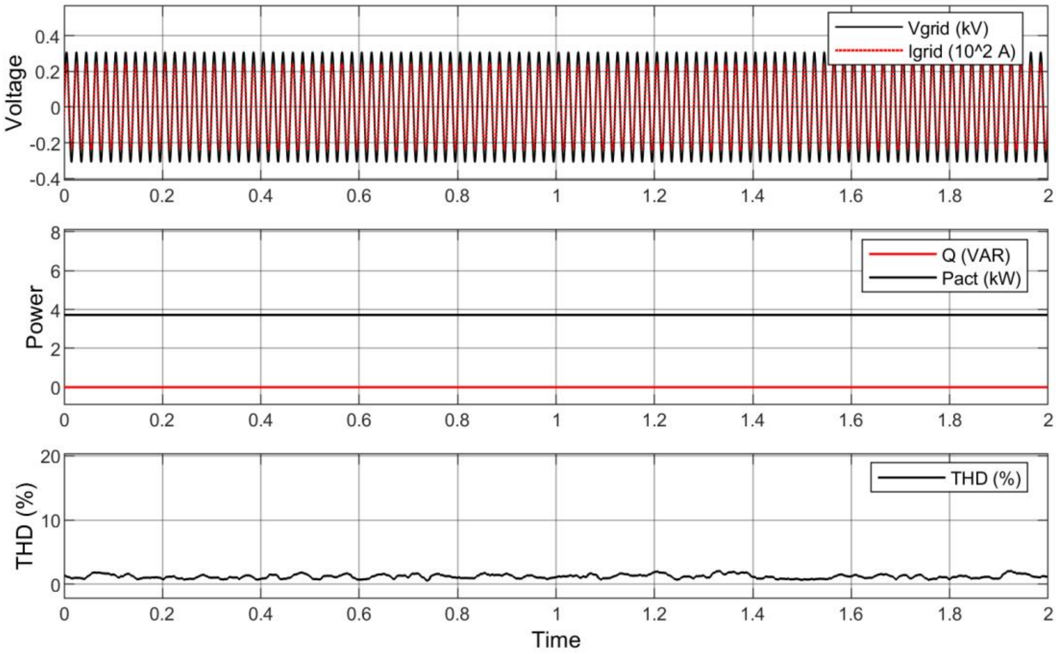

Figure 5.73. The obtained results of the developed CV-MPPT algorithm (DC-link voltage, injected active and reactive power, and THD) under full-power operating conditions

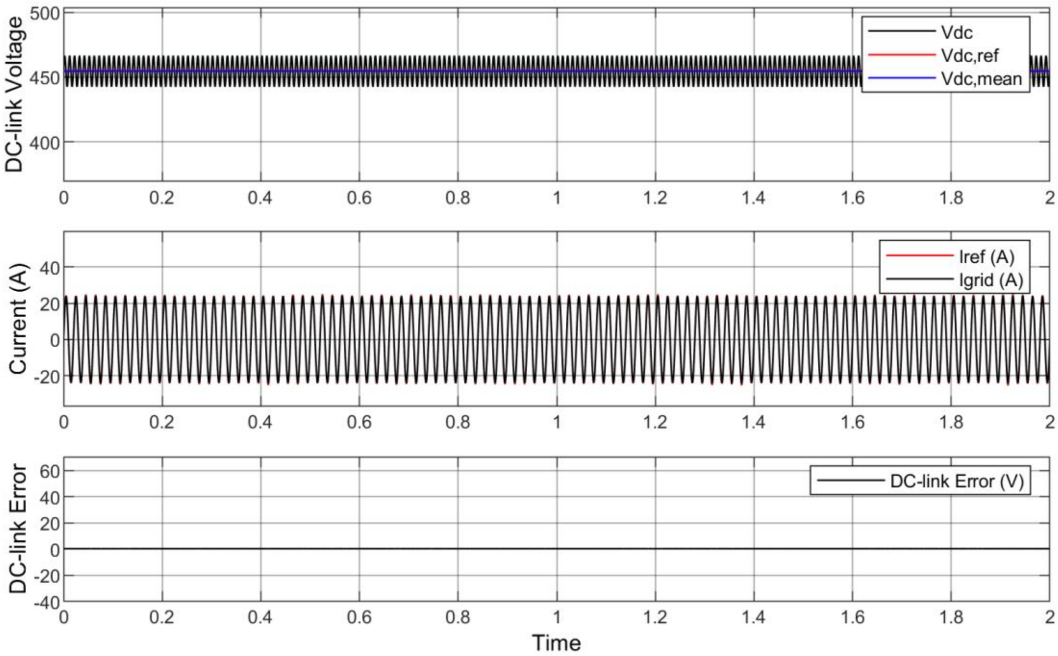

Figure 5.74. The obtained results of the developed CV-MPPT algorithm (DC-link voltage, grid current, and DC-link error) under full-power operating conditions

The obtained efficiency under the conventional CV-MPPT method is 97.53%. The resulting THD is observed to be 1.21%. The performance of the CV-MPPT algorithm under low-power operating conditions is shown in Figure 5.75 to Figure 5.77 below.

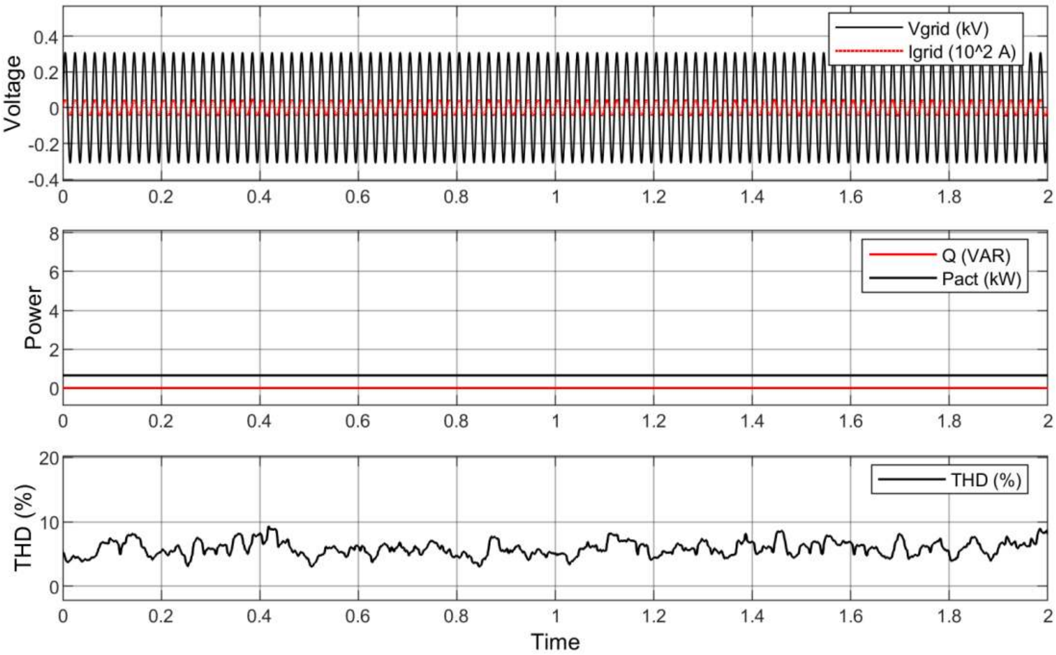

Figure 5.75. The obtained results of the developed CV-MPPT algorithm (dc-link voltage, injected active and reactive power, and THD) under low-power operating conditions

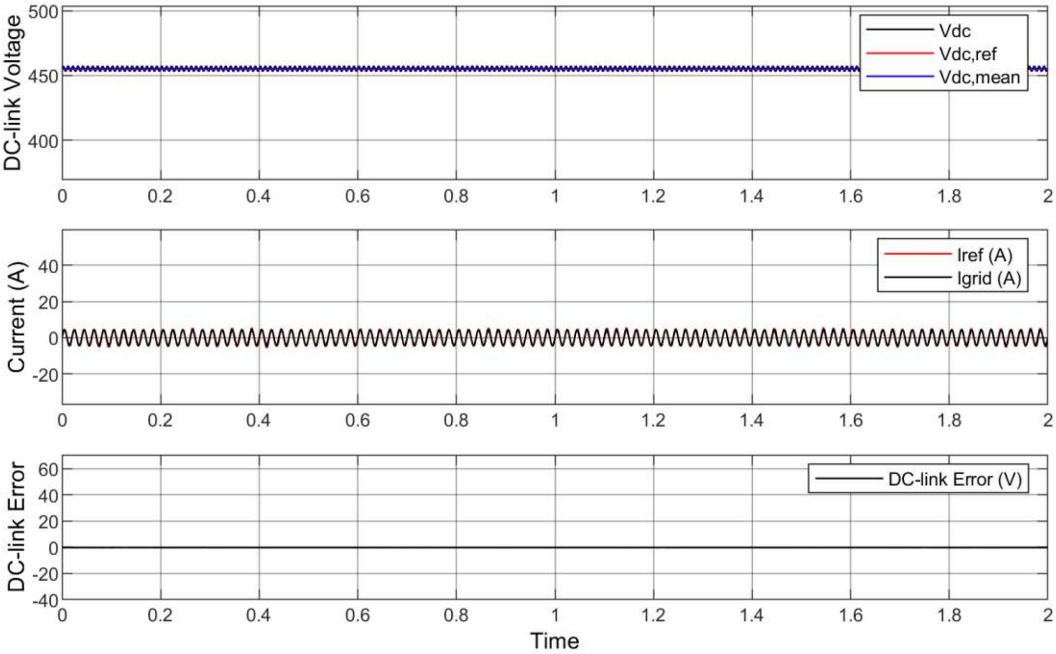

Figure 5.76. The obtained results of the developed CV-MPPT algorithm (DC-link voltage, grid current, and DC-link error) under low-power operating conditions

Under low-power operating conditions, the obtained CV-MPPT efficiency is 95.43%. Also, the resulting THD is 5.8%. The frequency spectrum of the injected grid current is shown in Figure 5.77, and it compares the conventional CV-MPPT method under low- and full-power operating conditions.

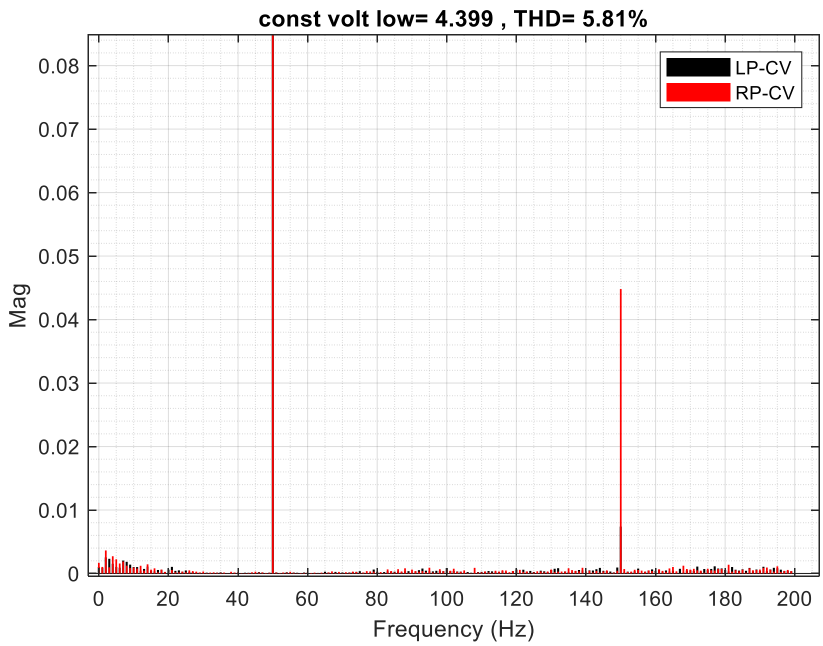

Figure 5.77. The injected grid current frequency spectrum under steady-state operating conditions, a comparison between developed MPPT methods, with a frequency resolution of 1 Hz

5.4. Summary of Results

The last section discussed proposed seven mitigation techniques and modifications to the P&O and InCon MPPT algorithms. The grid-connected PV system's enhanced control structure ensures the grid current's injection at the PCC with minimum delivered interharmonics, thus improving the PCC's PQ. The proposed mitigation techniques show a significant reduction in the emissions of interharmonics and THD with improvements in the tracking efficiencies of the MPPT algorithms, especially with low-power operating conditions. The performance characteristics of the proposed methods are depicted in Table 5.2. It can be observed that the utilization of the mitigation techniques proposed previously, which is characterized by modifying the MPPT operation, is highly affecting the perturbations of the DC-link voltage and its controller. The lowest obtained interharmonics emissions are for the proposed hybrid random MP&O, MInCon, and NN MPPT algorithms. Additionally, the CV-MPPT algorithm is considered a good candidate for minimizing the interharmonics-generating characteristics. However, some limitations are imposed on CV-MPPT and NN-MPPT algorithms, where the parameters of the inverter may change, and adaptive re-tuning is essential to ensure the best performance characteristic. Figure 5.78 and Figure 5.79 compare the obtained results under full-power operating conditions for the proposed mitigation methods.

Table 5.2. Summary of the obtained simulation results

Developed MPPT Algorithms	Rated Power			Low power			Interharmonic level
	THD (%)	η (%)	Oscillations	THD (%)	η (%)	Oscillations	
P&O	2.46	96.48	+++	12.43	89.4	+++	High
Modified P&O -V	2.06	96.71	++	10.33	91.19	++	Medium
Modified P&O -F	2.05	96.80	++	10.14	93.12	++	Medium
Modified P&O -HB	1.86	96.95	+	8.07	94.31	+	Low
InCon	2.49	96.51	+++	12.61	89.49	+++	High
Modified InCon -V	2.15	96.73	++	10.3	91.26	++	Medium
Modified InCon -F	2.13	96.81	++	9.87	93.11	++	Medium
Modified InCon HB	1.82	96.96	+	8.41	94.34	+	Low
Constant Voltage	1.21	97.53	+	5.8	95.43	+	Low
Neural Network	1.54	97.12	+	5.7	95.14	+	Low

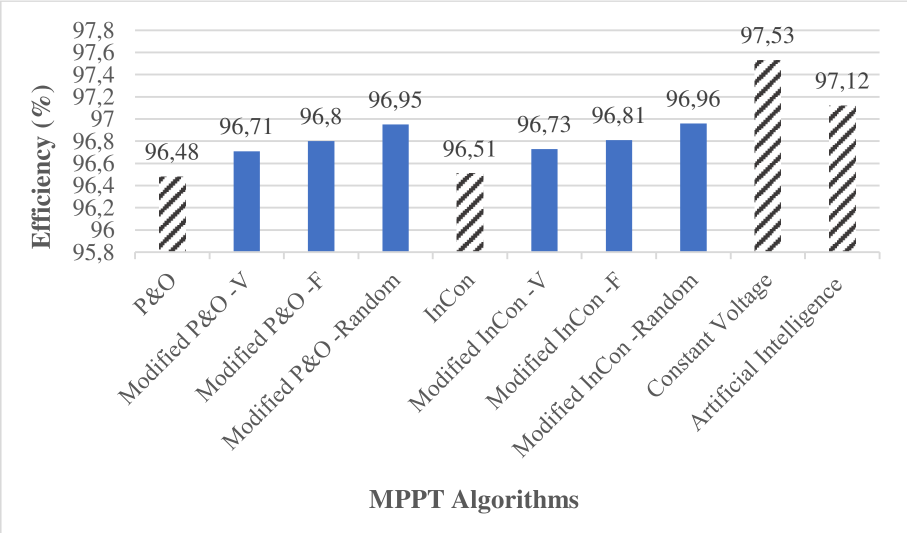

Figure 5.78. Comparison between the obtained efficiencies of the proposed MPPT algorithms under full-power operating conditions

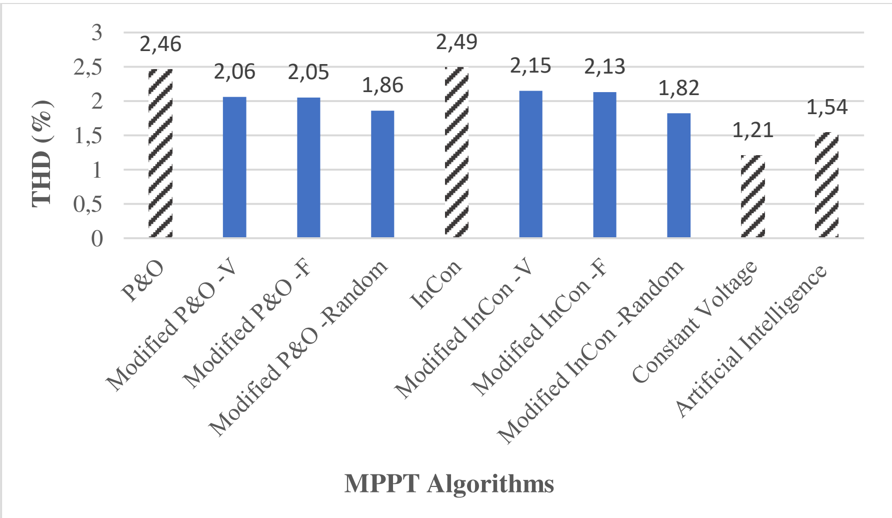

Figure 5.79. Comparison between the obtained THD values of the proposed MPPT algorithms under full-power operating conditions

Under low-power operating conditions, the obtained results are summarized in Figure 5.80 and Figure 5.81 below.

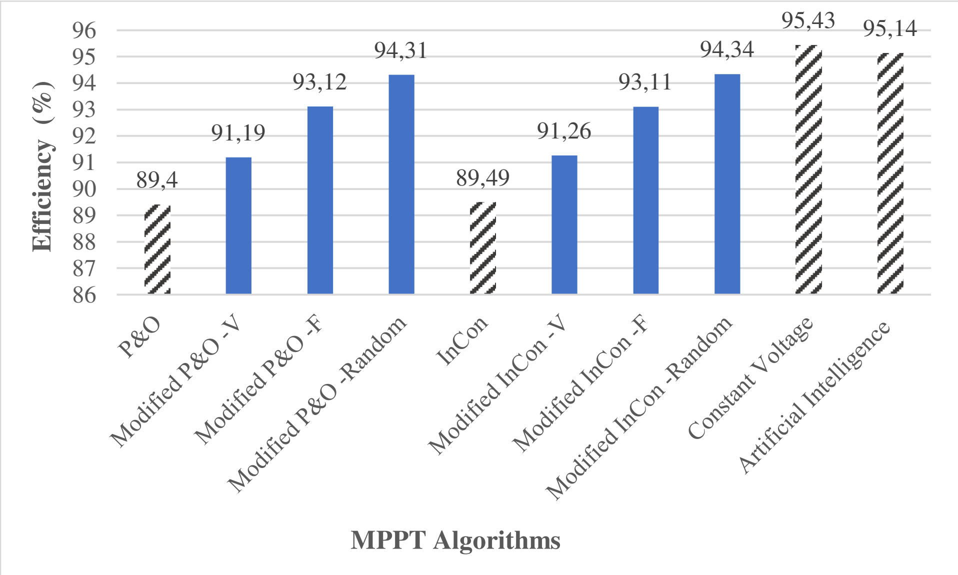

Figure 5.80. Comparison between the obtained efficiencies of the proposed MPPT algorithms under low-power operating conditions

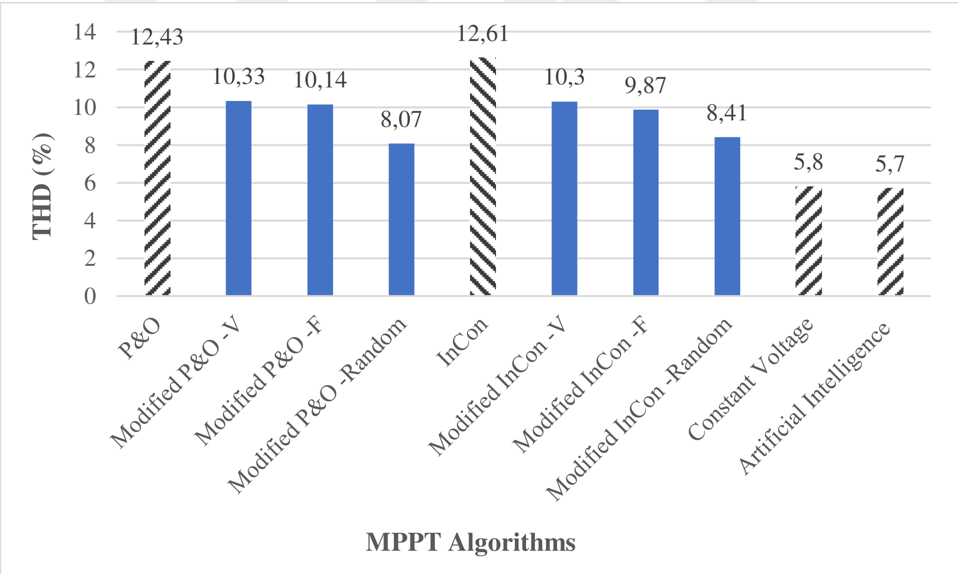

Figure 5.81. Comparison between the obtained THD values of the proposed MPPT algorithms under low-power operating conditions

5.5. Dynamical Response of the Proposed MPPT Algorithms

To evaluate the dynamical response of the proposed methods, the modified hybrid random P&O is selected to illustrate the interharmonics generating characteristic while changing the solar irradiance from 1000 W/m^2 to 800 W/m^2 to 600 W/m^2 to 1000 W/m^2, as indicated in Figure 5.82. The results in Figure 5.82 and Figure 5.83 show that the developed algorithm experienced high performance in terms of reducing the THD and interharmonics injection.

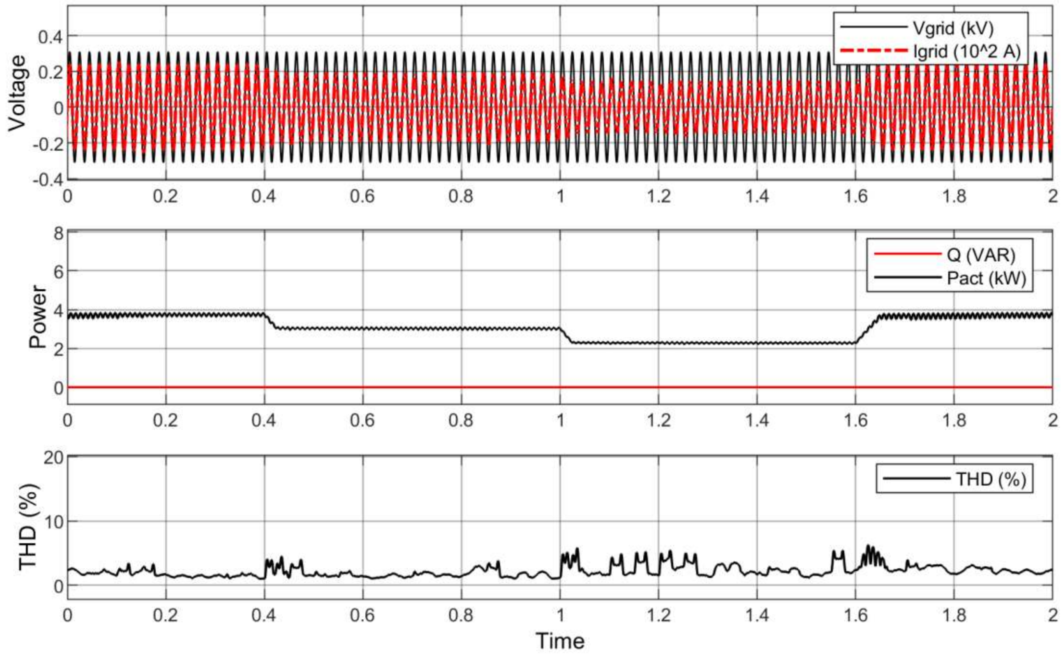

Figure 5.82. The obtained results of the proposed MP&O MPPT algorithm with the hybrid random technique (DC-link voltage, injected active and reactive power, and THD) operated under full-power operating conditions

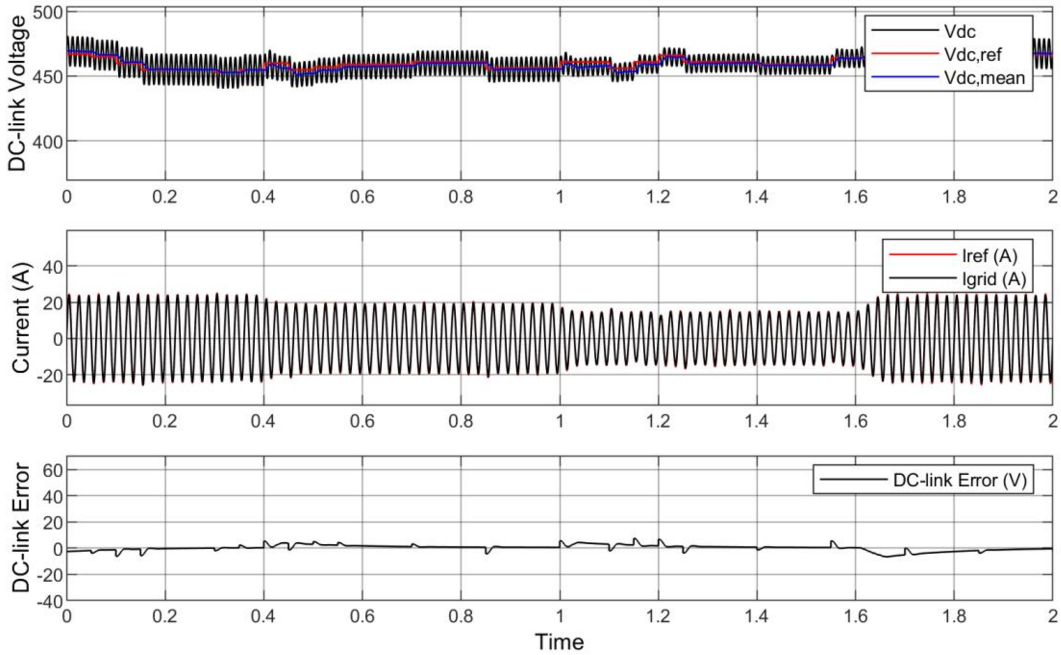

Figure 5.83. The obtained results of the proposed MP&O MPPT algorithm with the hybrid random technique (DC-link voltage, grid current, and DC-link error) operated under full-power operating conditions

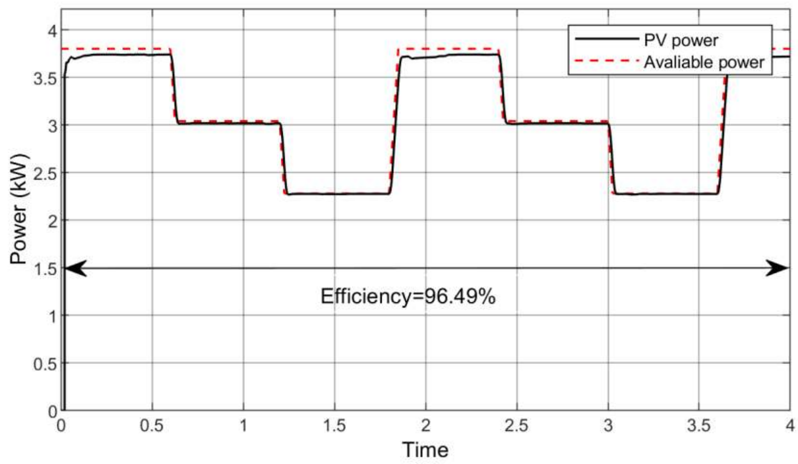

Figure 5.84. The efficiency resulted from the extracted PV power for the developed MPPT algorithm under different solar irradiances at full-power operating conditions

5.6. Multimission of the Proposed single-phase Grid-Connected PV System

Reactive power control and support are usually associated with the control and operation of grid-connected PV systems during faults that may raise the emissions of interharmonics at PCC. Different types of abnormalities could occur during the normal operation of the inverter. Not only to mention the voltage sag but also the other factors, such as the grid frequency deviation and the inverter components' aging effects with time. This section introduces a multimission profile containing the effect of LVRT, utility grid frequency deviation, and voltage sag/swell to investigate their impacts on the generating characteristic of interharmonics under different operating conditions.

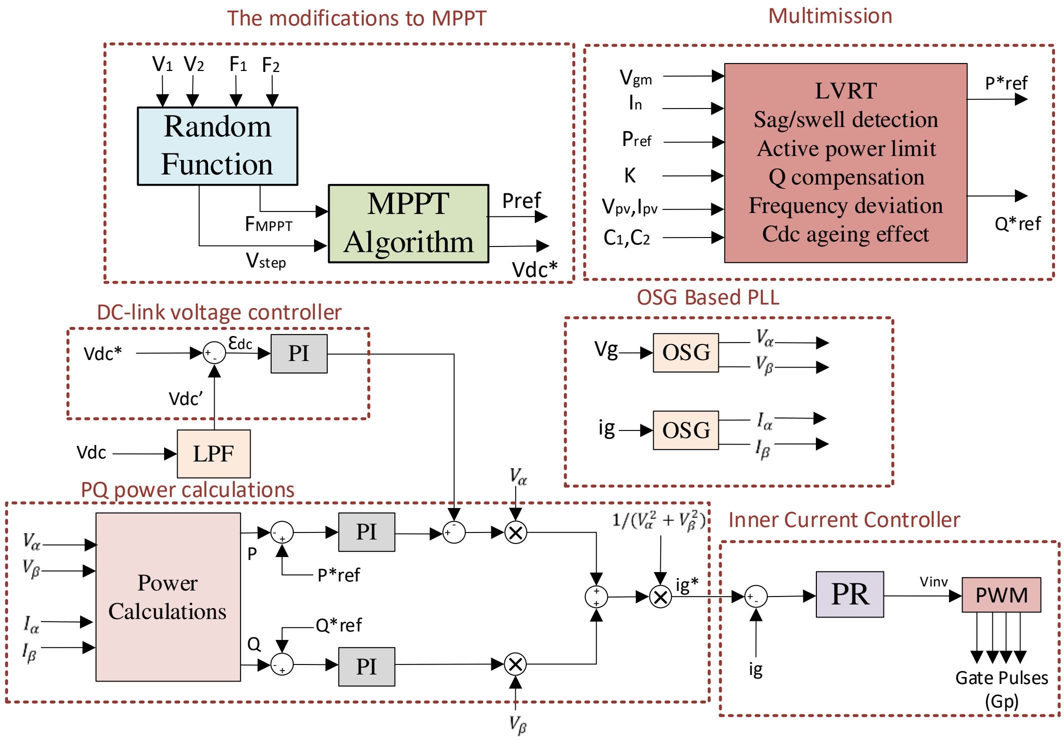

Figure 5.85. The modified control structure of the inverter

The control structure of the inverter is modified and enhanced to include the developed multimission profiles and the proposed interharmonics mitigation techniques, as shown in Figure 5.85. The simulation analysis is carried out under different operating conditions.

5.6.1. Dynamic Grid Support Capability

Many methods exist to control the reactive power injection for single-phase grid-connected PV systems. Droop control, which mimics the behavior of a synchronous generator, can be utilized. However, for single-phase systems, the grid feeder's X/R ratio is low. Therefore, this technique may not be feasible for reactive power support in grid-connected PV inverters. Another way is to use instantaneous power theory and an adaptive filtering scheme with directly synthesized power references. The main challenge in this method is the process of obtaining the synthesized power quantities. Nevertheless, another feasible solution is to use the single-phase PQ theory to flexibly control the active and reactive power in single-phase grid-connected PV systems. For this method, the grid control is performed in a stationary $\alpha\beta$ reference frame (Yang et al. 2019).

Grid monitoring is required to obtain the instantaneous grid voltage level and ensure proper operation of the LVRT. The system operation under normal operating conditions should deliver the maximum active power, i.e., Q=0, and minimize interharmonics emission. During the occurrence of a fault, the amount of active power may require to be limited to maintain a power factor value within the specified limit. The power reference values will be recalculated to specify the amount of active and reactive power to be injected into the grid. For instance, many codes are available for the amount of reactive power to be injected, e.g., the E.ON code (Luo et al. 2018) specifies the amount of Q as:

$$I_q = \begin{Bmatrix} 0 & 0.9\,pu \ \leq v_{gm} < 1.1\,pu \\ K\left(1 - v_{gm}\right) & 0.5\,pu \ \leq v_{gm} < 0.9\,pu \\ I_n & v_{gm} < 0.5\,pu \end{Bmatrix} \tag{5.4}$$

Where I_q is the reactive current, v_{gm} is the voltage magnitude, I_n is the nominal current, and k is an adjustment factor that is given by:

$$K = \frac{I_q/I_n}{1 - v_{gm}} \geq 2\,pu \tag{5.5}$$

A limitation is imposed on the total reactive power injected into the grid by:

$$|Q| \leq \sqrt{S_n - P^2} \tag{5.6}$$

It should be noted that without a reduction to the active power support, a sufficient amount of Q can be injected into the grid. Under the case of reactive power support, extended simulations are conducted to investigate the impacts of dynamic grid support and LVRT on the interharmonics generating characteristics and emissions from the single-phase grid-connected inverter. The previously developed model shown in Figure 5.85 is utilized for this purpose. A PLL-based grid monitoring technique is used to detect the variations in the grid voltage. A voltage sag of 0.8 pu is applied to the system at 0.395 seconds. The analysis is conducted under full- and low-power operating conditions, and the obtained results are shown in Figure 5.86 to Figure 5.97.

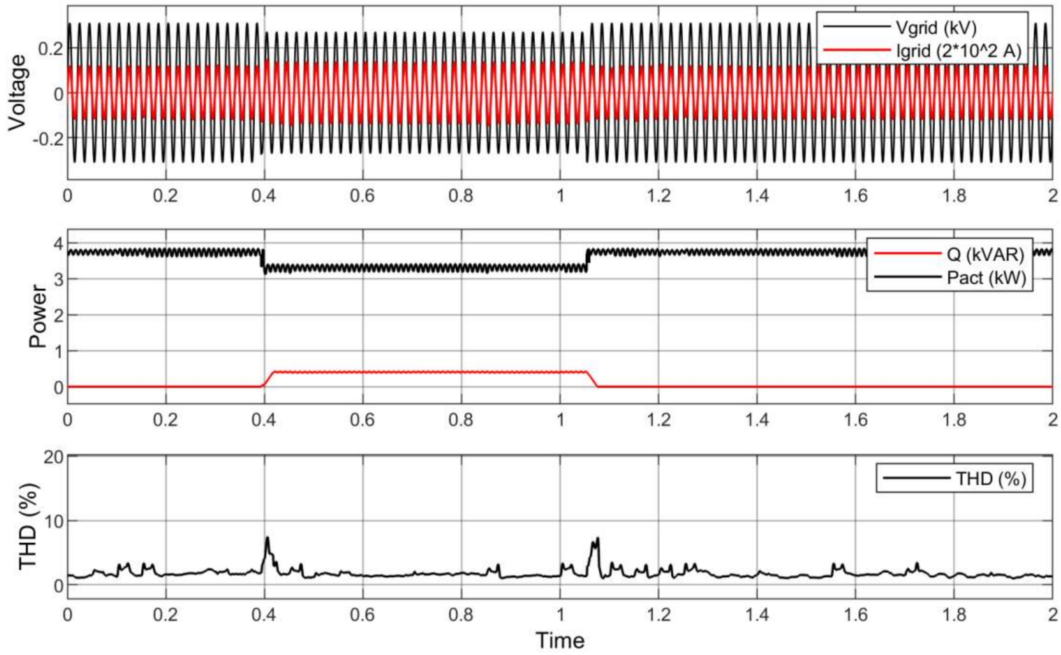

Figure 5.86. The obtained results of the proposed MP&O MPPT algorithm with the hybrid random technique (DC-link voltage, injected active and reactive power, and THD) under full-power operating conditions and LVRT

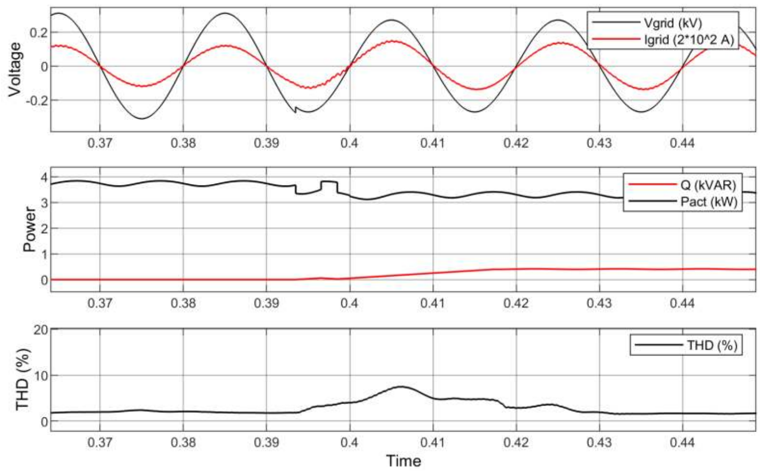

Figure 5.87. The moment of applying the fault- (DC-link voltage, injected active and reactive power, and THD) under full-power operating conditions and LVRT

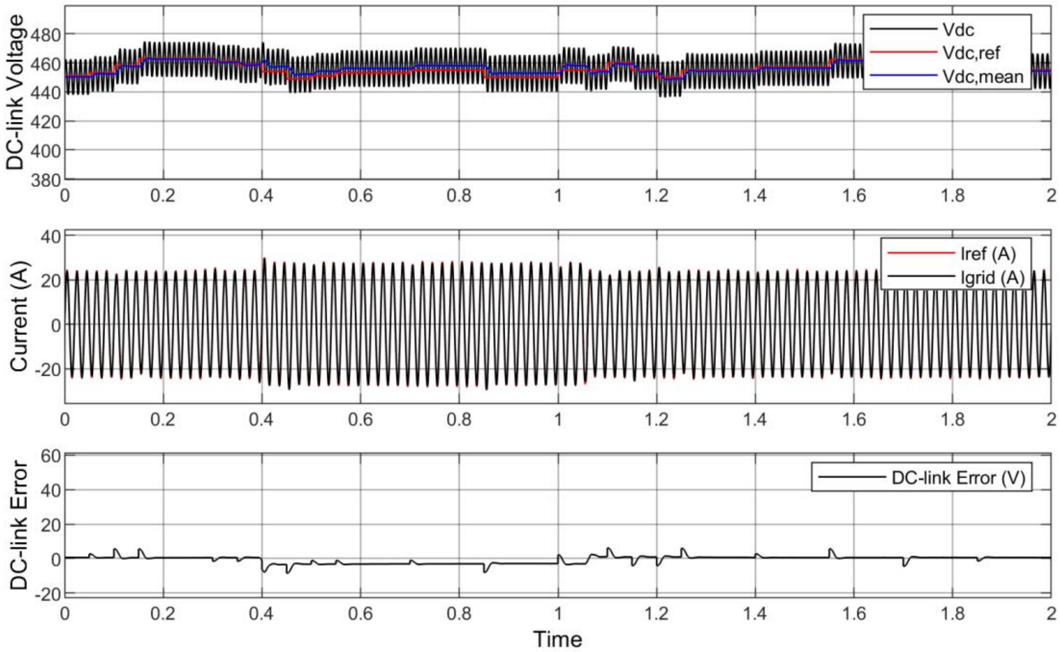

Figure 5.88. The obtained results of the proposed MP&O MPPT algorithm with the hybrid random technique (DC-link voltage, grid current, and DC-link error) under full-power operating conditions and LVRT

The results indicated that the obtained MPPT tracking efficiency is 96.82%, whereas the resulting THD is 1.87% before the fault occurrence and 3.91% during the LVRT. The injected reactive power is 400 VAR. It can be observed that the active power support is limited during the LVRT; the primary purpose is to maintain the power factor within the required utility grid requirements. The simulation is extended under the conventional P&O method to evaluate and validate the previous analysis under full-load operation conditions, as shown in Figure 5.89 and Figure 5.90.

It can be observed that the total harmonic distortion values are increased under these operating conditions with THD of 2.47% and MPPT efficiency of 96.32%. It can be included that the amount of injected reactive power is the same as in the previous case, which is 400 VAR. During the occurrence of fault with LVRT operation, the obtained THD increased to 4.52%.

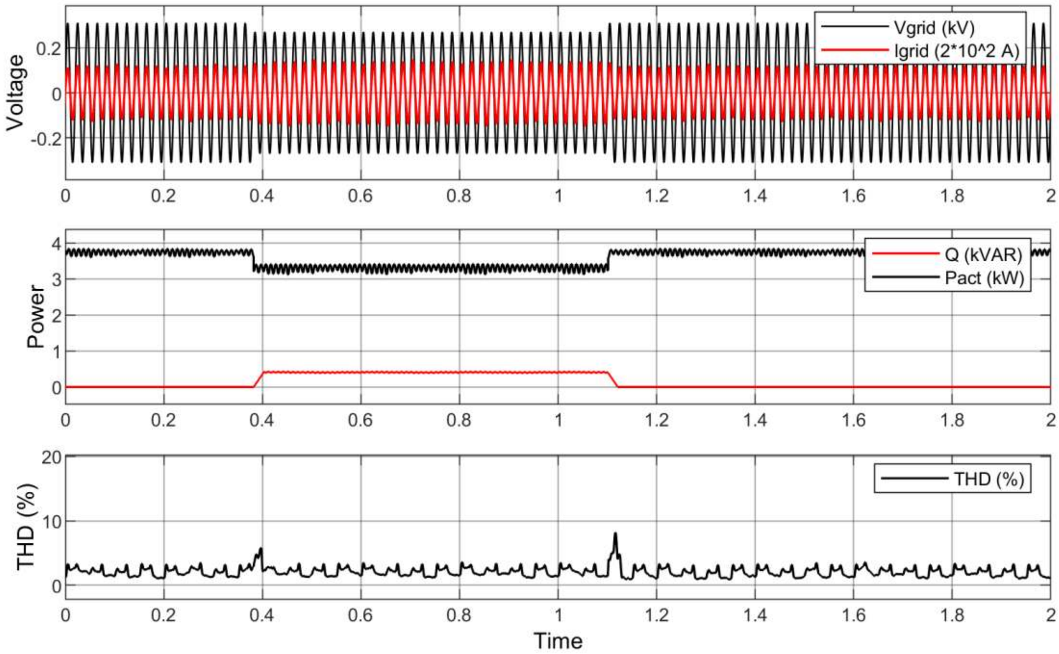

Figure 5.89. The obtained results of the developed P&O MPPT algorithm (DC-link voltage, injected active and reactive power, and THD) under full-power operating conditions and LVRT

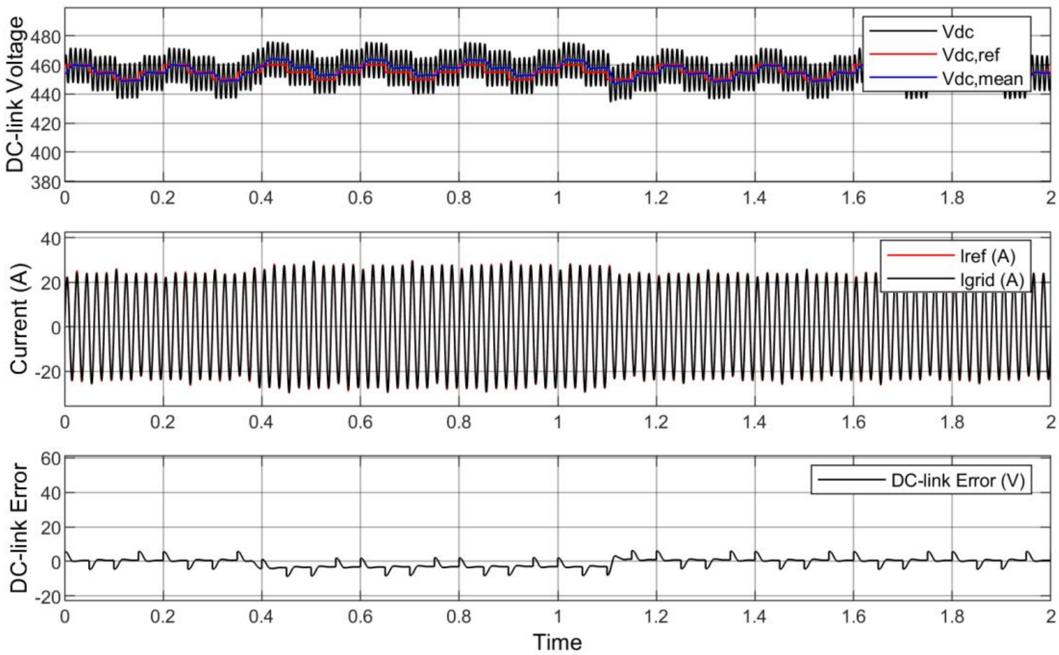

Figure 5.90. The obtained results of the developed P&O MPPT algorithm (DC-link voltage, grid current, and DC-link error) under full-power operating conditions and LVRT

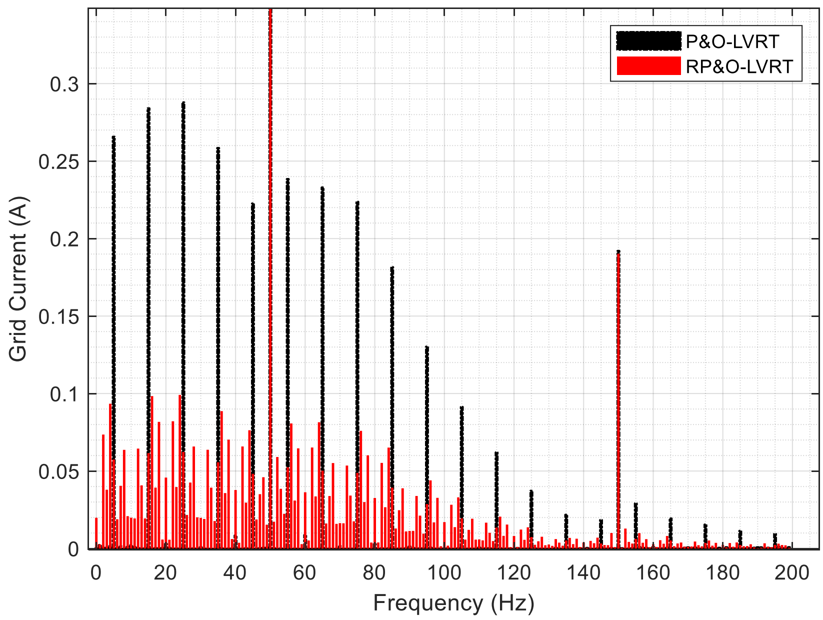

Figure 5.91. The injected grid current frequency spectrum before the operation of LVRT under full-power operating conditions and a frequency resolution of 1 Hz

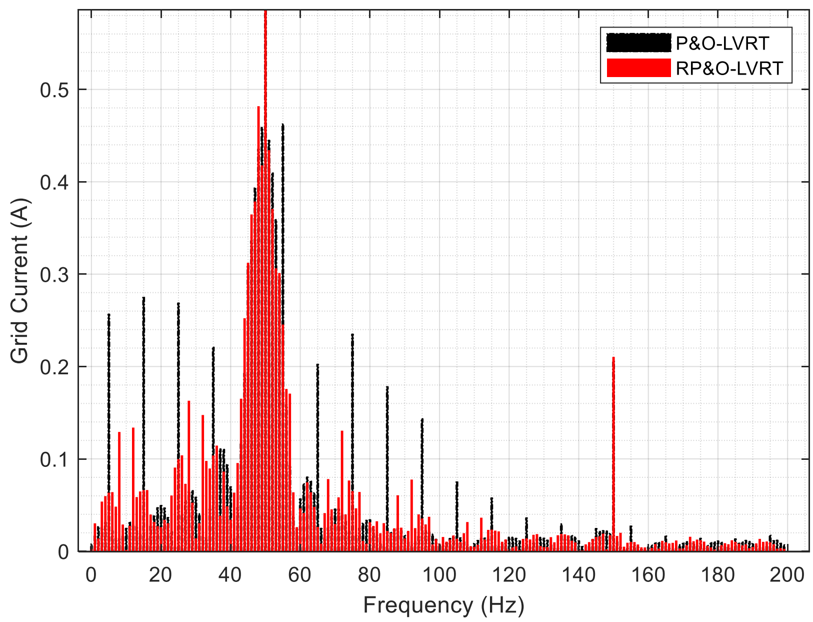

Figure 5.92. The injected grid current frequency spectrum (proposed MP&O and conventional P&O) during the fault occurrence and LVRT under full-power operating conditions and a frequency resolution of 1 Hz

The frequency spectrum of the injected grid current that compares the proposed MP&O with conventional MPPT algorithms is shown in Figure 5.92. It is evident that the proposed mitigation technique contributes to mitigating the interharmonics emissions in the frequency distribution. The analysis is extended for the low-power operating conditions for the proposed MPPT algorithm with a voltage sag of 0.7 pu, and the results are shown in Figure 5.93 and Figure 5.94.

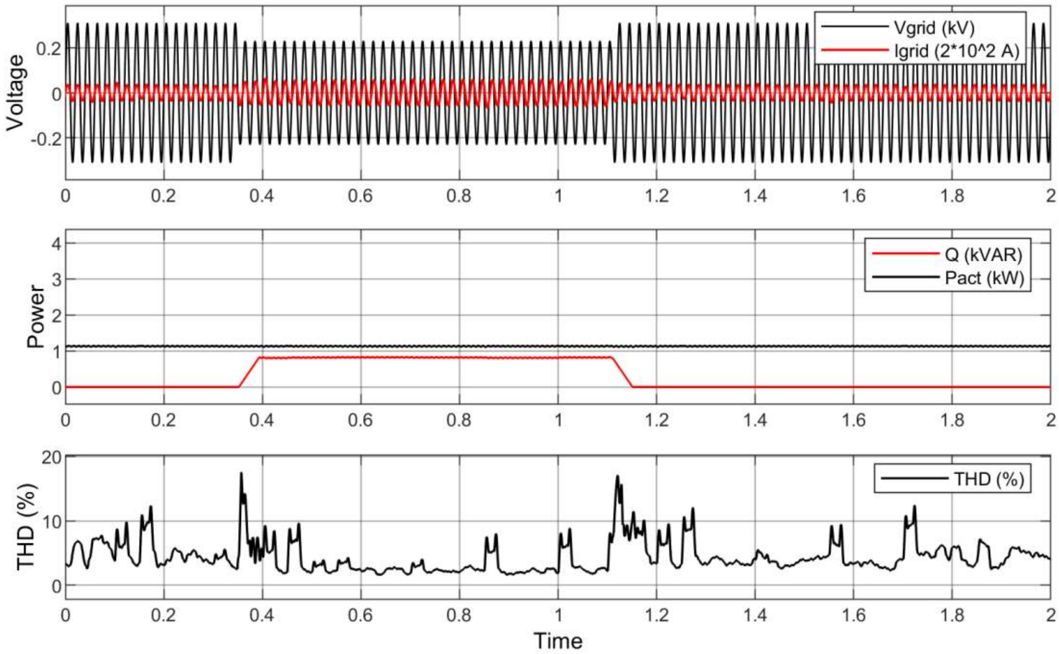

Figure 5.93. The obtained results of the proposed MP&O MPPT algorithm with the hybrid random technique (dc-link voltage, injected active and reactive power, and THD) under low-power operating conditions and LVRT

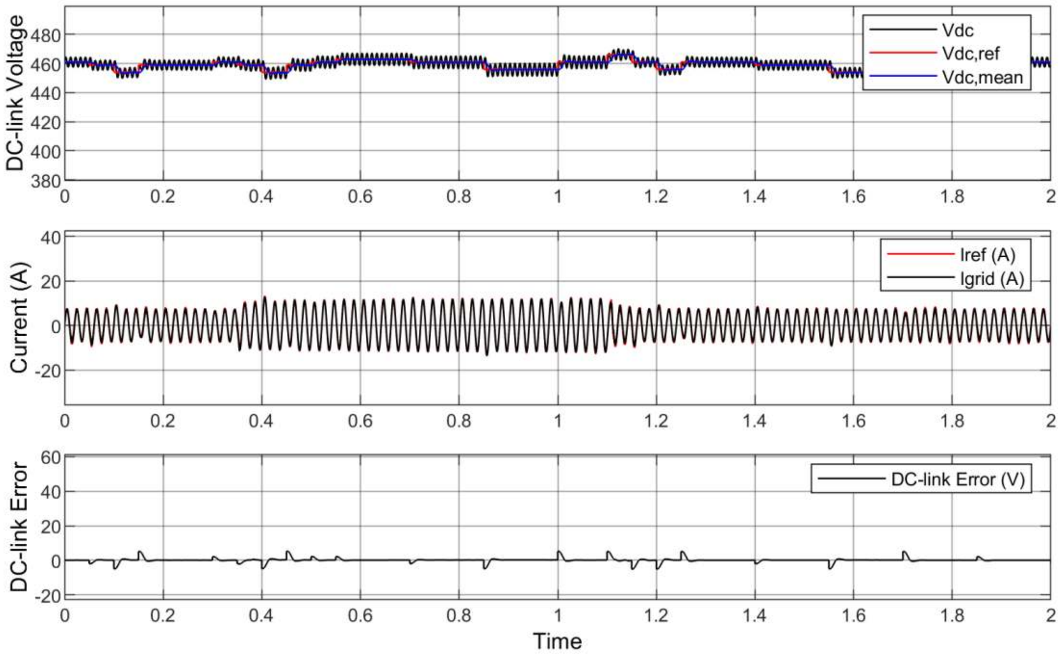

Figure 5.94. The obtained results of the proposed MP&O MPPT algorithm with the hybrid random technique (DC-link voltage, grid current, and DC-link error) under low-power operating conditions and LVRT

The obtained efficiency under this case is 95.77%, and the injected reactive power is 800 VAR. Before the occurrence of the fault, the THD was 5.82%, and during the LVRT operation, the obtained THD was 17.07%.

A comparison is conducted with the conventional P&O at low-power operating conditions for a voltage sag of 0.7 pu to evaluate the obtained results. The results are shown in Figure 5.95 and Figure 5.96. It can be observed that the active power under this criteria is kept the same without any limitation. The injected current is distorted more than in the previous case due to the low-power operating conditions and the fault occurrence.

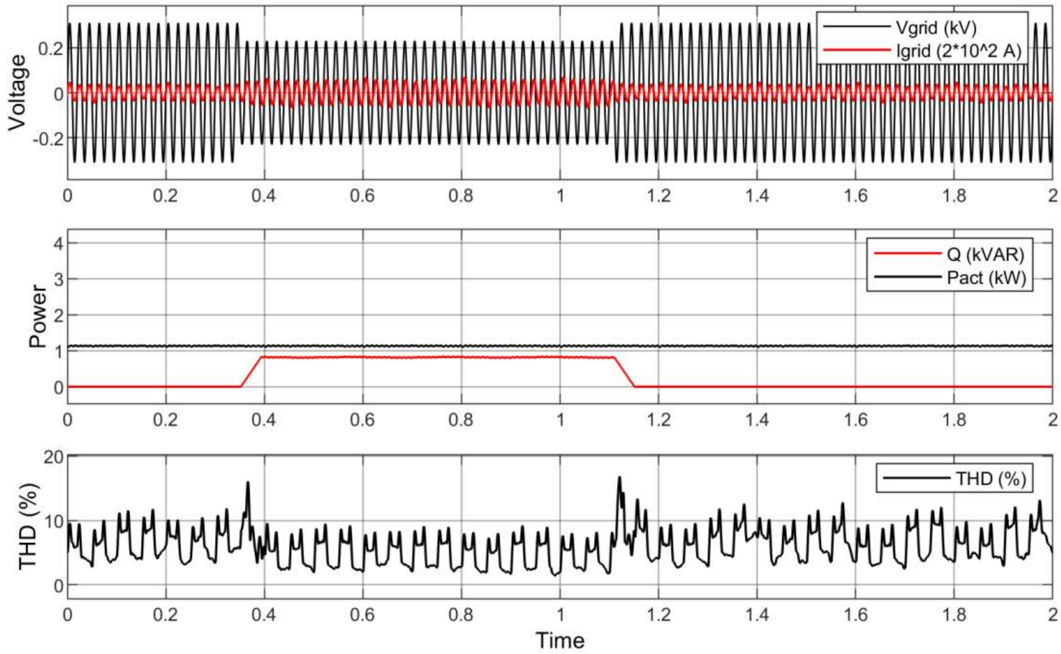

Figure 5.95. The obtained results of the developed P&O MPPT algorithm (dc-link voltage, injected active and reactive power, and THD) under low-power operating conditions and LVRT

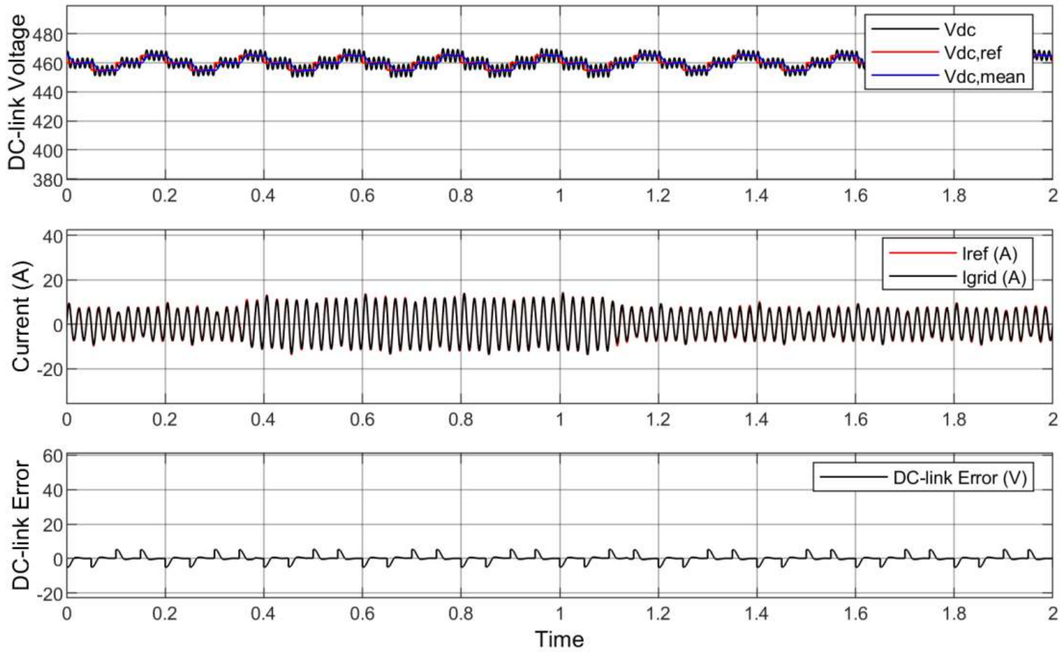

Figure 5.96. The obtained results of the developed P&O MPPT algorithm (DC-link voltage, grid current, and DC-link error) under low-power operating conditions and LVRT

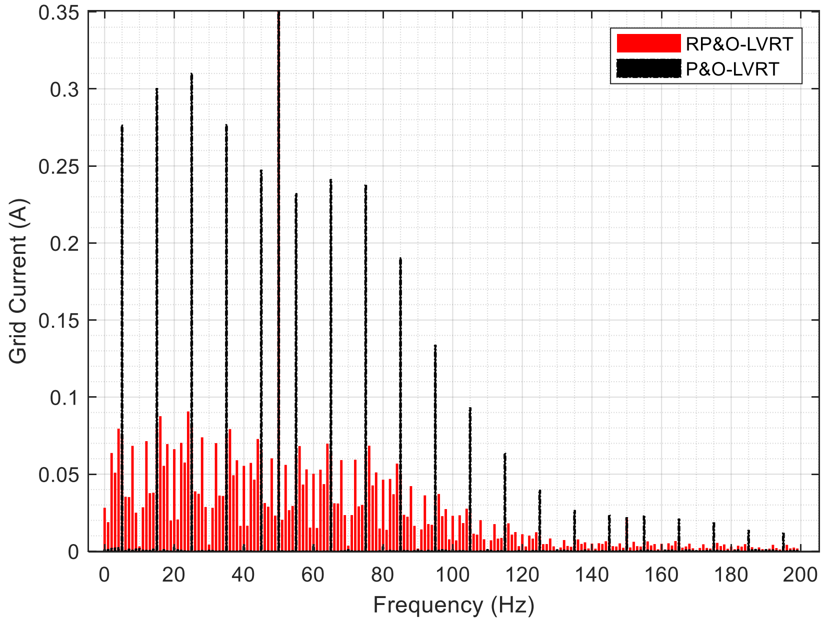

Figure 5.97. The injected grid current frequency spectrum (proposed MP&O and conventional P&O) during the fault occurrence and LVRT under low-power operating conditions and a frequency resolution of 1 Hz

The obtained tracking efficiency under the conventional P&O method is 93.06%, and the amount of injected reactive power is 800 VAR. Before the occurrence of the fault, the THD was 7.96%, and during the LVRT operation, the THD was 22.4%. It can be observed that in all power operating conditions, the proposed interharmonics mitigation technique significantly reduces the emissions injected into the grid.

5.6.2. Impact of Frequency Deviation on Interharmonics Generation

Abnormalities from the grid side at the PCC may occur in different forms, including fluctuations in the operating frequency. This section presents the impact of grid frequency deviation on interharmonics generating characteristics. The nominal grid frequency is 50 Hz, and a deviation is created by 0.5 Hz, which corresponds to a deviation of 1%, according to different grid codes (G. Landera et al. 2023). A comparison between the proposed mitigation technique and the conventional P&O method is shown in Figure 5.98 to Figure 5.104.

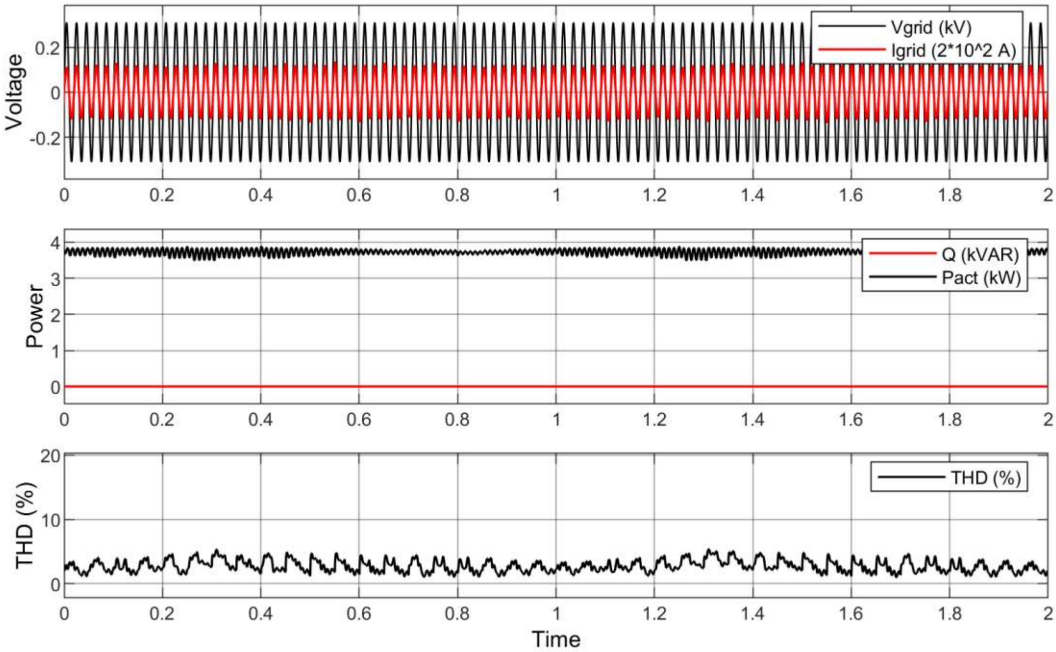

Figure 5.98. The obtained results of the developed P&O MPPT algorithm (dc-link voltage, injected active and reactive power, and THD) operated under full-power operating conditions and 0.5 Hz frequency deviation

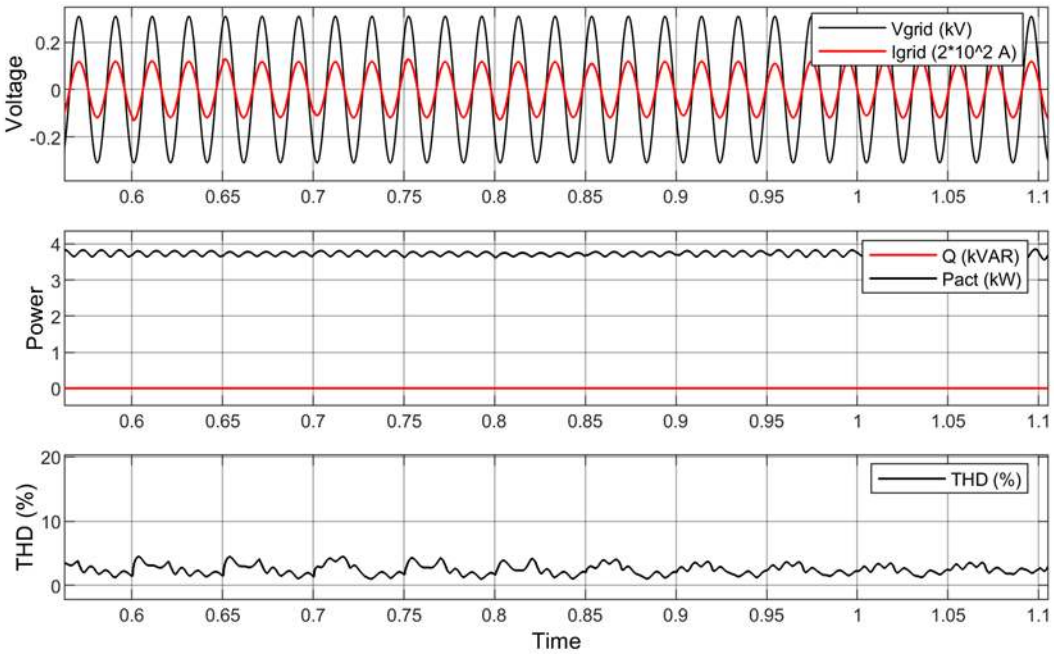

Figure 5.99. Detailed variations (dc-link voltage, injected active and reactive power, and THD) operated under the full-power operating conditions and 0.5 Hz frequency deviation

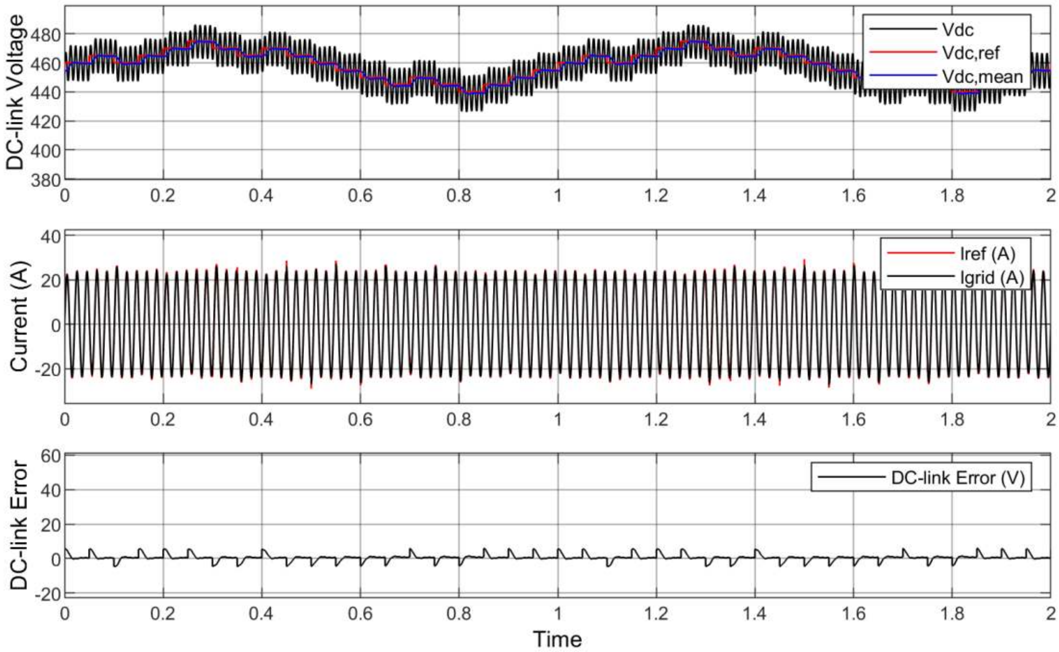

Figure 5.100. The obtained results of the developed P&O MPPT algorithm (DC-link voltage, grid current, and DC-link error) operated under full-power operating conditions and 0.5 Hz frequency deviation

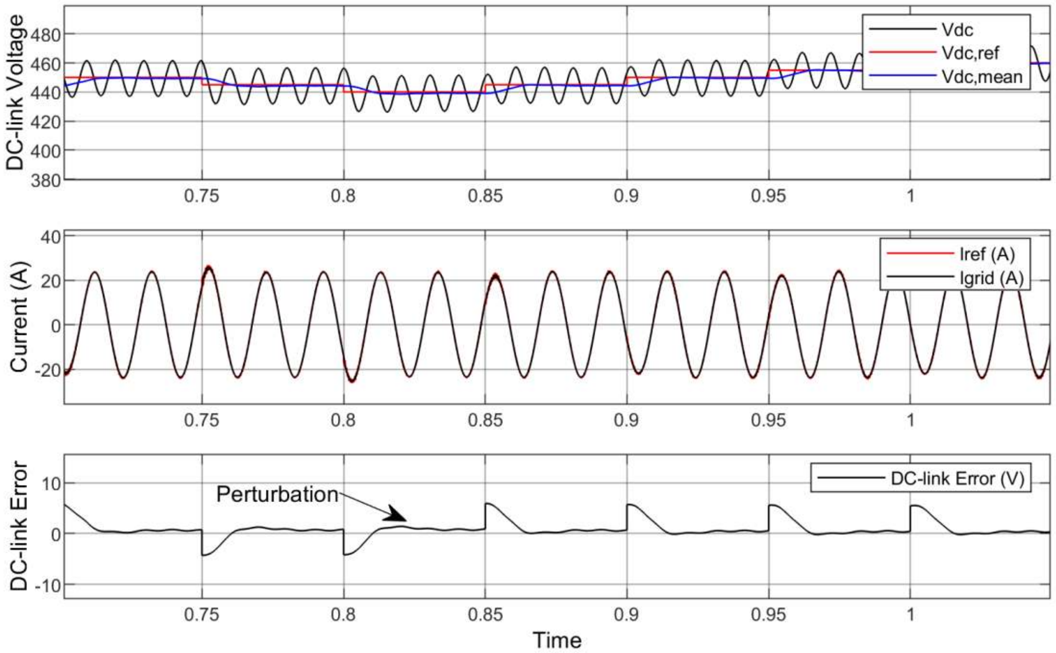

Figure 5.101. Detailed variations. (DC-link voltage, grid current, and DC-link error) operated under full-power operating conditions and 0.5 Hz frequency deviation

The current control loop encounters more fluctuations; thus, the interharmonics and harmonics distortion increases with the grid frequency deviations. The obtained efficiency under the conventional P&O method is 95.6%. Before the occurrence of the fault, the THD was 1.87%, and during the fault occurrence, the THD raised to 45.6%. The last results are compared with the developed MP&O MPPT algorithm, as indicated below.

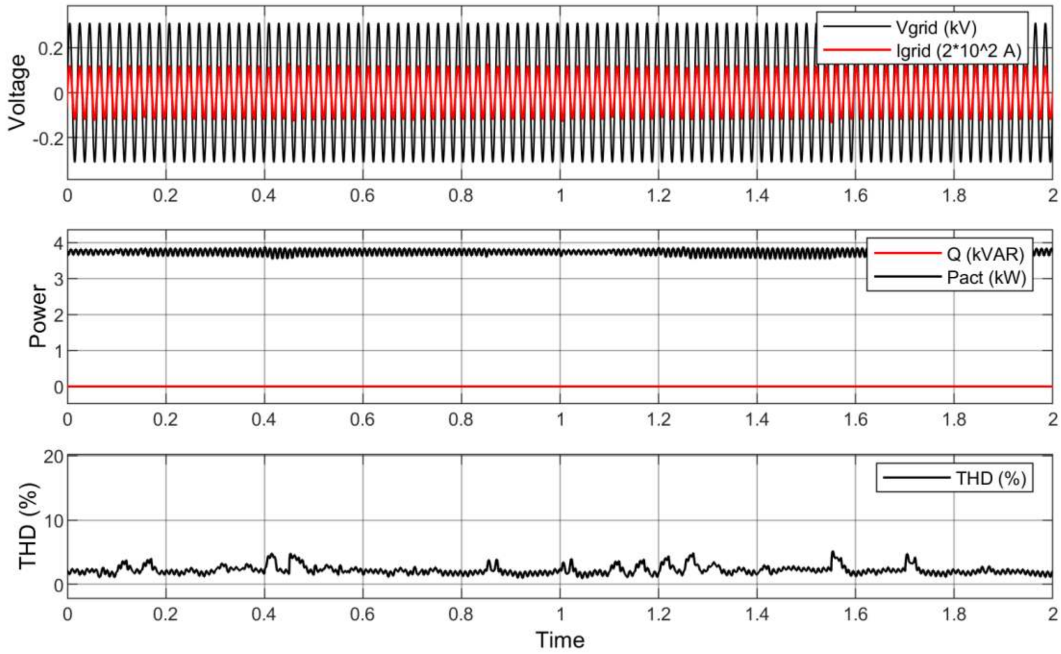

Figure 5.102. The obtained results of the proposed MP&O MPPT algorithm with the hybrid random technique (dc-link voltage, injected active and reactive power, and THD) operated under full-power operating conditions and 0.5 Hz frequency deviation

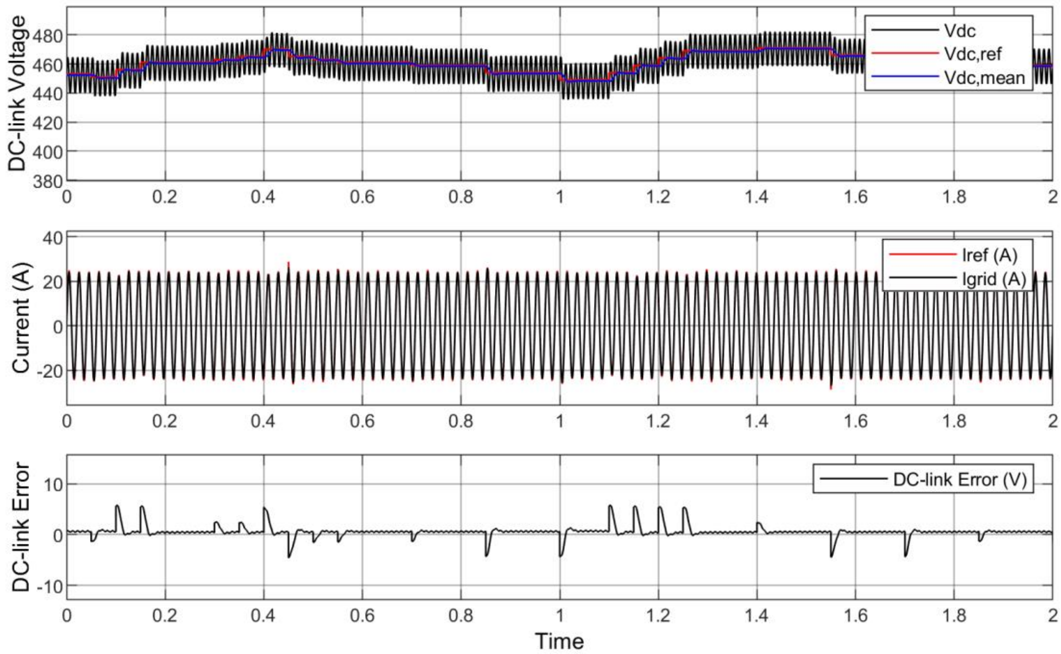

Figure 5.103. The obtained results of the proposed MP&O MPPT algorithm with the hybrid random technique (DC-link voltage, grid current, and DC-link error) operated under the full-power operating conditions and 0.5 Hz frequency deviation

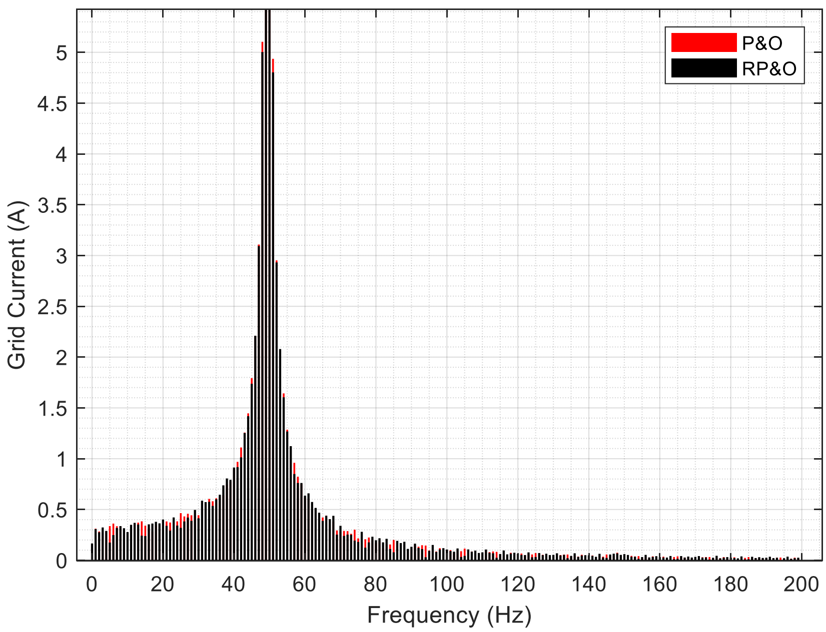

Figure 5.104. The injected grid current frequency spectrum with a frequency deviation of 1% under full-power operating conditions and a frequency resolution of 1 Hz

It can be observed that the non-uniform oscillations are increased in the grid current, injected active power, and the DC-link voltage. Also, it is evident that the grid frequency deviation affects the interharmonics generating characteristics and increases the emissions to the grid current. It is obvious from the THD waveform, as shown in Figure 5.98 and Figure 5.102. The obtained efficiency under the proposed MP&O method is 97.01%, and the THD is 41.23%.

5.6.3. Impact of DC-link Capacitance on Interharmonics Generation

By considering the aging factors of the inverter component, a deviation may be encountered with the operational time passed in hours (Plazas-Rosas et al. 2021). The literature mentioned that the utilization of a DC-link capacitor for around 3000 hours may reduce its value by 2% to 7%. Therefore, an average value will be used to investigate the impact of this deviation on the interharmonics generating characteristics.

The analysis will be conducted for full-power operating conditions, comparing the conventional P&O with the proposed hybrid random MP&O MPPT algorithm in terms of tracking efficiency and the generated interharmonics in the frequency spectrum of the grid current. A deviation of 5% is created in the capacitance value of the DC-link for the single-phase grid-connected PV system. The resulting grid ccurrent frequency spectrum is shown in Figure 5.105 and Figure 5.106. A summary of the results is depicted in Table 5.3. It can be observed that the proposed interharmonics mitigation technique reduces emissions in the frequency distribution compared to the conventional P&O method. In addition, a slight decrease in the interharmonics peaks is shown in the case of the 5% deviation in the DC-link capacitance.

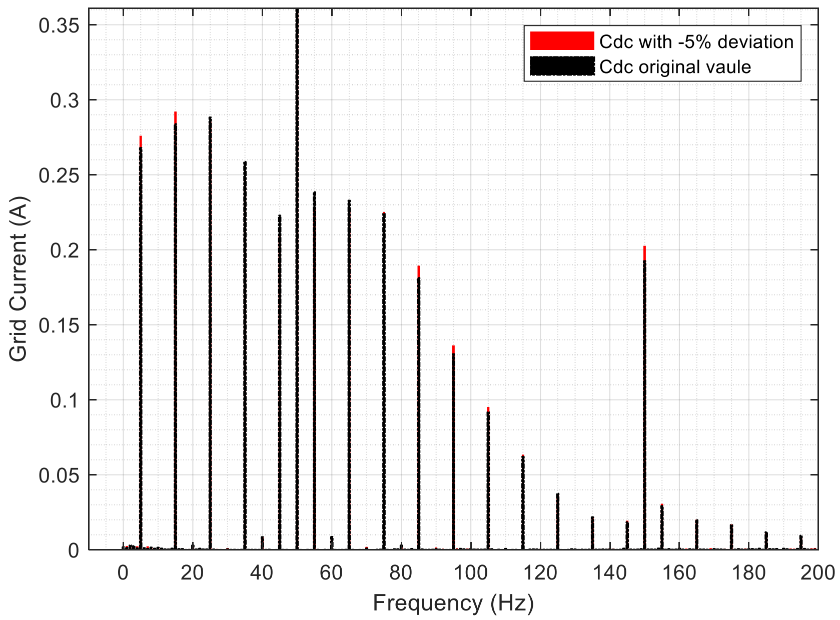

Figure 5.105. The injected grid current frequency spectrum with a capacitance deviation of 5% under full-power operating conditions and a frequency resolution of 1 Hz (P&O)

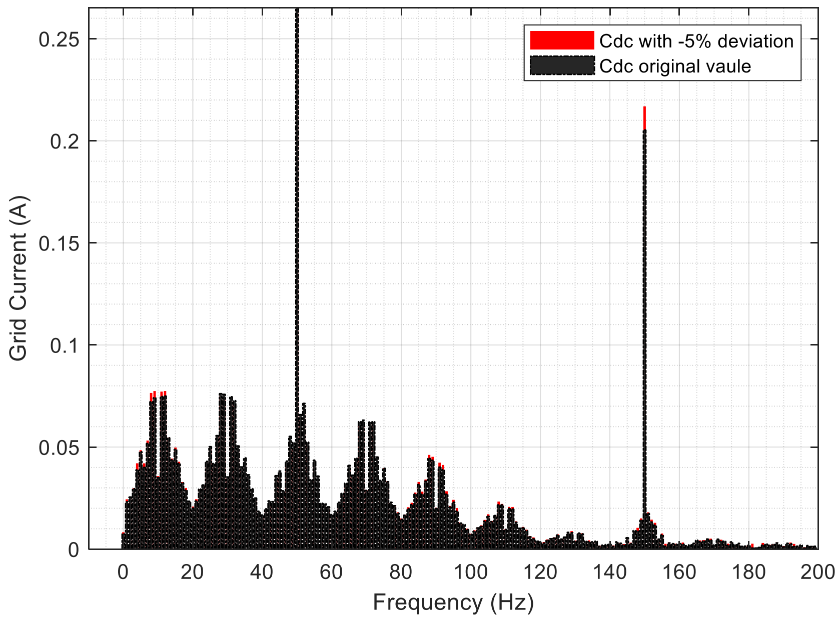

Figure 5.106. The injected grid current frequency spectrum with capacitance deviation of 5% under full rated power and a frequency resolution of 1 Hz (the proposed MPPT algorithm)

Table 5.3. Summary results for the deviation in the dc-link capacitance value

Parameters	THD (%)	η (%)	THD (%)	η (%)
Deviation Value	5%		0%	
P&O	2.51	96.46	2.46	96.48
Modified P&O -HB	1.91	96.88	1.86	96.95

5.6.4. Reduction of Interharmonics under Active and Reactive Power Support

The proposed interharmonics mitigation technique is discussed under the case of reactive power support to the grid. In this case, the effectiveness of the proposed mitigation technique is investigated under low-power operating conditions. From the previous discussion, the case for the hybrid random MP&O will be considered for the comparison and analysis of the DC-link variations and the interharmonics frequency spectrum, as shown in Figure 5.107 and Figure 5.108. A complete summary of the best results and the relationship between the reactive power injection and the characteristics of interharmonics is presented in Table 5.4.

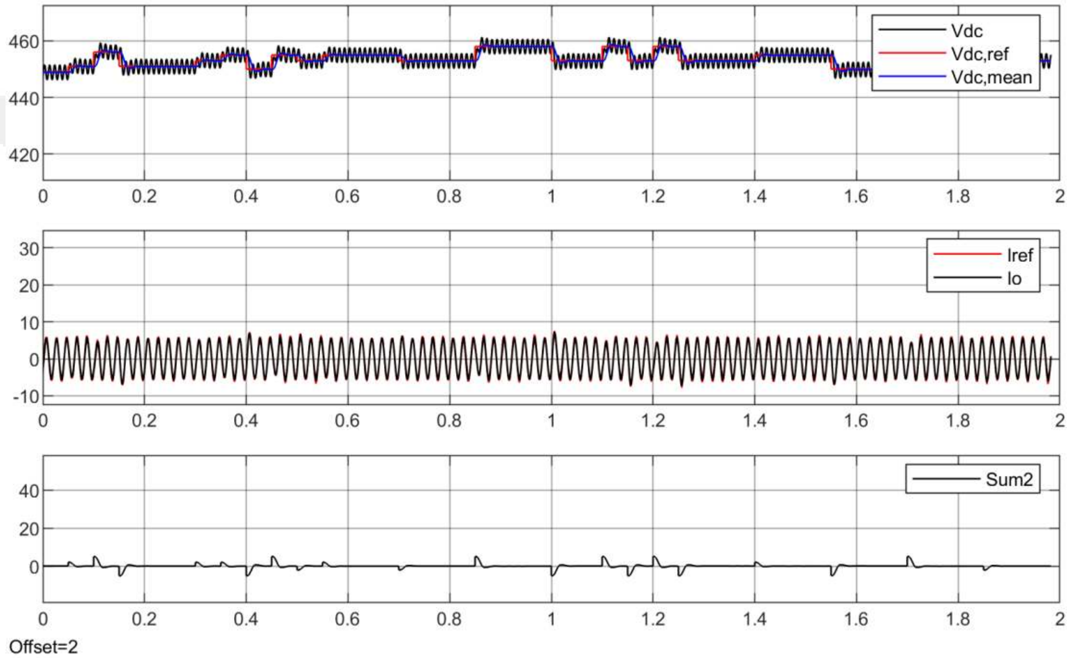

Figure 5.107. The simulation results for the proposed MP&O with the hybrid random technique (DC-link voltage, grid current, and DC-link error) operated under 5% of the rated active power and 500 VAR injected reactive power

It can be concluded from Table 5.4 that the magnitudes of the injected interharmonics are slightly reduced under reactive power support. This means that the reactive power injection, which stabilizes the grid voltage, reduces the interharmonics emissions that are injected into the grid current. Utilizing the proposed hybrid random MP&O along with the other proposed mitigation techniques significantly improves the overall performance, improves the THD, and reduces the interharmonics peaks in the frequency spectrum. For instance, the THD is reduced in case 5 from 10.57% to 6.28% under reactive power injection. Also, the THD is reduced from 12.55% to 6.28% in the second case. This includes the DC-link voltage being more stable under these operating conditions.

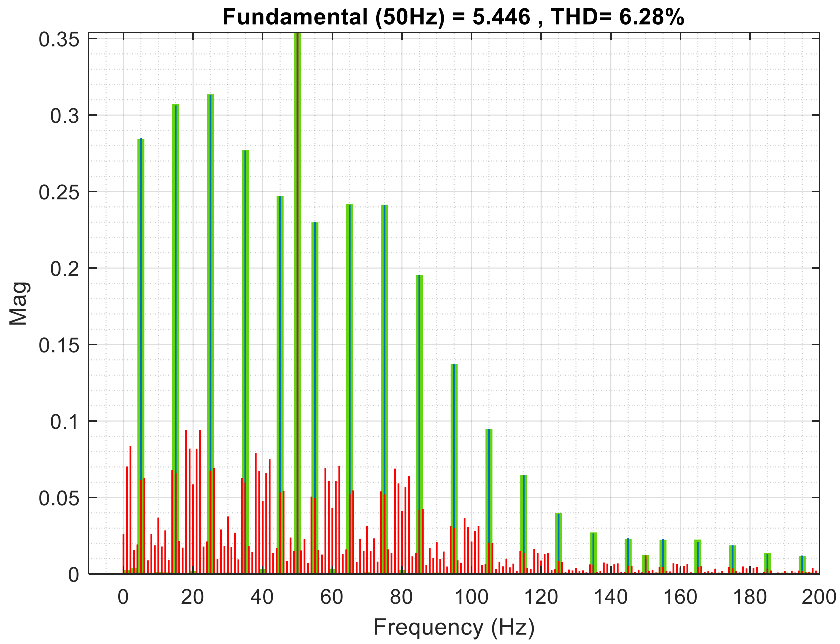

Figure 5.108. Frequency spectrum of grid current for the proposed MP&O (red color) compared to the conventional algorithms (green color)

Table 5.4. Different simulation cases under active and reactive power injection

Case	THD (%)	MPPT Parameters	Q (VAR)	P (%W)
1	2.47%	Fixed	0	100%
2	2.49%	Fixed	200	100%
3	12.55%	Fixed	0	5%
4	12.23%	Fixed	200	5%
5	10.57%	Fixed	500	5%
6	6.28%	MP&O-Proposed	500	5%

5.7. Summary

This chapter presents a development of the single-phase grid-connected control structure to enhance the overall performance and mitigate the generated interharmonics at the PCC. The proposed mitigation techniques are investigated and extended to other MPPT algorithms, such as the MInCon MPPPT algorithm. A comparison is conducted to evaluate the effectiveness of each method compared to the conventional algorithms. These methods are the modified step voltage (MP&O-v), modified sampling frequency (MP&O-f), hybrid random step-sampling frequency (MP&O), modified step voltage (MInCon -v), modified sampling frequency (MInCon -f), hybrid random step-sampling frequency (MInCon), and neural network MPPT algorithms, respectively. A multimission profile is proposed to investigate the impact of different grid faults and abnormalities on the generating characteristic of interharrmonics. In addition, the deviation effect of DC-link capacitance, the dynamical response of the developed system, dynamic grid support, LVRT, and grid frequency variations are also investigated. The results show that the proposed methods enhance the overall performance, reduce the generated interharmonics, reduce the total harmonic distortion (THD), and improve the MPPT algorithms tracking efficiencies. The simulations are conducted under full- and low-power operating conditions.

6. CONCLUSIONS AND FUTURE WORK

This chapter summarizes the main findings of the thesis, emphasizes the thesis contributions, presents the concluding remarks related to the thesis, and discusses the future aspects of the thesis for future work and studies.

6.1. Conclusions and featured remarks

Interest in PV technology has increased over the last few years due to its outstanding performance in distributed generating systems. Although with the great benefits of PV systems and their superior performance, increasing the penetration level of these grid-connected PV systems impacted the power quality of the utility grid, especially at the PCC. Power quality issues have started to be encountered with the increasing number of installed grid-connected PV systems, and among these issues are the waveform events, which include the interharmonics injection with the grid current. Therefore, enhancing the power delivery and quality for the grid-connected PV inverters is critical in developing renewable energy systems under high integration levels.

The enhancements of power delivery in grid-connected PV systems depend on the quality of the injected grid current and the control structure of the PV inverter, including the MPPT operation, to deliver interharmonics-free current waveform. The mitigation of interharmonics depends mainly on the operation of the MPPT algorithms and understanding the generating characteristics and the mechanism of emission for these interharmonics. However, the research on interharmonics from grid-connected PV systems is still premature, and more investigations are demanded to bridge the gaps in the literature. To cope with these challenges, the generating characteristics of interharmonics, emissions' mechanism, and the impacts of the inverter control structure and MPPT operation have been investigated, and therefore, to specify the primary origin behind interharmonics and the effects of different MPPT algorithms on the frequency separation of each interharmonic and the frequency spectrum of the injected grid current. Furthermore, this thesis proposes a mathematical development in investigating interharmonics, which is essential in developing various mitigation and detection techniques. This thesis proposes different interharmonics mitigation algorithms and case studies under different operating conditions with various power levels for single-phase grid-connected PV systems.

In this thesis, the impacts of the MPPT algorithms' control parameters on the aspects and generation characteristics of interharmonics have been investigated and examined. In this context, results show that with higher voltage step size and sampling frequency of the MPPT algorithm, the interharmonics peaks have been increased. However, changing the sampling frequency affects each interharmonic's frequency value in the grid current's frequency spectrum. Mathematical expressions are proposed to specify each interharmonic frequency in the frequency spectrum, which depends on the MPPT algorithms' control parameters. Also, mathematical development has been proposed to relate the MPPT control parameters to the DC-link voltage, which enhances the detection process. Results show that the perturbation of the DC-link voltage from the operation of the MPPT algorithm affects the proposed Fourier series terms of the DC-link voltage. Also, the results indicated that the control parameters of the inverter have a dominant effect on the generating characteristic of interharmonics. The results also concluded an important remark that the interharmonics peaks and allocations are almost the same for full- and low-power operating conditions.

The proposed interharmonics mitigation technique is developed based on mathematically modifying the MPPT algorithm control parameters to randomly change them between their optimal values. The developed algorithms ensure higher MPPT tracking efficiency while minimizing the interharmonics THD as the grid standards require for PV integrations. The developed mitigation technique has been applied to different proposed MPPT algorithms, which include modified step voltage P&O (MP&O-v), modified sampling frequency P&O (MP&O-f), hybrid random step voltage-sampling frequency P&O (MP&O), modified step voltage InCon (MInCon -v), modified sampling frequency InCon (MInCon -f), hybrid random step voltage-sampling frequency InCon (MInCon), and neural network MPPT algorithms, respectively. Under low-power operating conditions, the proposed MP&O-v improved the system performance by reducing the interharmonics emissions and THD by 16.89%, whereas the proposed MP&O-f is slightly better with 18.42% reduction. However, the proposed hybrid random MP&O has significantly enhanced the system performance with 35.04% and 24.4% reduction in interharmonics and THD and improved the tracking efficiency by 5.2% and 0.5%, under low- and full-power operating conditions, respectively. On the other hand, the proposed MICon-v enhanced the system performance by 15.83%, whereas the proposed MICon-f is slightly better with 16.9% reduction. Nevertheless, the proposed hybrid random MICon has potentially improved the system performance with 33.25% and 26.91% reduction in interharmonics and THD and improved the tracking efficiency by 5.1% and 0.46%, under low- and full-power operating conditions, respectively. The proposed NN-based MPPT algorithm shows an improvement of 54.1% and 38.15% reduction of interharmonics and THD, with tracking efficiency enhancement of 5.93% and 0.63%, under low- and full-power operating conditions, respectively.

A multimission profile is proposed in this thesis with the developed mitigation algorithms to evaluate the impacts of different grid side abnormalities, which include voltage sag/swell, dynamic grid support, LVRT, grid frequency deviations, and DC-link capacitance variations on the generating characteristics of interharmonics. Results show that the occurrence of voltage sag/swell increases the interharmonics injected into the grid current, whereas the grid frequency deviation highly impacted the current control loop and vastly increased the emissions. The variation of the DC-link capacitance has the most slight effect. The dynamic grid support, which includes reactive power injection and LVRT operation, improved the system performance and reduced the interharmonics emissions and THD by 13.5% by utilizing the proposed interharmonics mitigation technique. It has been observed that the magnitude of interharmonics emission injected into the grid current has been minimized for the proposed method, irrespective of the irradiance-interharmonics relation and variation while ensuring that the grid-connected PV system is delivering the maximum power with maximum tracking efficiency and minimum THD.

6.2. Future work

This research work can be extended, and possible study topics that are planned to be conducted in the future are listed below:

- A diagnostic technique based on artificial intelligence is planned to be developed utilizing this thesis's proposed mathematical development and expressions.
- Investigating the impacts of grid faults on the generating characteristic of interharmonics under different operating conditions.
- Investigating for any possibility of changing the power circuit topology to reduce the effect of interharmonics.
- It is planned to verify the proposed mitigation algorithms whose performance is tested theoretically and by simulation with an experimental prototype.

REFERENCES

Abdlrahem, Abdlmnam, Ganesh K. Venayagamoorthy, and Keith A. Corzine. 2013. “Frequency Stability and Control of a Power System with Large PV Plants Using PMU Information.” Pp. 1–6 in *2013 North American Power Symposium (NAPS)*. IEEE.

Ahmad, Riaz, Ali F. Murtaza, and Hadeed Ahmed Sher. 2019. “Power Tracking Techniques for Efficient Operation of Photovoltaic Array in Solar Applications – A Review.” *Renewable and Sustainable Energy Reviews* 101(November 2017):82–102.

Alaaeddin, M. H., S. M. Sapuan, M. Y. M. Zuhri, E. S. Zainudin, and Faris M. AL-Oqla. 2019. “Photovoltaic Applications: Status and Manufacturing Prospects.” *Renewable and Sustainable Energy Reviews* 102(December 2018):318–32.

Alam, Md Aftab, S. V. A. V. Prasad, and Mohammed Asim. 2022. “Comparison and Analysis of Transformer-Less Topologies for Grid-Connected PV Systems.” *2022 2nd International Conference on Emerging Frontiers in Electrical and Electronic Technologies, ICEFEET 2022*.

Anurangi, R. O., Asanka S. Rodrigo, and Upuli Jayatunga. 2018. “Effects of High Levels of Harmonic Penetration in Distribution Networks with Photovoltaic Inverters.” Pp. 1–6 in *2017 IEEE International Conference on Industrial and Information Systems, ICIIS Proceedings*.

Beites, Luis F., Julio G. Mayordomo, Araceli Hernández, and Rafael Asensi. 2001. “Harmonics, Interharmonics and Unbalances of Arc Furnaces: A New Frequency Domain Approach.” *IEEE Transactions on Power Delivery* 16(4):661–68.

Blaabjerg, Frede, John K. Pedersen, and Paul Thoegersen. 1997. “Improved Modulation Techniques for PWM-VSI Drives.” *IEEE Transactions on Industrial Electronics* 44(1):87–95.

Blaabjerg, Frede, Remus Teodorescu, Marco Liserre, and Adrian V. Timbus. 2006. “Overview of Control and Grid Synchronization for Distributed Power Generation Systems.” *IEEE Transactions on Industrial Electronics* 53(5):1398–1409.

Blaabjerg, Frede, Yongheng Yang, Dongsheng Yang, and Xiongfei Wang. 2017. “Distributed Power-Generation Systems and Protection.” *Proceedings of the IEEE* 105(7):1311–31.

Boscaino, Valeria, Vito Ditta, Giuseppe Marsala, Nicola Panzavecchia, Giovanni Tinè, Valentina Cosentino, Antonio Cataliotti, and Dario Di Cara. 2024. “Grid-Connected Photovoltaic Inverters: Grid Codes, Topologies and Control Techniques.” *Renewable and Sustainable Energy Reviews* 189:113903.

Chicco, Gianfranco, Jürgen Schlabbach, and Filippo Spertino. 2009. “Experimental Assessment of the Waveform Distortion in Grid-Connected Photovoltaic Installations.” *Solar Energy* 83(7):1026–39.

Choudhary, Piyush and Rakesh Kumar Srivastava. 2019. "Sustainability Perspectives- a Review for Solar Photovoltaic Trends and Growth Opportunities." *Journal of Cleaner Production* 227:589–612.

Djokic, S., J. Meyer, F. Möller, R. Langella, and A. Testa. 2015. "Impact of Operating Conditions on Harmonic and Interharmonic Emission of PV Inverters." *2015 IEEE International Workshop on Applied Measurements for Power Systems, AMPS 2015 - Proceedings*.

Dogga, Raveendhra and M. K. Pathak. 2019. "Recent Trends in Solar PV Inverter Topologies." *Solar Energy* 183(April 2018):57–73.

Du, Yang and Dylan Dah-Chuan Lu. 2018. *Power System Harmonics, Harmonic Distortion Caused by Single-Phase Grid- Connected PV Inverter*. Rijeka.

Du, Yang, Dylan Dah Chuan Lu, Grace M. L. Chu, and Weidong Xiao. 2015. "Closed-Form Solution of Time-Varying Model and Its Applications for Output Current Harmonics in Two-Stage PV Inverter." *IEEE Transactions on Sustainable Energy* 6(1):142–50.

Du, Yang, Dylan Dah Chuan Lu, Geoffrey James, and David J. Cornforth. 2013. "Modeling and Analysis of Current Harmonic Distortion from Grid Connected PV Inverters under Different Operating Conditions." *Solar Energy* 94:182–94.

Ellis, A., R. Nelson, E. Von Engeln, J. MacDowell, L. Casey, E. Seymour, and W. Peter. 2012. "Reactive Power Performance Requirements for Wind and Solar Plants." Pp. 1–8 in *2012 IEEE Power and Energy Society General Meeting*. IEEE.

Elsheikh, Ammar H., Swellam W. Sharshir, Mohamed Abd Elaziz, A. E. Kabeel, Wang Guilan, and Zhang Haiou. 2019. "Modeling of Solar Energy Systems Using Artificial Neural Network: A Comprehensive Review." *Solar Energy* 180(October 2018):622–39.

Elvira-Ortiz, David A., Daniel Morinigo-Sotelo, Oscar Duque-Perez, Roque A. Osornio-Rios, and Rene J. Romero-Troncoso. 2019. "Study of the Harmonic and Interharmonic Content in Electrical Signals from Photovoltaic Generation and Their Relationship with Environmental Factors." *Journal of Renewable and Sustainable Energy* 11(4):043502.

Enslin, Johan H. R. and Peter J. M. Heskes. 2004. "Harmonic-Interaction between a Large Number of Distributed Power Inverters and the Distribution Network." *IEEE Transactions on Power Electronics* 19(6):1586–93.

Etier, I., M. H. Abderrazzaq, A. Al Tarabsheh, O. A. Saraereh, and M. AlBdour. 2016. "The Impact of Large Scale Photovoltaic Systems on the Harmonic Increase in Distribution Networks." *Jordan Journal of Mechanical and Industrial Engineering* 10(4):239–44.

Fekete, Kresimir, Zvonimir Klaic, and Ljubomir Majdandzic. 2012. "Expansion of the Residential Photovoltaic Systems and Its Harmonic Impact on the Distribution Grid." *Renewable Energy* 43:140–48.

Femia, Nicola, Giovanni Petrone, Giovanni Spagnuolo, and Massimo Vitelli. 2005. "Optimization of Perturb and Observe Maximum Power Point Tracking Method." *IEEE Transactions on*

Power Electronics 20(4):963–73.

G. Landera, Yandi, Oscar C. Zevallos, Rafael C. Neto, Jose F. d. Costa Castro, and Francisco A. S. Neves. 2023. "A Review of Grid Connection Requirements for Photovoltaic Power Plants." *Energies 2023, Vol. 16, Page 2093* 16(5):2093.

Gallo, D., R. Langella, A. Testa, J. C. Hernandez, I. Papic, B. Blazic, and J. Meyer. 2013. "Case Studies on Large PV Plants: Harmonic Distortion, Unbalance and Their Effects." in *IEEE Power and Energy Society General Meeting*.

Gawhade, Pragya and Amit Ojha. 2021. "Recent Advances in Synchronization Techniques for Grid-Tied PV System: A Review." *Energy Reports* 7:6581–99.

Guerrero-Lemus, Ricardo, Benjamín González-Díaz, Gerardo Ríos, and Ramzi N. Dib. 2015. "Study of the New Spanish Legislation Applied to an Insular System That Has Achieved Grid Parity on PV and Wind Energy." *Renewable and Sustainable Energy Reviews* 49:426–36.

Hernández-Callejo, Luis, Sara Gallardo-Saavedra, and Víctor Alonso-Gómez. 2019. "A Review of Photovoltaic Systems: Design, Operation and Maintenance." *Solar Energy* 188(March):426–40.

IEA. 2023. "Renewables Analysis and Forecast 2028." *International Energy Agency*, 1–143.

Infield, David G., Peter Onions, Anton D. Simmons, and Gordon A. Smith. 2004. "Power Quality from Multiple Grid-Connected Single-Phase Inverters." *IEEE Transactions on Power Delivery* 19(4):1983–89.

Jain, Shailendra. 2014. *Power Quality: An Introduction*. Elsevier Inc.

Jithin, Kolampurath, Puthan Purayil Haridev, Nanappan Mayadevi, Raveendran Pillai Harikumar, and Valiyakulam Prabhakaran Mini. 2023. "A Review on Challenges in DC Microgrid Planning and Implementation." *Journal of Modern Power Systems and Clean Energy* 11(5):1375–95.

Kabalcı, Ersan. 2020. "Review on Novel Single-Phase Grid-Connected Solar Inverters: Circuits and Control Methods." *Solar Energy* 198(October 2019):247–74.

Karimi-Ghartemani, Masoud and M. Reza Iravani. 2005. "Measurement of Harmonics/Inter-Harmonics of Time-Varying Frequencies." *IEEE Transactions on Power Delivery* 20(1):23–31.

Katiraei, Farid and Julio Romero Agüero. 2011. "Solar PV Integration Challenges." *IEEE Power and Energy Magazine* 9(3):62–71.

Katiraei, Farid, Konrad Mauch, and Lisa Dignard-Bailey. 2007. "Integration of Photovoltaic Power Systems in High-Penetration Clusters for Distribution Networks and Mini-Grids." *International Journal of Distributed Energy Resources* 3(3).

Kivimaki, Jyri, Sergei Kolesnik, Moshe Sitbon, Teuvo Suntio, and Alon Kuperman. 2017. "Revisited Perturbation Frequency Design Guideline for Direct Fixed-Step Maximum Power Point Tracking Algorithms." *IEEE Transactions on Industrial Electronics* 64(6):4601–9.

Langella, R., A. Testa, S. Z. Djokic, J. Meyer, and M. Klatt. 2016. “On the Interharmonic Emission of PV Inverters under Different Operating Conditions.” Pp. 733–38 in *Proceedings of International Conference on Harmonics and Quality of Power*. IEEE Computer Society.

Langella, Roberto, Alfredo Testa, Jan Meyer, Friedemann Moller, Robert Stiegler, and Sasa Z. Djokic. 2016. “Experimental-Based Evaluation of PV Inverter Harmonic and Interharmonic Distortion Due to Different Operating Conditions.” *IEEE Transactions on Instrumentation and Measurement* 65(10):2221–33.

Li, Chun. 2018. “Unstable Operation of Photovoltaic Inverter from Field Experiences.” *IEEE Transactions on Power Delivery* 33(2):1013–15.

Liu, Y., J. Bebic, B. Kroposki, J. de Bedout, and W. Ren. 2008. “Distribution System Voltage Performance Analysis for High-Penetration PV.” Pp. 1–8 in *2008 IEEE Energy 2030 Conference*. IEEE.

Luo, Xing, Jihong Wang, Jacek D. Wojcik, Jianguo Wang, Decai Li, Mihai Draganescu, Yaowang Li, and Shihong Miao. 2018. “Review of Voltage and Frequency Grid Code Specifications for Electrical Energy Storage Applications.” *Energies 2018, Vol. 11, Page 1070* 11(5):1070.

M. Ciobotaru. 2009. “Reliable Grid Condition Detection and Control of Single- Phase Distributed Power Generation Systems.” Ph.D. dissertation, Aalborg Univ, Denmark.

Menti, Anthoula, Thomas Zacharias, and John Milias-Argitis. 2011. “Harmonic Distortion Assessment for a Single-Phase Grid-Connected Photovoltaic System.” *Renewable Energy* 36(1):360–68.

Messo, T., J. Jokipii, A. Aapro, and T. Suntio. 2014. “Time and Frequency-Domain Evidence on Power Quality Issues Caused by Grid-Connected Three-Phase Photovoltaic Inverters.” in *2014 16th European Conference on Power Electronics and Applications, EPE-ECCE Europe 2014*. Institute of Electrical and Electronics Engineers Inc.

Mlazi, Nsulwa John, Maranya Mayengo, Geminpeter Lyakurwa, and Baraka Kichonge. 2024. “Mathematical Modeling and Extraction of Parameters of Solar Photovoltaic Module Based on Modified Newton–Raphson Method.” *Results in Physics* 57:107364.

Montoya, Francisco G., Raúl Baños, Alfredo Alcayde, and Francisco M. Arrabal-Campos. 2019. “Analysis of Power Flow under Non-Sinusoidal Conditions in the Presence of Harmonics and Interharmonics Using Geometric Algebra.” *International Journal of Electrical Power & Energy Systems* 111:486–92.

Morey, Meghraj, Nitin Gupta, Man Mohan Garg, and Ajay Kumar. 2023. “A Comprehensive Review of Grid-Connected Solar Photovoltaic System: Architecture, Control, and Ancillary Services.” *Renewable Energy Focus* 45:307–30.

Motahhir, Saad, Aboubakr El Hammoumi, and Abdelaziz El Ghzizal. 2019. “The Most Used MPPT Algorithms: Review and the Suitable Low-Cost Embedded Board for Each Algorithm.” *Journal of Cleaner Production* (xxxx):118983.

Murillo-Yarce, Duberney, José Alarcón-Alarcón, Marco Rivera, Carlos Restrepo, Javier Muñoz, Carlos Baier, and Patrick Wheeler. 2020. "A Review of Control Techniques in Photovoltaic Systems." *Sustainability 2020, Vol. 12, Page 10598* 12(24):10598.

Nduka, Onyema S. and Bikash C. Pal. 2017. "Harmonic Domain Modeling of PV System for the Assessment of Grid Integration Impact." *IEEE Transactions on Sustainable Energy* 8(3):1154–65.

NREL. 2014. *ADVANCED INVERTER FUNCTIONS TO SUPPORT HIGH LEVELS OF DISTRIBUTED SOLAR*.

Nyamathulla, Shaik and Dhanamjayulu Chittathuru. 2023. "A Review of Multilevel Inverter Topologies for Grid-Connected Sustainable Solar Photovoltaic Systems." *Sustainability 2023, Vol. 15, Page 13376* 15(18):13376.

Oliva, Alejandro R. and Juan Carlos Balda. 2003. "A PV Dispersed Generator: A Power Quality Analysis within the IEEE 519." *IEEE Transactions on Power Delivery* 18(2):525–30.

de Oliveira, Daniel Ramalho, Marcelo Antonio Alves Lima, Leandro Rodrigues Manso Silva, Danton Diego Ferreira, and Carlos Augusto Duque. 2021. "Second Order Blind Identification Algorithm with Exact Model Order Estimation for Harmonic and Interharmonic Decomposition with Reduced Complexity." *International Journal of Electrical Power & Energy Systems* 125:106415.

Oliveira, W. R., Anésio L. F. Filho, and Jorge Cormane. 2019. "A Contribution for the Measuring Process of Harmonics and Interharmonics in Electrical Power Systems with Photovoltaic Sources." *International Journal of Electrical Power & Energy Systems* 104:481–88.

Pinto, Rita, Sílvio Mariano, Maria Do Rosário Calado, and José Felippe De Souza. 2016. "Impact of Rural Grid-Connected Photovoltaic Generation Systems on Power Quality." *Energies* 9(9):1–15.

Plazas-Rosas, Ramiro Alejandro, Martha Lucia Orozco-Gutierrez, Giovanni Spagnuolo, Édinson Franco-Mejía, and Giovanni Petrone. 2021. "DC-Link Capacitor Diagnosis in a Single-Phase Grid-Connected PV System." *Energies 2021, Vol. 14, Page 6754* 14(20):6754.

Raveendhra, Dogga, Rajana Poojitha, Beeramangalla Lakshminarasaiah Narasimharaju, Aliona Dreglea, Fang Liu, Daniil Panasetsky, Mukesh Pathak, and Denis Sidorov. 2023. "Part-I: State-of-the-Art Technologies of Solar Powered DC Microgrid with Hybrid Energy Storage Systems-Architecture Topologies." *Energies 2023, Vol. 16, Page 923* 16(2):923.

Ravindran, Vineetha, Tatiano Busatto, Sarah K. Ronnberg, Jan Meyer, and Math Bollen. 2019. "Time-Varying Interharmonics in Different Types of Grid-Tied PV Inverter Systems." *IEEE Transactions on Power Delivery* PP(c):1.

Ravindran, Vineetha, Sarah K. Rönnberg, and Math H. J. Bollen. 2019. "Interharmonics in PV Systems: A Review of Analysis and Estimation Methods; Considerations for Selection of an Apt Method." *IET Renewable Power Generation* 13(12):2023–32.

De Rosa, Francesco, Roberto Langella, Adolfo Sollazzo, and Alfredo Testa. 2005. "On the Interharmonic Components Generated by Adjustable Speed Drives." *IEEE Transactions on Power Delivery* 20(4):2535–43.

Sangwongwanich, Ariya and Frede Blaabjerg. 2019. "Mitigation of Interharmonics in PV Systems With Maximum Power Point Tracking Modification." *IEEE Transactions on Power Electronics* 34(9):8279–82.

Sangwongwanich, Ariya, Yongheng Yang, Dezso Sera, and Frede Blaabjerg. 2017a. "Interharmonics from Grid-Connected PV Systems: Mechanism and Mitigation." *2017 IEEE 3rd International Future Energy Electronics Conference and ECCE Asia, IFEEC - ECCE Asia 2017* 722–27.

Sangwongwanich, Ariya, Yongheng Yang, Dezso Sera, and Frede Blaabjerg. 2017b. "Interharmonics from Grid-Connected PV Systems: Mechanism and Mitigation." Pp. 722–27 in *IEEE 3rd International Future Energy Electronics Conference and ECCE Asia*. Institute of Electrical and Electronics Engineers Inc.

Sangwongwanich, Ariya, Yongheng Yang, Dezso Sera, Hamid Soltani, and Frede Blaabjerg. 2018a. "Analysis and Modeling of Interharmonics from Grid-Connected Photovoltaic Systems." *IEEE Transactions on Power Electronics* 33(10):8353–64.

Sangwongwanich, Ariya, Yongheng Yang, Dezso Sera, Hamid Soltani, and Frede Blaabjerg. 2018b. "Analysis and Modeling of Interharmonics from Grid-Connected Photovoltaic Systems." *IEEE Transactions on Power Electronics* 33(10):8353–8364.

Santhoshi, B. Kavya, K. Mohana Sundaram, and Sanjeevikumar Padmanaban. 2019. "Critical Review of PV Grid-Tied Inverters." *Energies* 12(10):1921.

Shubbak, Mahmood H. 2019. "Advances in Solar Photovoltaics: Technology Review and Patent Trends." *Renewable and Sustainable Energy Reviews* 115(July):109383.

Silva, Vera, Miguel Lopez-Botet-Zulueta, and Ye Wang. 2016. "Impact of High Penetration of Variable Renewable Generation on Frequency Dynamics in the Continental Europe Interconnected System." *IET Renewable Power Generation* 10(1):10–16.

Singh, Bhuwan Pratap, Sunil Kumar Goyal, and Shahbaz Ahmed Siddiqui. 2019. "Grid Connected-Photovoltaic System (GC-PVS): Issues and Challenges." P. 594 in *Conf. Ser.: Mater. Sci. Eng.*

Sinsel, Simon R., Rhea L. Riemke, and Volker H. Hoffmann. 2020. "Challenges and Solution Technologies for the Integration of Variable Renewable Energy Sources—a Review." *Renewable Energy* 145:2271–85.

Srivastava, Rachit, A. N. Tiwari, and V. K. Giri. 2020. "A Glance View on Performance of PV Plants Commissioned at Different Places in the World." *Energy for Sustainable Development* XX(Xx):1–39.

Sufyan, M., N. A. Rahim, Bilal Eid, and S. R. S. Raihan. 2019. "A Comprehensive Review of

Reactive Power Control Strategies for Three Phase Grid Connected Photovoltaic Systems with Low Voltage Ride through Capability." *Renewable Sustainable Energy* 042701(11).

Taylor, N. and A. Jäger-Waldau. 2019. "Low Carbon Energy Observatory Photovoltaics Technology Development Report 2018." *European Commission, Luxemburg* EUR 29916(JRC118300).

Teodorescu, R., M. Liserre, and P. Rodriguez. 2011. *Grid Converters for Photovoltaic and Wind Power Systems*. New York: IEEE-Wiley.

Testa, Alfredo, M. F. Akram, R. Burch, G. Carpinelli, G. Chang, V. Dinavahi, C. Hatziadoniu, W. M. Grady, E. Gunther, M. Halpin, P. Lehn, Y. Liu, R. Langella, M. Lowenstein, A. Medina, T. Ortmeyer, S. Ranade, P. Ribeiro, N. Watson, J. Wikston, and W. Xu. 2007. "Interharmonics: Theory and Modeling." *IEEE Transactions on Power Delivery* 22(4):2335–48.

V, Beena, Jayaraju M, and Sebin Davis K. 2018. "Active and Reactive Power Control of Single Phase Transformerless Grid Connected Inverter for Distributed Generation System." 13(1):150–57.

Varma, Rajiv K., Shah Arifur Rahman, Tim Vanderheide, and Michael D. N. Dang. 2016. "Harmonic Impact of a 20-MW PV Solar Farm on a Utility Distribution Network." *IEEE Power and Energy Technology Systems Journal* 3(3):89–98.

Vilar, Carolina, Julio Usaola, and Hortensia Amarís. 2003. "A Frequency Domain Approach to Wind Turbines for Flicker Analysis." *IEEE Transactions on Energy Conversion* 18(2):335–41.

Xiao, Xu, Adam J. Collin, Sasa Z. Djokic, Sergey Yanchenko, Friedemann Moller, Jan Meyer, Roberto Langella, and Alfredo Testa. 2017. "Analysis and Modelling of Power-Dependent Harmonic Characteristics of Modern PE Devices in LV Networks." *IEEE Transactions on Power Delivery* 32(2):1014–23.

Yang, Yongheng, Katherine A. Kim, Frede Blaabjerg, and Ariya Sangwongwanich. 2019. *Advances in Grid-Connected Photovoltaic Power Conversion Systems*. Duxford, United Kingdom: Elsevier.

Yang, Yongheng, Huai Wang, and Frede Blaabjerg. 2014. "Reactive Power Injection Strategies for Single-Phase Photovoltaic Systems Considering Grid Requirements." *IEEE Transactions on Industry Applications* 50(6):4065–76.

Yang, Yongheng, Keliang Zhou, and Frede Blaabjerg. 2016. "Current Harmonics from Single-Phase Grid-Connected Inverters-Examination and Suppression." *IEEE Journal of Emerging and Selected Topics in Power Electronics* 4(1):221–33.

Yu, Yiqing, Wei Zhao, Lei Chen, Qing Wang, and Songling Huang. 2020. "Power Measurement Accuracy Analysis in the Presence of Interharmonics." *Measurement* 154:107484.

Žnidarec, Matej, Zvonimir Klaić, Damir Šljivac, and Boris Dumnić. 2019. "Harmonic Distortion Prediction Model of a Grid-Tie Photovoltaic Inverter Using an Artificial Neural Network." *Energies* 12(5).

CURRICULUM VITAE

Ibrahem Hussein, He received the B.Sc. and M.Sc. degrees in Electrical Engineering from Birzeit University in 2013 and King Fahd University of Petroleum and Minerals (KFUPM) in 2017, the latter with a scholarship fully funded by KFUPM, respectively. His research interests include renewable energy resources, machine failure analysis and pattern recognition, and power system planning and reliability analysis.

SCI Journals and International Conferences

- **Ibrahem Hussein**, Çelik, Ö. & A. Teke, A. “A hybrid random parameters modification to MPPT algorithm to mitigate interharmonics from single-phase grid-connected PV systems”, Energy Reports 8, 6234–6244 (2022).
- **Ibrahem Hussein**, Çelik, Ö. & Teke, A. “An Efficient Mitigation Technique for Interharmonics Emission from Single-Phase Grid-Connected PV Systems Under Active and Reactive Power Support”, (Under review), 2024.
- **Ibrahem Hussein,** Zakariya Al-Hamouz, Mohammad Abido, and Abdulaziz Milhem “On the Mathematical Modeling of Line-Start Permanent Magnet Synchronous Motors under Static Eccentricity”, Energies, 2018.
- **Ibrahem Hussein**, Z. Al-Hamouz, "Neural Network Based Detection Technique for Eccentricity Fault in LSPMS Motors", 2018 IEEE Innovations in Intelligent Systems and Applications Conference, pp. 1-5, 2018.
- **Ibrahem Hussein** and Ahmet teke, “Evaluation of Sustainable Campus at Çukurova University: The Case of PVs with EVs”, (Under review), 2024.
- **Ibrahem Hussein** and M. Almuhaini "Reliability Assessment Of Integrated Wind-Storage Systems Using Monte Carlo Simulation", IEEE Conf. - SSD, Germany, 2016.
- **Ibrahem Hussein**, Ayyoub Hourani, and Samir A. Baiyat "Modeling and Simulation of Intelligent Cruise Control System", IEEE Conf.-GCC, Bahrain, 2017.
- **Ibrahem Hussein** and Ali T. Al-Awami "Reliability Assessment Of Sustainable Photovoltaic- Electric Vehicles System", IEEE Conf.-GCC, Bahrain, 2017.

Dissertations:

- **MS Thesis Title:** “A Novel Method For Detecting Eccentricity In Line Start Permanent Magnet Synchronous Motors”, KFUPM, Feb 2017.